

C.B.

I-20

# Acoustic Interactions Between an Altitude Test Facility and Jet Engine Plumes — Theory and Experiments

K. K. Ahuja, K. C. Massey, and A. J. Fleming  
Georgia Tech Research Institute  
Atlanta, GA

and

C. K. W. Tam  
Consultant  
Florida State University  
Tallahassee, FL

and

R. R. Jones, III  
Sverdrup Technology, Inc./AEDC Group

January 1992

Final Report for Period May 1990 through October 1991

PROPERTY OF U.S. AIR FORCE  
AEDC TECHNICAL LIBRARY

**TECHNICAL REPORTS  
FILE COPY**

Approved for public release; distribution is unlimited.

**ARNOLD ENGINEERING DEVELOPMENT CENTER  
ARNOLD AIR FORCE BASE, TENNESSEE  
AIR FORCE SYSTEMS COMMAND  
UNITED STATES AIR FORCE**

## NOTICES

When U. S. Government drawings, specifications, or other data are used for any purpose other than a definitely related Government procurement operation, the Government thereby incurs no responsibility nor any obligation whatsoever, and the fact that the Government may have formulated, furnished, or in any way supplied the said drawings, specifications, or other data, is not to be regarded by implication or otherwise, or in any manner licensing the holder or any other person or corporation, or conveying any rights or permission to manufacture, use, or sell any patented invention that may in any way be related thereto.

Qualified users may obtain copies of this report from the Defense Technical Information Center.

References to named commercial products in this report are not to be considered in any sense as an endorsement of the product by the United States Air Force or the Government.

This report has been reviewed by the Office of Public Affairs (PA) and is releasable to the National Technical Information Service (NTIS). At NTIS, it will be available to the general public, including foreign nations.

## APPROVAL STATEMENT

This report has been reviewed and approved.



PAUL LACASSE, Capt, CF  
Propulsion Division  
Directorate of Technology  
Deputy for Operations

FOR THE COMMANDER



KEITH L. KUSHMAN  
Director of Technology  
Deputy for Operations

REPORT DOCUMENTATION PAGE			Form Approved OMB No. 0704-0188	
Public reporting burden for this collection of information is estimated to average 1 hour per response, including the time for reviewing instructions, searching existing data sources, gathering and maintaining the data needed, and completing and reviewing the collection of information. Send comments regarding this burden estimate or any other aspect of this collection of information, including suggestions for reducing this burden, to Washington Headquarters Services, Directorate for Information Operations and Reports, 1215 Jefferson Davis Highway, Suite 1204, Arlington, VA 22202-4302, and to the Office of Management and Budget, Paperwork Reduction Project (0704-0188), Washington, DC 20503.				
1. AGENCY USE ONLY (Leave blank)	2. REPORT DATE January 1992	3. REPORT TYPE AND DATES COVERED Final - May 1990 - October 1991		
4. TITLE AND SUBTITLE  Acoustic Interactions Between an Altitude Test Facility and Jet Engine Plumes - Theory and Experiments		5. FUNDING NUMBERS  NAS1-19061 (Task 1) PN - DD22EW MIPR EY7483-90-0007		
6. AUTHOR(S) Ahuja, K. K., Massey, K. C., and Fleming, A. J., GTRI, and Tam, C. K. W., Florida State Univ., and Jones, R. R., III, Sverdrup Technology, Inc., AEDC Group				
7. PERFORMING ORGANIZATION NAME(S) AND ADDRESS(ES)  Georgia Tech Research Institute Georgia Institute of Technology Atlanta, GA 30032-0800		8. PERFORMING ORGANIZATION REPORT NUMBER  A8612-001		
9. SPONSORING/MONITORING AGENCY NAME(S) AND ADDRESS(ES) National Aeronautics and Space Administration Langley Research Center Hampton, VA 23665-5225  Arnold Engineering Development Center/DOT Arnold Air Force Base, TN 37389-5000		10. SPONSORING/MONITORING AGENCY REPORT NUMBER  AEDC-TR-91-20		
11. SUPPLEMENTARY NOTES  Available in Defense Technical Information Center (DTIC).				
12a. DISTRIBUTION/AVAILABILITY STATEMENT  Approved for public release; distribution is unlimited.			12b. DISTRIBUTION CODE	
13. ABSTRACT (Maximum 200 words)  The overall objective of the effort described in this report was to develop an understanding of the physical mechanisms involved in the flow/acoustic interactions experienced in full-scale altitude engine test facilities. This is done by conducting subscale experiments and through development of a theoretical model. Model cold jet experiments with an axisymmetric convergent nozzle are performed in a test setup that simulates a supersonic jet exhausting into a cylindrical diffuser. The measured data consist of detailed flow visualization data and acoustic spectra for a free and a ducted plume. It is shown that duct resonance is most likely responsible for the low frequency, high intensity whistles measured in the full-scale facility. This is further confirmed by theoretical calculations. Theoretical calculations also indicate that the higher discrete tones observed in the measurements are related to the screech phenomena.  Limited experiments on the sensitivity of a free 2-D, C-D nozzle to externally imposed sound are also presented. It is shown that a 2-D, C-D nozzle with a cutback is less excitable than a 2-D nozzle with no cutback. At a pressure ratio of 1.5, unsteady separation from the diverging walls of the nozzle is noticed. This separation switches from one wall to the opposite wall thus providing an unsteady deflection of the plume. It is shown that this phenomenon is related to the venting provided by the cutback section.				
14. SUBJECT TERMS screech, altitude test facilities, instability waves, flow/acoustic interactions, jet noise, flow visualization, ejectors			15. NUMBER OF PAGES 172	
			16. PRICE CODE	
17. SECURITY CLASSIFICATION OF REPORT UNCLASSIFIED	18. SECURITY CLASSIFICATION OF THIS PAGE UNCLASSIFIED	19. SECURITY CLASSIFICATION OF ABSTRACT UNCLASSIFIED	20. LIMITATION OF ABSTRACT Same as Report	

## **PREFACE**

The effort described in this report was sponsored by the Arnold Engineering Development Center, (AEDC), Tennessee, through NASA Langley Research Center under contract NAS1-19061. The NASA technical monitor was Dr. Jack Seiner. The AEDC point of contact was Dr. Ralph Jones, who provided all information needed to design the nozzle and relevant test configurations.

The authors are grateful to Mr. Glen Lazalier of AEDC who visited the test facility with Dr. Jones a number of times during the course of this program and provided valuable comments.

The Air Force monitors for this program were Major (CF) R. G. Foster and Captain (CF) J. E. P. Lacasse, AEDC/DOTP.

The reproducibles used in the publication of this report were supplied by the authors. AEDC has neither edited nor altered this manuscript.

## TABLE OF CONTENTS

SECTION	PAGE
1 INTRODUCTION.....	5
1.1 Background.....	5
1.2 Program Objectives.....	6
1.3 Report Outline.....	7
2 MODEL JET/DIFFUSER EXPERIMENTS.....	8
2.1 Objective.....	8
2.2 Model Configuration.....	8
2.3 Test Conditions.....	13
2.4 Flow Visualization.....	13
2.4.1 Water Injection.....	15
2.4.2 Oil Flow Visualization.....	15
2.4.3 Phase-Locked Laser Schlieren Flow Visualization.....	41
2.5 Initial Acoustic Diagnostics for the Ducted Jet.....	46
2.6 Free Jet Versus Ducted Jet - Acoustic Data.....	46
2.7 Further Tests to Confirm Duct Resonance.....	73
2.8 Concluding Comments.....	83
3 JET/DIFFUSER STABILITY CALCULATIONS.....	85
3.1 Supersonic Jet/Diffuser Flow Model and Analysis.....	85
3.2 Duct Acoustic Modes.....	89
3.3 The Dominant Kelvin-Helmholtz Instability Wave.....	112
3.4 Screech Tone Characteristics and Generation.....	124
3.4.1 Analysis of Screech Tone Frequency Data.....	124
3.4.2 Correlation With The Dominant Instability Wave Mode of Supersonic Jets....	127
3.4.3 Screech Tone Generation Mechanism.....	129
3.4.4 Feedback Acoustic Waves.....	131
4 PLUME DEFLECTION SENSITIVITY TO SOUND.....	139
4.1 Objective.....	139
4.2 Test Nozzle.....	139
4.3 Acoustic Source.....	139
4.4 Plume Sensitivity Experiment.....	146
4.5 Additional Interesting Data.....	155

**TABLE OF CONTENTS (Cont.)**

<b>SECTION</b>	<b>PAGE</b>
<b>5</b>	<b>OVERALL CONCLUSIONS AND RECOMMENDATIONS FOR</b>
	<b>FUTURE WORK..... 161</b>
<b>5.1</b>	<b>Axisymmetric Jet Diffuser Flows..... 161</b>
<b>5.2</b>	<b>2-D, C-D Nozzle Flows..... 163</b>
	<b>APPENDIX..... 166</b>
	<b>REFERENCES..... 168</b>

## SECTION 1

### INTRODUCTION

#### 1.1 Background

Altitude test cells are routinely used to test aero-engines during their development phases. Often, these cells are also used to test propulsion system enhancements after entering service. In a typical installation, the engine is contained in a large test cell where the engine inlet is supplied with conditioned air through a direct connection to the test cell air supply system. The engine inlet is aerodynamically isolated from the test cell. The test cell is maintained at the desired altitude pressure through the combined action of the facility exhaust compressors and the pumping action of the engine exhaust as it enters the test cell exhaust gas management system (EGMS) which, in its most common form, is a cylindrical diffuser. In such an installation, the high energy engine exhaust stream may contain acoustic and/or fluid dynamic characteristics that can couple with the resonant modes of the test cell and/or the (EGMS) to produce strong undesirable pressure fluctuations.

In isolated full-scale engine tests conducted at Arnold Engineering Development Center (AEDC) in Tennessee it has become apparent that, for certain operating conditions and test geometries, when engines exhaust supersonically into the EGMS, high intensity discrete tones (whistles) are heard (ref. 1.1). Sound pressure levels as high as 170 dB have been measured within the facility exhaust system. These whistles appear to be unrelated to the screech commonly observed in free jets and whose frequency can now be calculated with a high degree of accuracy (Ref. 1.2).

When these high intensity tones are heard, it appears that the phenomenon responsible for these tones also is directly or indirectly responsible for producing large vibrations in the test cells and other related test facility ducting (ref. 1.1).

The above-described phenomenon has been observed for both axisymmetric, under-expanded nozzles and for two-dimensional, convergent-divergent (2-D, C-D) nozzles. For the 2-D, C-D nozzle, it appears that for certain flow operating conditions, the whole jet body physically deflects in the manner of a fluidic jet. This is also accompanied by a high amplitude (in excess of 165 db) discrete tone.

The physical mechanisms responsible for the discrete tones described above and their interactions with the flow needs to be understood so that a corrective action can be taken in a timely manner. Or if it is known in advance as to what range of flow conditions for given geometric test

configuration produces an unacceptable interaction, then that range of flow conditions can be avoided until an appropriate control methodology has been implemented.

## 1.2 Program objectives

The overall objective of this effort thus is to develop an understanding of the physical mechanisms involved in the flow/acoustic interactions experienced in the full-scale altitude engine test facilities of AEDC. Such an understanding will contribute to the identification of control methods and/or design practices to avoid such interactions.

The specific objectives of the program are three-fold:

### (1) Model Jet Diffuser Experiment

Conduct model jet experiments with model-scale axisymmetric convergent nozzles in a test set-up that will simulate a supersonic jet exhausting into a cylindrical diffuser. Conduct these experiments with a view to obtain better understanding of jet flow/sound interactions in a ducted environment.

### (2) Jet/Diffuser Stability Calculations

Investigate the ability of available aeroacoustic computational methods to predict the potential for acoustic interaction between a supersonic plume and a cylindrical diffuser. In particular, determine the influence of mean flow on acoustic modes of a cylindrical diffuser and develop computer codes for the determination of shear layer instability waves in a ducted environment.

### (3) Plume Sensitivity

Conduct experiments to assess the sensitivity of a two-dimensional convergent-divergent nozzle to external excitation at scale frequencies commensurate with those experienced in acoustic interactions at AEDC.

The first objective was accomplished through acquisition of detailed flow visualization and acoustic measurements of a 1:48 scale-model test facility specifically designed and fabricated for this task.

The theoretical effort under the second objective was directed by the experimental findings.

The "plume sensitivity" experiments under the third objective consisted of only flow visualization.

### 1.3 Report Outline

The model-jet diffuser test facility and experiments are first described in Section 2. This is followed, in Section 3, by a description of the theoretical calculations and comparisons with experimental data. The "plume sensitivity" measurements for the 2-D, C-D nozzle are then presented in Section 4. Finally, the overall conclusions and recommendations are provided in Section 5.

It should be noted that throughout the report the words "diffuser" and "ejector" are used interchangeably. For all experimental observations reported, the exhaust diffuser was operated in an unstarted condition (i.e., subsonic flow always existed in portions of diffuser allowing pressure communication from entrance to exit). The term "ducted" indicates the complete sub-scale facility consisting of the jet, the diffuser, the test cell sections surrounding the jet nozzle and downstream of the jet nozzle.

## SECTION 2

### MODEL JET/DIFFUSER EXPERIMENTS

#### 2.1 Objective

The objective of the effort described in this section was to employ a sub-scale cold flow facility to model a full-scale configuration for which an interaction had been experienced at AEDC. During the full-scale interaction, two high amplitude discrete frequencies were experienced, 85 Hz and 140 Hz. A model-scale axisymmetric convergent nozzle was used in a test set-up to simulate a supersonic jet exhausting into a cylindrical diffuser. These experiments were conducted with a view to obtain a better understanding of jet flow/sound interactions in a ducted environment.

#### 2.2 Model Configuration

Based upon the specifications and sketches provided by personnel at AEDC, the model jet-diffuser configuration shown in Figures 2.1, 2.2 and 2.3 were designed and fabricated. The nozzle is connected to an 18 inch diameter plenum/muffler (see ref. 2.1 for details). The air to the plenum is provided by a compressor capable of providing 17 lbm/sec of dry air continuously. The jet exhausts from a 0.484 inch diameter round convergent nozzle attached to a 2 inch inner diameter (ID) supply duct. The test cell has an ID of 6.50 inches and is made out of transparent acrylic. To simulate variations in test cell secondary or cooling flow, the test cell is connected to a secondary air supply through four inlets connected to a manifold. The test cell, along with the manifold, can be slid over the jet exhaust supply duct. This allows one to control the distance between the jet exit and the cylindrical diffuser (ejector) located downstream of the jet exit.

The supply duct is attached to an existing 18-inch diameter muffler/plenum at GTRI's flow visualization facility. Various photographic views of the facility are shown in Figure 2.4.

Figure 2.4a shows only the free-jet configuration. The framework shown in this picture is a three dimensional traverse arrangement that allows the positioning of a microphone or a pitot probe at suitable locations around the jet exit for various appropriate measurements.

Figure 2.4b and 2.4c show the complete configuration of the jet, diffuser and the test cell. The diffuser section and the secondary supply manifold is seen clearly in the side view of the facility in Figure 2.4c.

Two separate cylindrical ejectors were designed. The inner diameter of each ejector is 2.62 inches. The ratios of the length of the ejector to ejector diameter of the two ejectors are 1 and 3, respectively. The circular disk that supports the ejector has two 0.25 inch diameter through bores

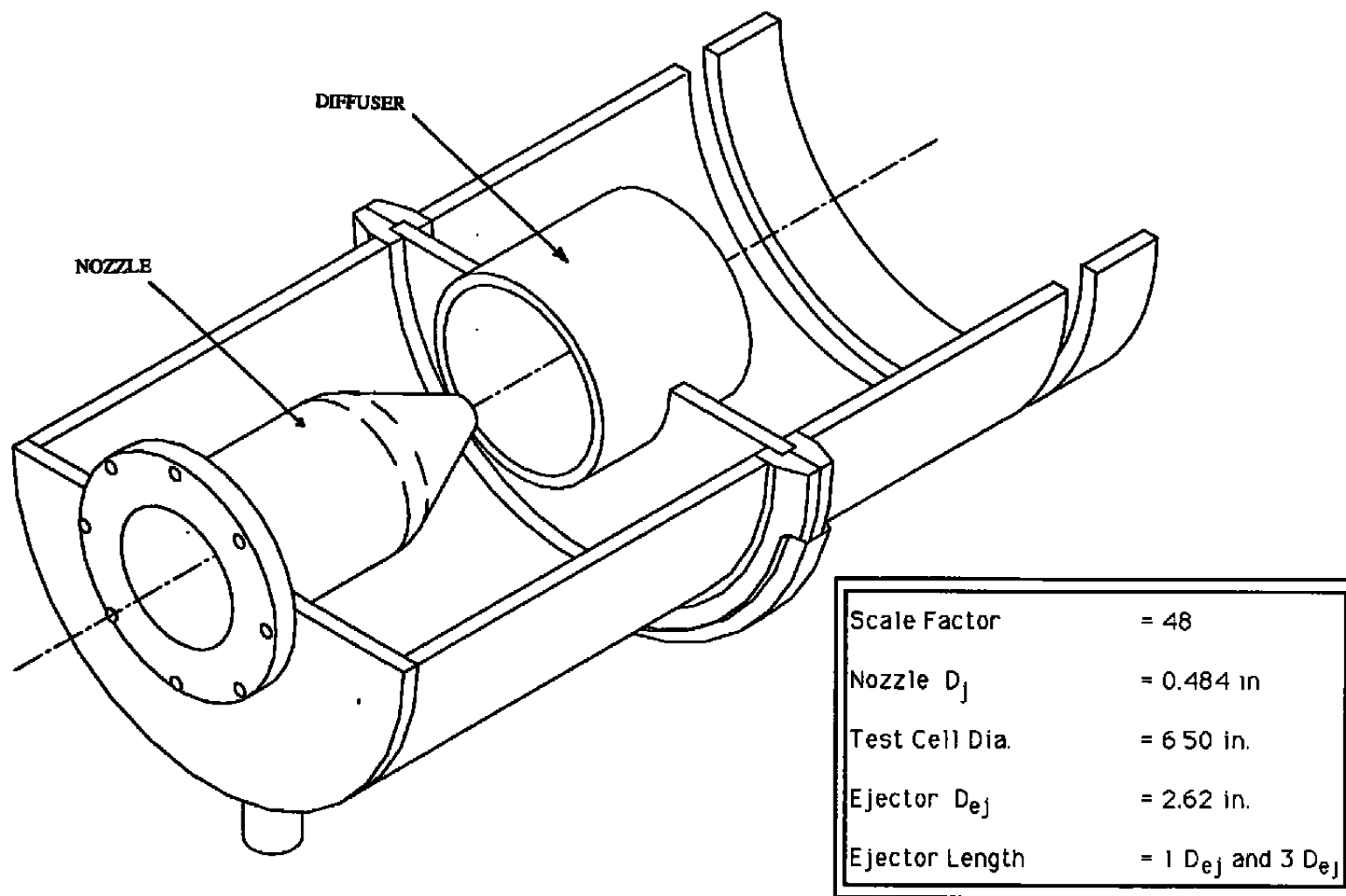


Figure 2.1 Subscale axisymmetric jet/diffuser configuration.

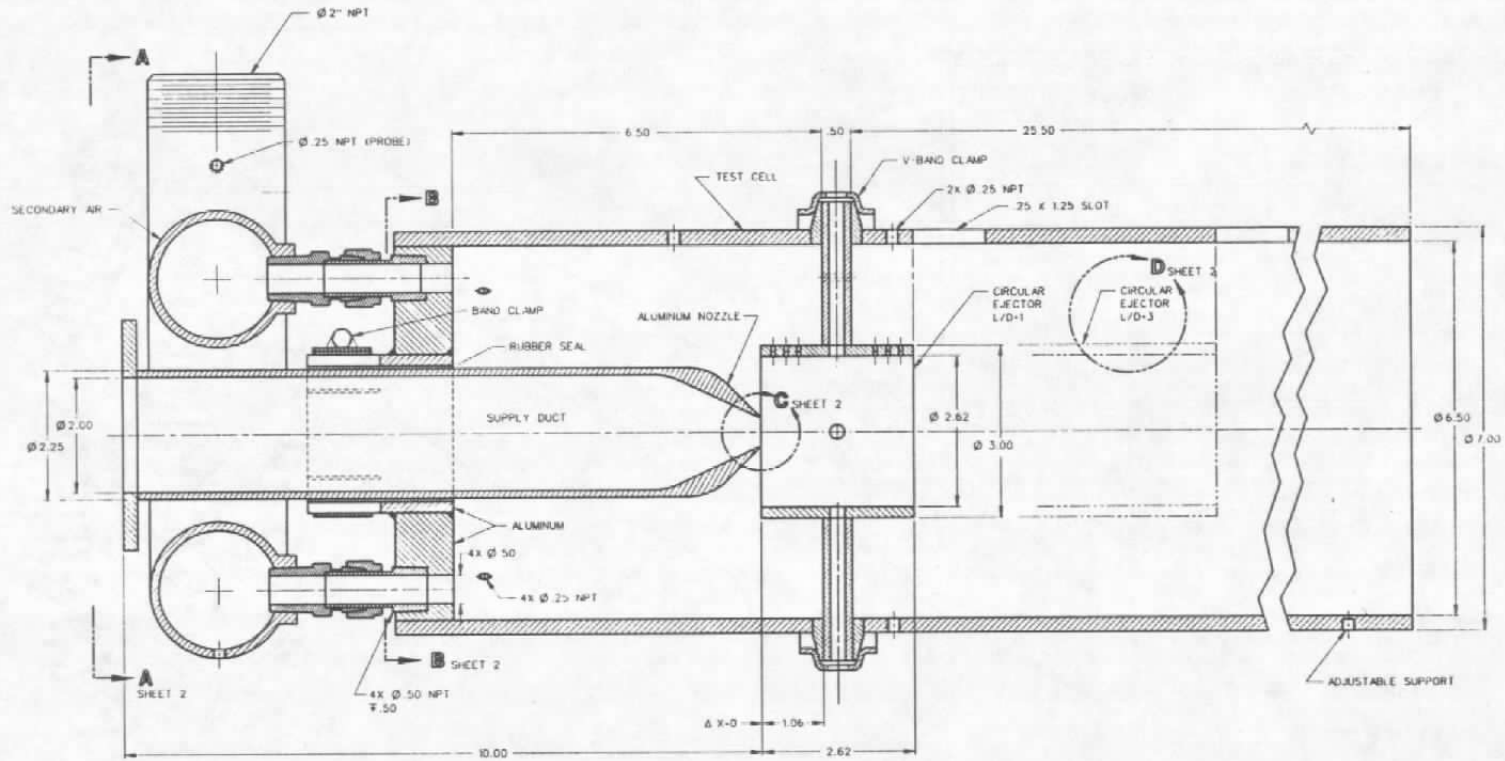
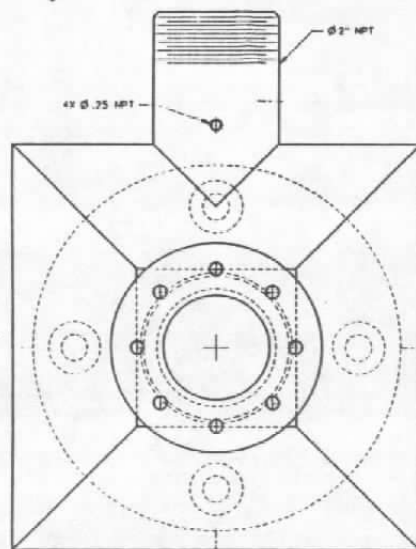
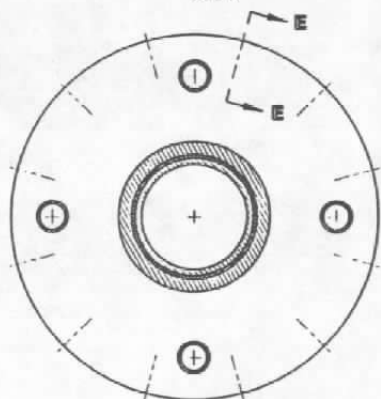


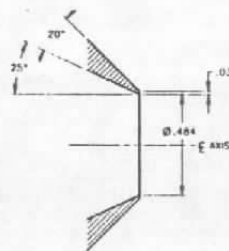
Figure 2.2 Axisymmetric model jet/diffuser configuration.



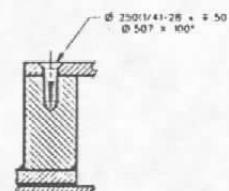
VIEW A-A  
SCALE 1:1



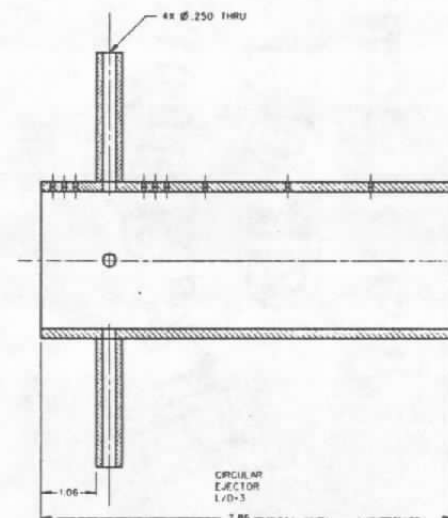
SECTION B-B  
SCALE 1:1



VIEW C  
SCALE 4:1



SECTION E-E  
SCALE 1:1  
ROTATED CCW 15°



DETAIL D  
SCALE 1:1

Figure 2.3 Model jet/diffuser configuration component details.

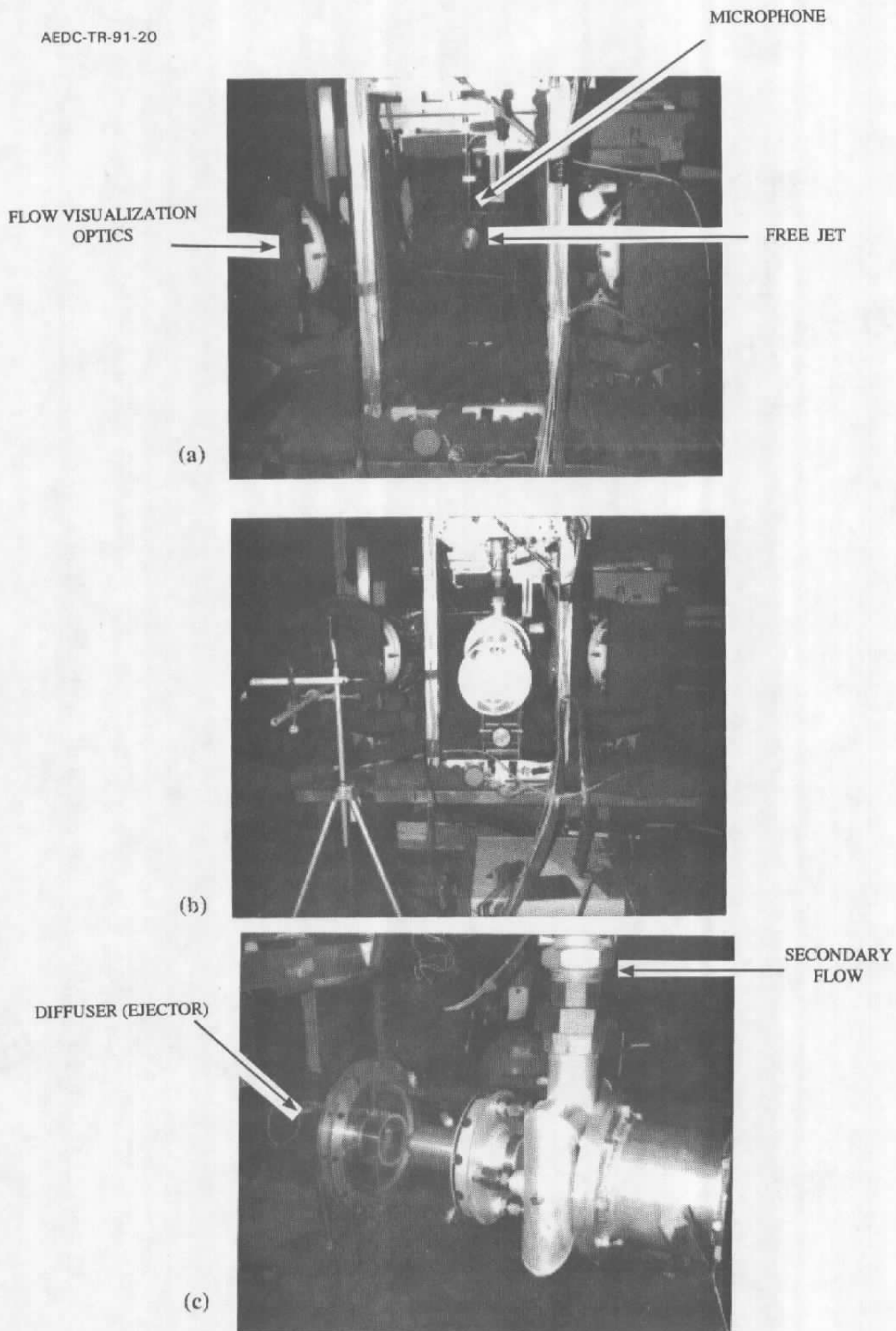


Figure 2.4 Axisymmetric jet/diffuser configuration: (a) free jet alone, (b) and (c) ducted jet. (Part of the flow visualization optics can also be seen.)

in two orthogonal planes. These bores are incorporated to allow laser beams to enter the ejector. A cylindrical lens is mounted at the junction of one of these bores and the ejector inner wall. This provides a laser sheet for flow visualization. A number of 0.25 inch diameter inlets are added to the test cell wall and the secondary supply manifold so that either smoke can be added into the test cell directly from these inlets, or smaller tubes carrying smoke or water can be injected into the test cell and be positioned at critical locations such as at the lip of the jet nozzle. Suitable pressure ports have been added to both the ejector wall and the test cell wall to measure static pressures.

To measure velocity profiles at the exit of the ejector, a 0.25 inch by 1.25 inch slot is provided on the test cell wall to accommodate pitot static probes. The methods of flow visualization and microphone mountings will be described separately later with the results for flow visualization and acoustic measurements.

It should be noted that the scale factor for this sub-scale facility with the smaller ejector is 1/48. The ejector in the full-scale facility included a divergent conical section whereas that used here is a straight circular section. Thus, the sub-scale facility with the smaller ejector represents a generic model of the full-scale configuration maintaining common nozzle and ejector area and length ratios. The longer ejector was included to allow a limited assessment of variations in model geometry.

### 2.3 Test Conditions

The majority of the tests were carried out first with the free jet and then with the ducted jet. The free jet was operated at plenum pressure ratios corresponding to fully-expanded mach numbers of 0.8, 1.0, 1.1, 1.2, 1.3, 1.4, 1.5, 1.6, and 1.7. The same plenum pressure ratio, with respect to the ambient pressure, was maintained for the ducted jet. (As discussed later, it provided minor differences in the fully-expanded jet exit mach numbers for the larger ejector.) The nozzle exit was located at a distance of 0.3 nozzle diameters from the ejector inlet for all tests.

### 2.4 Flow Visualization

A number of flow visualization schemes were tried to examine the flow behavior in the ejector and on the walls of the test cell. These schemes included:

- (1) Water injection combined with laser sheet and laser scattering.
- (2) Oil-flow visualization.
- (3) Laser schlieren visualization.

To improve the quality of the flow visualization, especially of the ducted jet near its exit, two transparent flat-walls were provided in the test cell upstream of the disc that held the ejector. This can be seen in Figure 2.5.

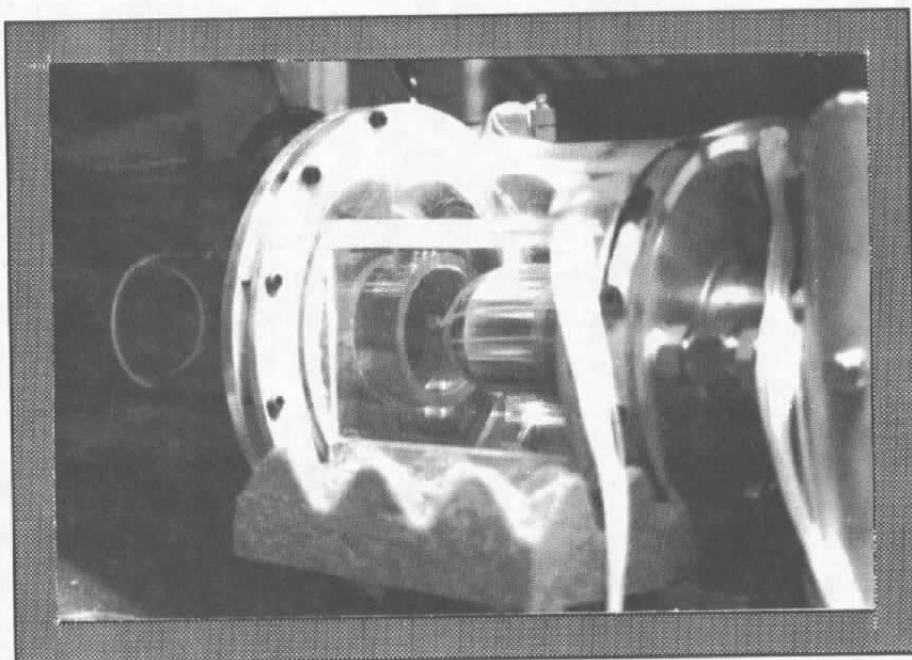


Figure 2.5 Test cell with partly flattened walls.

The approach for each of the three methods of flow visualization and the results therefrom is presented below.

#### 2.4.1 Water Injection

As shown in Figures 2.6 through 2.11, plastic bottles filled with colored water were used to supply the fluid for visualization. These bottles were equipped with small plastic tubes as shown in these figures. One end of these tubes was connected to the bottle, whereas the other was placed at a suitable location in the vicinity of the site of flow visualization. The lower than ambient pressure inside the ejector and in the vicinity of the jet allowed the water to be sucked through the tubes for easy flow visualization. The flow was visualized with the help of a laser sheet or a cylinder of laser beam normally used in schlieren visualization in the same test facility.

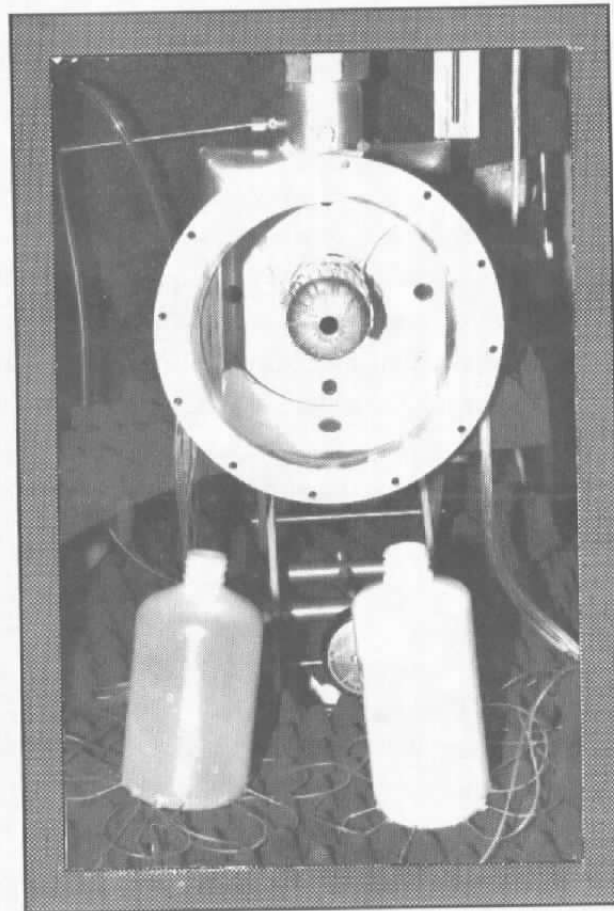
Most useful information about the flow behavior was obtained by examining the flow visualization videos taken during the tests.

A detailed examination of the flow visualization by water injection revealed that the jet appeared to contain a rotational component downstream of the ejector inlet. In addition, it appeared that the jet might have been impinging on the ejector wall surface some distance downstream of the ejector inlet. To understand the nature of this flow phenomenon somewhat better, the oil-flow visualization described below was obtained.

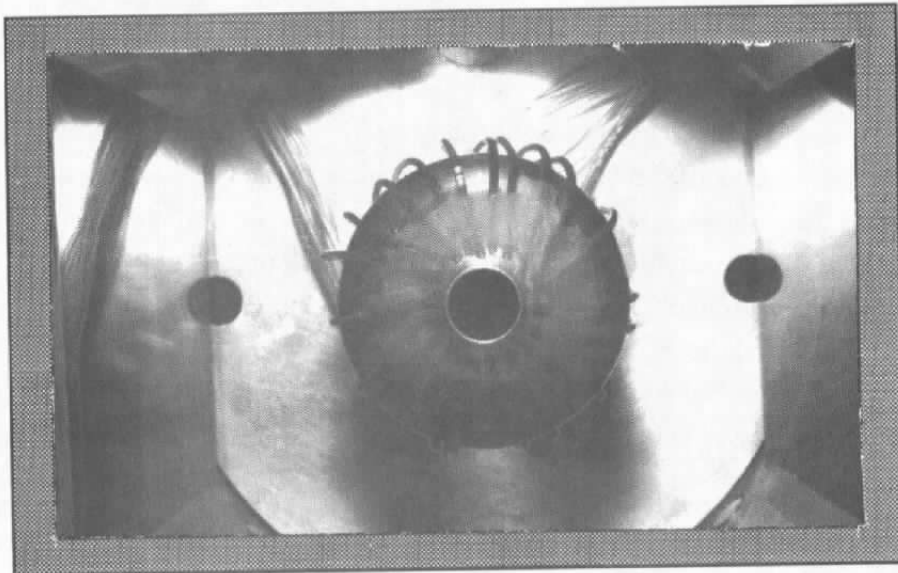
#### 2.4.2 Oil Flow Visualization

In the video pictures taken by injecting water droplets in the jet and by illuminating the jet flow with laser light, it appeared that the jet just downstream of the ejector inlet had a swirling (spiral) component of velocity. It was not absolutely certain in these flow visualization studies, however, if the jet was actually touching the diffuser inner wall or not. It was also not quite clear if there was any back-flow towards the jet exit along the ejector wall. An oil-flow surface visualization method was, therefore, implemented. Oil mixed with fluorescent dye was used to coat the inner surface of the diffuser. Figure 2.12 shows a view of the flow behavior in the vicinity of the nozzle and the diffuser inlet for a jet Mach number of 1.7 for the larger diffuser ejector with  $L/D=3$ . Note that the oil was smeared along the length of the diffuser only over the semi-circular portion facing the reader. On turning the flow on, the whole surface, including the side onto which oil was not applied was found to be covered by the dye indicating that the flow over the surface was indeed moving in a spiral manner.

The presence of the spiral oil flow pattern is abundantly clear in the photographs shown in Figure 2.12. In fact, each time a new coat of oil dye was applied, the upstream test-cell surface



(a)



(b)

Figure 2.6 Nozzle and open test cell; (a) along with water bottles used in visualizing the flow, (b) close up of tubes and flat plates.

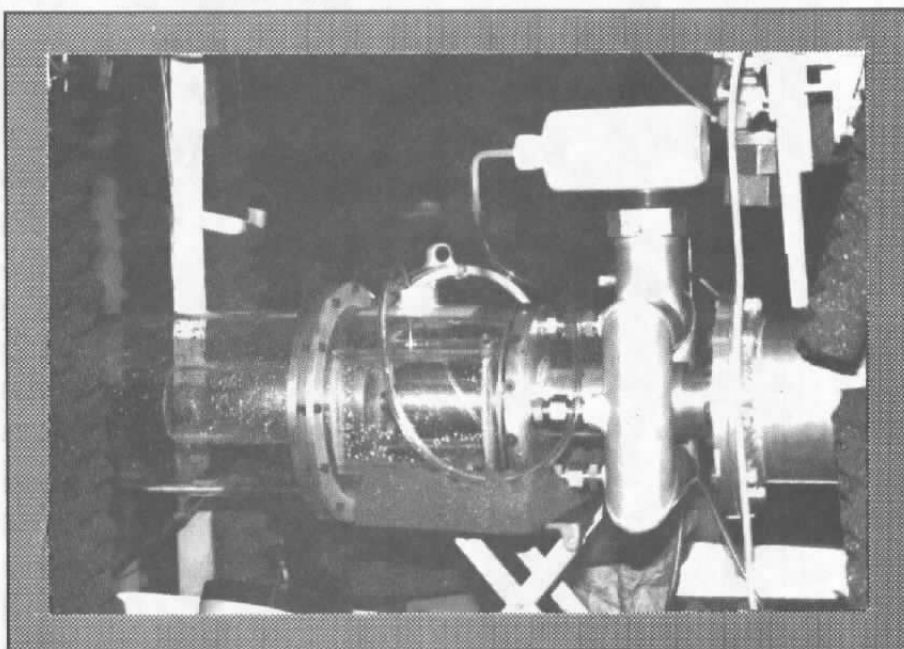


Figure 2.7 Experiment with water dropped into flow.

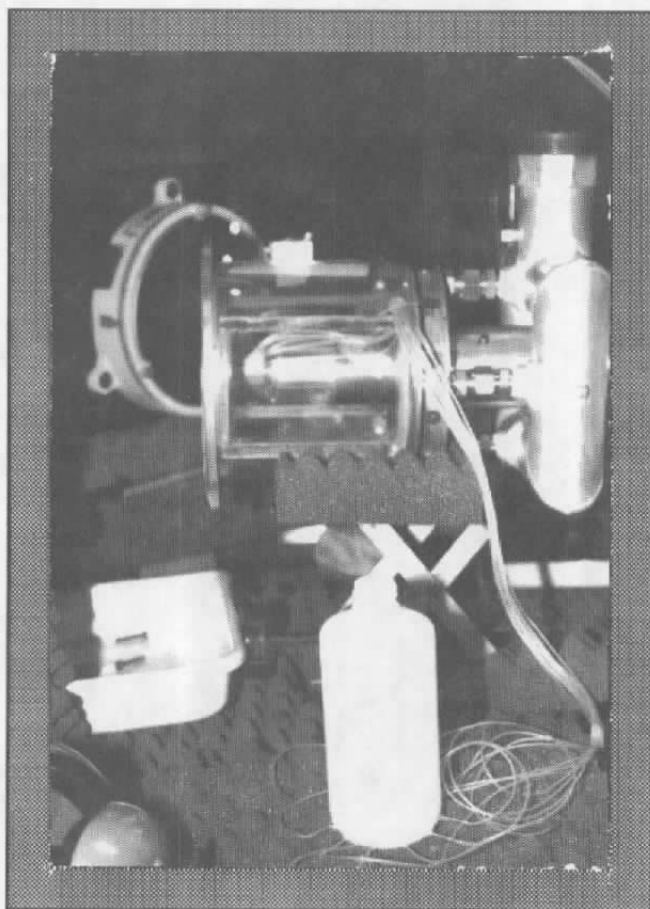


Figure 2.8 Bottle used for injecting water into top half of nozzle.

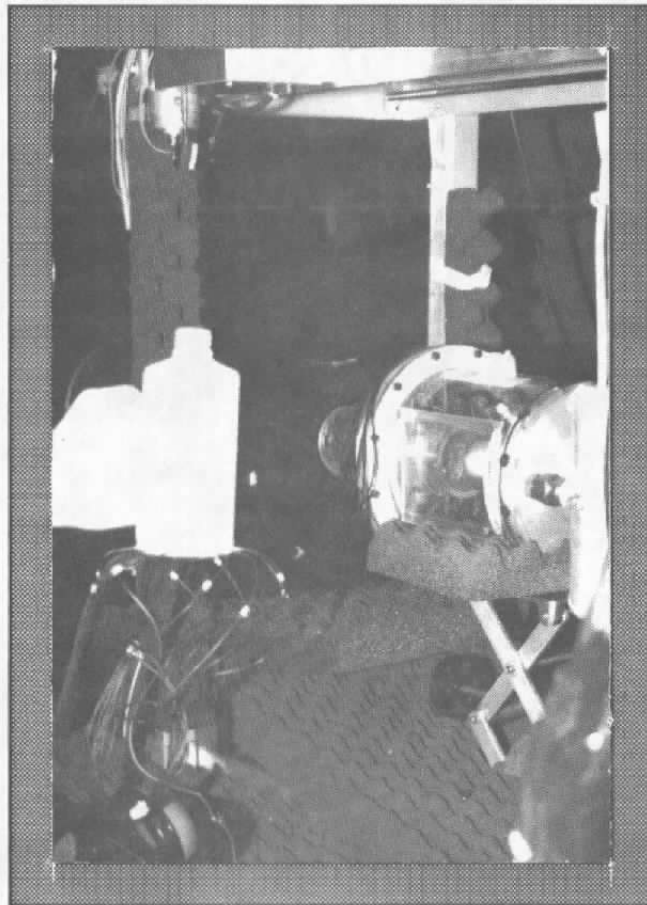


Figure 2.9 Bottle used for injecting water into static pressure ports of ejector.

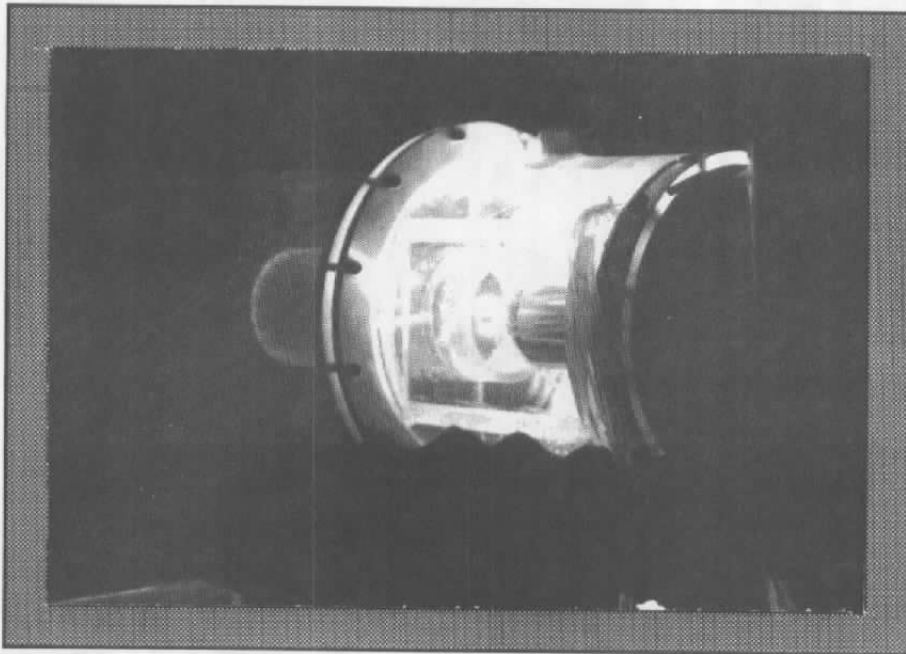


Figure 2.10 Laser sheet passed through jet cross section.

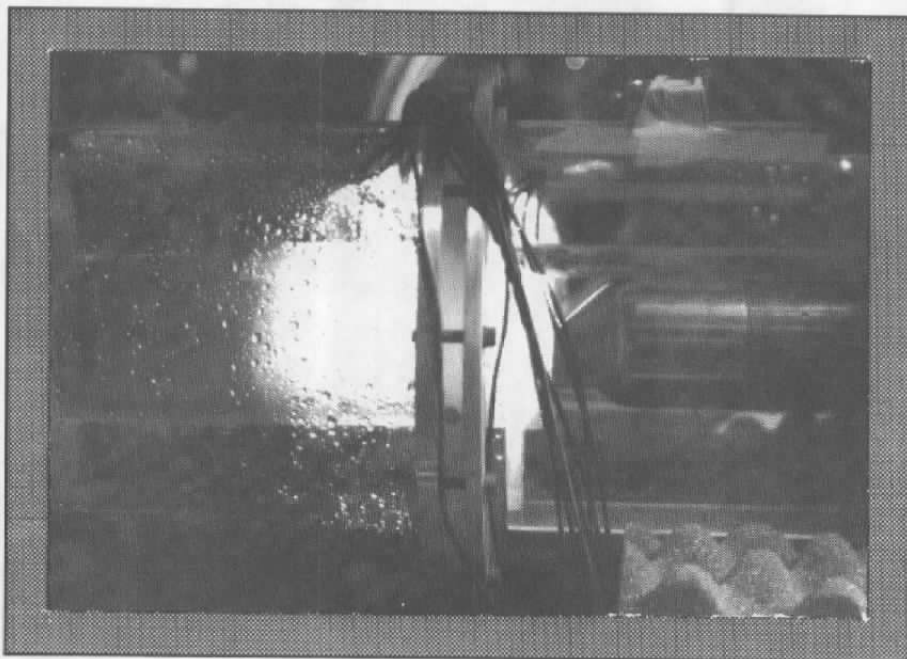


Figure 2.11 Test cell wall flow visualization.

area surrounding the main jet nozzle always appeared to get sputtered by oil dye that moved to the upstream locations from the downstream locations. The presence of the dye pigments on the interior wall of the test cell is also evident in Figure 2.12. These visualizations also indicated that the flow over the wall surface was indeed moving from the diffuser inlet towards the upstream direction. The behavior of the flow along the complete length of the ejector duct is visualized in Figures 2.13, 2.14, and 2.15 for three Mach numbers, namely, 1.7, 1.4, and 0.8. For each Mach number, three photographs are shown. As mentioned above and shown in the sketch on the top left corner of these three figures, the oil and dye was smeared over only one half of the diffuser inner wall surface (side A). Figure (a) is a typical picture of the oil dye coated over diffuser wall surface before the flow was turned on. Views of both sides (side A and side B) of the diffuser are then shown after the flow was turned on. It is seen that much of the dye pigments has moved from the downstream locations and has actually collected in the upstream region. In fact, the spiral motion appears to be present only up to the plane of the disc to which the diffuser is mounted. At further downstream locations, flow appears to straighten out. It may well be that, at this location, the jet actually touches the inner surface of the diffuser. Other likely phenomenon is that, at this location, the flow moving upstream along the surface may meet the flow moving downstream (stagnation region). Additional quantitative data need to be acquired to understand the precise nature of the flow behavior inside the diffuser.

A comparison of the flow patterns for the three Mach numbers indicates that the angle of the spiral is a strong function of the jet Mach number. The lower the Jet Mach number, the smaller is the angle of the spiral, until at  $M = 0.8$ , the flow is almost straight.

The tubes shown in Figure 2.12 (b) were used to inject water droplets for flow visualization of the main jet. These tubes were left in place for the present oil-flow visualizations. (The water injection was prohibited for this case.) To ensure that the tubes themselves were not responsible for the spiral pattern, additional measurements need to be made by removing the tubes.

Flow visualization downstream of the diffuser plate and within the test-cell duct was also made by smearing the oil dye all around the inner surface of this duct. These visualizations for a range of operating jet pressure ratios and nominal Mach numbers are shown in Figures 2.16 thru 2.20. In each figure, the data for identical reservoir pressure is compared for the shorter ( $L/D=1$ ) and the longer ( $L/D=3$ ) diffusers. Here, data for five Mach numbers, namely, 1.7, 1.4, 1.3, 1.1, and 0.8 are presented. With few exceptions, a spiral pattern is seen in most pictures here also. Most of the dye pigments appear to have collected on the wall surface of the duct in the plane of the diffuser exit.

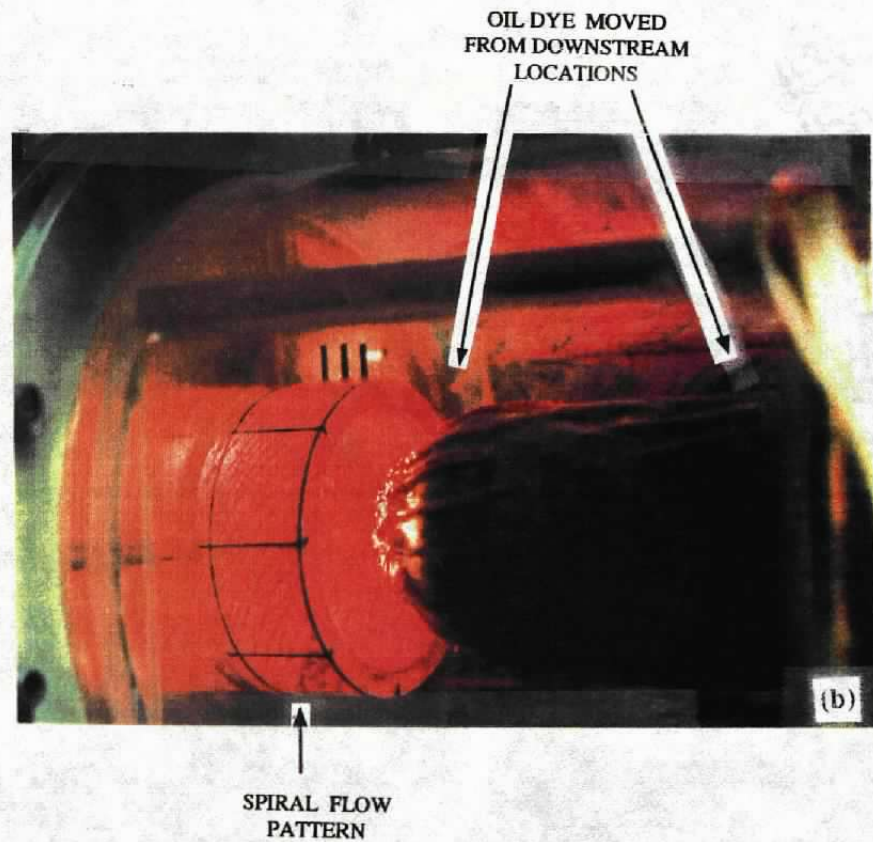
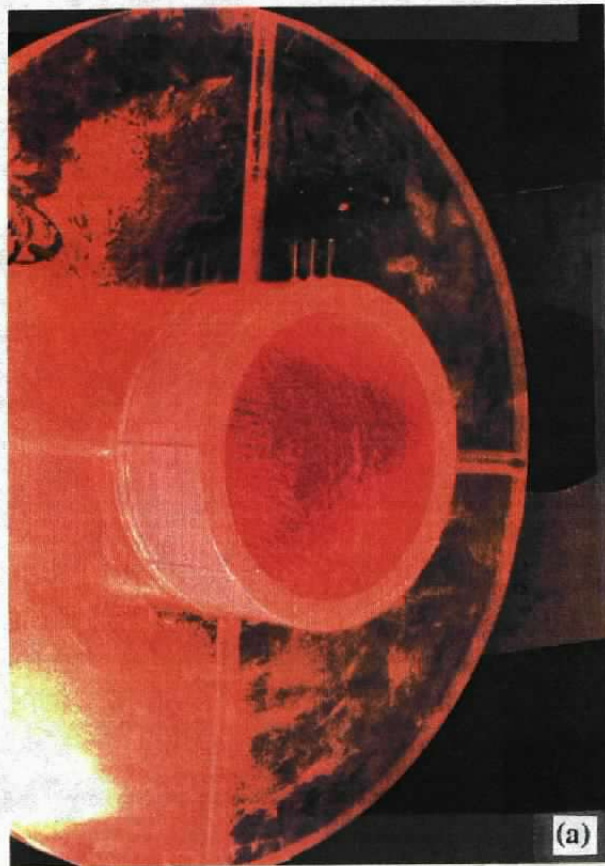


Figure 2.12 Ejector inlet flow visualization. ( $\xi_1 = 4.936$ ,  $M_j \approx 1.7$ ,  $L/D = 3$ )

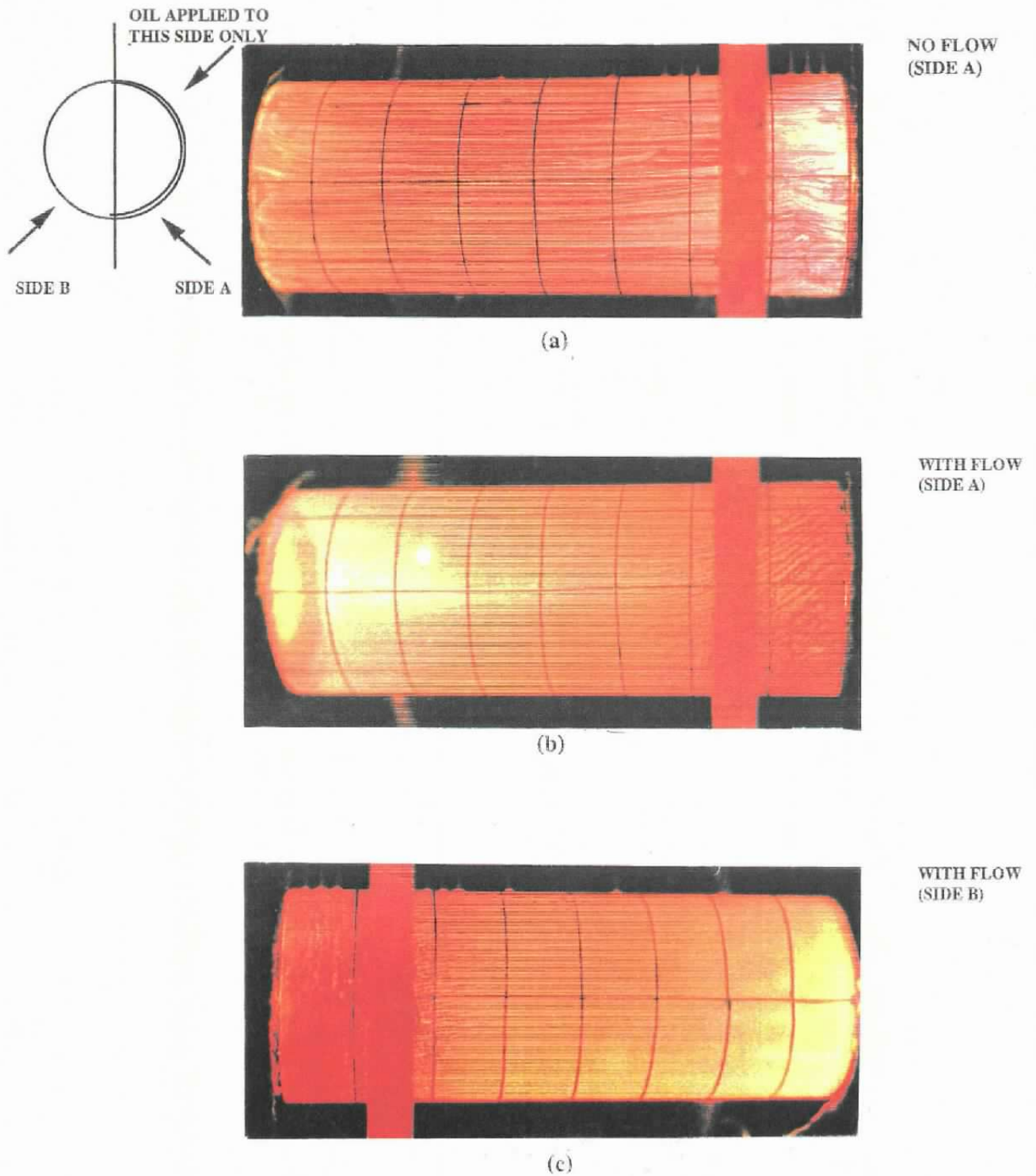


Figure 2.13 Ejector flow visualization. ( $\xi_1 = 4.936$ ,  $M_j \approx 1.7$ ,  $L/D = 3$ )

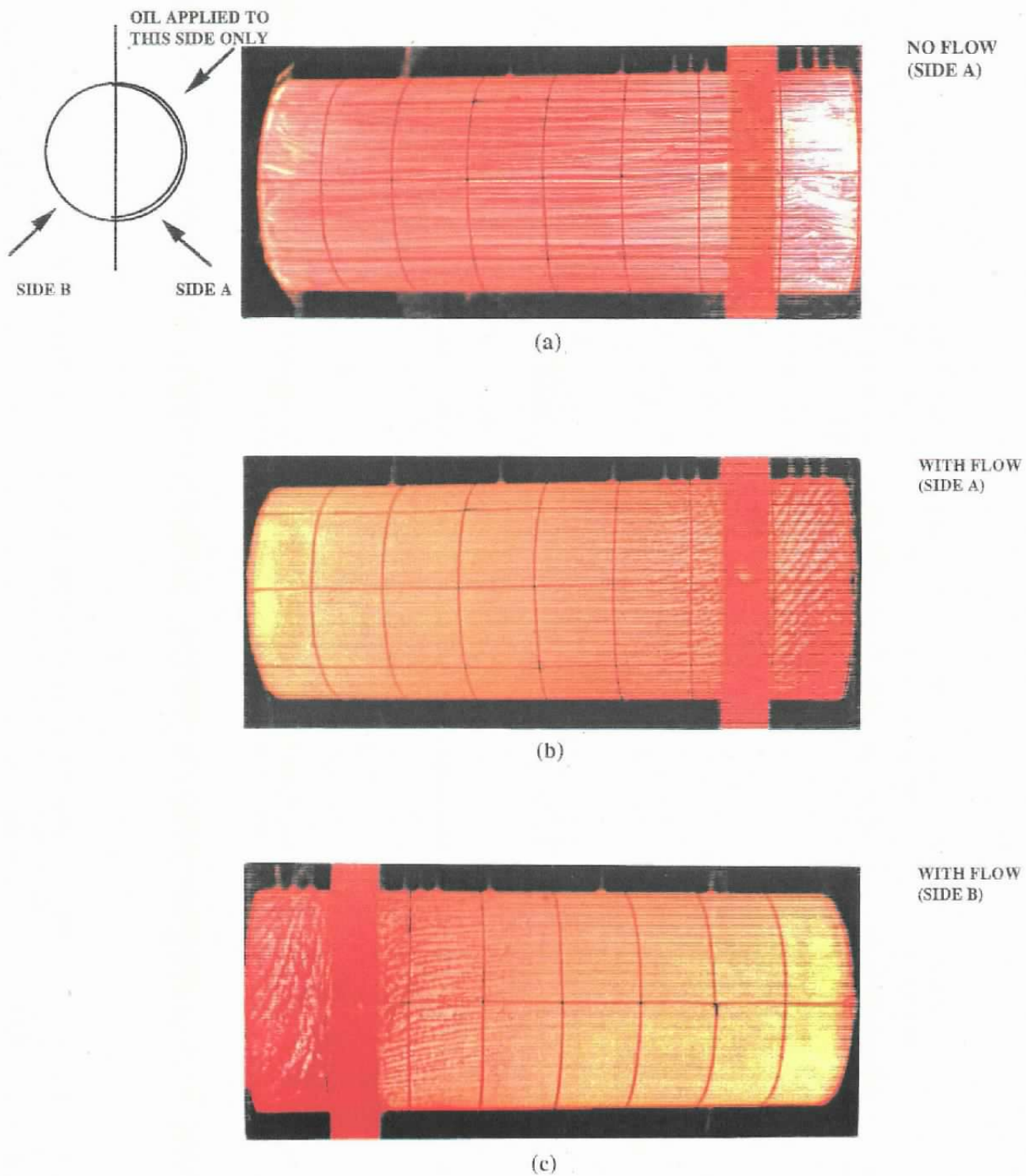


Figure 2.14 Ejector flow visualization. (  $\xi_1 = 3.182$ ,  $M_j = 1.4$ ,  $L/D = 3$  )

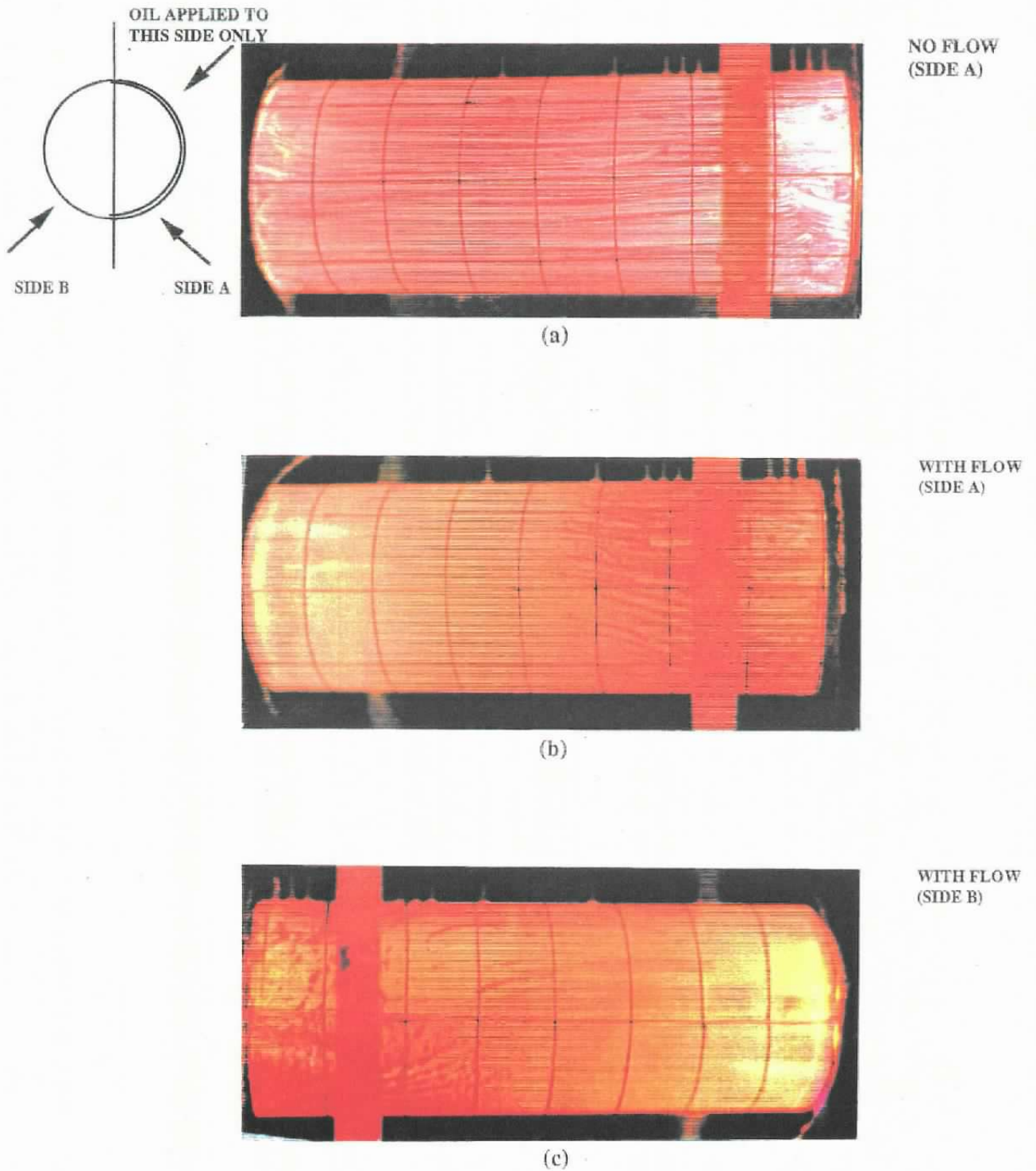
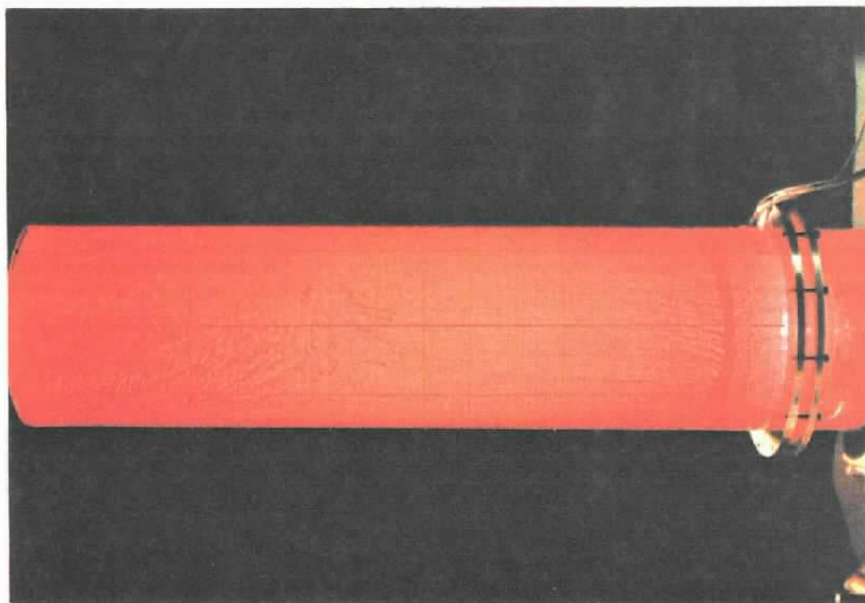


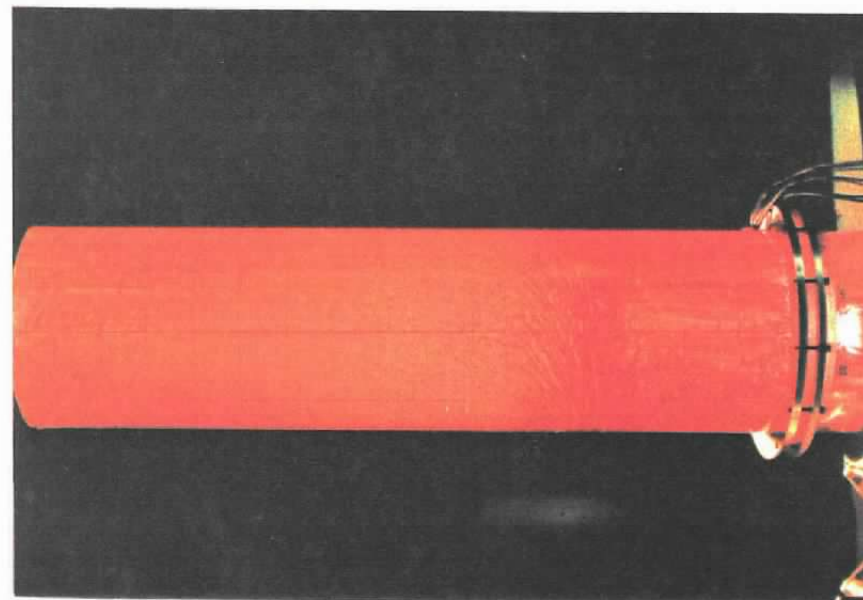
Figure 2.15 Ejector flow visualization. ( $\xi_1 = 1.52$ ,  $Mj \approx 0.8$ ,  $L/D = 3$ )

**$L/D = 1$**

**$L/D = 3$**



(a)

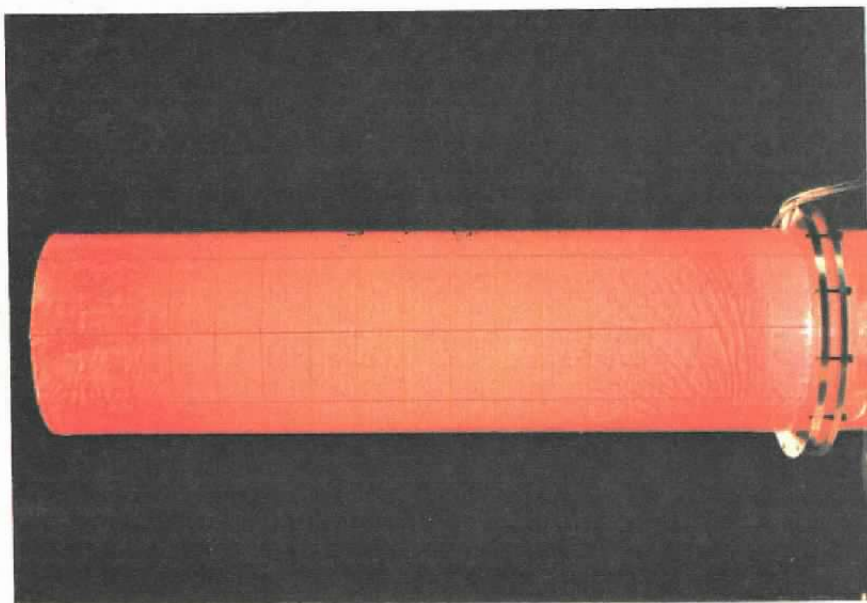


(b)

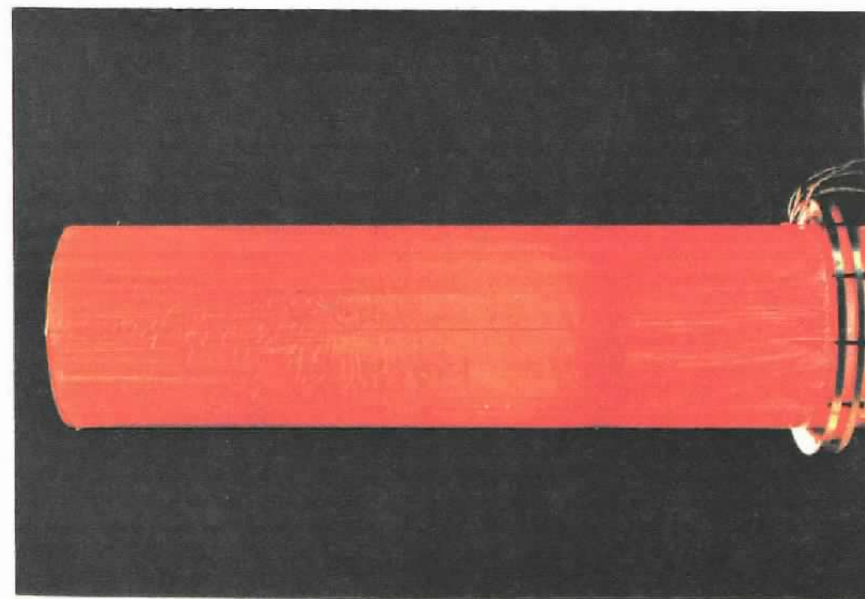
Figure 2.16 Test cell flow visualization. ( $\xi_1 = 4.936$ ,  $M_j \approx 1.7$ )

**$L/D = 1$**

**$L/D = 3$**



(a)

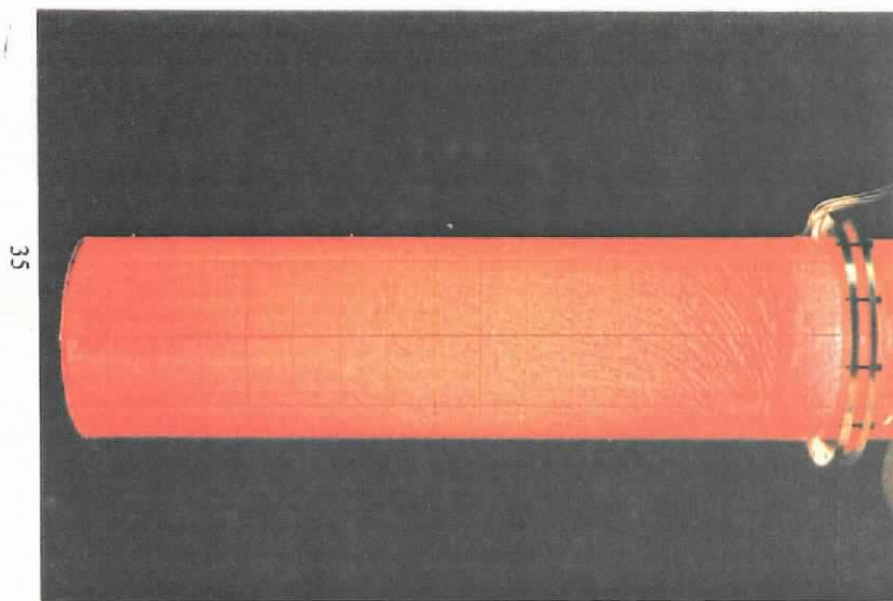


(b)

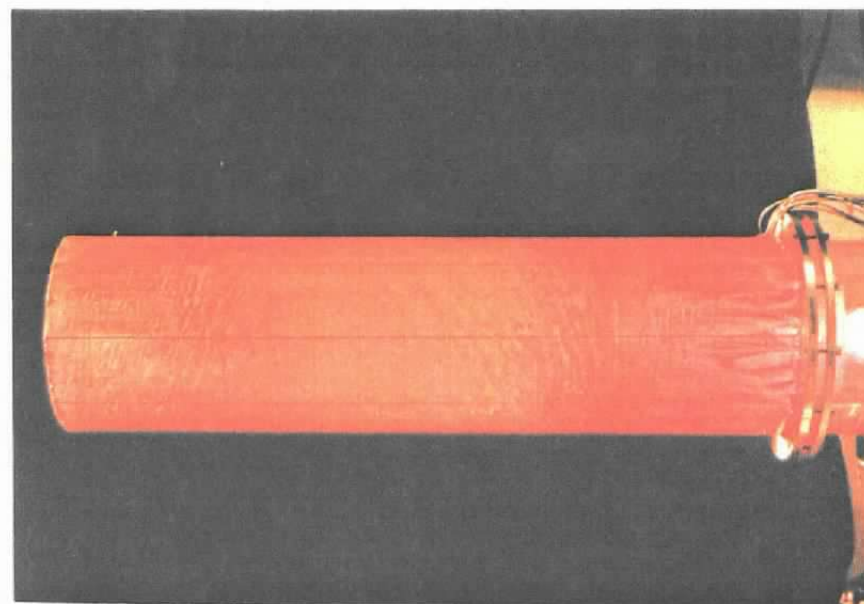
Figure 2.17 Test cell flow visualization. ( $\xi_1 = 3.182$ ,  $M_j \approx 1.4$ )

**$L/D = 1$**

**$L/D = 3$**



(a)

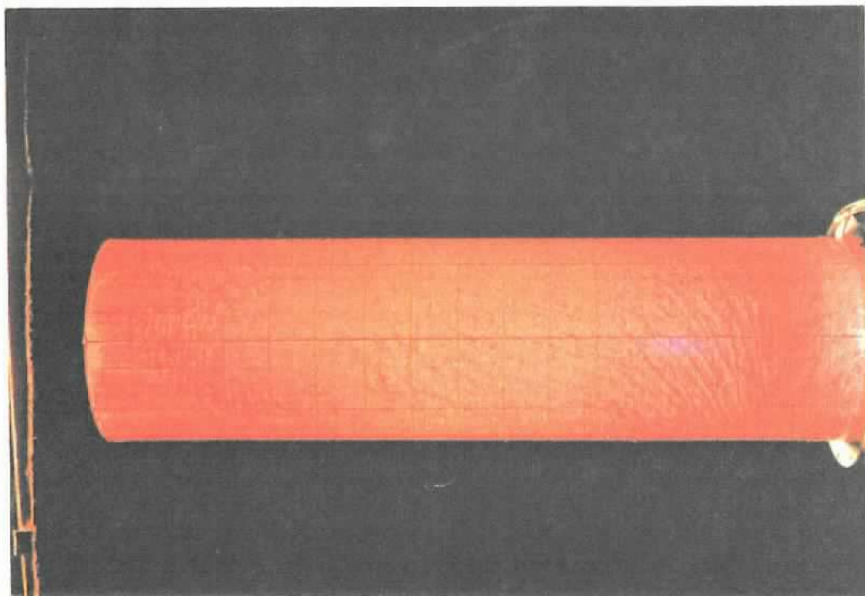


(b)

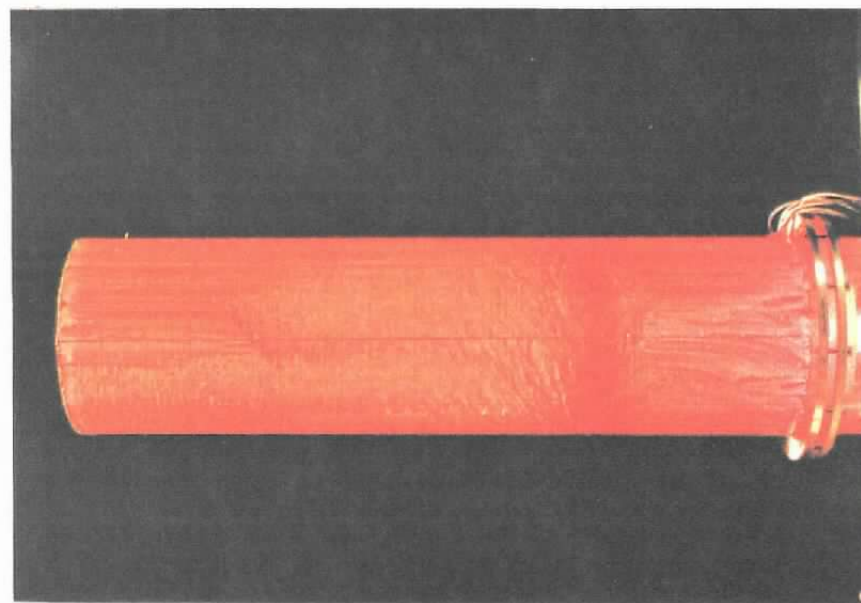
Figure 2.18 Test cell flow visualization. ( $\xi_1 = 2.771$ ,  $M_j \approx 1.3$ )

$L/D = 1$

$L/D = 3$



(a)

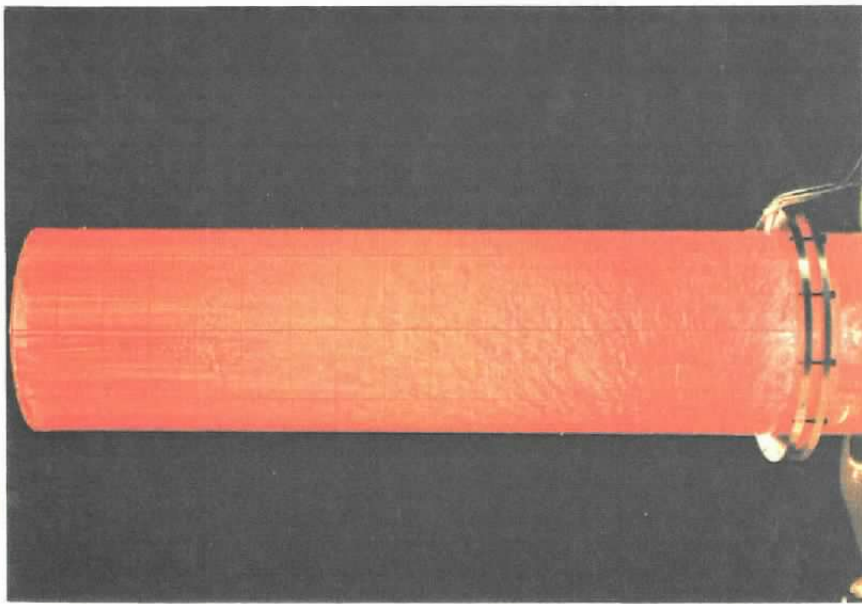


(b)

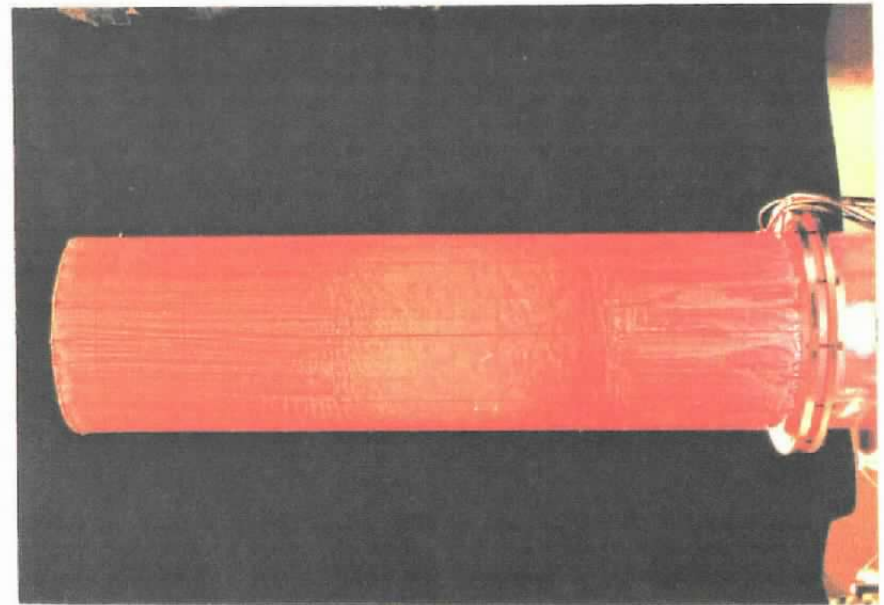
Figure 2.19 Test cell flow visualization. ( $\xi_1 = 2.135$ ,  $M_j \approx 1.1$ )

$L/D = 1$

$L/D = 3$



(a)



(b)

Figure 2.20 Test cell flow visualization. ( $\xi_1 = 1.52$ ,  $M_j \approx 0.8$ )

The flow patterns are arguably a function of jet Mach number and the diffuser length. These results are expected to provide considerable help in planning the direction of any future quantitative measurements to understand the flow phenomenon associated with ducted jets and the nature of resulting flow/acoustic interactions.

#### 2.4.3 Phase-Locked Laser Schlieren Flow Visualization

The now-popular technique of phase locked flow visualization (refs. 2.1-2.3) was used to visualize the evolution of instability waves in the jet. A Helium-Argon laser was used as the source of light. A microphone located in the plane of the exit of the free jet was used to trigger the laser strobe in the manner described by Ahuja et al (refs. 2.1 - 2.3) to freeze the motion of the self-excited instability waves in the underexpanded supersonic jets. In the present study, such photographs could be obtained only for the free-jet. The double layered round surfaces of the ejector and the outer test cell proved to be a hindrance in visualizing the flow within the diffuser using this technique.

Figures 2.21 through 2.28 show the phase-locked schlieren flow visualizations of the free jet at fully-expanded Mach numbers of 1.1, 1.2, 1.27, 1.3, 1.34, 1.4, 1.5, and 1.6. On each photograph are provided the relevant jet operating data.  $P_T$  refers to the reservoir gauge pressure,  $M$  refers to the calculated fully-expanded Mach number,  $f_s$  refers to the strobe frequency,  $L_s$  refers to the sound pressure level (SPL) at the strobe frequency, and  $R$  and  $\Theta$  refer to the distance and polar angle of the microphone from the center of the free jet nozzle. Note that, in most cases, the strobe frequency is the same as the dominant screech frequency.

It is seen from these schlieren photographs that, at the lower Mach numbers, the instability waves start out to be axisymmetric, and thus they correspond to  $n = 0$  or axisymmetric mode (see Figure 2.22 and 2.23). At the smallest Mach number, the screech amplitude was rather weak. This is why it was difficult to capture a well-defined wave at  $M = 1.1$  (see Figure 2.21). Likewise, at  $M = 1.3$ , the modes of instability waves appeared to switch back and forth from  $n = 0$  (axisymmetric) to  $n = 1$  (helical or flapping mode). It was, therefore, difficult to lock on to a dominant tone and visualize a well-defined structure in the flow (see Figure 2.24). At the higher Mach numbers, however, the nonaxisymmetric mode ( $n=1$ ) appears to dominate as seen in Figures 2.25 through 2.28.

As seen later in Section 3, these data provided considerable guidance in developing and validating the theoretical calculations.

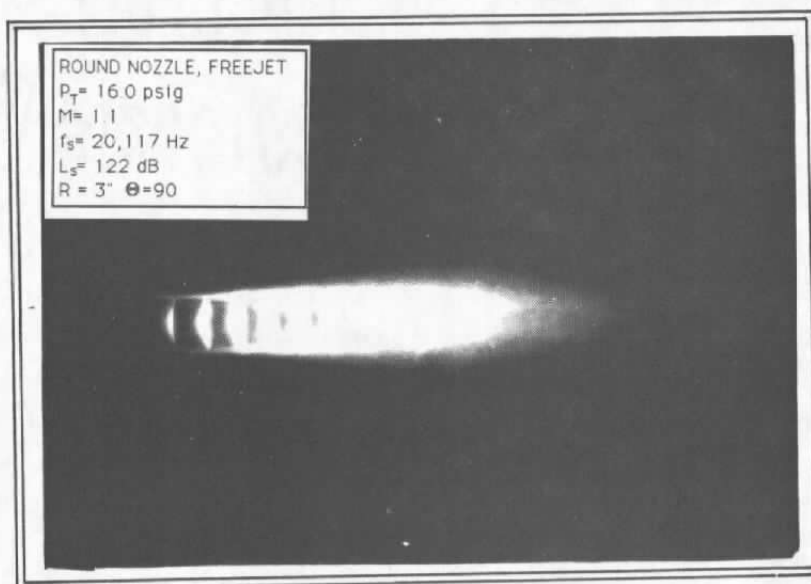


Figure 2.21 Laser schlieren flow visualization.

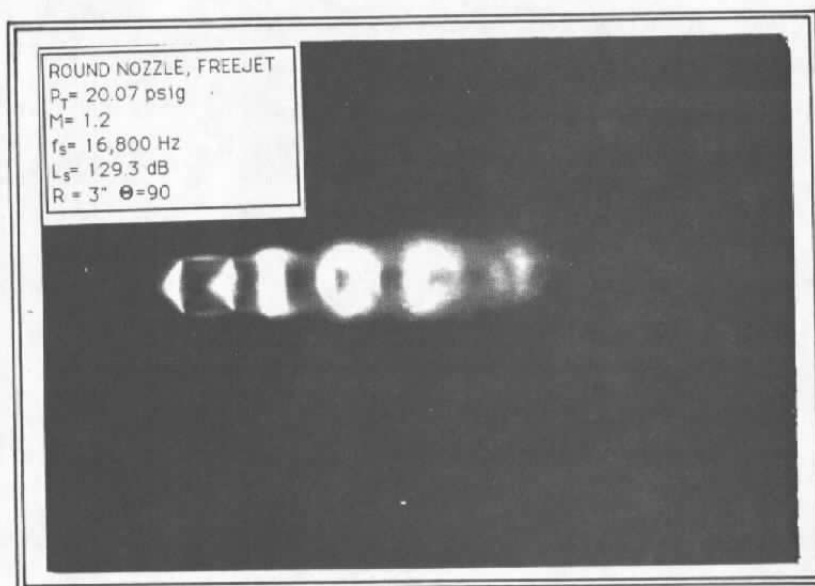


Figure 2.22 Laser schlieren flow visualization.



Figure 2.23 Laser schlieren flow visualization.

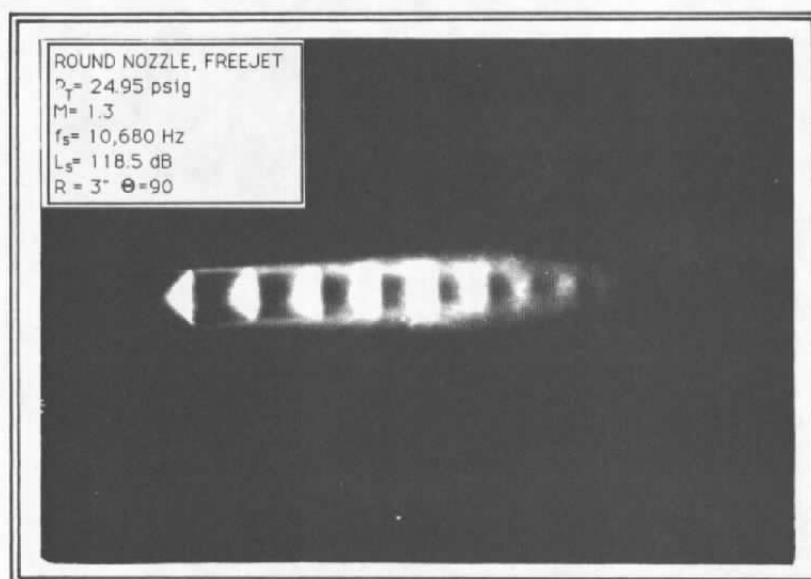


Figure 2.24 Laser schlieren flow visualization.

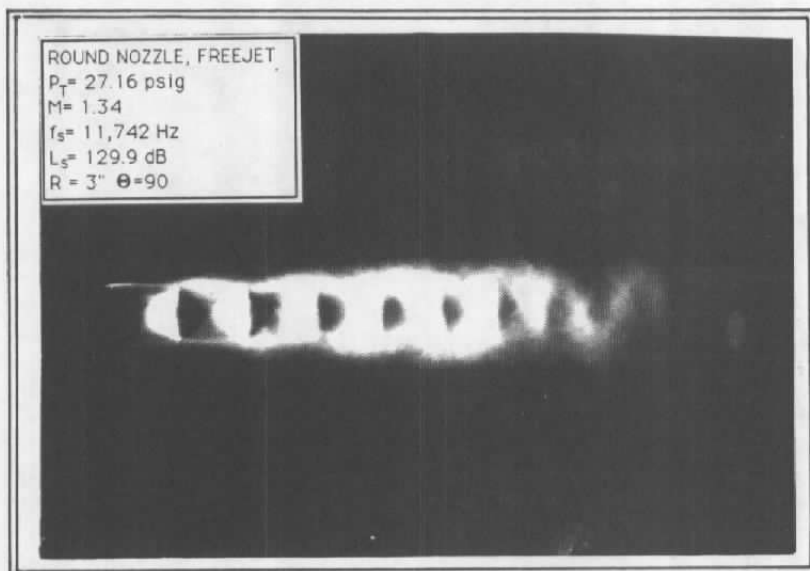


Figure 2.25 Laser schlieren flow visualization.



Figure 2.26 Laser schlieren flow visualization.

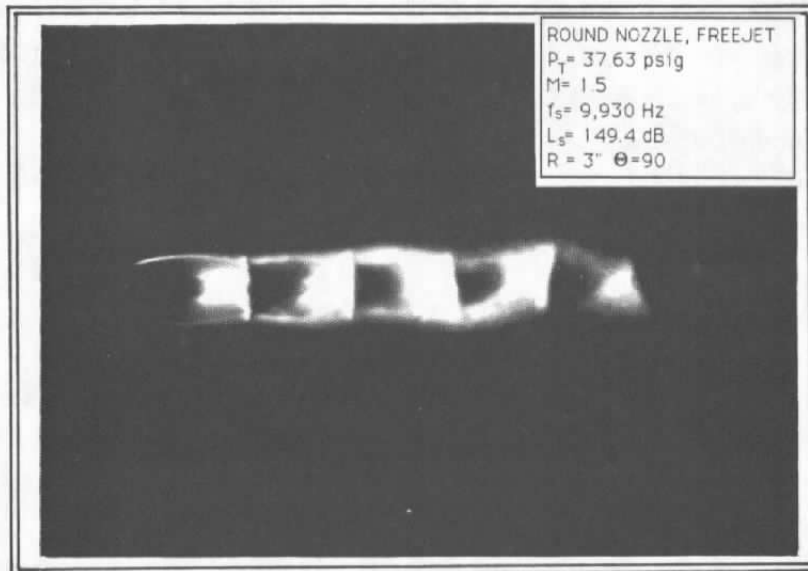


Figure 2.27 Laser schlieren flow visualization.

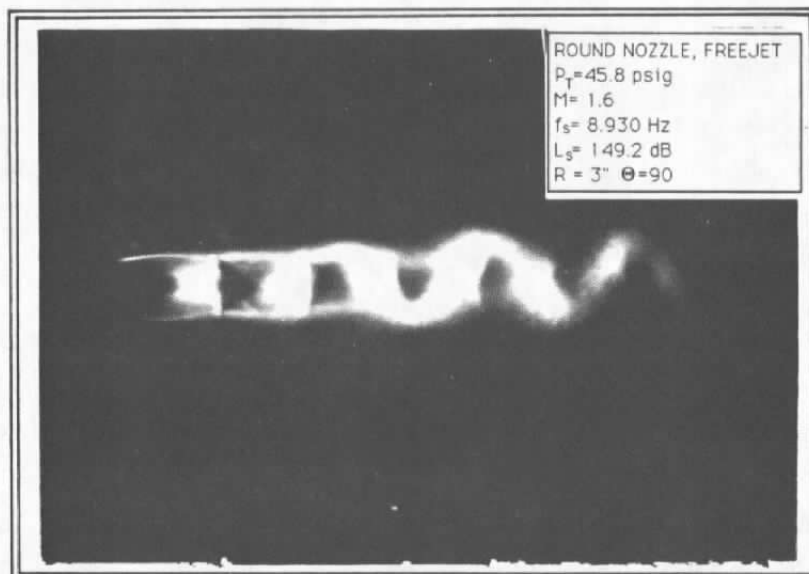


Figure 2.28 Laser schlieren flow visualization.

## 2.5 Initial Acoustic Diagnostics for the Ducted Jet

In the full-scale tests at AEDC, the high intensity tones were measured with the secondary mass flow rate maintained at 10 percent of that of the main jet. To establish how critical the presence of the secondary mass-flow was to the character of the measured noise spectra, acoustic data for the plume operated at fixed jet exit Mach numbers were acquired for a range of secondary mass flow rates. The secondary mass flow rates were as high as 100 percent of those of the primary mass flow rates. It was found that the presence of the secondary flow made little difference to the measured noise spectrum. This was found to be true for both the shorter and the longer ejector.

The data for the longer ejector with  $L_{ej}/D_{ej} = 3$  are presented below.

The acoustic data were acquired by a 1/4 inch Bruel and Kjaer (B&K), type 4136 microphone, in conjunction with B & K Cathode follower (type 2619). The microphone for the acoustic measurements with the diffuser and test cell configuration was located in the plane of the test cell exit at a distance of 12 nozzle exit diameters (12 inches) from the jet center line. All of the measurements presented here were acquired with the nozzle located at 0.15 inches from the ejector inlet ( $x_{ej}/D_{ej} = 0.3$ ).

Typical results are shown in Figures 2.29 and 2.30. Notice that all of the pertinent information appears on the top right corner of each plot. Here  $D_{ej}$  refers to the ejector inner diameter, and  $D_e$  refers to the nozzle exit diameter. In Figure 2.29, spectra for  $M_j = 1.3$  are compared for no secondary mass flow with  $\dot{m}_2 = 45\% \dot{m}_1$ . Likewise, in Figure 2.30, spectra for  $M_j = 1.6$  are compared for  $\dot{m}_2 = 80\% \dot{m}_1$ . Clearly, identical noise spectra are obtained with and without the secondary flow. Such insensitivity of the noise characteristics to the secondary air flow is also consistent with results from the full-scale facility.

In view of these findings, it was decided to disconnect the secondary flow supply. The inlet to the secondary manifold was then blanked off, and all of the remaining data presented in this report are those with no secondary mass flow ( $Q = 0$ ).

## 2.6 Free Jet Versus Ducted Jet - Acoustic Data

The acoustic spectra on an exterior microphone were compared for the free jet with those for the ducted jet. Typical results for a range of plume Mach numbers are shown in Figures 2.31. As before, all pertinent information appears on the top right corner of each plot. For these comparison plots, the microphone position with respect the main nozzle exit remained unchanged; the ejector and the test cell were simply added to the free-jet configuration. Any changes observed

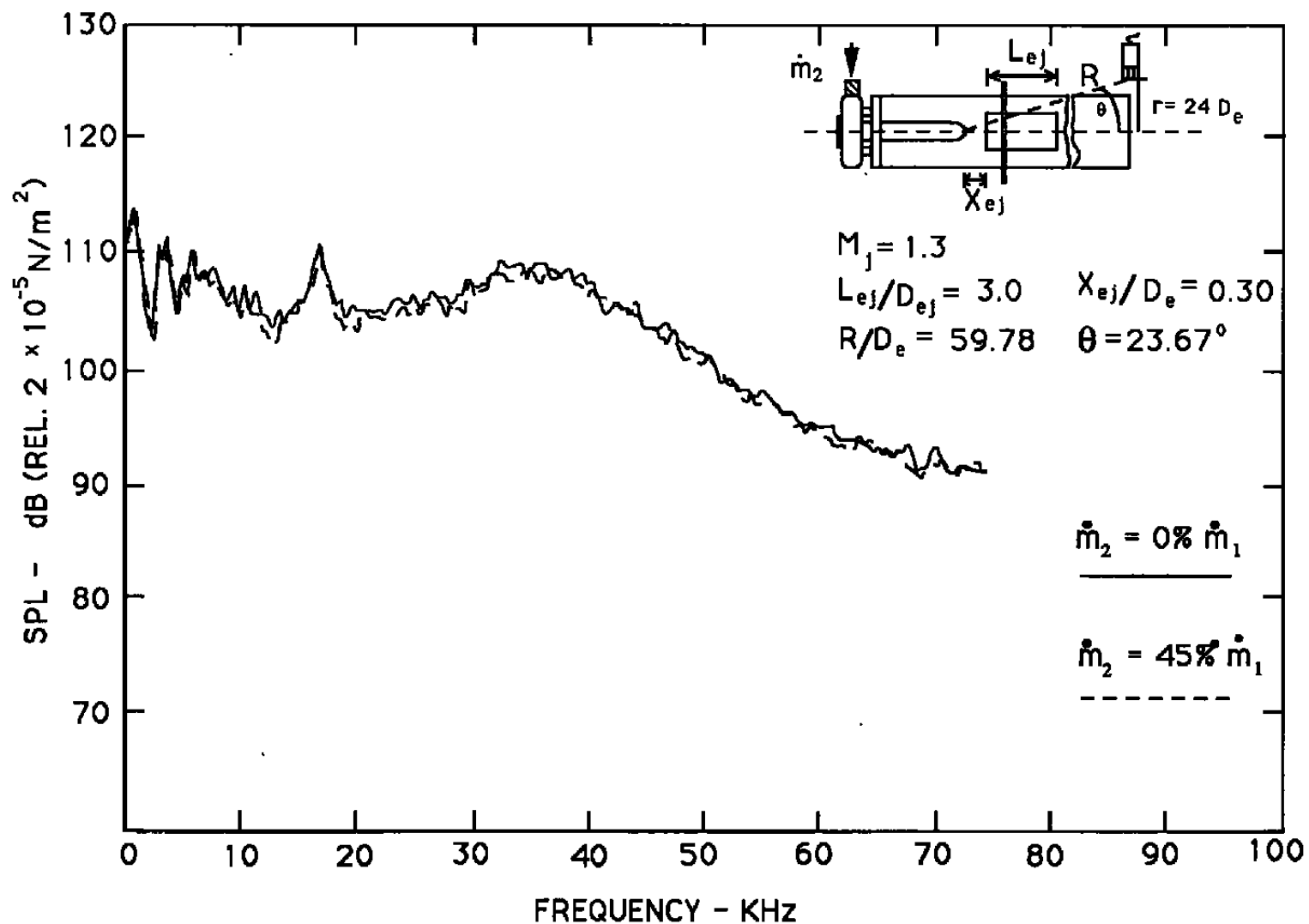


Figure 2.29 Effect of secondary mass flow on the exterior microphone noise spectra.

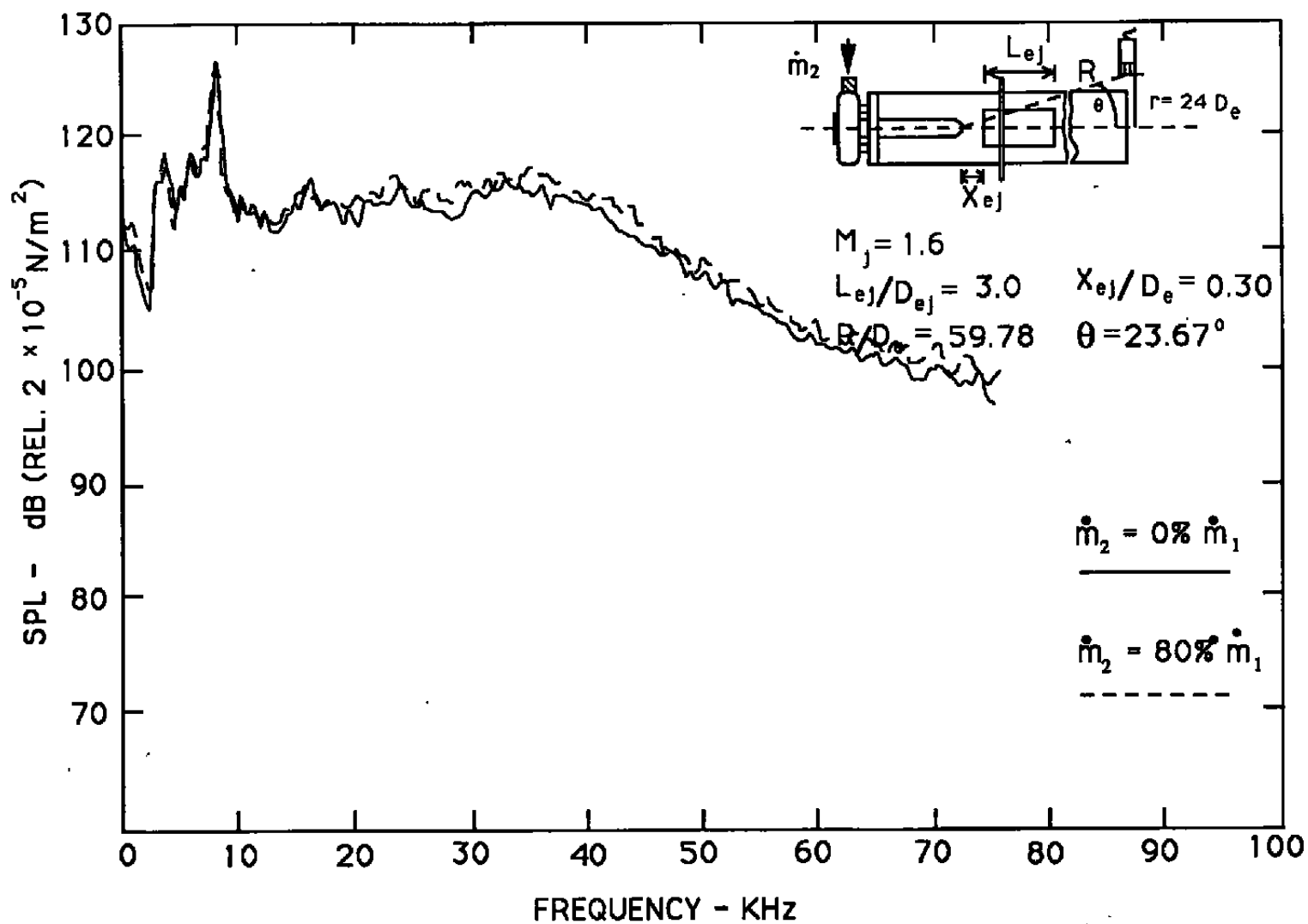


Figure 2.30 Effect of secondary mass flow on the exterior microphone noise spectra.

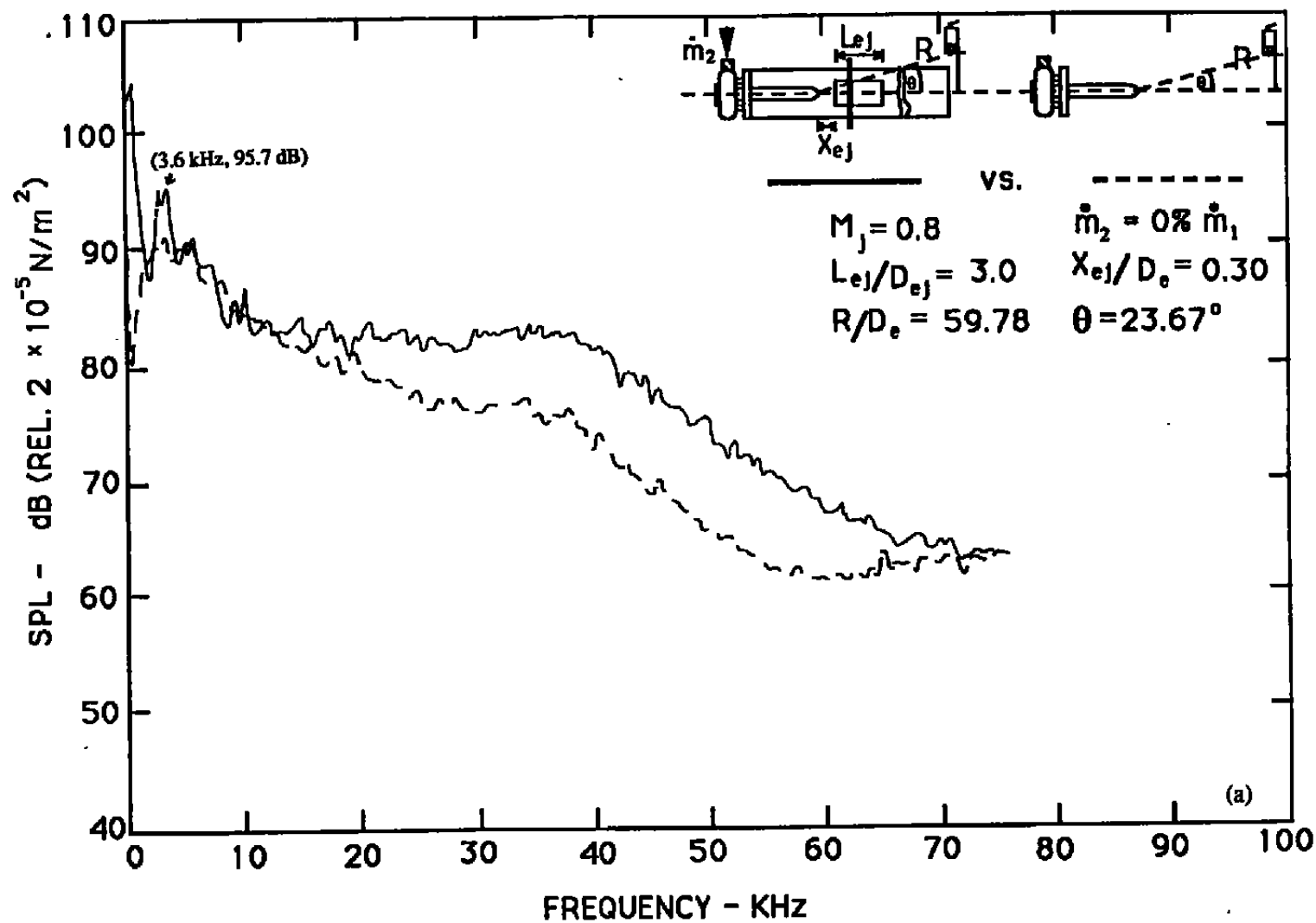


Figure 2.31 Effect of adding the ducted configuration on the acoustic spectra measured by an exterior microphone.  $M_j =$  : (a) 0.8, (b) 1.2, (c) 1.4, and (d) 1.6.

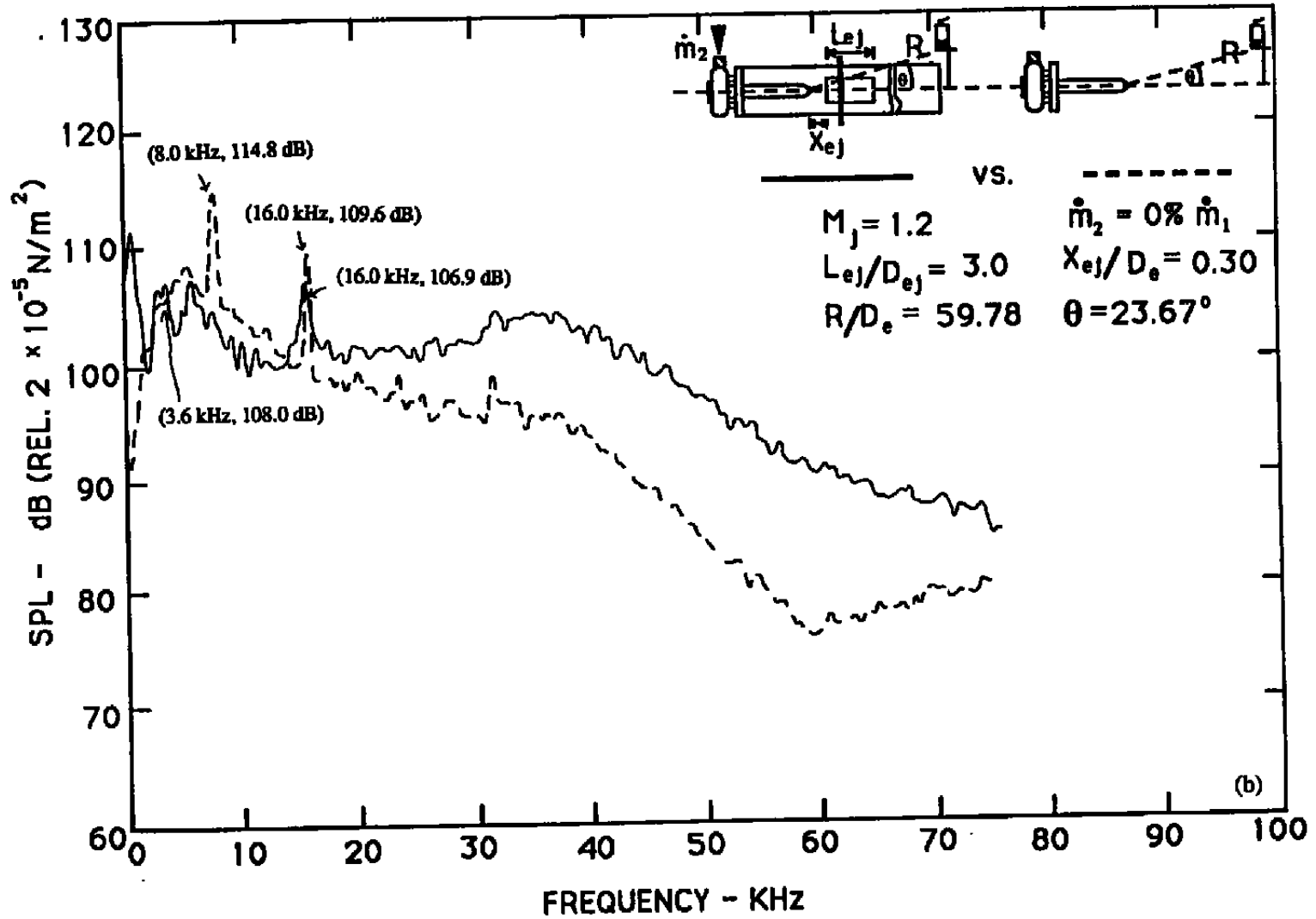


Figure 2.31 (continued from previous page)

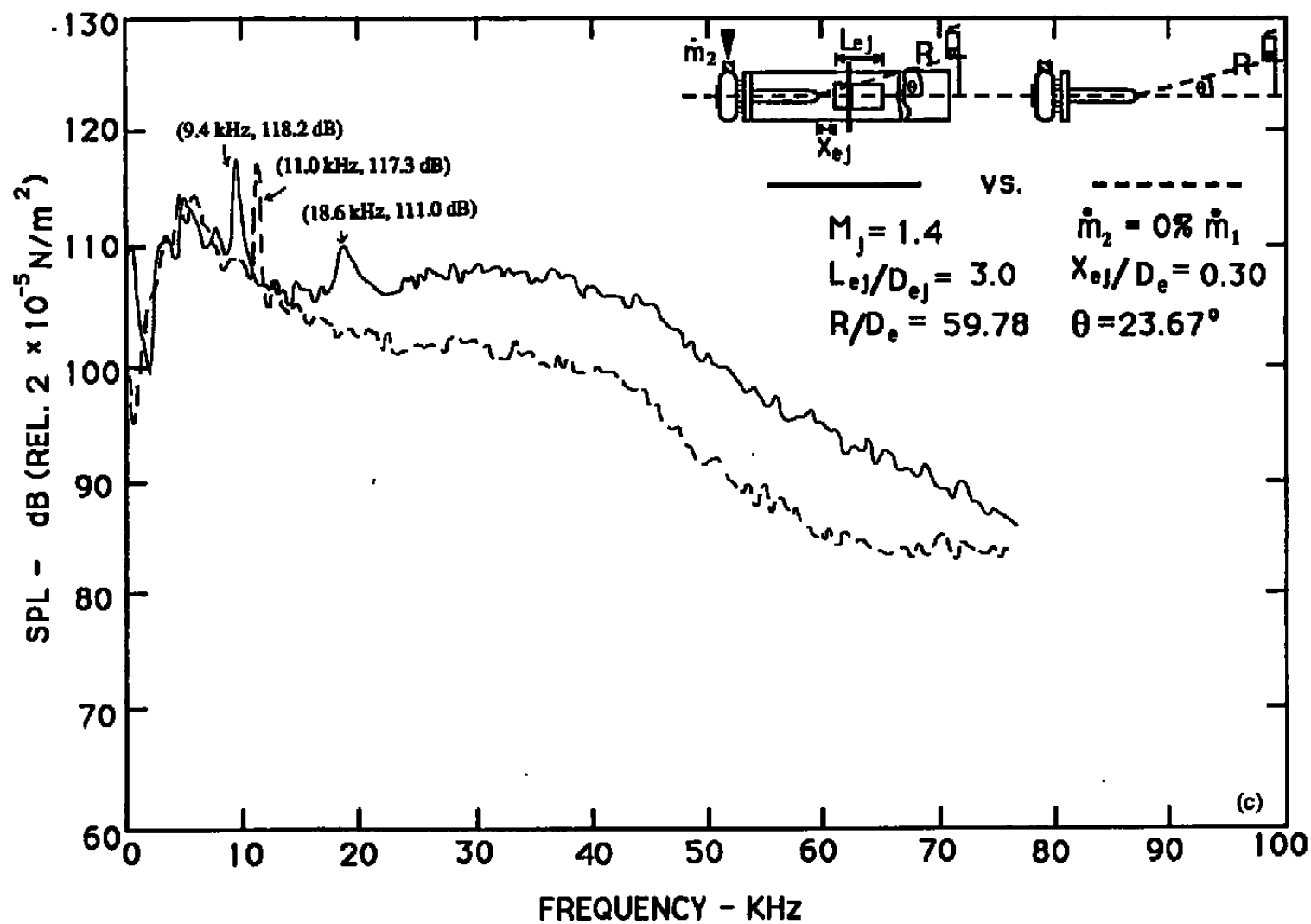


Figure 2.31 (continued from previous page)

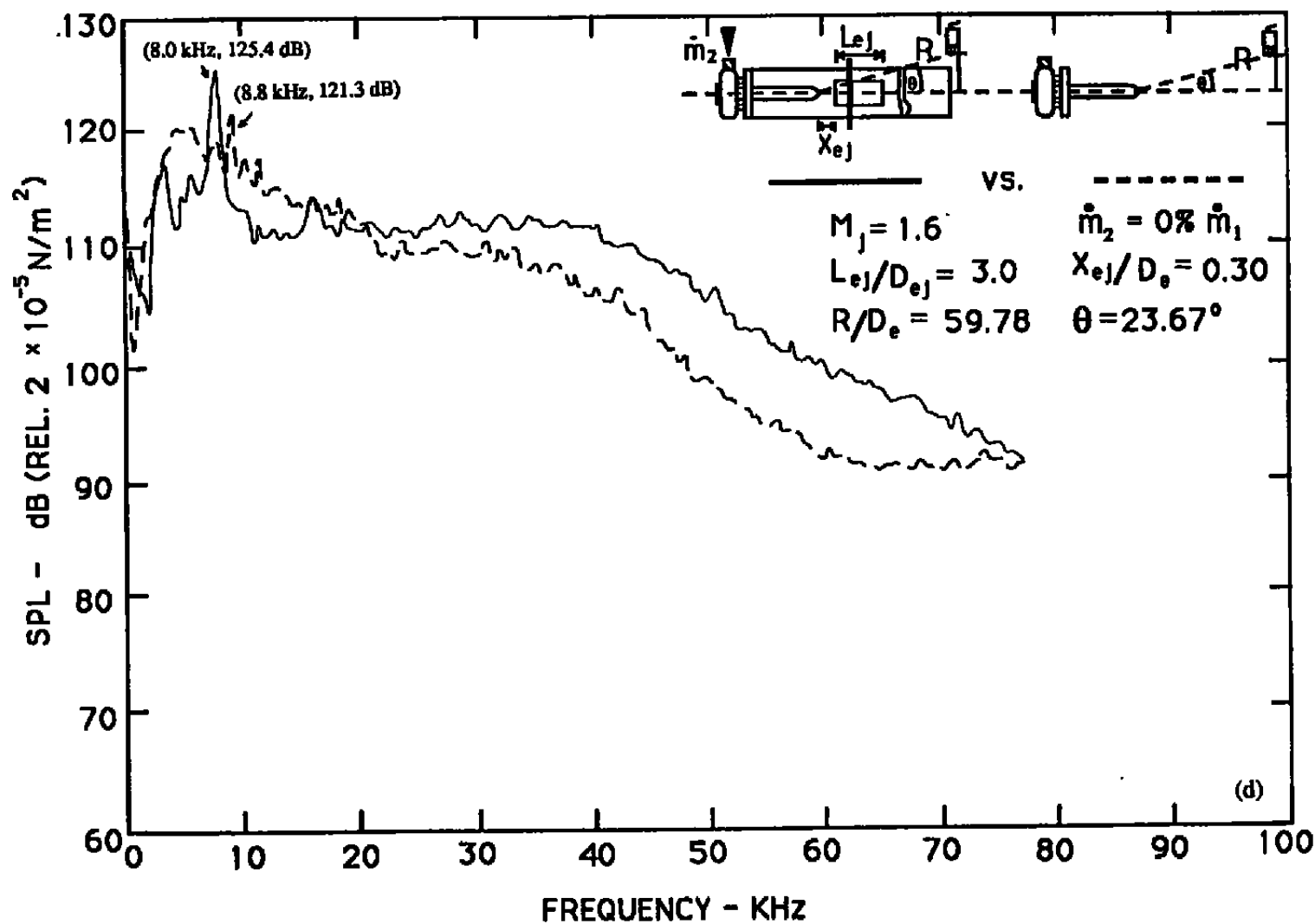


Figure 2.31 (continued from previous page)

in the noise spectra are thus those due to the addition of the ducting. Our goal is to identify if these changes are due to enhanced flow/sound interaction, by pure duct resonance, or by a combination of the two, or by some other mechanism.

The following observations are made from these results:

1. Effect of adding the ejector and the test cell is to produce a low frequency tone (at 3.6 kHz in Figure 2.31a) and also to increase the broadband noise considerably at all Mach numbers. In fact the increase in broadband noise is as much as 8 decibels at  $M = 1.4$ .
2. Since the broad band noise has increased by a rather large amount, the so called "broadband amplification" may well be the cause of this. If so, this must be produced by very high sound pressure levels and attendant excitation of instability waves within the ejector.

The far-field acoustic data presented above did not display particularly unusual discrete tones in the measured spectra. The broadband noise was, however, found to increase considerably at all frequencies. It was speculated that it is possible that there may exist discrete tones that may not be propagating to the far field. It was, therefore, decided to make measurements by a 1/4-inch condenser microphone mounted flush with the wall of the test cell. An existing hole in the test cell section located about 111 degrees with respect to the downstream jet axis was utilized to mount the microphone. The microphone was thus located just upstream of the nozzle exit plane. For comparison, identical data were acquired with the microphone located exactly at the same location with respect to the nozzle exit but with the free jet alone. This was done both for the shorter and the longer ejector. The data were acquired for a total of nine fully-expanded jet Mach numbers of the free jet, namely, 0.8, 1.0, 1.1, 1.2, 1.3, 1.4, 1.5, 1.6, and 1.7. It should be noted that, with the ejector and the test cell in place, the quoted Mach numbers were calculated assuming the back pressure to be the same as that of the ambient even though there was some reduction in the back pressure. Data for constant operating pressure ratio, with the true back pressure accounted for, are discussed in Appendix I. As seen below, this fact does not seem to change the conclusions from our measurements about the observed phenomenon. The main effect on the spectral character is one of shifting the screech frequencies to a somewhat lower values for the ducted jet. This is because the true Mach numbers are somewhat larger than those quoted in the figures below due to the back pressure being somewhat lower than the ambient pressure.

The narrow band noise spectra for the smaller ejector for the above mentioned nine Mach numbers are shown in Figures 2.32 through 2.40. Likewise, similar data for the longer ejector are

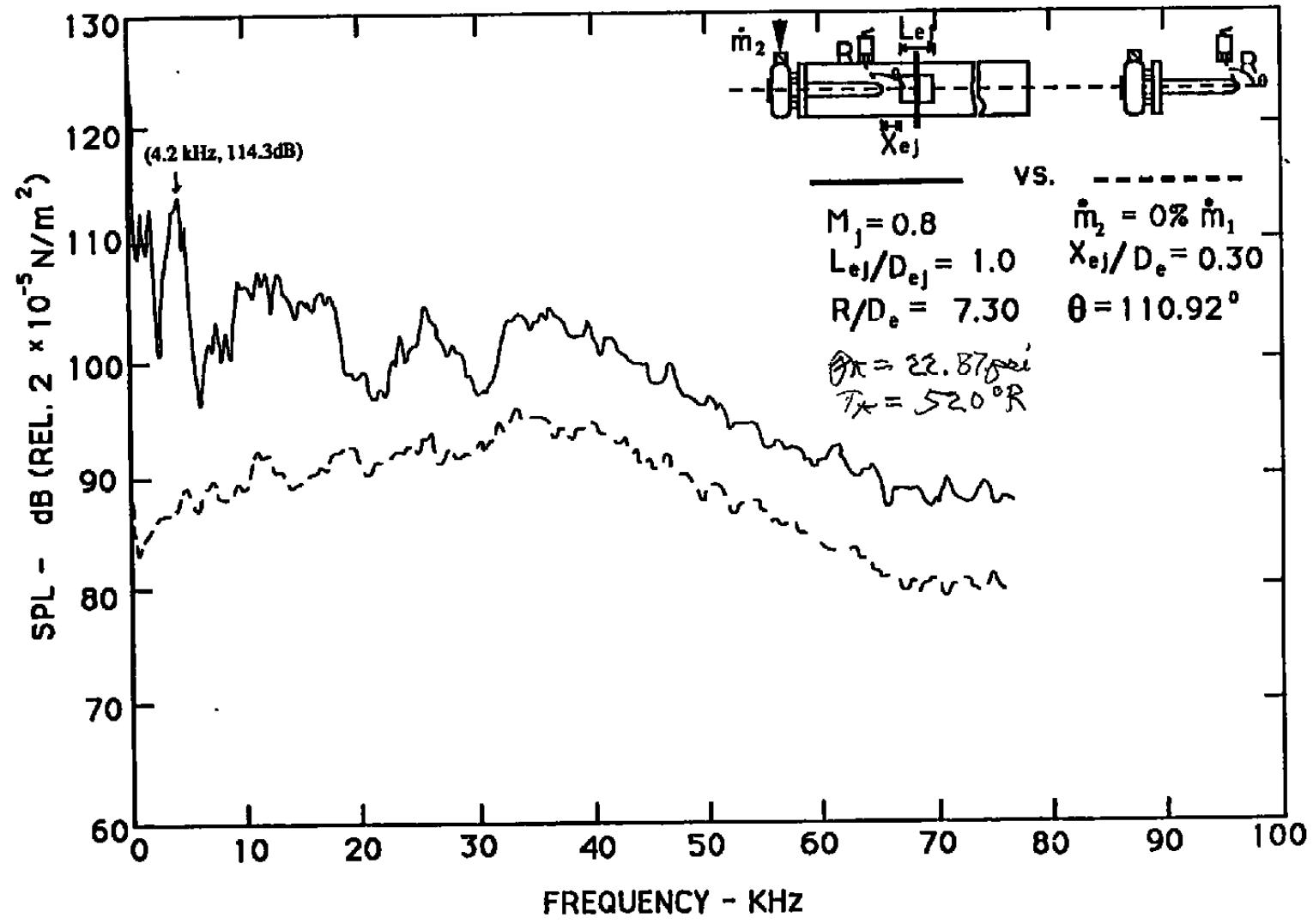


Figure 2.32 Effect of adding the ducted configuration on the acoustic spectra measured by an interior microphone.

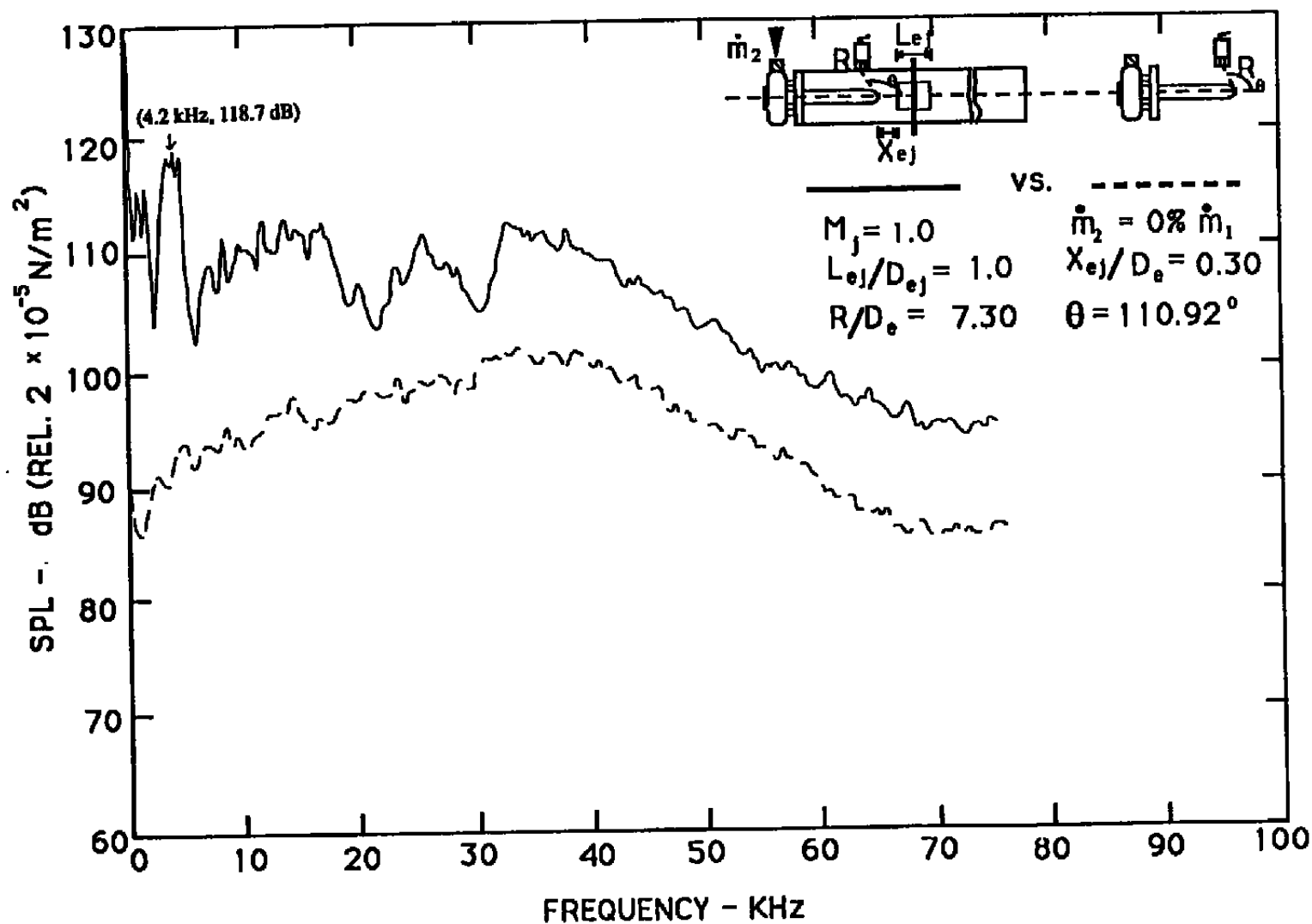


Figure 2.33 Effect of adding the ducted configuration on the acoustic spectra measured by an interior microphone.

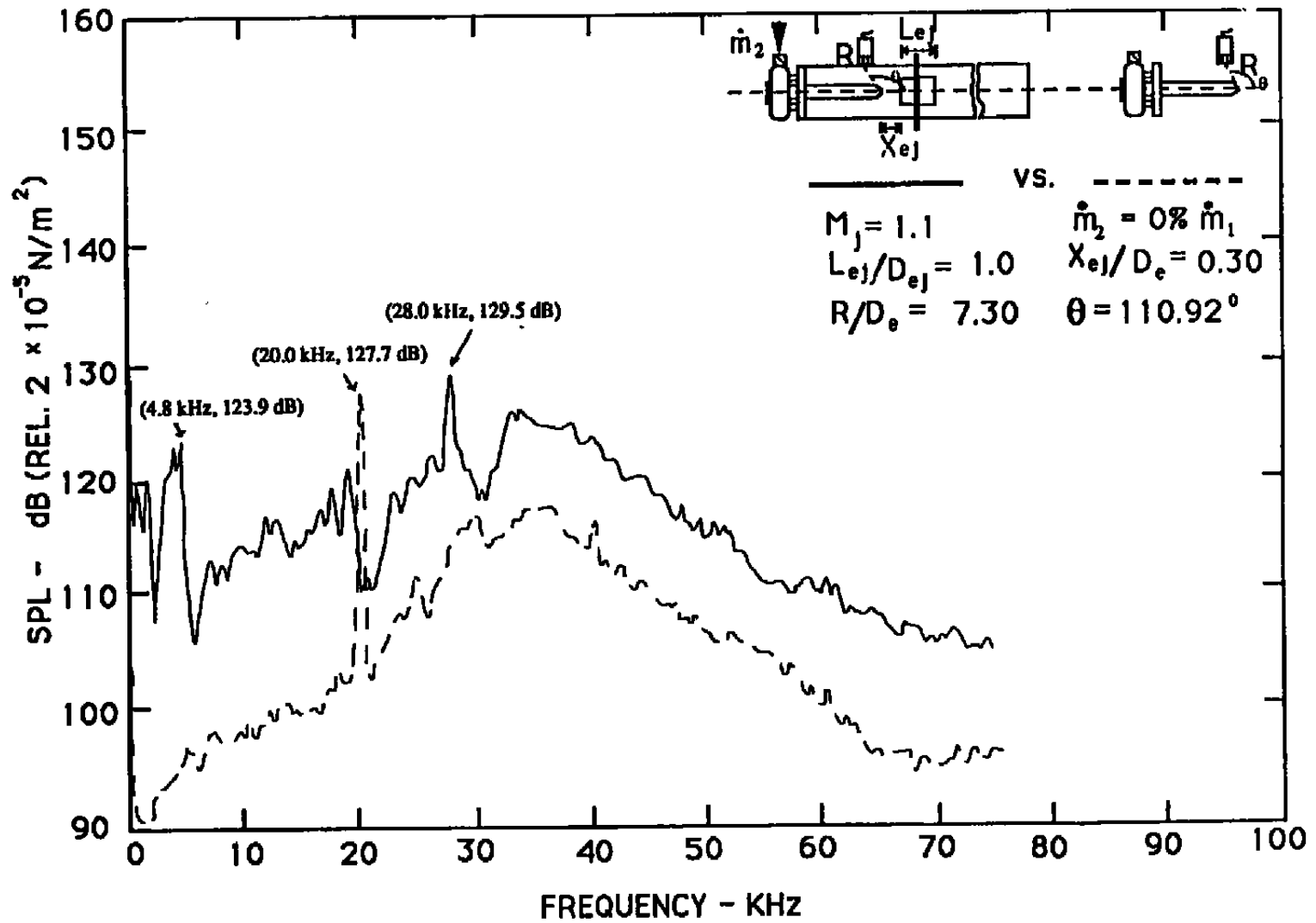


Figure 2.34 Effect of adding the ducted configuration on the acoustic spectra measured by an interior microphone.

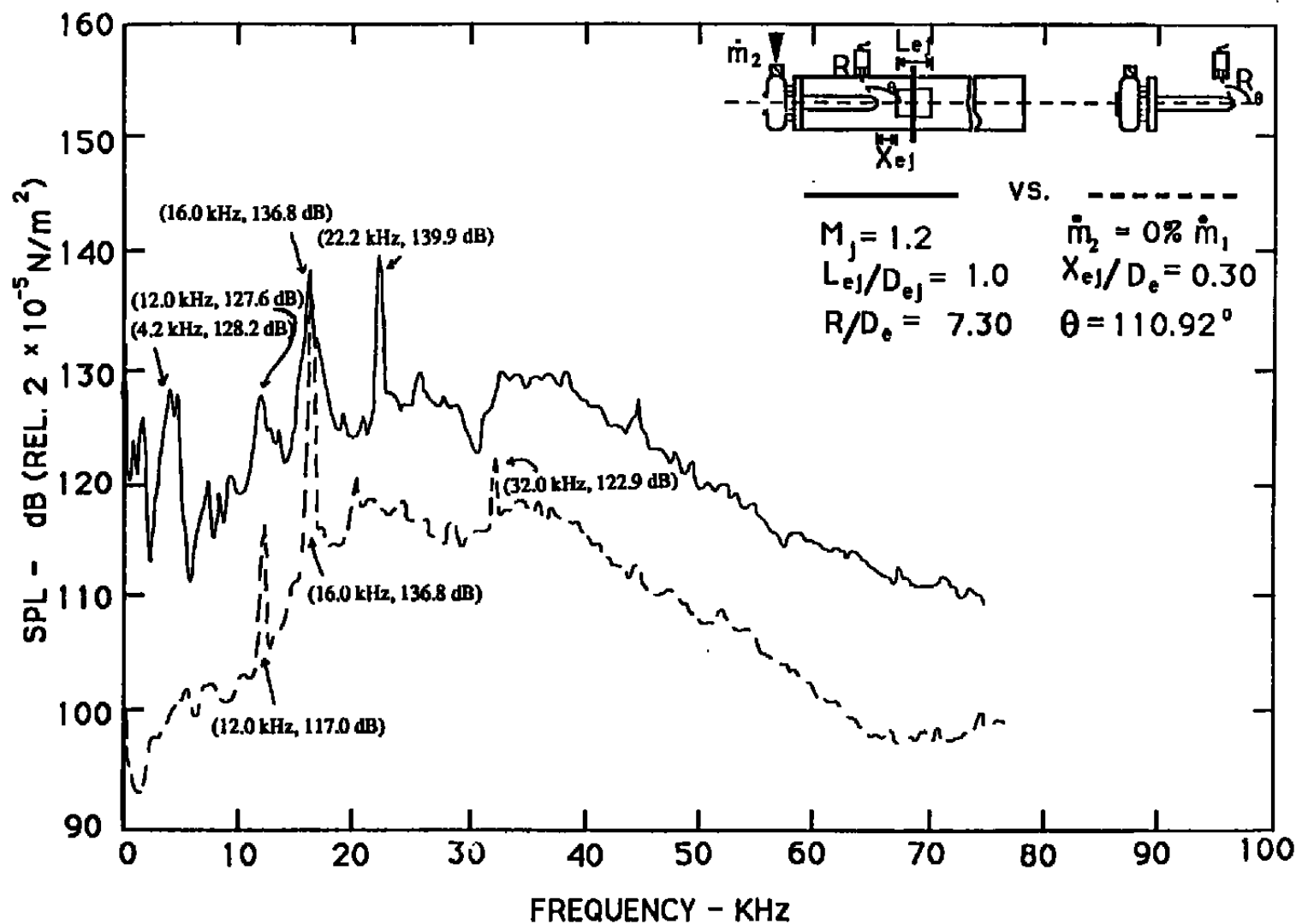


Figure 2.35 Effect of adding the ducted configuration on the acoustic spectra measured by an interior microphone.

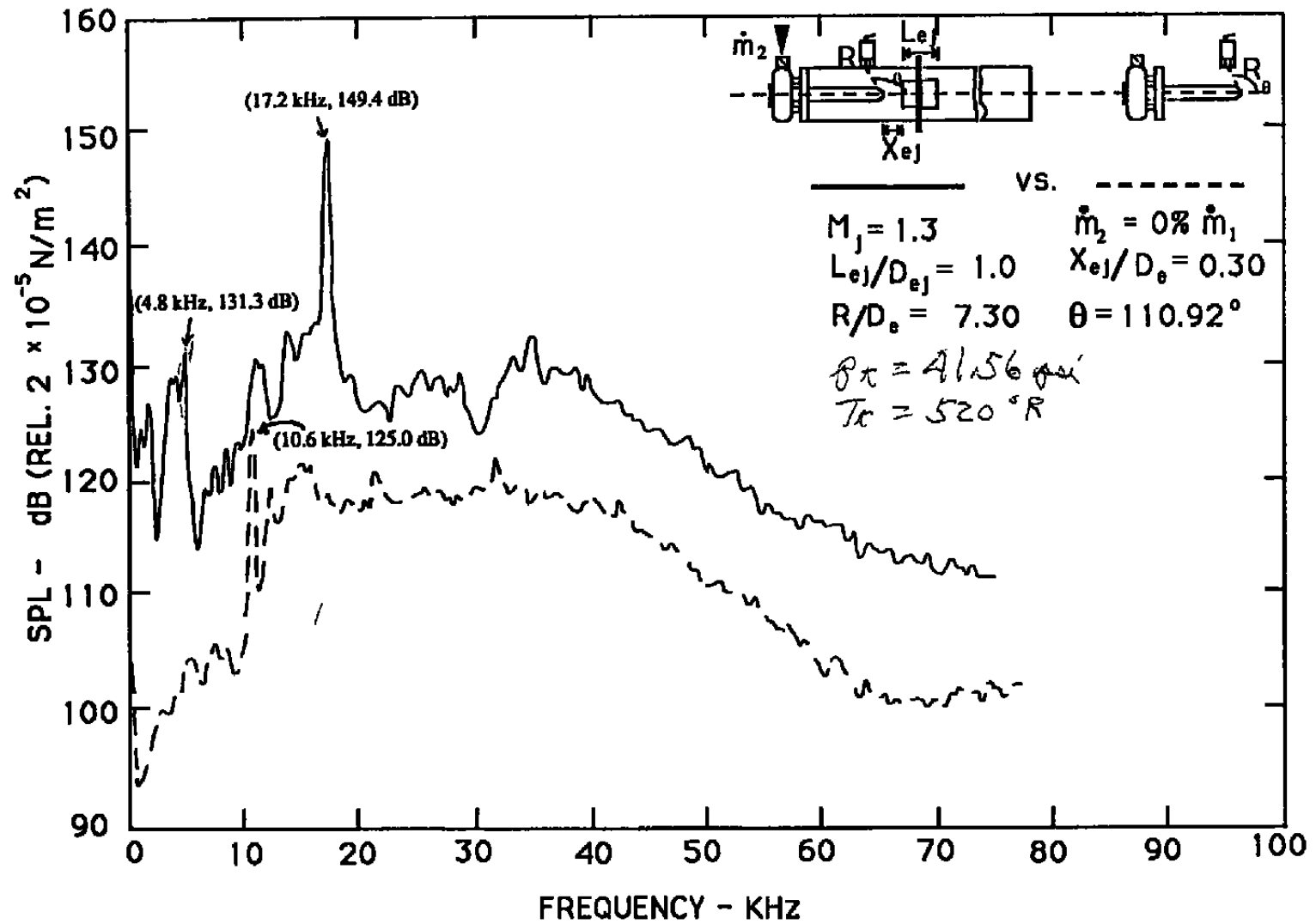


Figure 2.36 Effect of adding the ducted configuration on the acoustic spectra measured by an interior microphone.

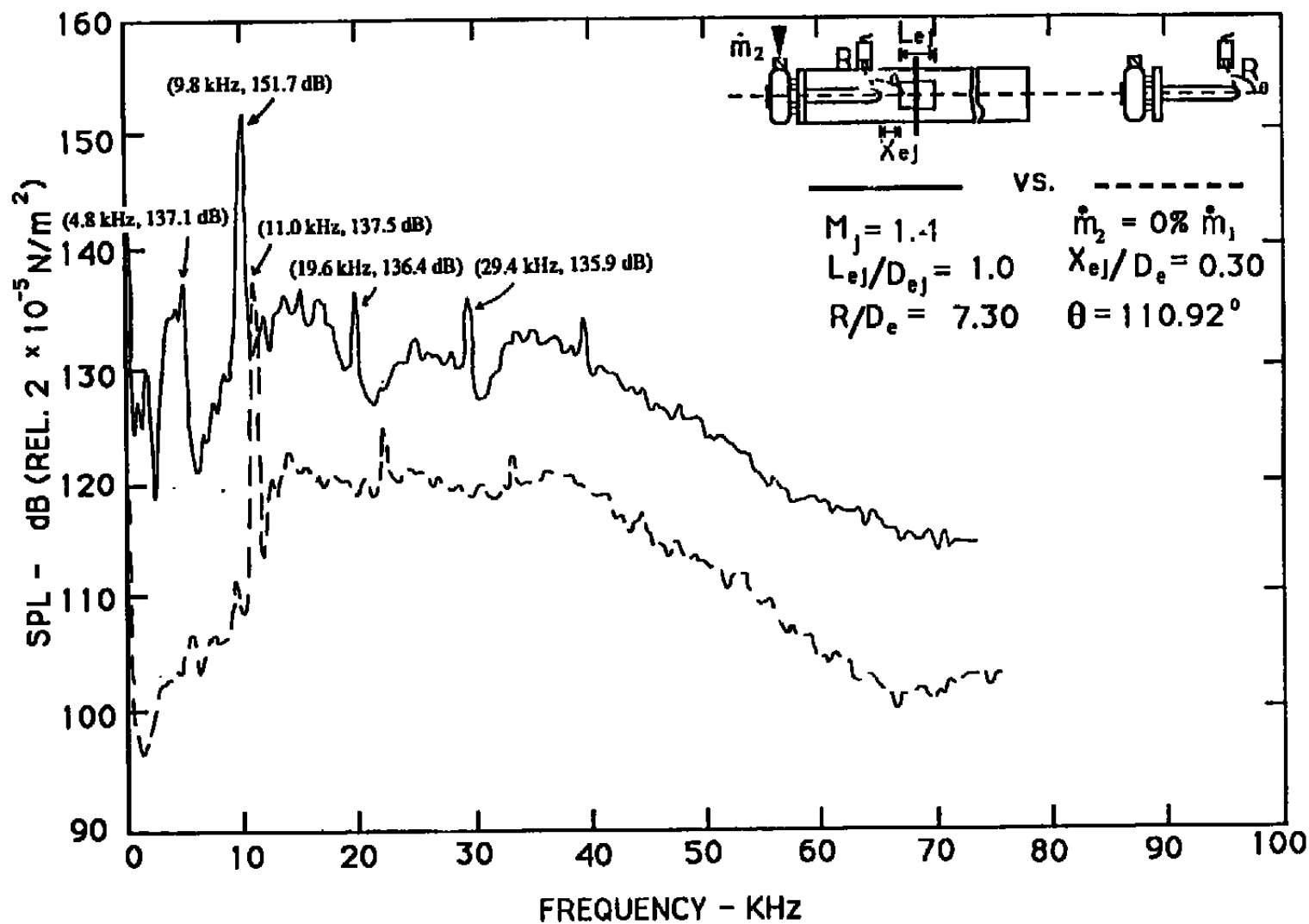


Figure 2.37 Effect of adding the ducted configuration on the acoustic spectra measured by an interior microphone.

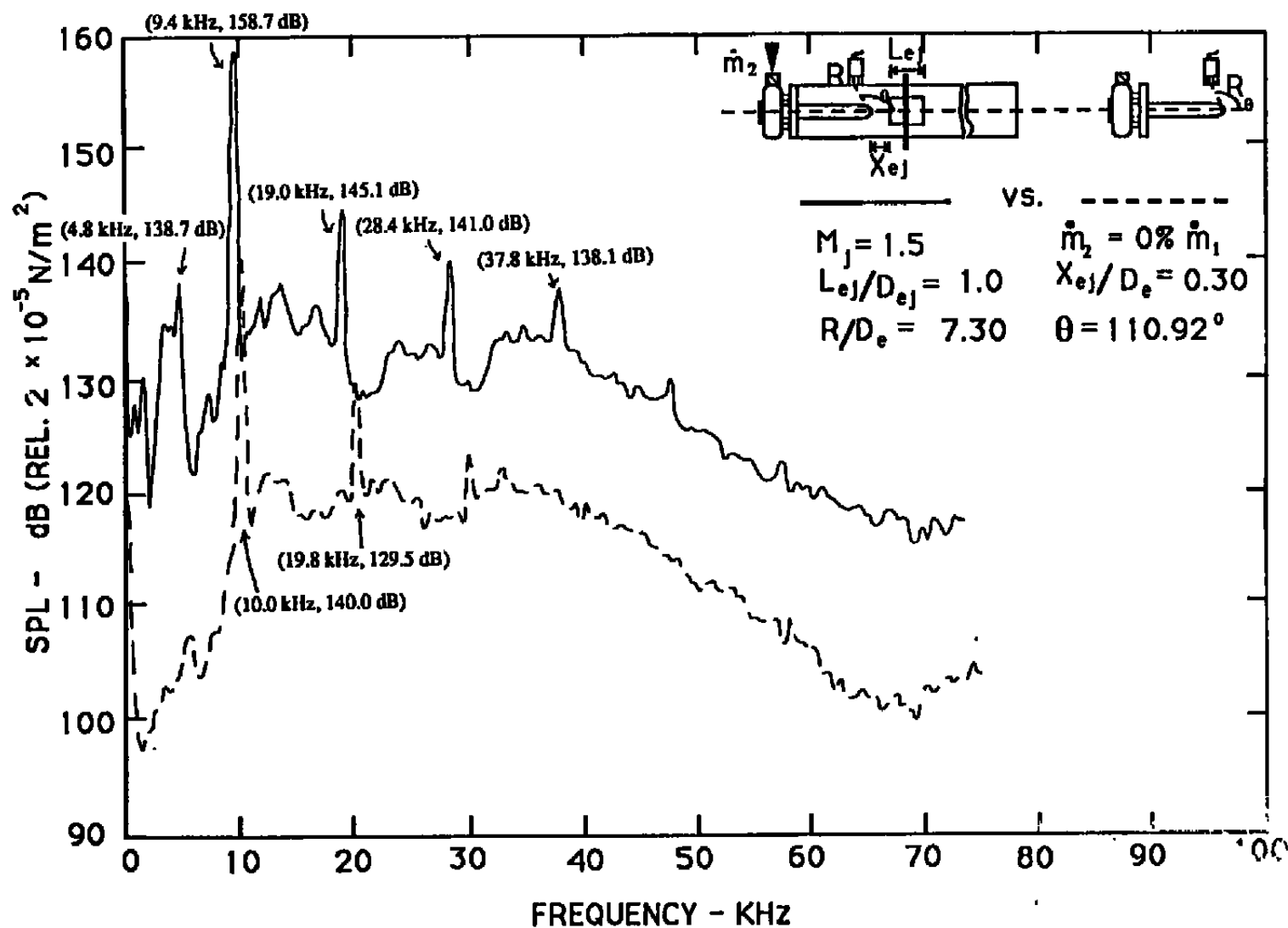


Figure 2.38 Effect of adding the ducted configuration on the acoustic spectra measured by an interior microphone.

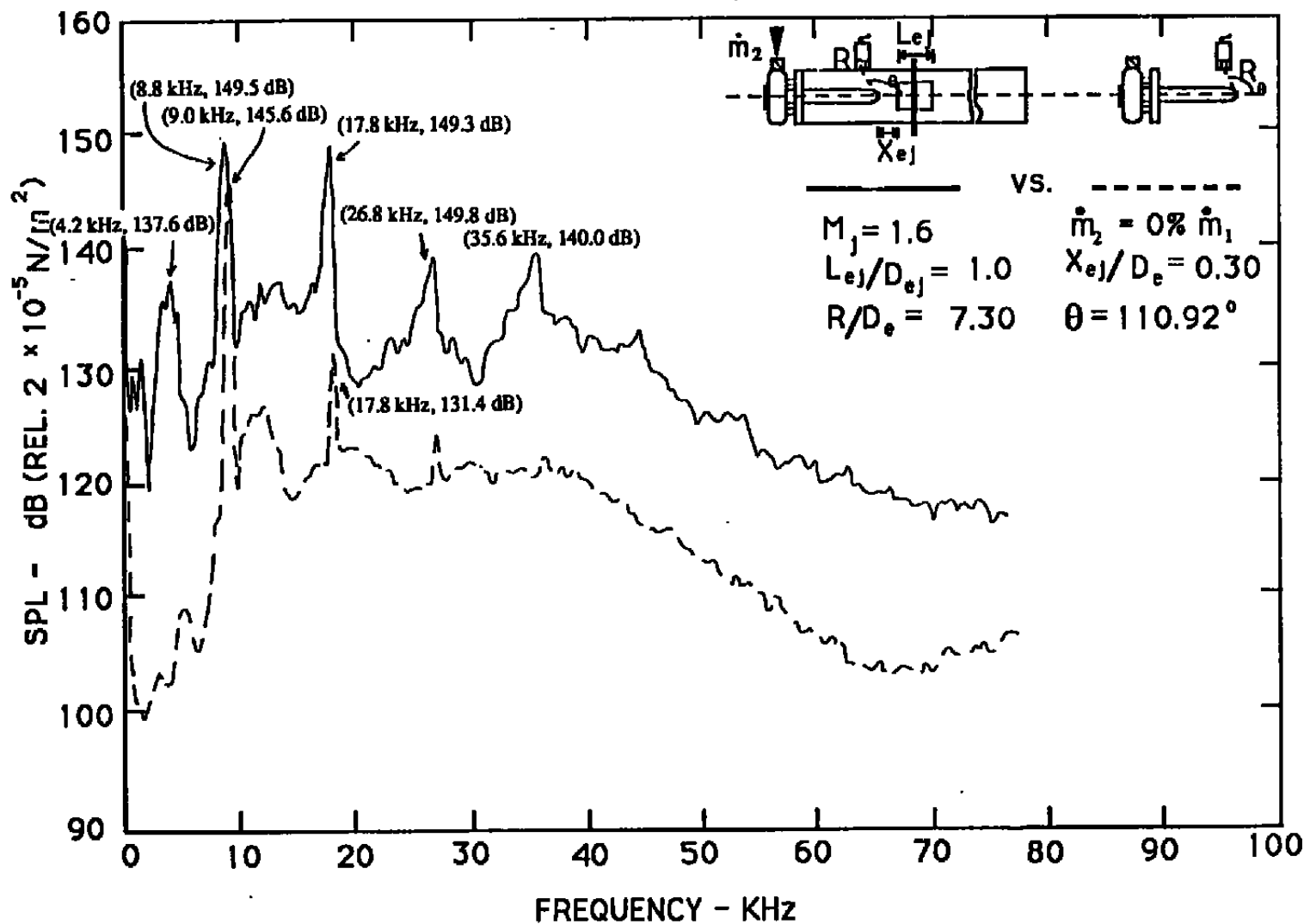


Figure 2.39 Effect of adding the ducted configuration on the acoustic spectra measured by an interior microphone.

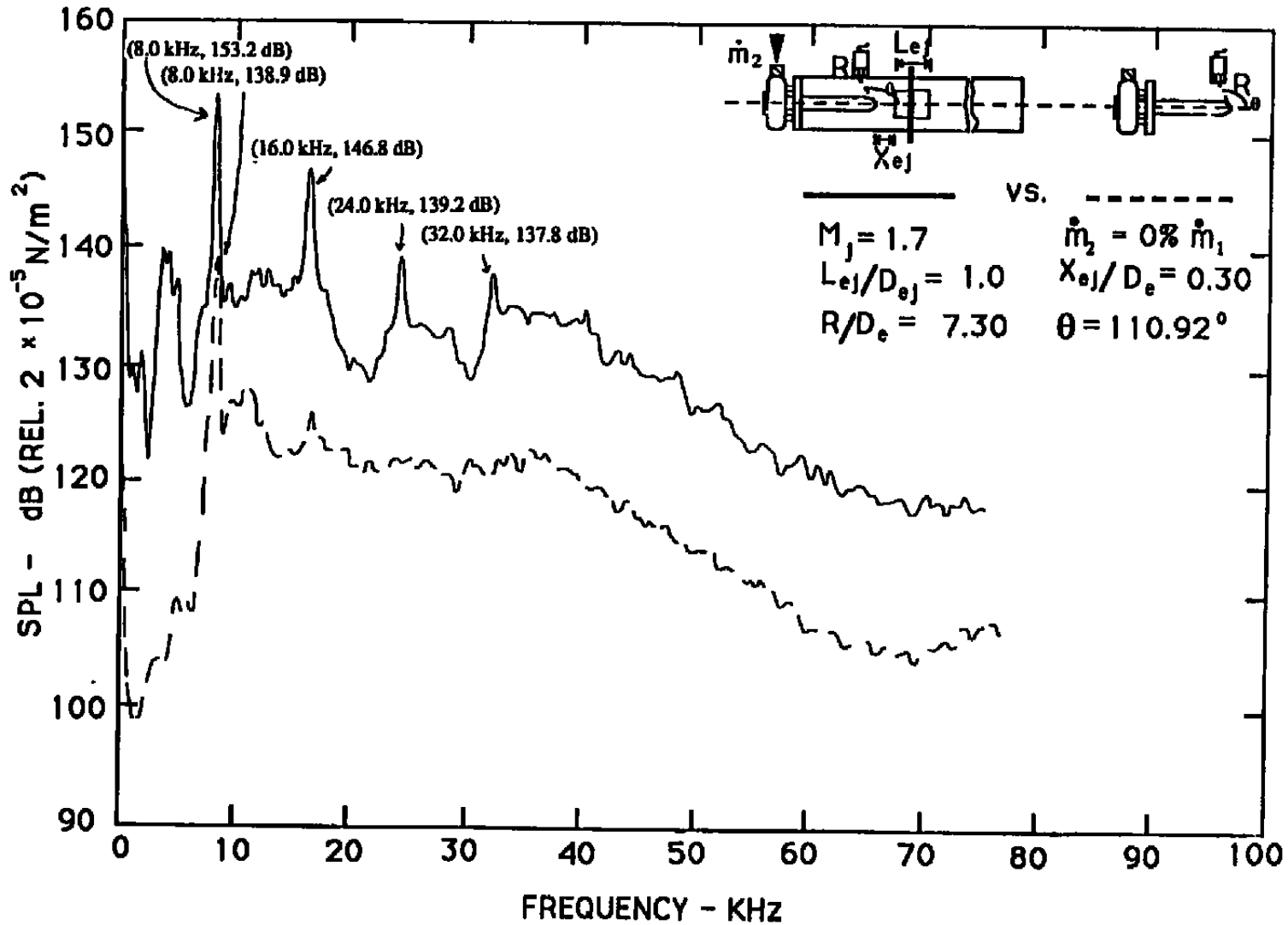


Figure 2.40 Effect of adding the ducted configuration on the acoustic spectra measured by an interior microphone.

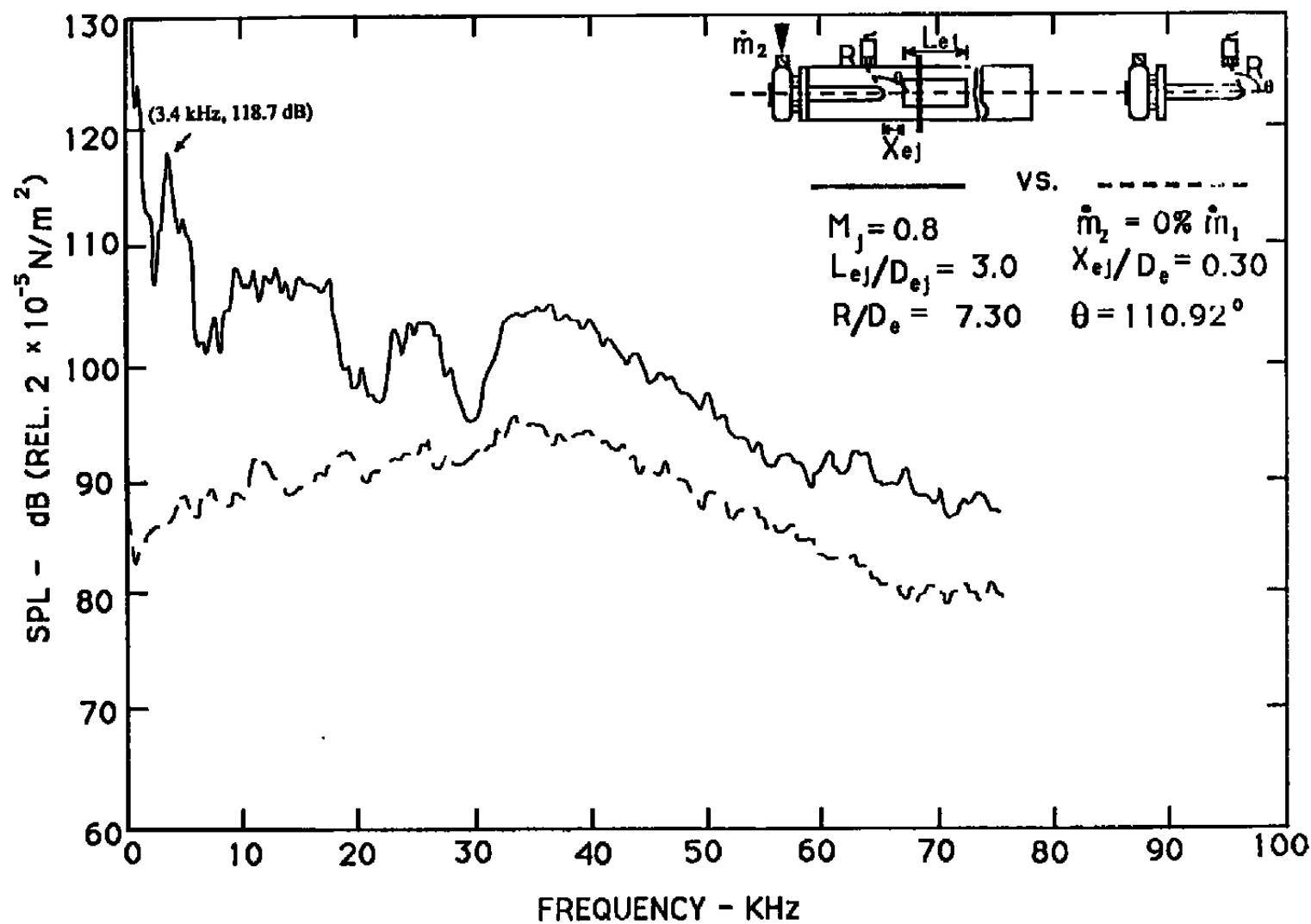


Figure 2.41 Effect of adding the ducted configuration on the acoustic spectra measured by an interior microphone.

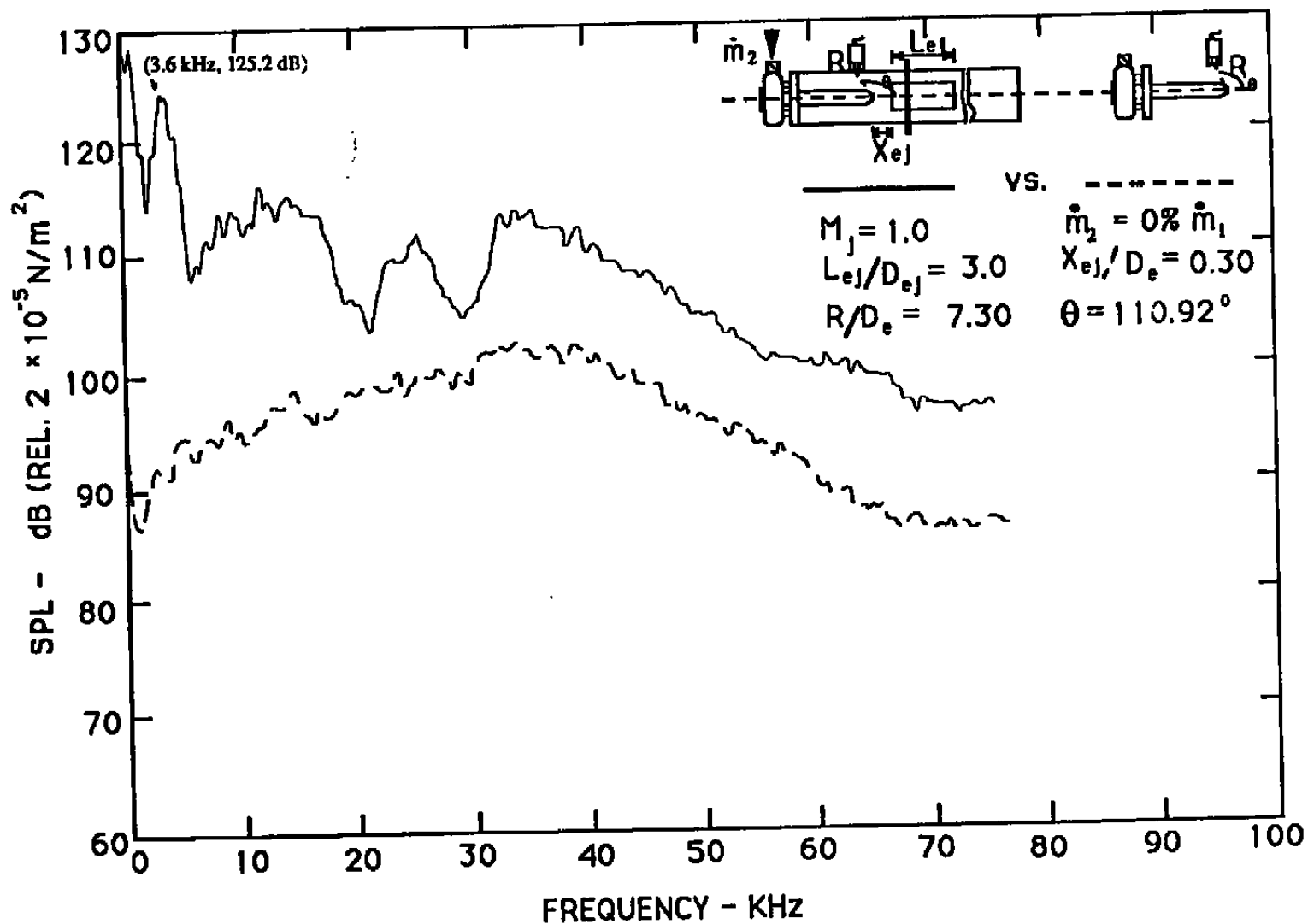


Figure 2.42 Effect of adding the ducted configuration on the acoustic spectra measured by an interior microphone.

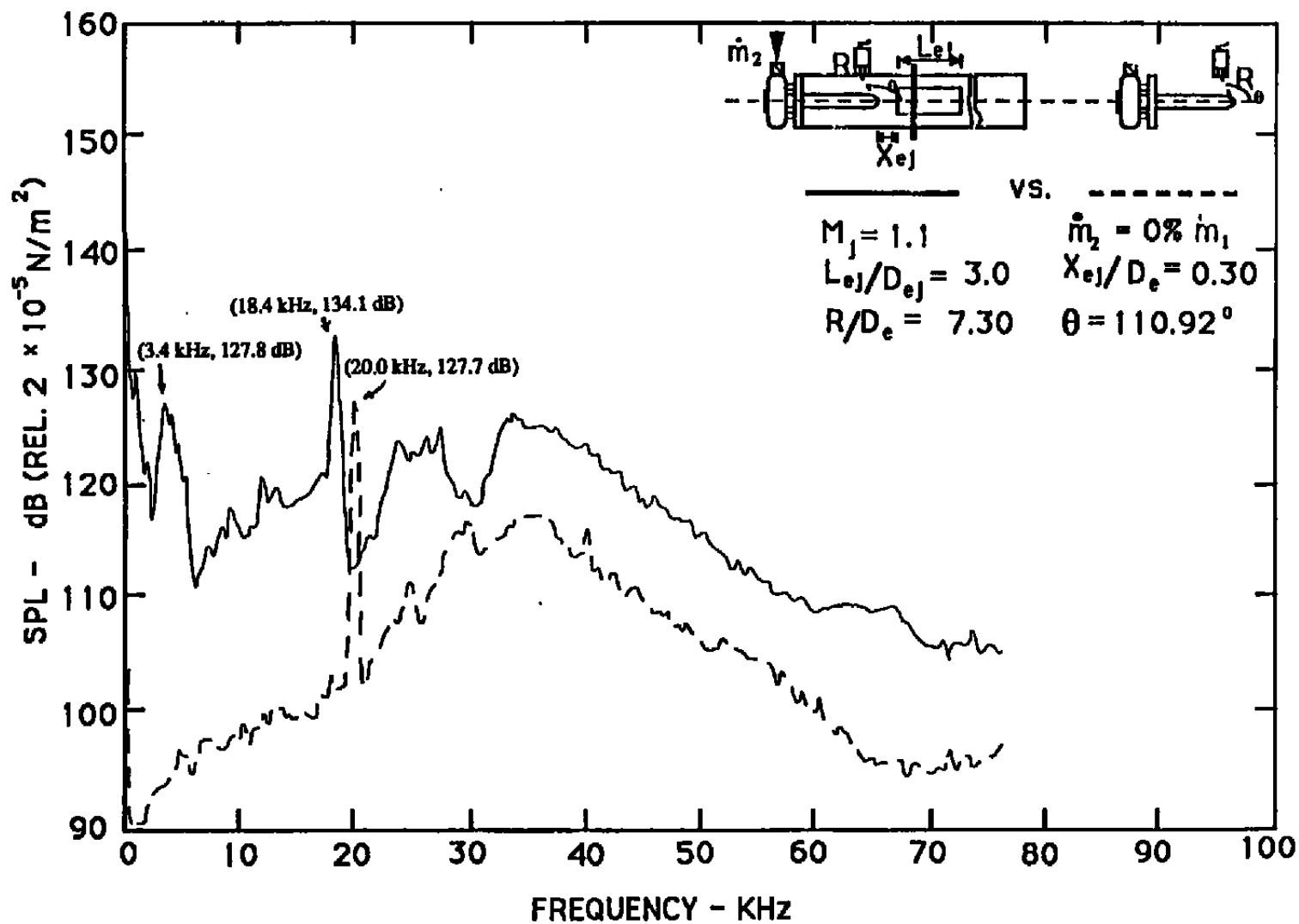


Figure 2.43 Effect of adding the ducted configuration on the acoustic spectra measured by an interior microphone.

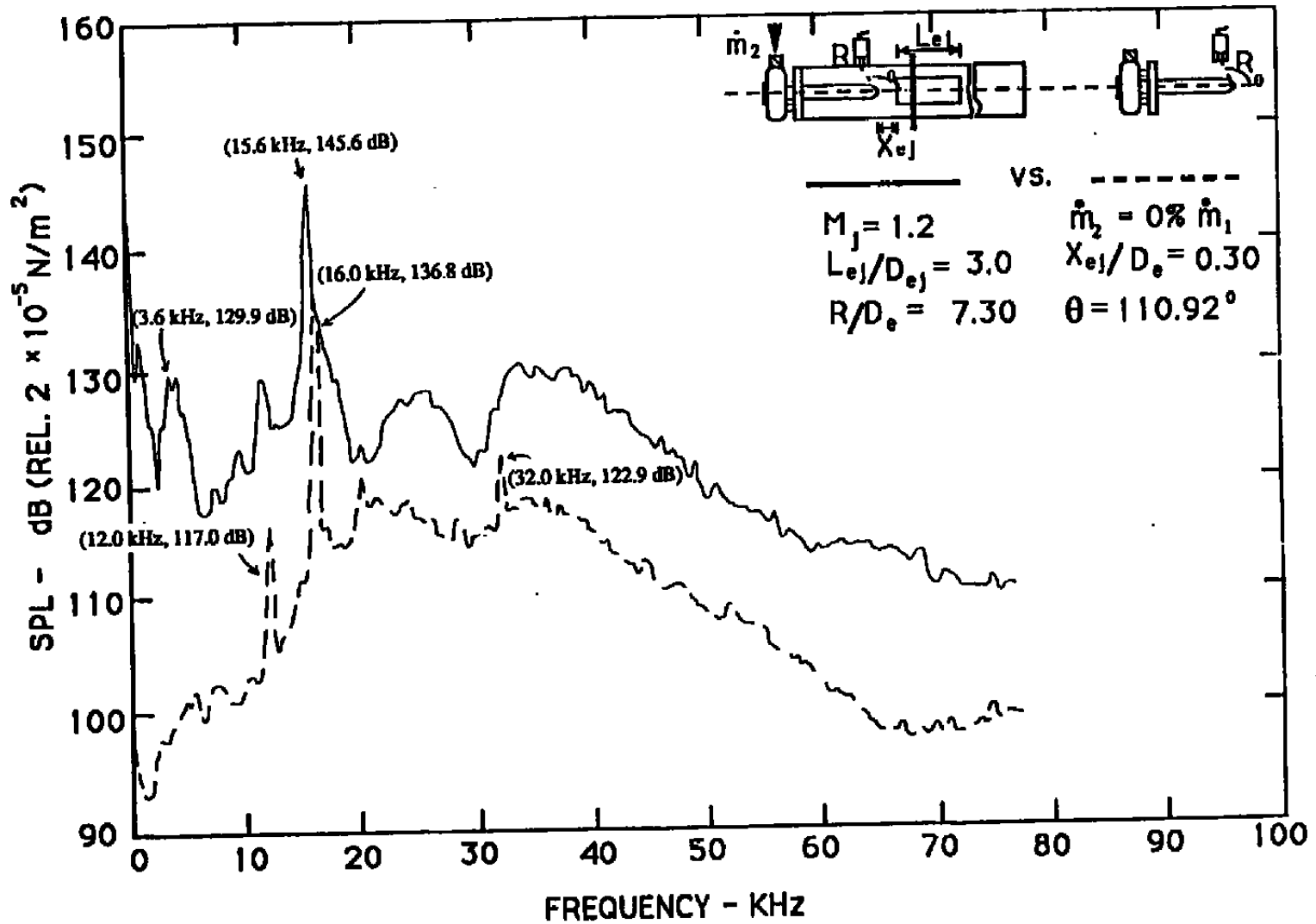


Figure 2.44 Effect of adding the ducted configuration on the acoustic spectra measured by an interior microphone.

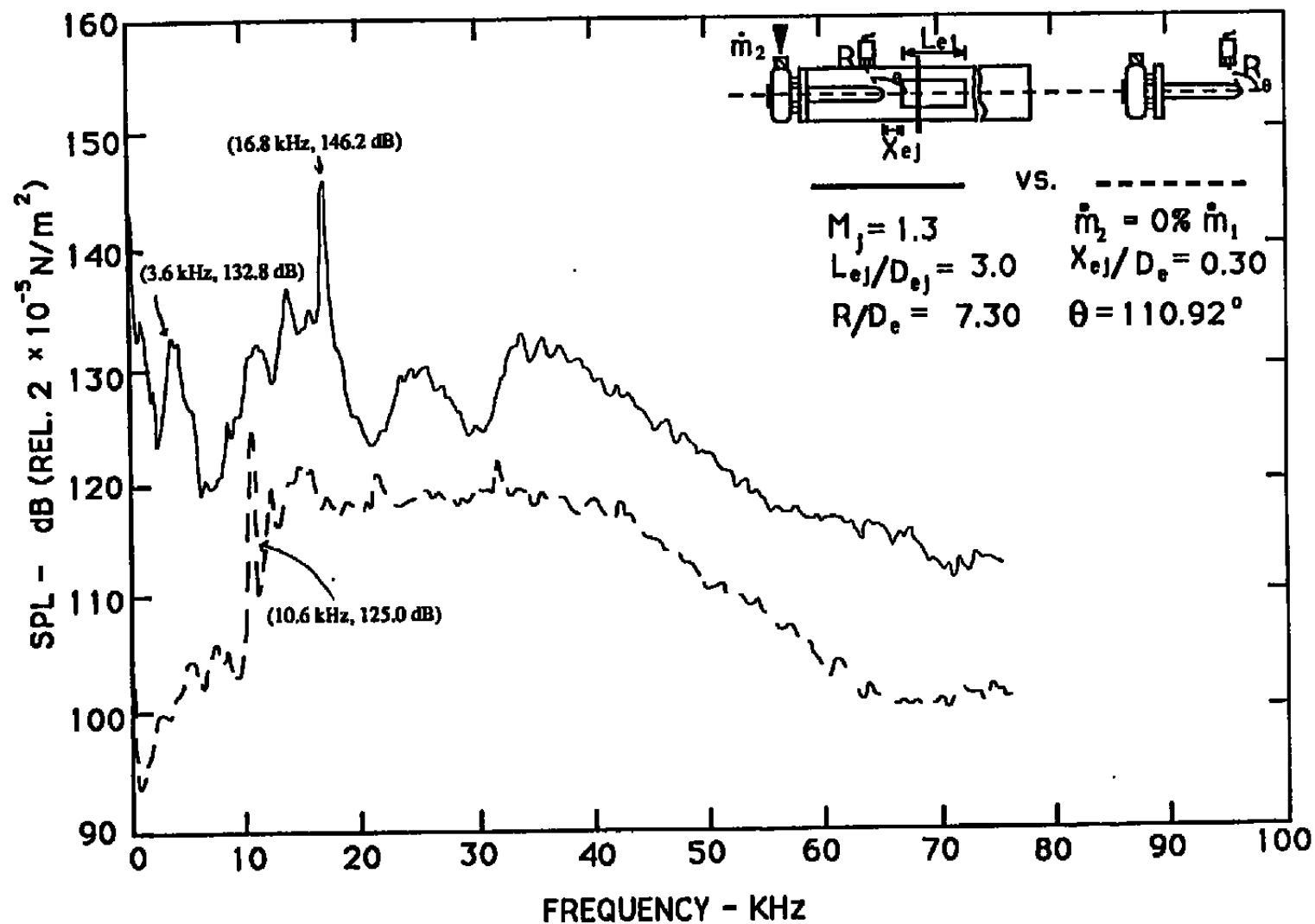


Figure 2.45 Effect of adding the ducted configuration on the acoustic spectra measured by an interior microphone.

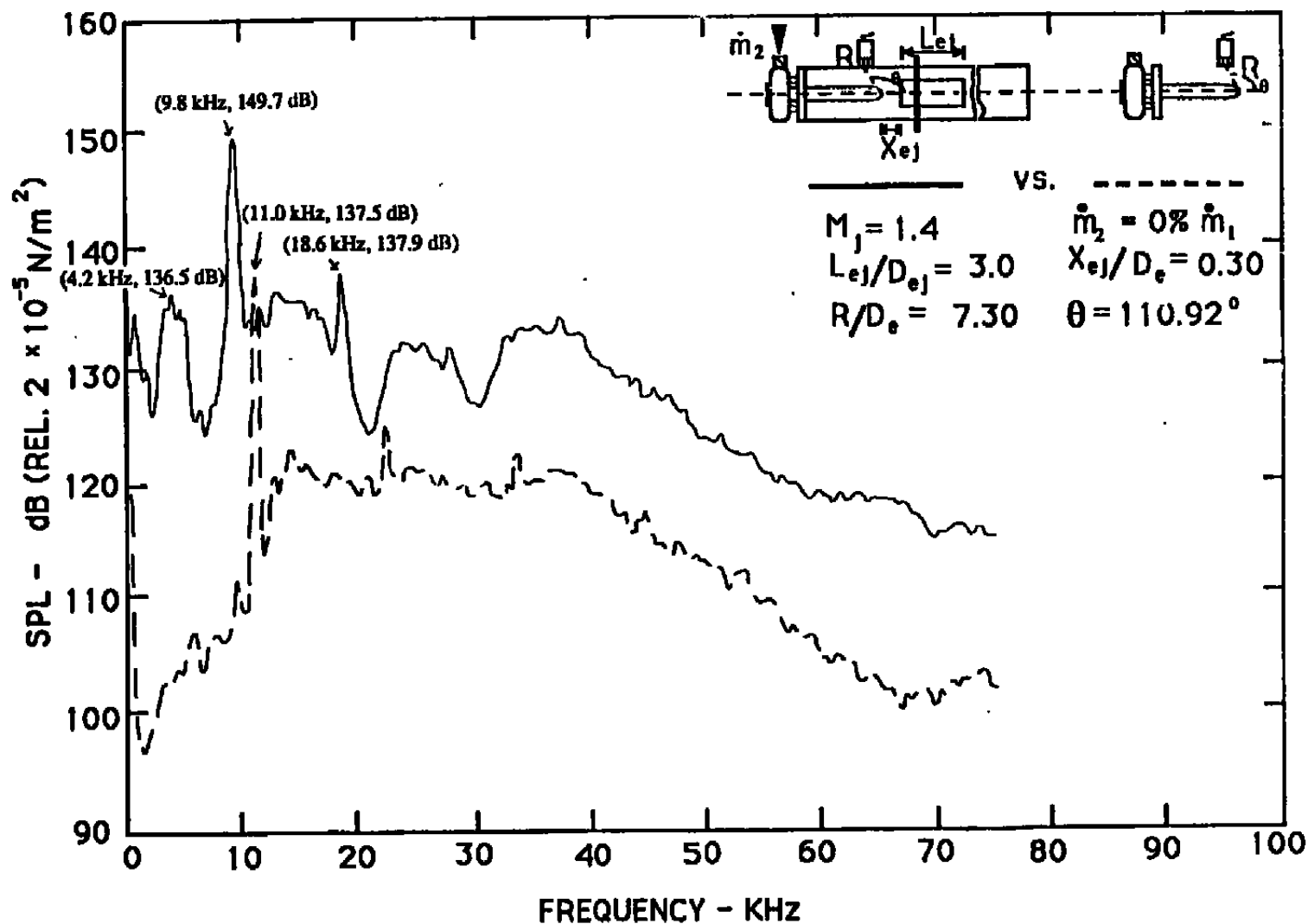


Figure 2.46 Effect of adding the ducted configuration on the acoustic spectra measured by an interior microphone.

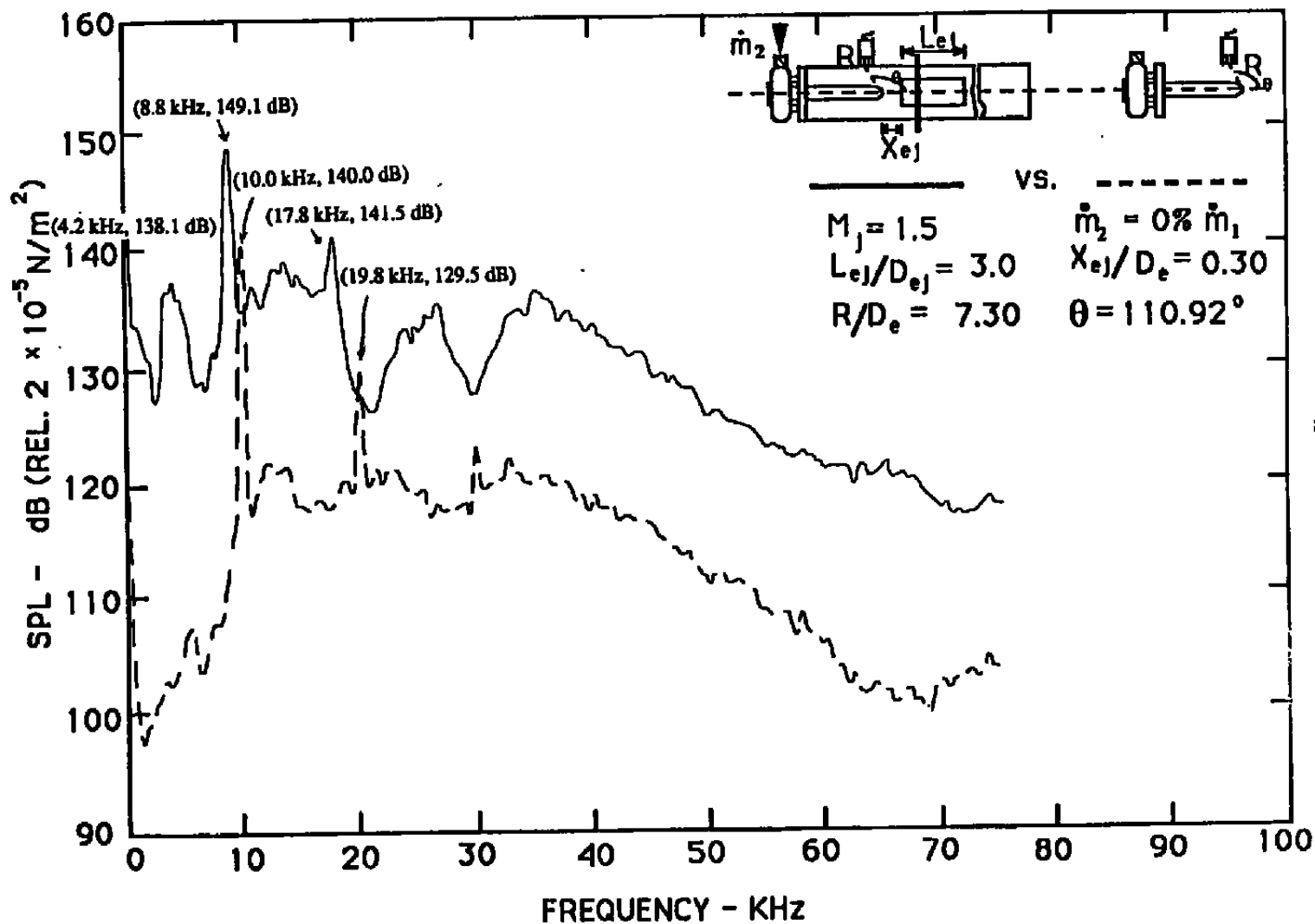


Figure 2.47 Effect of adding the ducted configuration on the acoustic spectra measured by an interior microphone.

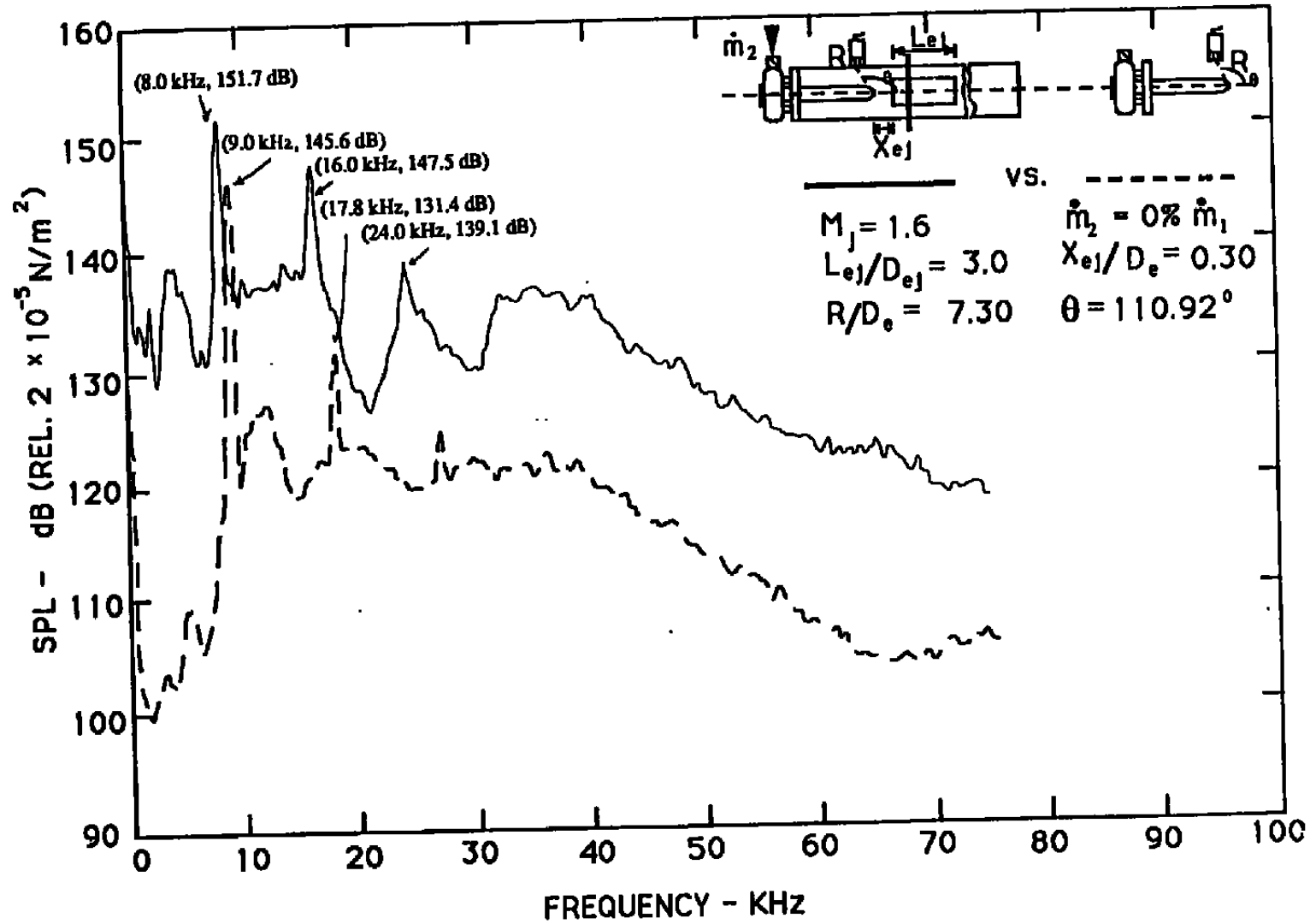


Figure 2.48 Effect of adding the ducted configuration on the acoustic spectra measured by an interior microphone.

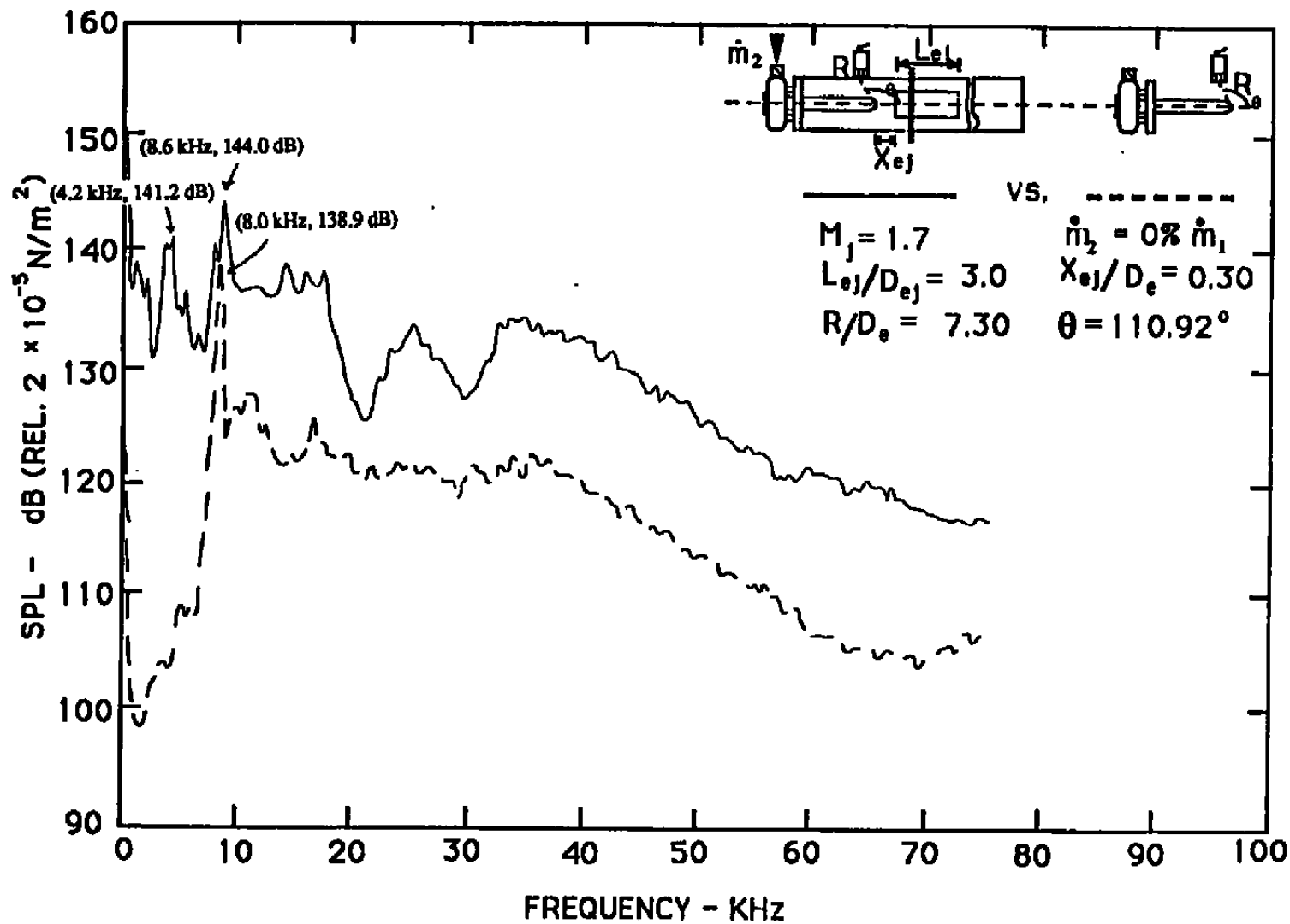


Figure 2.49 Effect of adding the ducted configuration on the acoustic spectra measured by an interior microphone.

shown in Figures 2.41 through 2.49. In each figure, the free jet noise data are compared with the ducted jet noise data at the same jet plenum pressures.

The following observations are noteworthy about the in-duct acoustic signatures:

1. As for the far field acoustic spectra, the in-duct signatures also show 8 to 10 decibels broadband noise increase at all frequencies.
2. Noise at the screech frequency and its harmonics increases by more than 10 decibels at most Mach numbers. This increase in amplitude is believed to be due to the fact that most of the energy at this frequency is trapped within the reverberant interior of the test cell.
3. A well-defined and high-amplitude discrete tone is obtained between 3 and 5 kHz. This frequency is mostly about 4.2 kHz for the smaller ejector and about 3.4 kHz for the larger ejector. It should be recalled that no dominant tone was observed in the far field spectra. Purely based upon geometrical scaling of the ejector diameter, a tone at a frequency of 4 kHz was expected to be observed. (The frequency for the full-scale facility was 85 Hz. The scale factor was 48.)
4. An additional set of tones is seen at lower frequencies for both ejectors between DC and 2 kHz. The levels of these tones are higher for the longer ejector.
5. A comparison of the in-duct noise spectra for the shorter and the longer ejector indicates that with the exception of the very low frequency tones alluded to under item 4 above, changing the ejector length has little effect on the general features of the measured spectra. The broadband noise levels essentially remain unchanged. Even the levels of the above-noted frequency between 3 and 5 kHz are almost the same for the two ejectors.

Based upon these observations, it appears that the frequency between 3 and 5 kHz, may well be associated with the duct resonance. This conclusion is derived from the fact that this frequency essentially did not change on changing the jet Mach number. Changing the duct length by a factor of three changed this frequency from 4.2 kHz to 3.4 kHz. The bandwidth of the spectral analysis over a frequency range of 100 kHz was 200 Hz. The fact that the frequency remained almost constant for a given ejector for all jet mach numbers, indicates that this frequency is associated with some form of duct resonance and is not related to excitation of flow instability modes. This explanation also seems to fit with the arguments based upon calculations of the

resonances associated with normal acoustic modes of the jet/diffuser as described in the next section on theoretical results. Also additional tests performed in the absence of flow and in the presence of artificially generated sound, further confirmed the presence of duct resonance. This is described below.

## 2.7 Further Tests to Confirm Duct Resonance

To establish that the low frequency tones in the frequency range 3-4kHz were indeed due to some form of duct resonance, artificially generated sound was used to excite acoustic duct modes in the test configuration in the absence of any flow. In particular, the following four tests were performed:

### Test 1:

An acoustic driver was mounted in the manner shown in Figure 2.50 at the inlet of the secondary air supply manifold. Broadband noise was injected into the test-cell.

### Test 2:

An acoustic driver was connected to an inverse conical horn. The horn was 1 inch in diameter at the driver source opening and converged to a 1/4 inch diameter (See Figure 2.51 a). A 1/4 inch diameter tube extension was then connected to the smaller end of this horn. The tube was attached to the 1/4 inch diameter bore in the disc holding the ejector so as to inject sound inside the ejector duct. A photographic view of this arrangement is shown in Figure 2.51 (b).

### Test 3:

An acoustic driver was placed outside the test cell exit and in-duct microphone noise spectra were measured with and without the test-cell ducting in place (configuration not shown).

### Test 4:

A jet exhausting from a 1/2 inch diameter tube was placed outside the test cell exhaust in the manner shown in Figure 2.52. In-duct noise spectra for the free jet and the ducted configuration were compared to identify acoustic resonances.

In each case, strong tones were obtained at the lower frequencies for which duct resonance was suspected in the with-flow data presented earlier. Typical data are shown in Figures 2.53 (a) and (b) for Test 1, Figures 2.54 (a) and (b) for Test 2, Figure 2.55 for Test 3, and Figure 2.56 for Test 4.

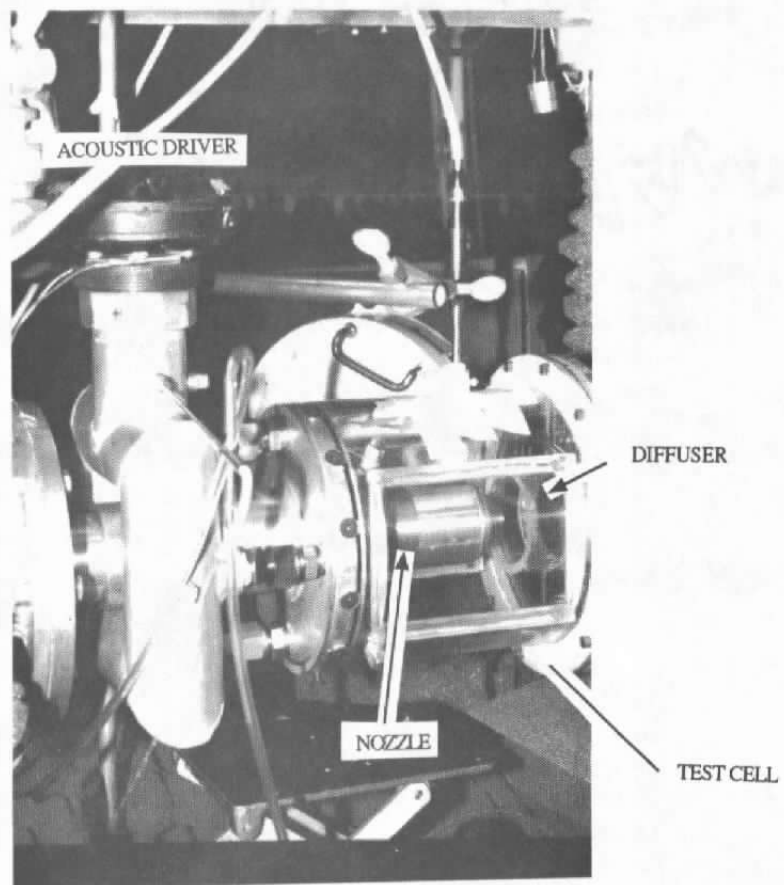


Figure 2.50 Acoustic driver mounted at the secondary air supply inlet.

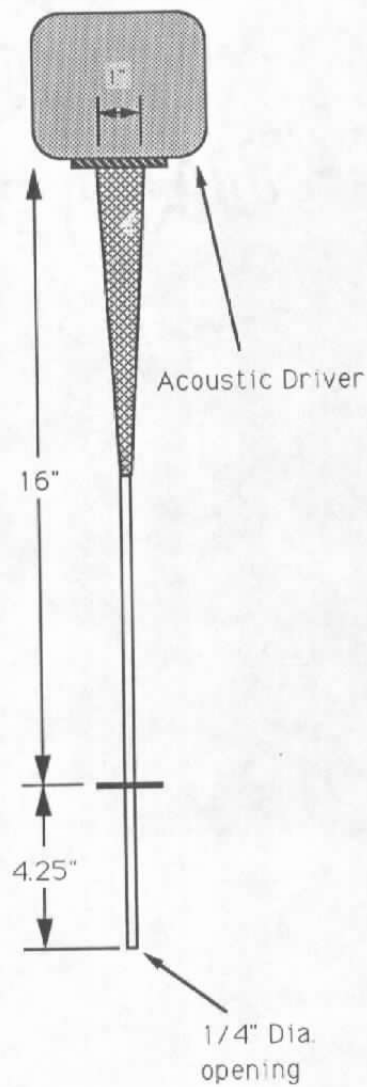


Figure 2.51 (a) The point sound source.

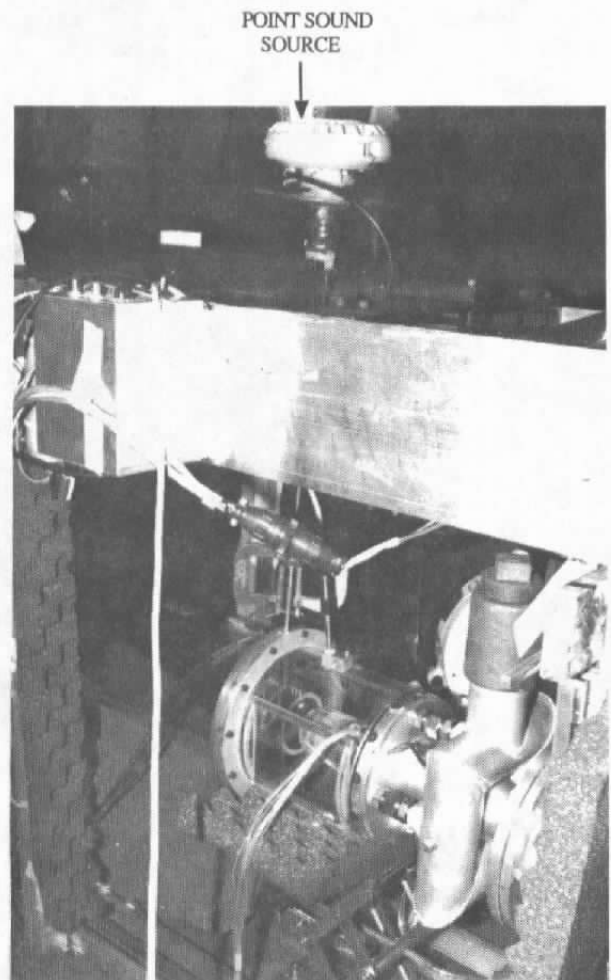


Figure 2.51 (b) Point sound source injected into the ejector.

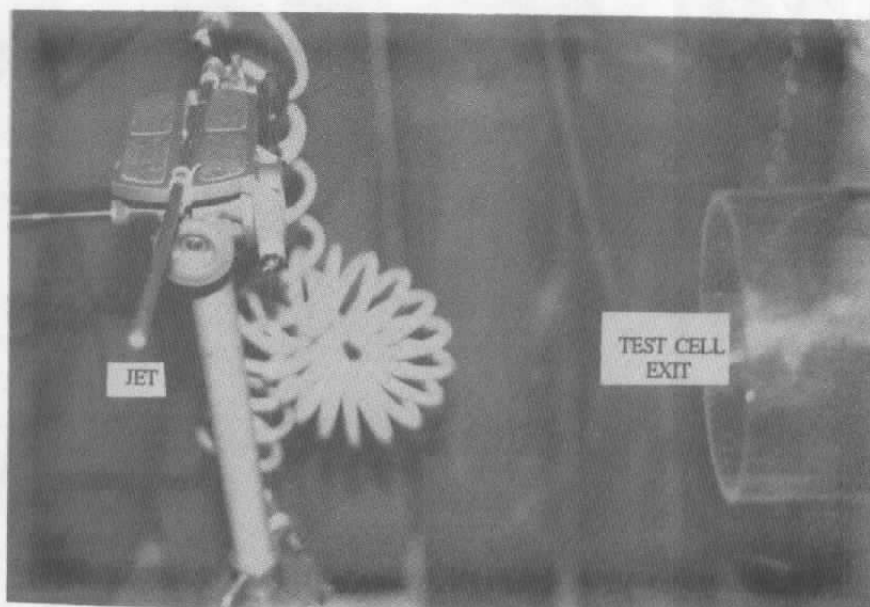


Figure 2.52 A small jet exhaust used to excite duct resonance.

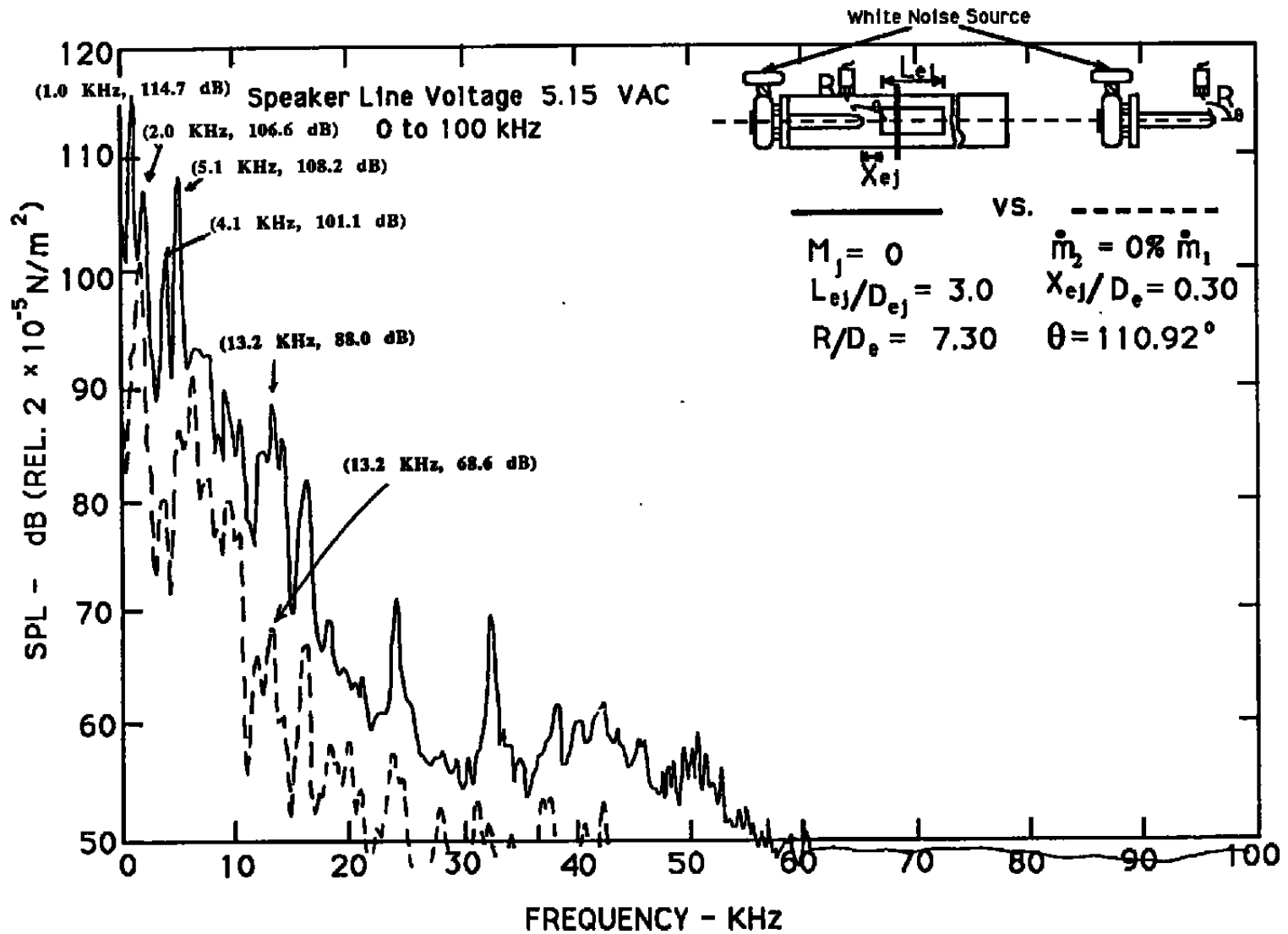


Figure 2.53 (a) Acoustic resonance produced during test 1 (0 - 100 KHz).

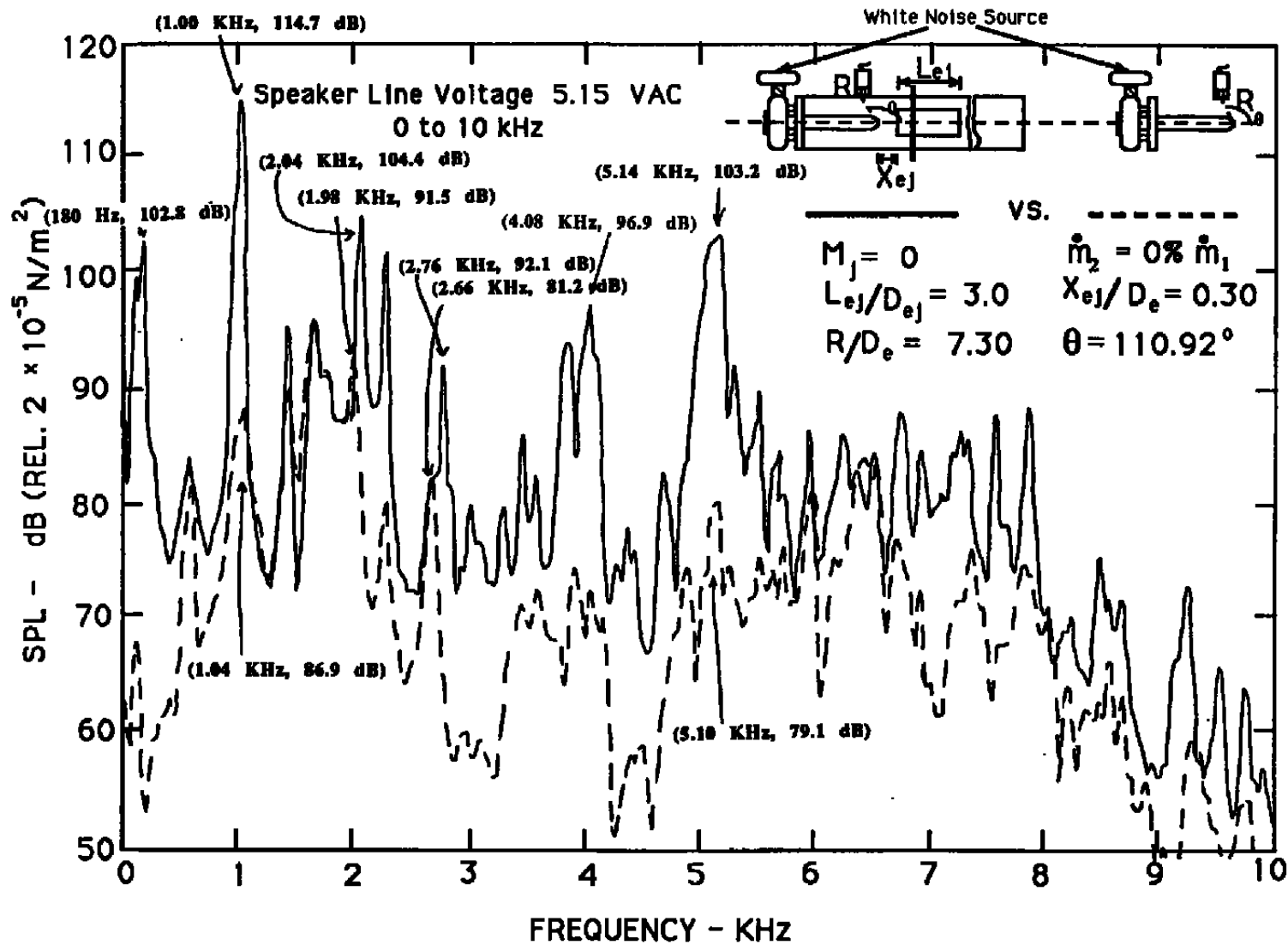


Figure 2.53 (b) Acoustic resonance produced during test 1 (0 - 10 KHz).

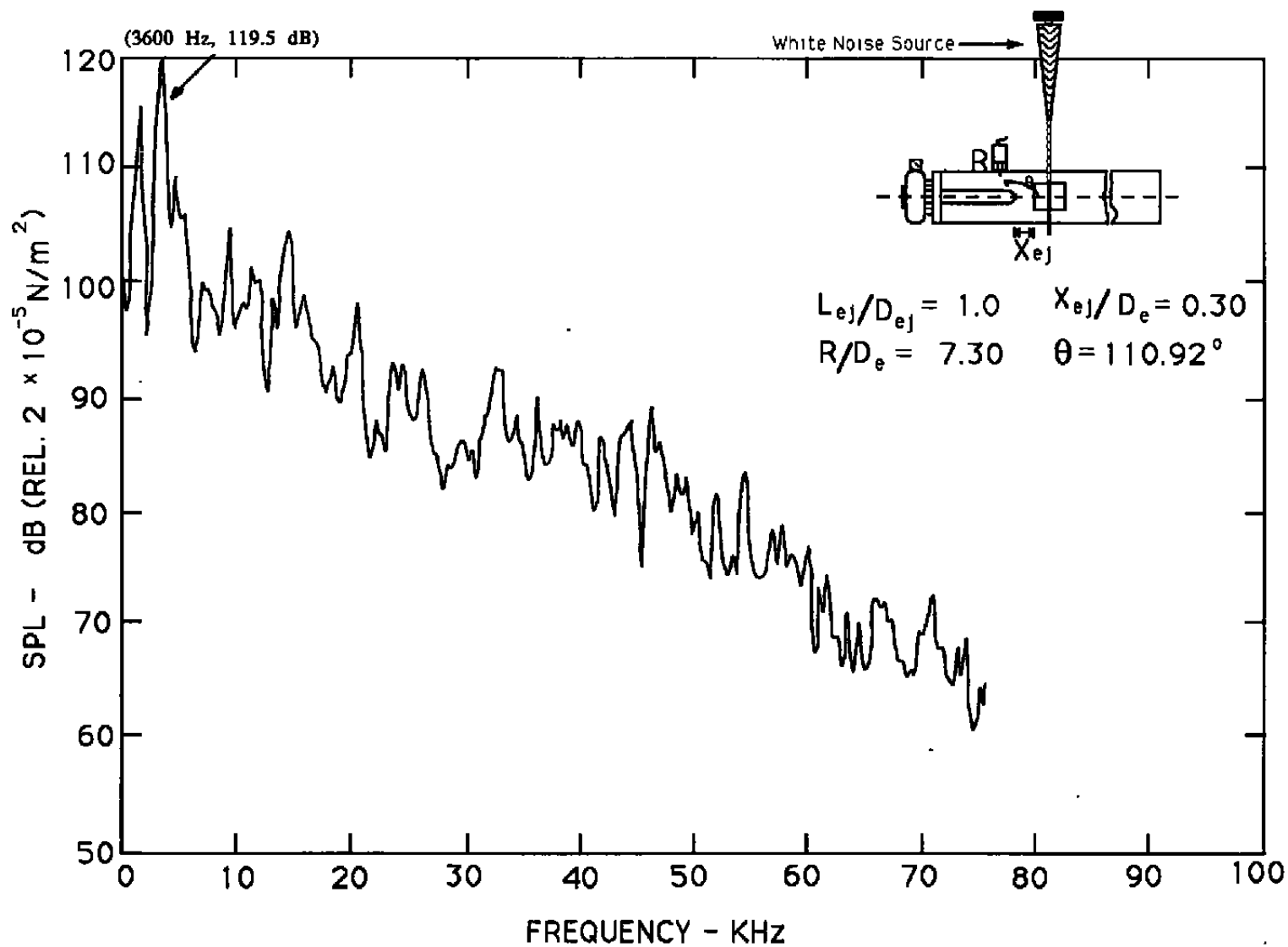


Figure 2.54 (a) Acoustic resonance produced during test 2.

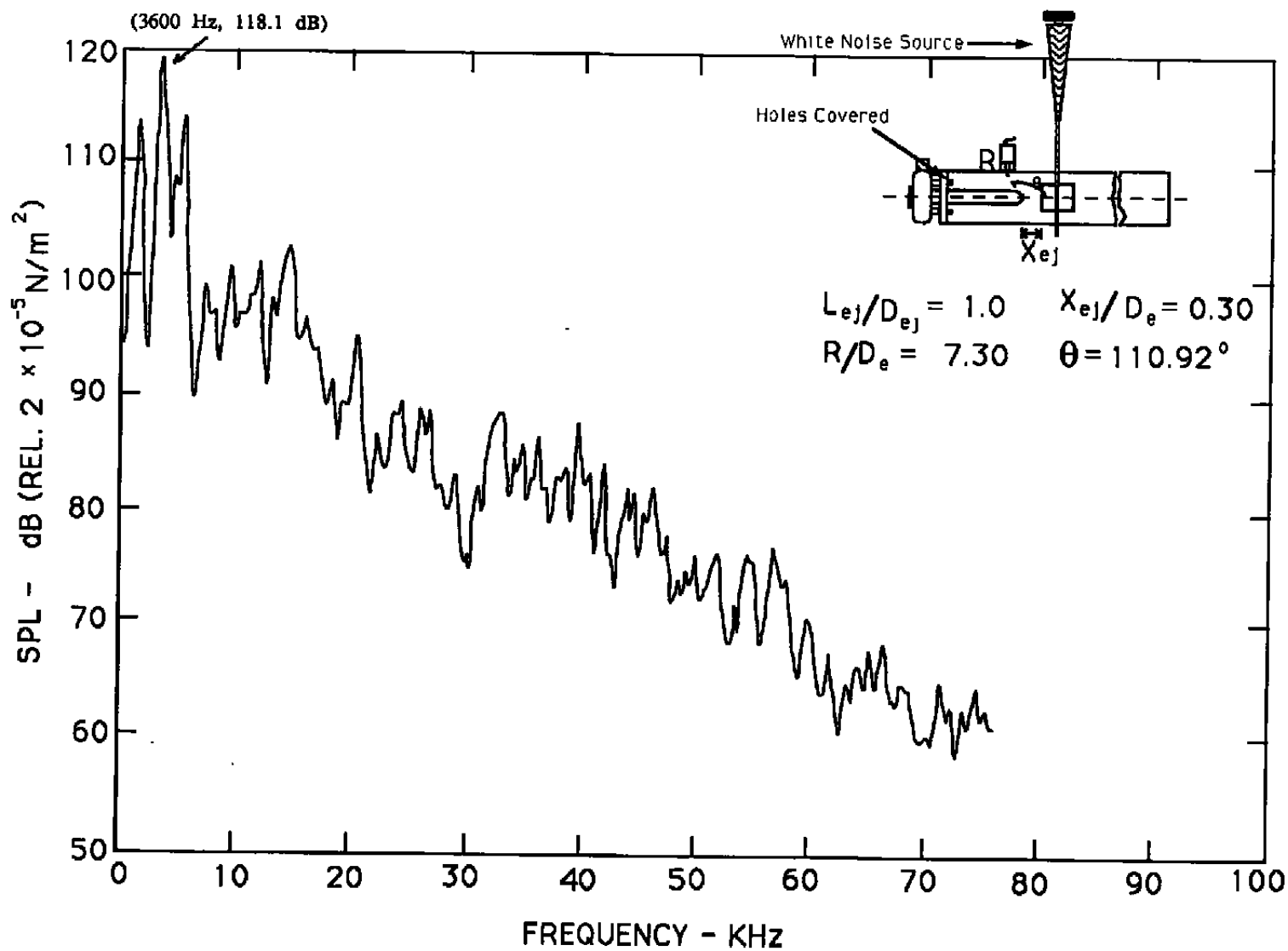


Figure 2.54 (b) Acoustic resonance produced during test 2.  
 (Tube exits for secondary flow covered.)

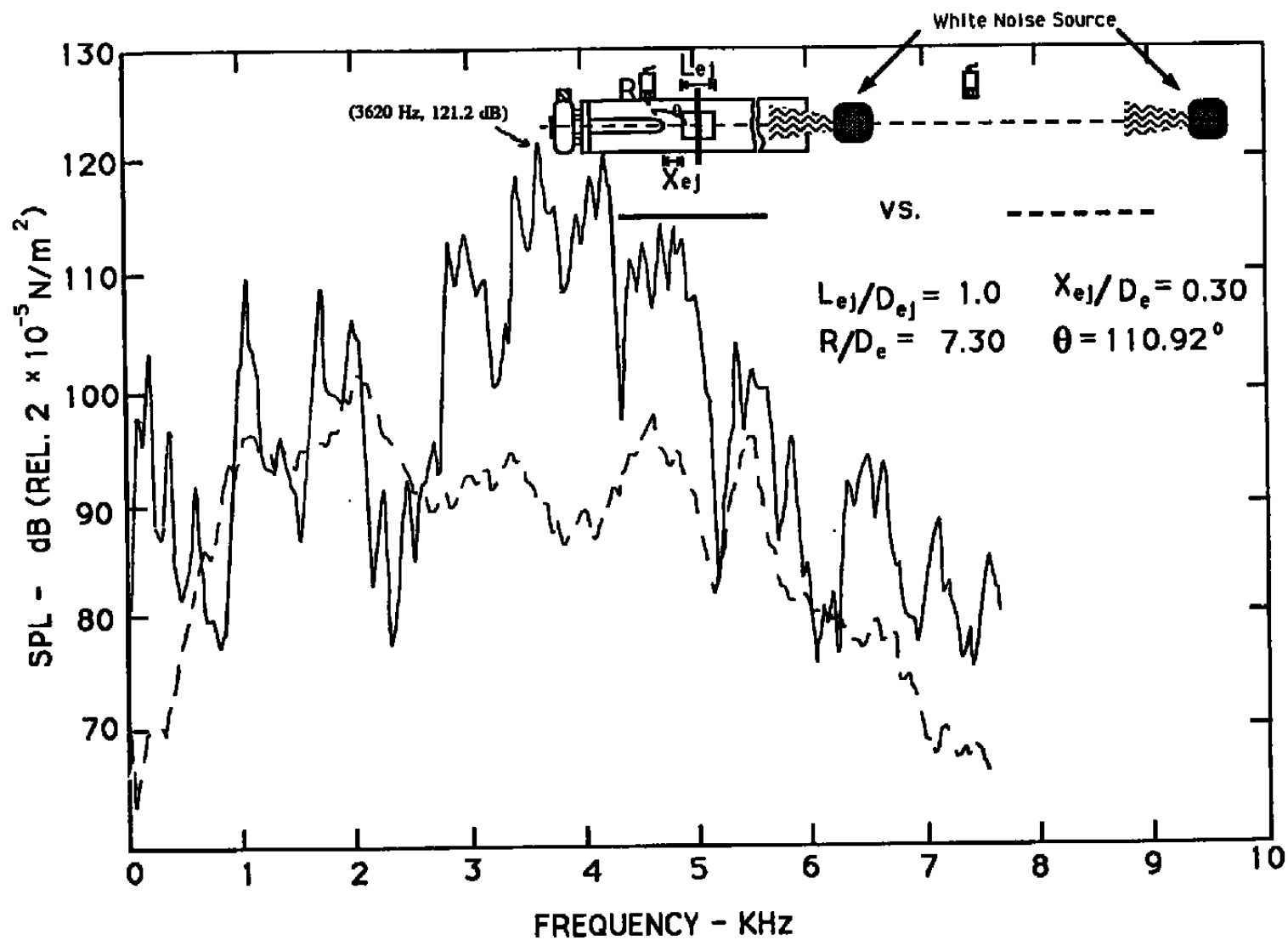


Figure 2.55 Acoustic resonance produced during test 3.

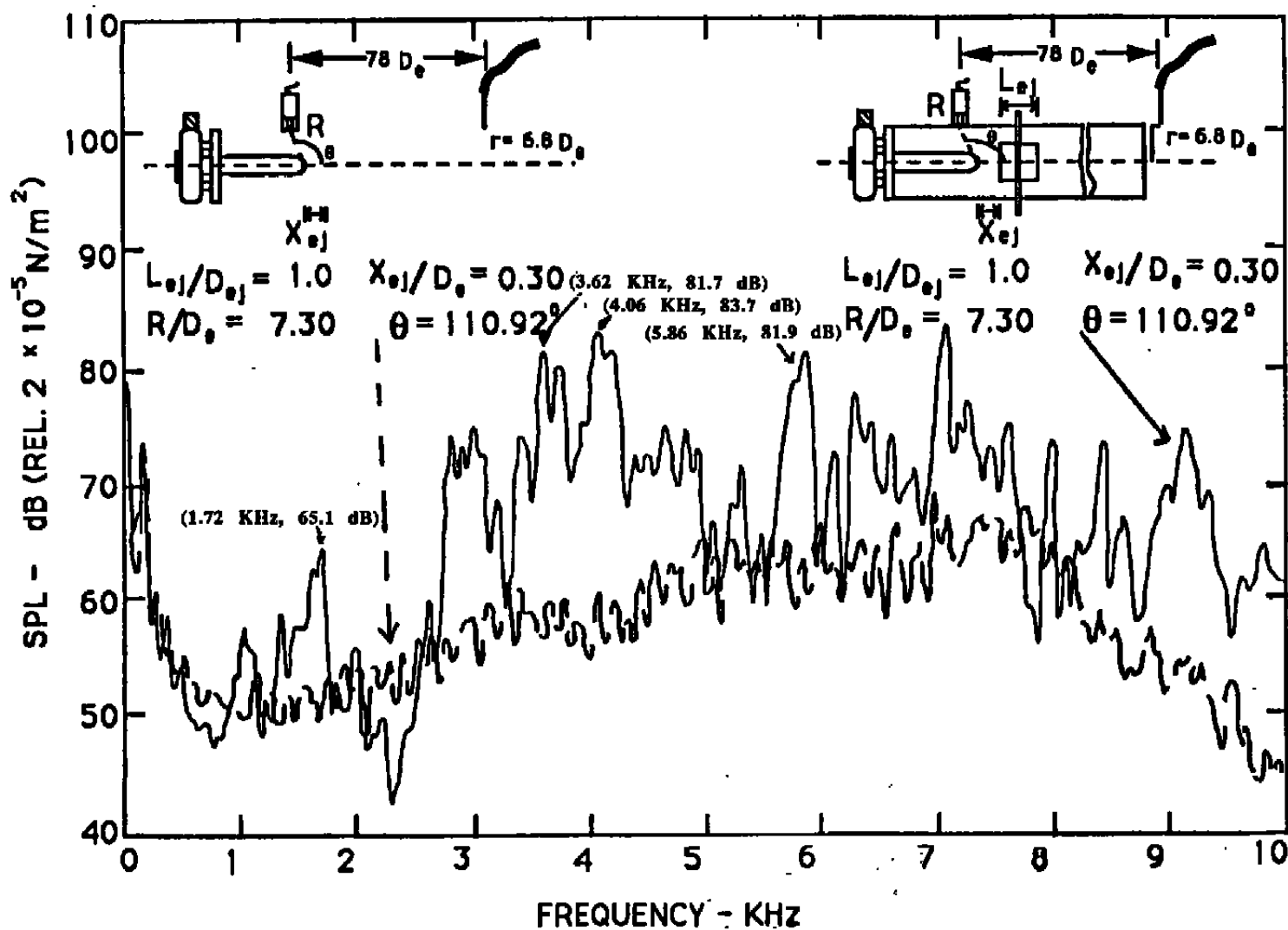


Figure 2.56 Acoustic resonance produced during test 4.

For Test 1, with the driver mounted at the secondary flow inlet, Figure 2.53a shows a comparison of the noise spectra, analyzed to a frequency range of 100 kHz, between the unducted and the ducted configuration. Data for the larger ejector are shown. As expected, noise at all frequencies increased on installing the ducted configuration, as the noise that would normally radiate in all directions is now confined within the reverberant interior of the test cell. But notice that few additional tones have also been excited including those at 4.1 kHz and 5.1 kHz. These are believed to be those due to duct resonance. This is seen in somewhat more detail in Figure 2.53b where the spectra have been expanded by reanalyzing and replotting the data only up to 10 kHz (instead of 100 kHz as shown in Figure 2.53a).

Data for Test 2 were repeated with the four tubes connecting the manifold and the test cell blocked. This was to isolate any effects due to potential resonance of the tubes and the manifold and the ducting located upstream. A comparison of Figures 2.54 (a) and 2.54 (b) shows that identical spectra were obtained for the blocked and unblocked secondary air supply tubes. Existence of resonance peaks at 3.6 KHz is quite clear in this case. Data for the unducted configuration were not obtained in this case for identical location of the point source opening relative to the microphone, but the data for other locations displayed no peaks at 3.6 KHz.

Data for Test 3 are shown in Figure 2.55. This time, the data for the smaller ejector are shown. Resonance at a frequency around 4 kHz is obtained.

Finally similar resonances are noticed around 4kHz with Test 4 conducted with a small jet exhaust located outside the test cell exit. These data are shown in Figure 2.56.

These tests, thus, further confirm that the high intensity tones measured in full-scale facility at 85 Hz and 140 was in all likelihood a result of duct resonance.

The narrow band region at the very low frequencies between DC and 2 kHz appeared to change with changing the ejector length. These results still need to be examined further.

## 2.8 Concluding Comments

The measurements reported in this section indicate that the noise spectra of the ducted configuration is characterized by the dominance of a number of spectral peaks. The narrow band spectral tones attributable to screech for the free jet are still noticed for the ducted configuration. These frequencies remain roughly the same as for the free jet. Any changes in frequency observed are attributable to minor differences in the jet Mach number for the ducted configuration since all

measurements for a constant nominal Mach number were acquired at the same operating reservoir pressure. It is found that, compared to the free jet, the levels of these discrete tones increase by as much 10dB as measured by an in-duct microphone. This is to be expected, since the most of the upstream propagating acoustic energy generated during the screech-related feedback process is trapped in the test cell. This, in addition to the fact that the test-cell enclosure is reverberant, accounts for the higher levels of screech type tones at the induct microphone locations. That these narrow band tones are indeed related to feedback phenomena are discussed in great detail in the next section.

In addition to the screech-type narrowband tones, tones with somewhat broader half-widths are also measured for the ducted configuration. These tones, falling in the range of 3 kHz to just above 4 kHz, are attributable to some form of duct resonance. It is shown that the frequencies of these tones do not change much on changing the flow conditions. Additional tests performed by exciting the interior of the ducted configuration in the absence of any flow with artificially generated sound further support the contention that the broader tones measured between 3-4 kHz are those due to duct resonances. Further confirmation of these findings is provided in the next section based upon theoretical findings.

### SECTION 3

## JET/DIFFUSER STABILITY CALCULATIONS

The purpose of the theoretical part of this investigation is to provide physical interpretations and analysis of the findings of the companion experimental study described in the last section on the aeroacoustics of jet/diffuser flow. Experimental measurements indicate that the spectrum of the noise of the flow is dominated by tones and resonances. Here tones are referred to the spectral peaks of very narrow half-widths. On the other hand, spectral peaks with broader half-widths and not so well-defined peak frequencies are referred to as resonances. It is our belief that the tones are jet screech tones generated by feedback loops. These feedback loops are driven by the large-scale instability waves of the jet flow. The resonances are associated with the normal acoustic modes of the jet/diffuser. Because the flow is highly turbulent, the normal mode resonances are not sharp. In the following, the normal acoustic modes of the flow system and the characteristics of the instability waves of the supersonic jet are analyzed. The results are then used to explain and to correlate experimental observations.

### 3.1 Supersonic Jet/Diffuser Flow Model and Analysis

The ejector flow is, needless to say, very complicated. Since it is not known conclusively that the duct mode resonance is, indeed, responsible for the observed low frequency tones a very detailed analysis is deemed unwarranted. It is believed that a simple ejector jet flow model such as a vortex sheet supersonic jet housed inside a circular duct may be a reasonable first analytical model. Such a model does contain the essential physics crucial to the interaction between the oscillatory motion of the jet and the enclosing duct. Furthermore, results of such a relatively simple model would provide valuable initial estimates of the frequency or the wave number for refined calculations of the resonance frequency when a more realistic model is used. To the authors knowledge, the acoustic modes of a vortex sheet (top hat profile) supersonic jet inside a rigid circular duct have not been analyzed before. Thus the results provided here are new.

Consider a supersonic jet bounded by a vortex sheet inside a rigid circular duct as shown in Figure 3.1. The fully-expanded radius of the jet  $R_j$ , is related to the nozzle exit radius,  $R$ , by the requirement of conservation of mass flux. If  $M_d$  is the nozzle design Mach number ( $M_d = 1.0$  for a convergent nozzle) and  $M_j$  is the fully-expanded Mach number of

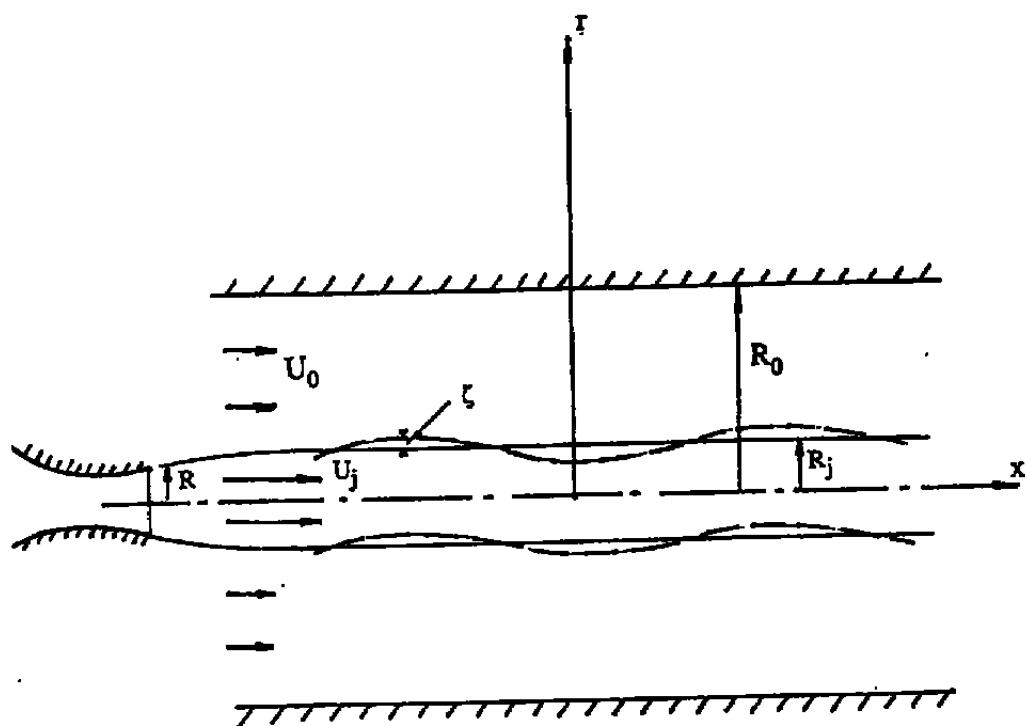


Figure 3.1 Ejector flow configuration

the jet then  $R_j$  is given by

$$R_j/R = \left[ \left( 1 + \frac{\gamma-1}{2} M_j^2 \right) / \left( 1 + \frac{\gamma-1}{2} M_d^2 \right) \right]^{\frac{\gamma+1}{4(\gamma-1)}} (M_d/M_j)^{1/2}.$$

Let the time independent mean flow be  $\rho = \bar{\rho}(r)$ ,  $u = \bar{u}(r)$  and  $\bar{p} = \text{constant}$ , where  $r$  is the radial coordinate. The linearized equations of motion of an inviscid, compressible, non-heat conducting flow in cylindrical coordinates are,

$$\bar{\rho} \left( \frac{\partial v}{\partial t} + \bar{u} \frac{\partial v}{\partial x} \right) = -\frac{\partial p}{\partial r} \quad (1)$$

$$\bar{\rho} \left( \frac{\partial w}{\partial t} + \bar{u} \frac{\partial w}{\partial x} \right) = -\frac{1}{r} \frac{\partial p}{\partial \theta} \quad (2)$$

$$\bar{\rho} \left( \frac{\partial u}{\partial t} + \bar{u} \frac{\partial u}{\partial x} + v \frac{d\bar{u}}{dr} \right) = -\frac{\partial p}{\partial x} \quad (3)$$

$$\frac{\partial p}{\partial t} + \bar{u} \frac{\partial p}{\partial x} + \gamma \bar{p} \left( \frac{1}{r} \frac{\partial r v}{\partial r} + \frac{1}{r} \frac{\partial w}{\partial \theta} + \frac{\partial u}{\partial x} \right) = 0 \quad (4)$$

where  $(u, v, w)$  are velocity components in the  $(x, r, \theta)$  directions. Let us look for duct mode solutions of the form

$$p = \hat{p}(r) e^{i(kx + n\theta - \omega t)}. \quad (5)$$

Upon eliminating all other variables in favor of  $\hat{p}$  the governing equation is

$$\frac{d^2 \hat{p}}{dr^2} + \left[ \frac{1}{r} - \frac{1}{\bar{\rho}} \frac{d\bar{\rho}}{dr} + \frac{2k}{(\omega - \bar{u}k)} \frac{d\bar{u}}{dr} \right] + \left[ \frac{\bar{\rho}(\omega - \bar{u}k)^2}{\gamma \bar{p}} - k^2 - \frac{n^2}{r^2} \right] \hat{p} = 0. \quad (6)$$

For the case of a vortex sheet (or top hat profile) jet, (6) reduces to:  $r \leq R_j$ ,

$$\frac{d^2 \hat{p}_j}{dr^2} + \frac{1}{r} \frac{d\hat{p}_j}{dr} + \left[ \frac{(\omega - u_j k)^2}{a_j^2} - k^2 - \frac{n^2}{r^2} \right] \hat{p}_j = 0 \quad (7)$$

$R_j \leq r \leq R_o$

$$\frac{d^2 \hat{p}_o}{dr^2} + \frac{1}{r} \frac{d\hat{p}_o}{dr} + \left[ \frac{(\omega - u_o k)^2}{a_o^2} - k^2 - \frac{n^2}{r^2} \right] \hat{p}_o = 0 \quad (8)$$

where subscript  $j$  or  $o$  indicates whether the variable is associated with a physical quantity inside or outside the jet.  $a_j$  and  $a_o$  are the speeds of sound. The mean flow velocity outside the jet is taken to be  $u_o$ , which may be zero.

The dynamic and kinematic boundary conditions at the vortex sheet  $r = R_j$  are,

$$\hat{p}_j = \hat{p}_o \quad (9)$$

$$\frac{1}{\rho_j(\omega - u_j k)} \frac{d\hat{p}_j}{dr} = \frac{1}{\rho_o(\omega - u_o k)} \frac{d\hat{p}_o}{dr}. \quad (10)$$

At the duct wall,  $r = R_j$ , the boundary condition is

$$\frac{d\hat{p}_o}{dr} = 0. \quad (11)$$

The solution of (7), which is finite at  $r = 0$ , is

$$\hat{p}_j = A J_n(\lambda_j r) \quad (12)$$

where  $\lambda_j = [(\omega - u_j k)^2 / a_j^2 - k^2]^{1/2}$  and  $J_n$  is the Bessel function of order  $n$ .  $A$  is an arbitrary constant. The branch cuts for  $\lambda_j$  are taken so that  $-\pi/2 < \arg \lambda_j \leq \pi/2$ . The solution of (8) which satisfies boundary condition (11) is

$$\hat{p}_o = B[Y'_n(\phi R_o)J_n(\phi r) - Y_n(\phi r)J'_n(\phi R_o)] \quad (13)$$

where  $\phi = [\omega^2 / a_o^2 - 2M_o \omega k / a_o - (1 - M_o^2)k^2]^{1/2}$ ,  $0 \leq \arg \phi < \pi$ .  $M_o = u_o / a_o$  is the Mach number of the mean flow outside the jet.  $Y_n$  is the  $n^{\text{th}}$  order Neumann function. Substitution of (12) and (13) into (9) and (10) yields two homogeneous algebraic equations for the two unknowns  $A$  and  $B$ . In order to have a non-trivial solution, the determinant of the coefficient matrix must be equal to zero. This leads to the following dispersion relation for  $\omega$  and  $k$ .

$$\begin{aligned} & \frac{\lambda_j J'_n(\lambda_j R_j)}{\rho_j(\omega - u_j k)^2} [Y'_n(\phi R_o)J_n(\phi R_j) - J'_n(\phi R_o)Y_n(\phi R_j)] \\ & - \frac{\phi J_n(\lambda_j R_j)}{\rho_o(\omega - u_o k)^2} [Y'_n(\phi R_o)J'_n(\phi R_j) - J'_n(\phi R_o)Y'_n(\phi R_j)] = 0. \end{aligned} \quad (14)$$

At  $\phi = 0$ , the Neumann function becomes infinite. This occurs when  $k = \frac{-\omega}{a_o(1-M_o)}$  and  $k = \frac{\omega}{a_o(1+M_o)}$ .

Dispersion relation (14) provides an algebraic relationship between wave number  $k$  and frequency  $\omega$ . There are two basic types of solutions. They are:

- (a) Acoustic wave modes.
- (b) Kelvin-Helmholtz instability waves.

The acoustic wave modes are solutions in which both  $k$  and  $\omega$  are real. The instability wave solutions involve real  $k$  and complex  $\omega$  with imaginary  $\omega$  greater than zero for temporal instability or real  $\omega$  and complex  $k$  for spatial instability. It is to be noted that for comparisons with experiments spatial instability waves are more relevant.

Acoustic wave solutions of dispersion relation (14) can further be divided into two classes with totally different characteristics. Those solutions, see Figure 3.2, which are located in the sector of the  $\omega$ - $k$  plane bounded by the lines  $\omega = ka_0(1 + M_0)$  and  $\omega = -ka_0(1 - M_0)$  including the  $\omega$ -axis are the diffuser duct modes. They are the regular duct acoustic modes modified by the presence of the supersonic jet. Solutions to the left of the line  $\omega = -ka_0(1 - M_0)$  are the upstream and downstream propagating acoustic wave modes associated with the supersonic jet. These modes are found and their importance recognized only recently (see ref. 3.1, 3.2 and 3.3). A rather remarkable characteristic of these wave modes is that they are attached and guided by the jet. The portion of the solution curve in the  $\omega$ - $k$  plane with negative group velocity ( $\partial\omega/\partial k < 0$ ) represents upstream waves. These acoustic wave modes propagate upstream toward the nozzle exit following the supersonic jet. One peculiar property of these upstream propagating wave modes is that they are confined to specific frequency bands. The implication of the unusual property of these modes will be discussed further later on.

### 3.2 Duct Acoustic Modes

The duct modes are given by the roots of (14), i.e.,  $\omega = \omega(k)$ . There are many duct modes. They are usually classified by the azimuthal mode number  $n$  ( $n = 0, 1, 2, 3, \dots$ ) and a radial mode number  $m$  ( $m = 1, 2, 3, \dots$ ).  $n = 0$  corresponds to the axisymmetric configuration.  $n = 1$  corresponds to the helical or flapping ( $n = \pm 1$ ) configuration. The radial mode number indicates the number of nodes the eigenfunction has in the radial direction.

Numerical solutions of (14) have been carried out at  $M_o = 0$  and  $M_j = 1.1, 1.2, 1.3, 1.4, 1.5$  and  $1.6$  for a flow geometry identical to that of the companion experiments. For each jet Mach number, the dispersion relation for  $n = 0, 1, 2$  and  $m = 1, 2, 3$  are calculated. They are expressed in nondimensional form  $W = W(k)$  where  $W = \omega R/u_j$  and  $k$  is nondimensionalized by  $R$ . The dispersion relations of these duct modes are shown in Figures 3.3 to 3.20. An examination of these dispersion relations indicate that for a given jet Mach number, the  $n = 1, m = 1$  mode has the lowest frequency. It is, therefore, the mode most likely to be excited. Since  $\omega$  is not a linear function of  $k$ , all the duct mode waves are dispersive. As is well-known the energy of dispersive waves propagate with group velocity  $\frac{\partial\omega}{\partial k}$ . Now if the group velocity of a wave is zero the energy of the wave will not propagate away. Instead it will remain localized. In the case of the jet ejector flow, these waves which are in a sense trapped inside the duct are prime candidates for inducing resonance. We will call these waves resonance waves. Figure 3.21 shows the calculated

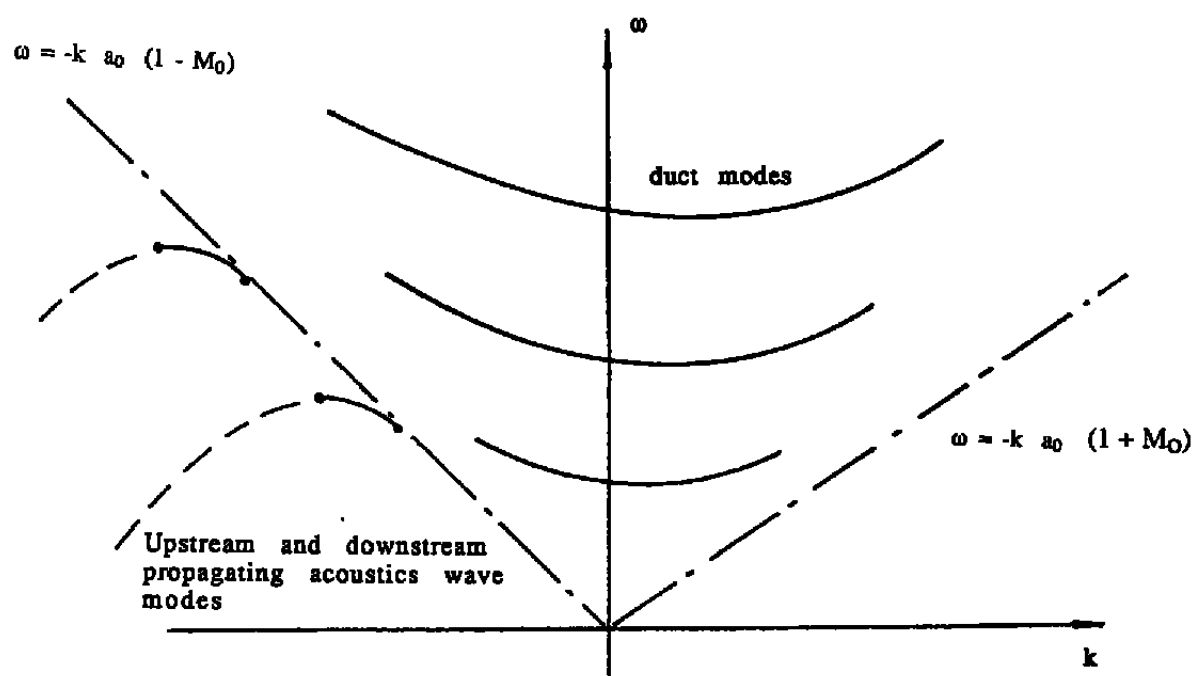


Figure 3.2 Locations of the duct modes and the upstream and downstream propagating acoustic wave modes in the  $\omega$ - $k$  plane

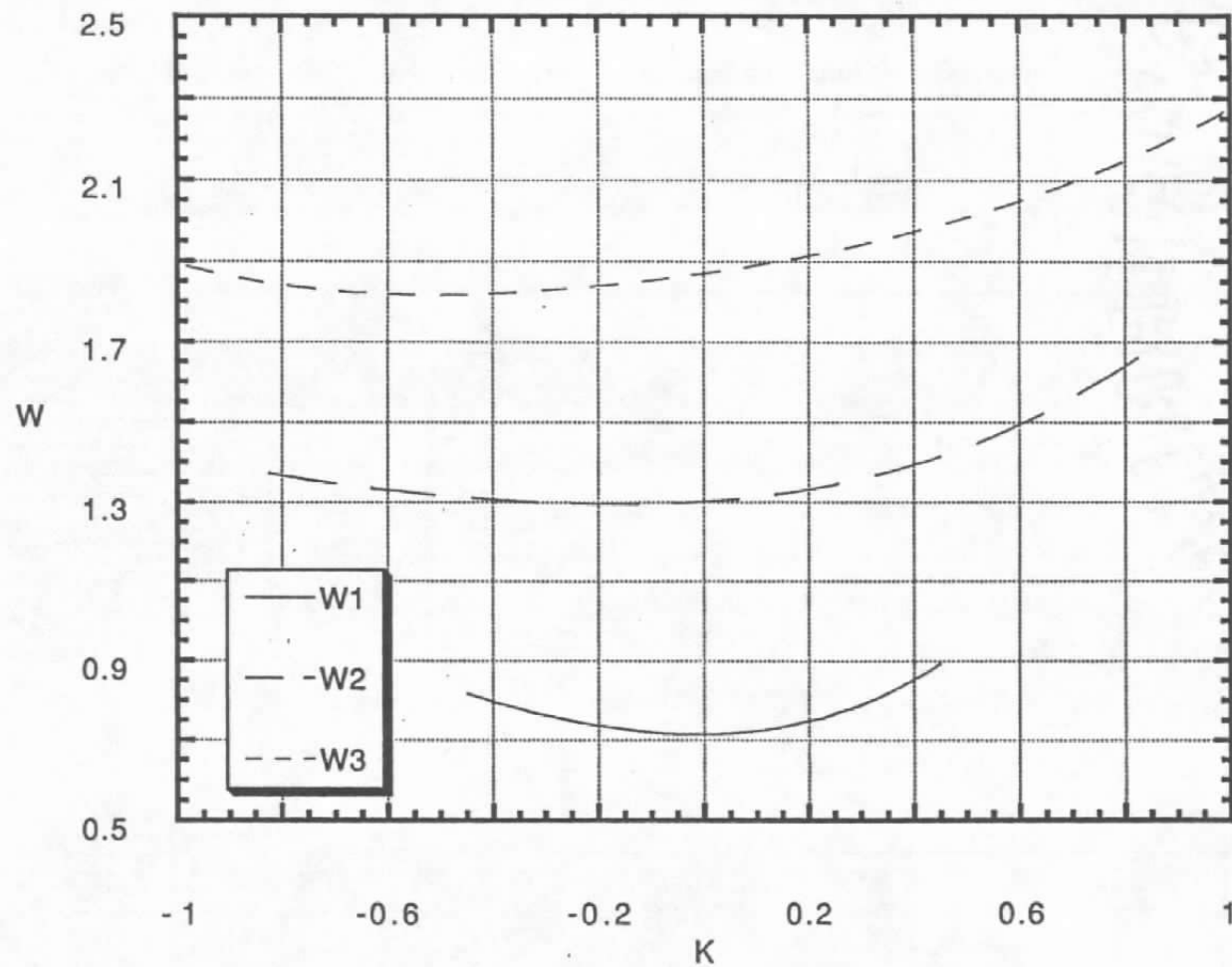


Figure 3.3 Dispersion relation of the first three radial duct modes at  $M_j=1.1$ , mode 0

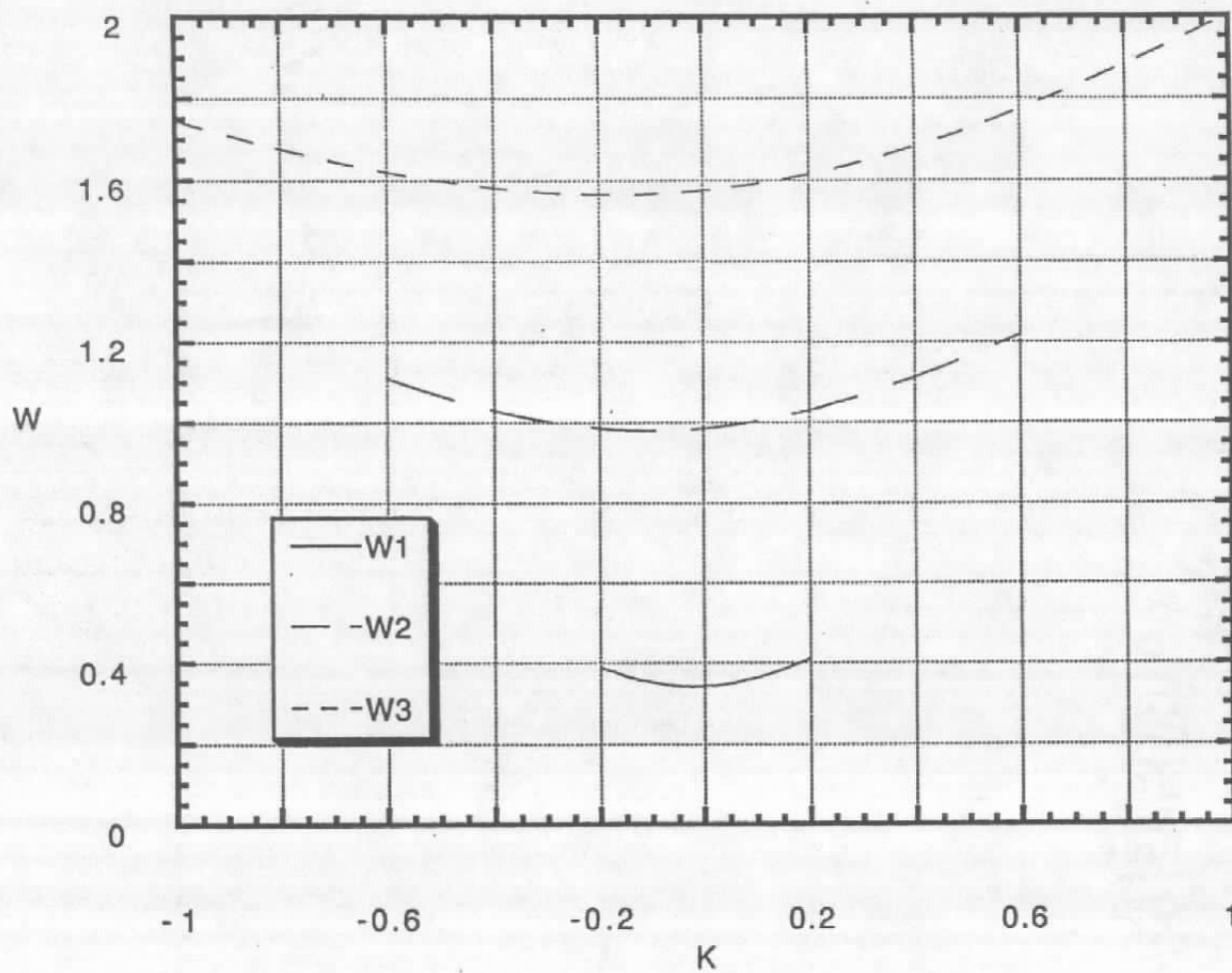


Figure 3.4

Dispersion relation of the first three radial duct modes  
at  $M_j=1.1$ , mode 1

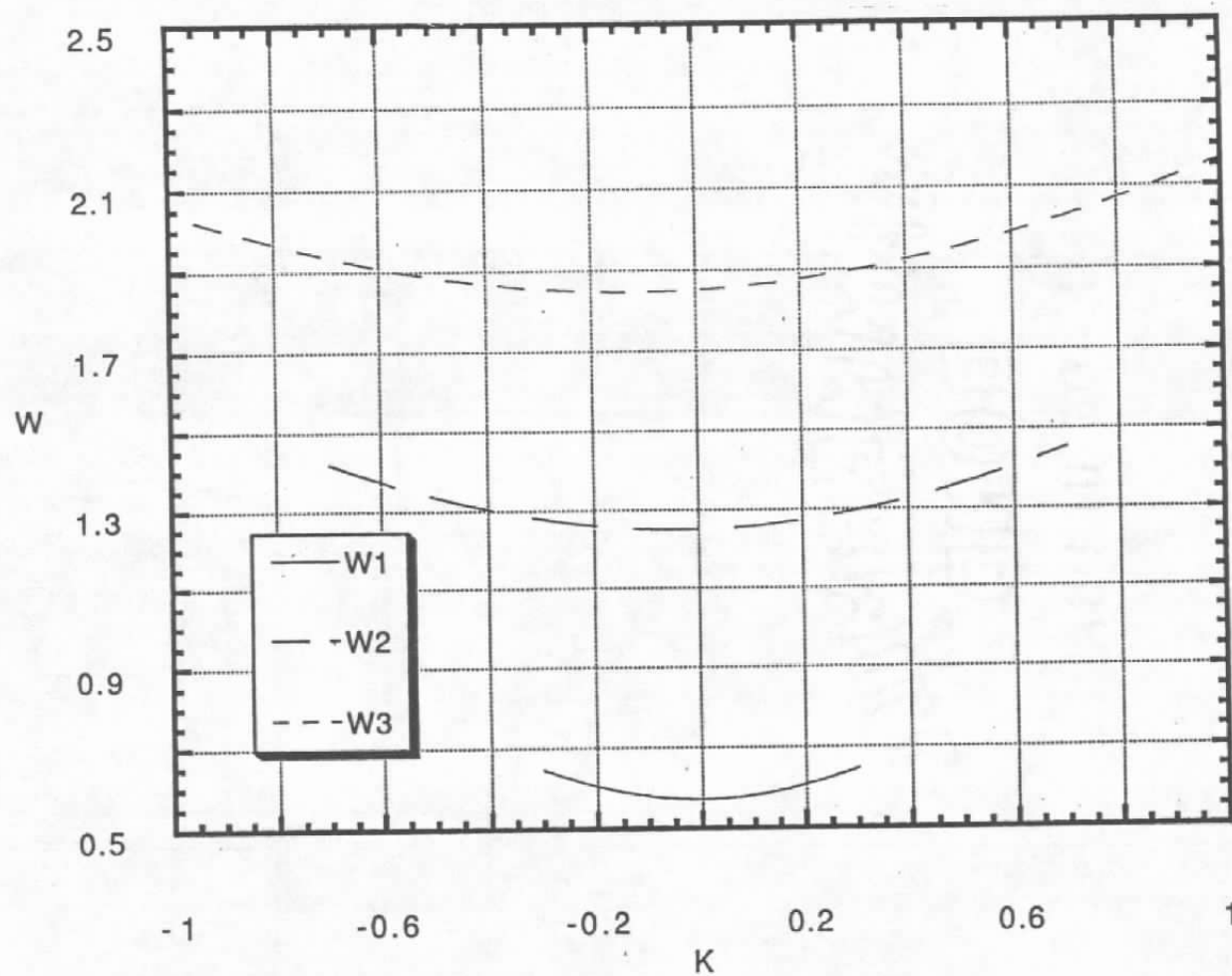


Figure 3.5 Dispersion relation of the first three radial duct modes at  $M_j=1.1$ , mode 2

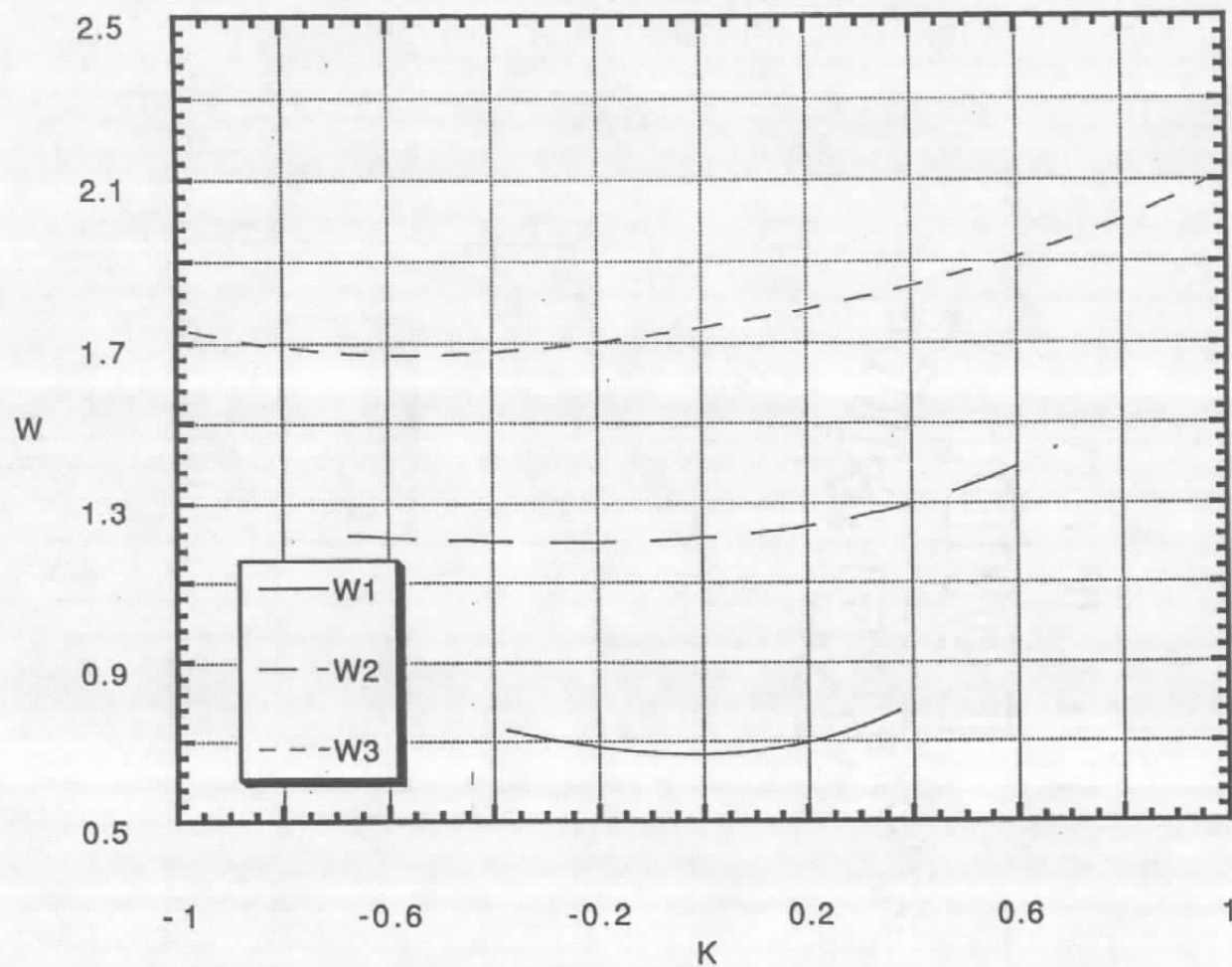


Figure 3.6 Dispersion relation of the first three radial duct modes at  $M_j=1.2$ , mode 0

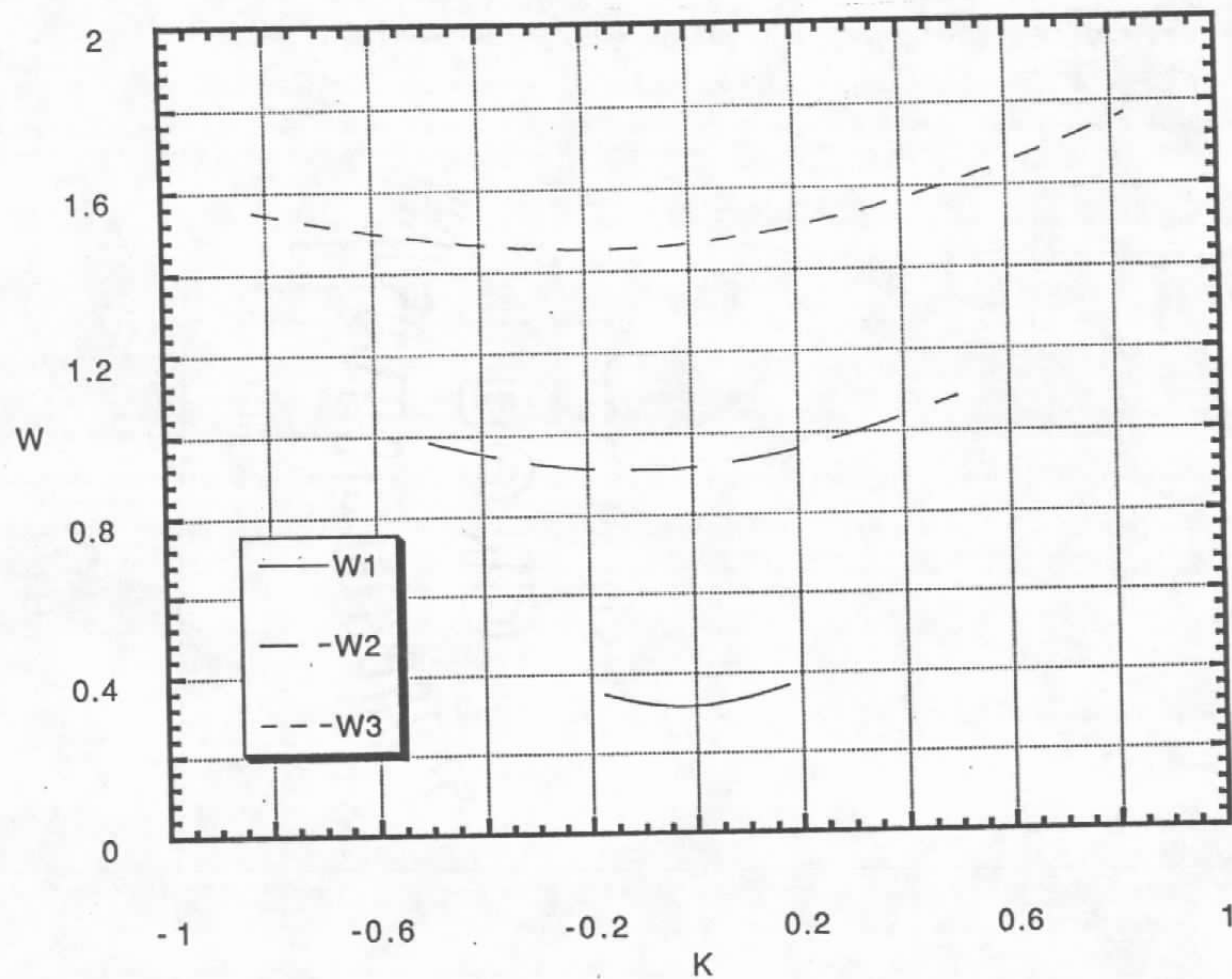


Figure 3.7 Dispersion relation of the first three radial duct modes at  $M_j=1.2$ , mode 1

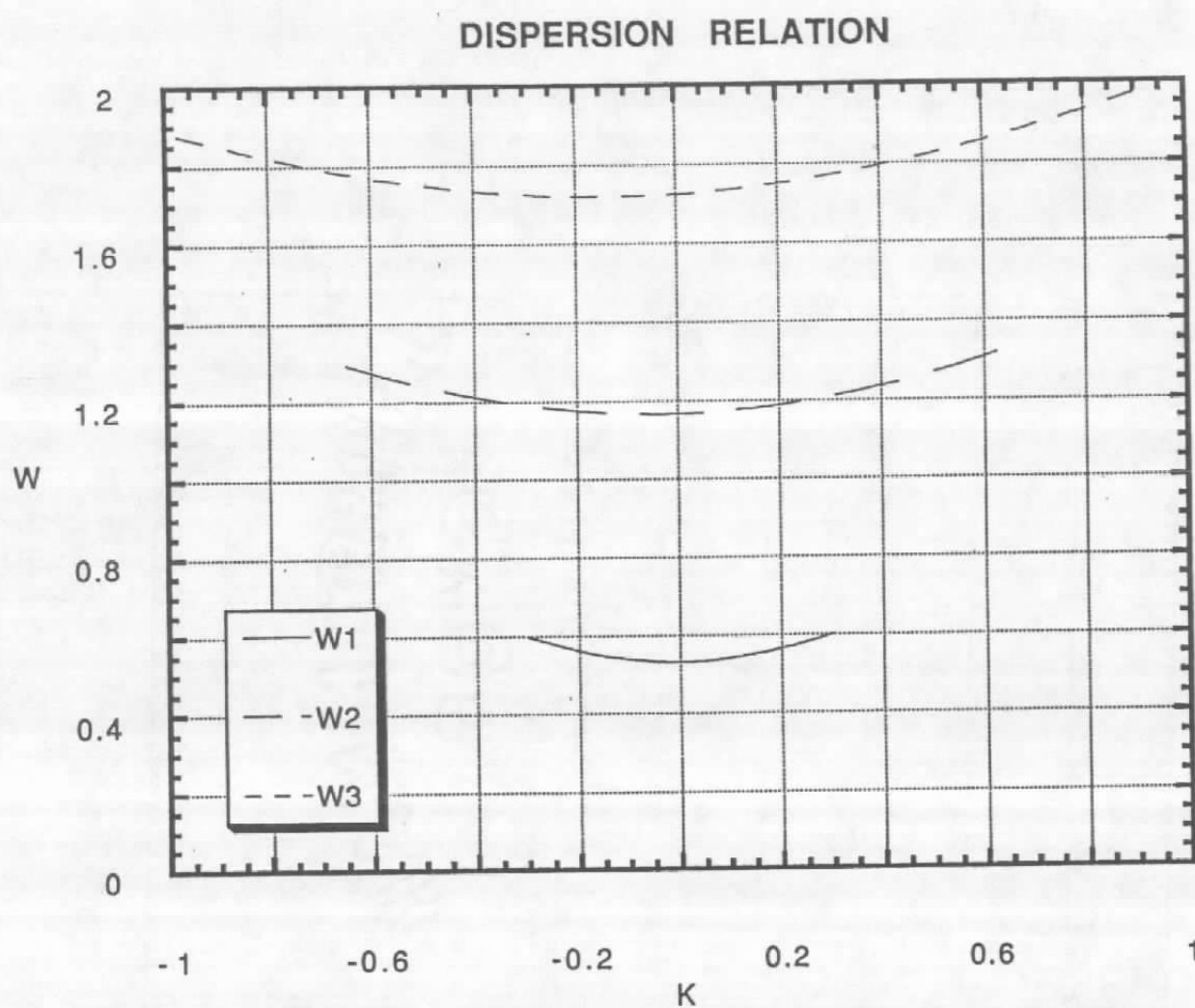


Figure 3.8

Dispersion relation of the first three radial duct modes  
at  $M_j=1.2$ , mode 2

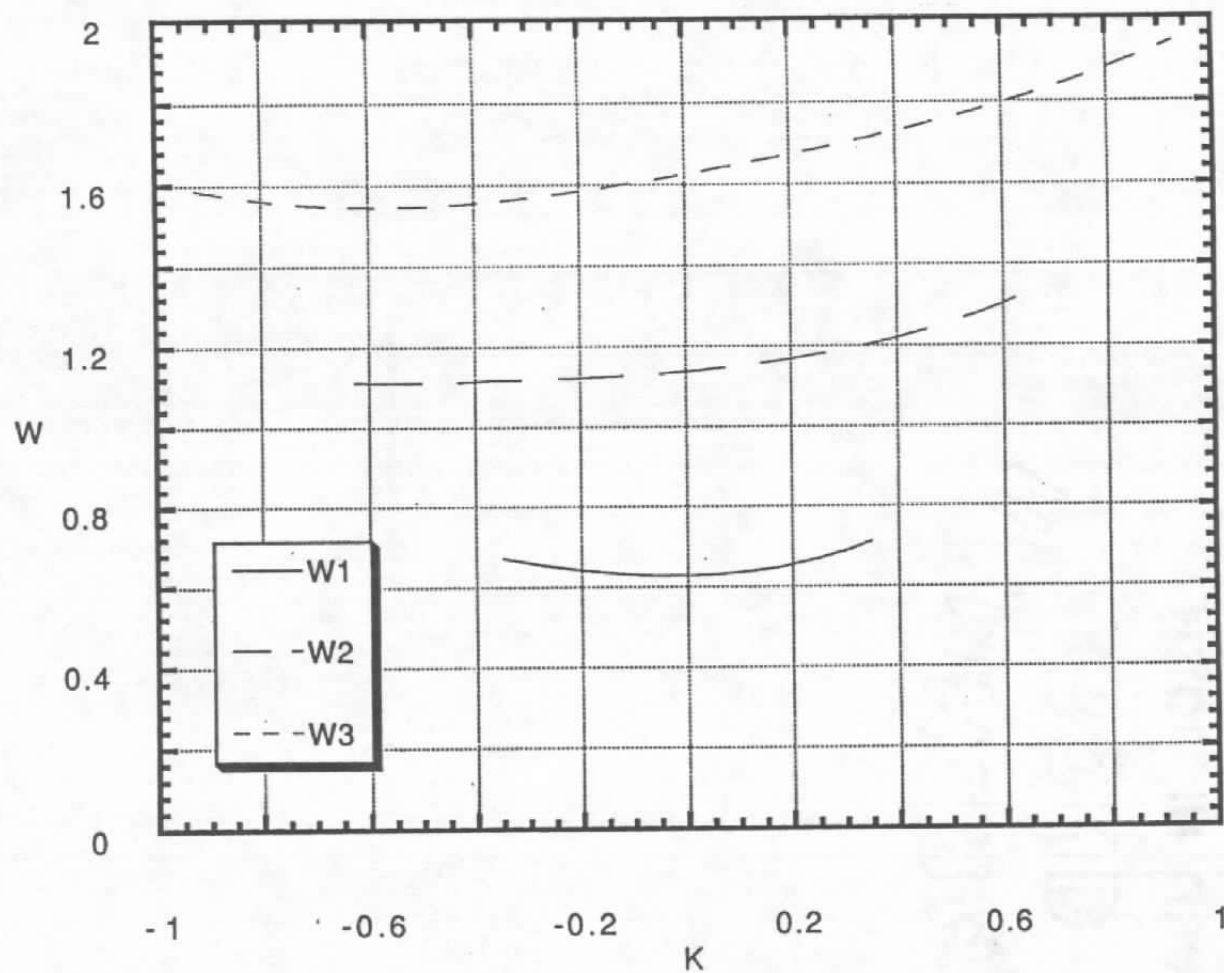


Figure 3.9 Dispersion relation of the first three radial duct modes at  $M_j=1.3$ , mode 0

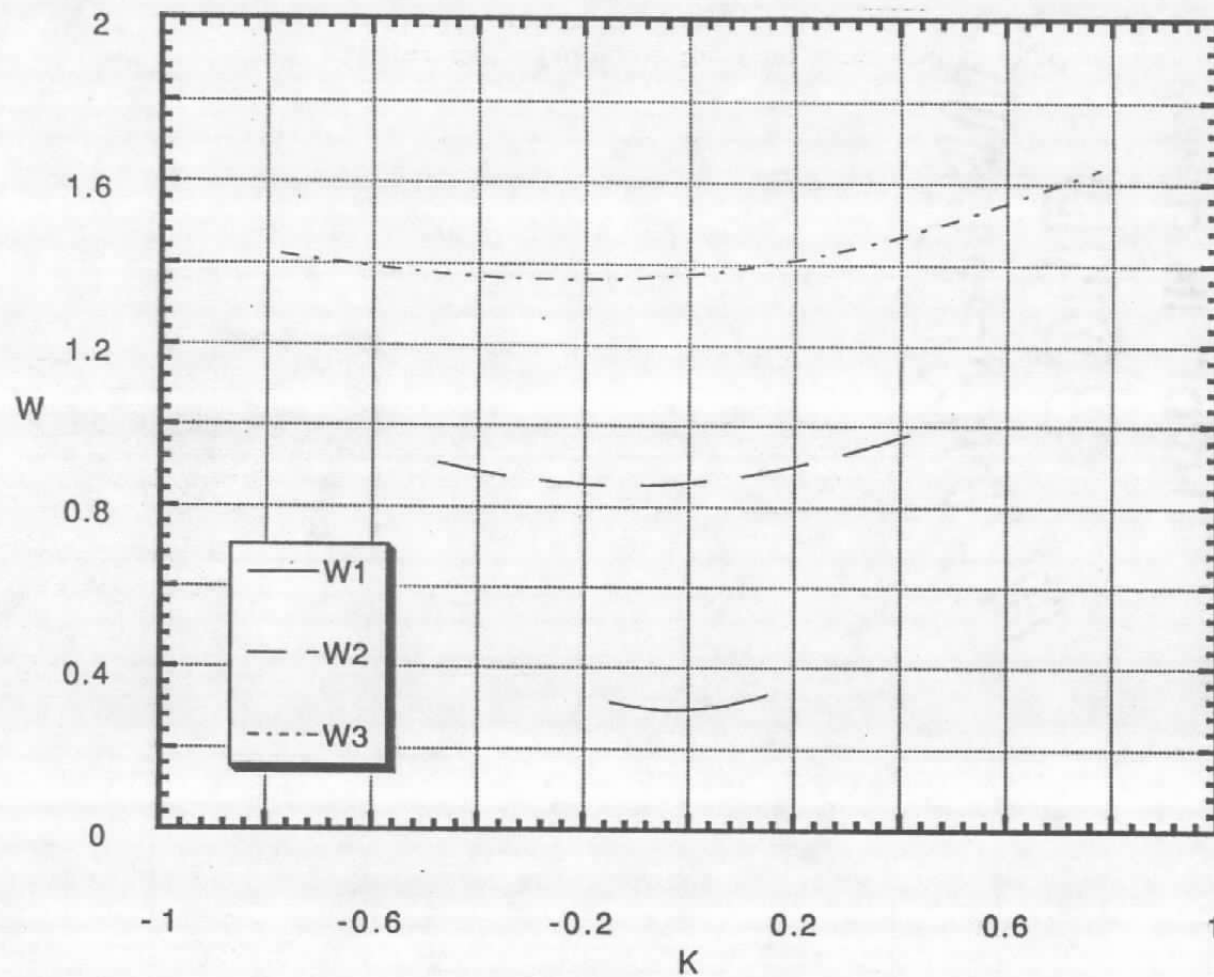


Figure 3.10 Dispersion relation of the first three radial duct modes at  $M_j=1.3$ , mode 1

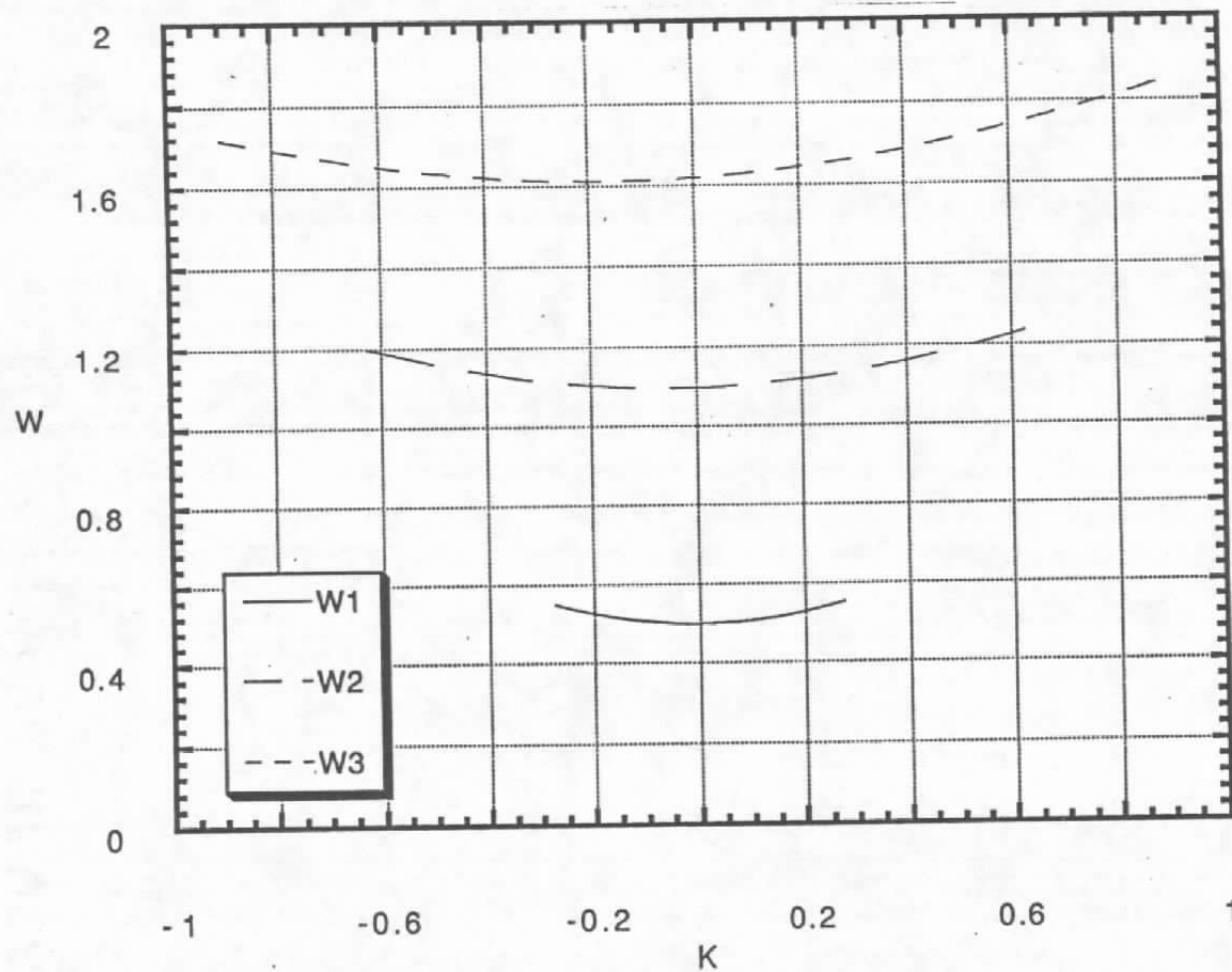


Figure 3.11 Dispersion relation of the first three radial duct modes at  $M_j=1.3$ , mode 2

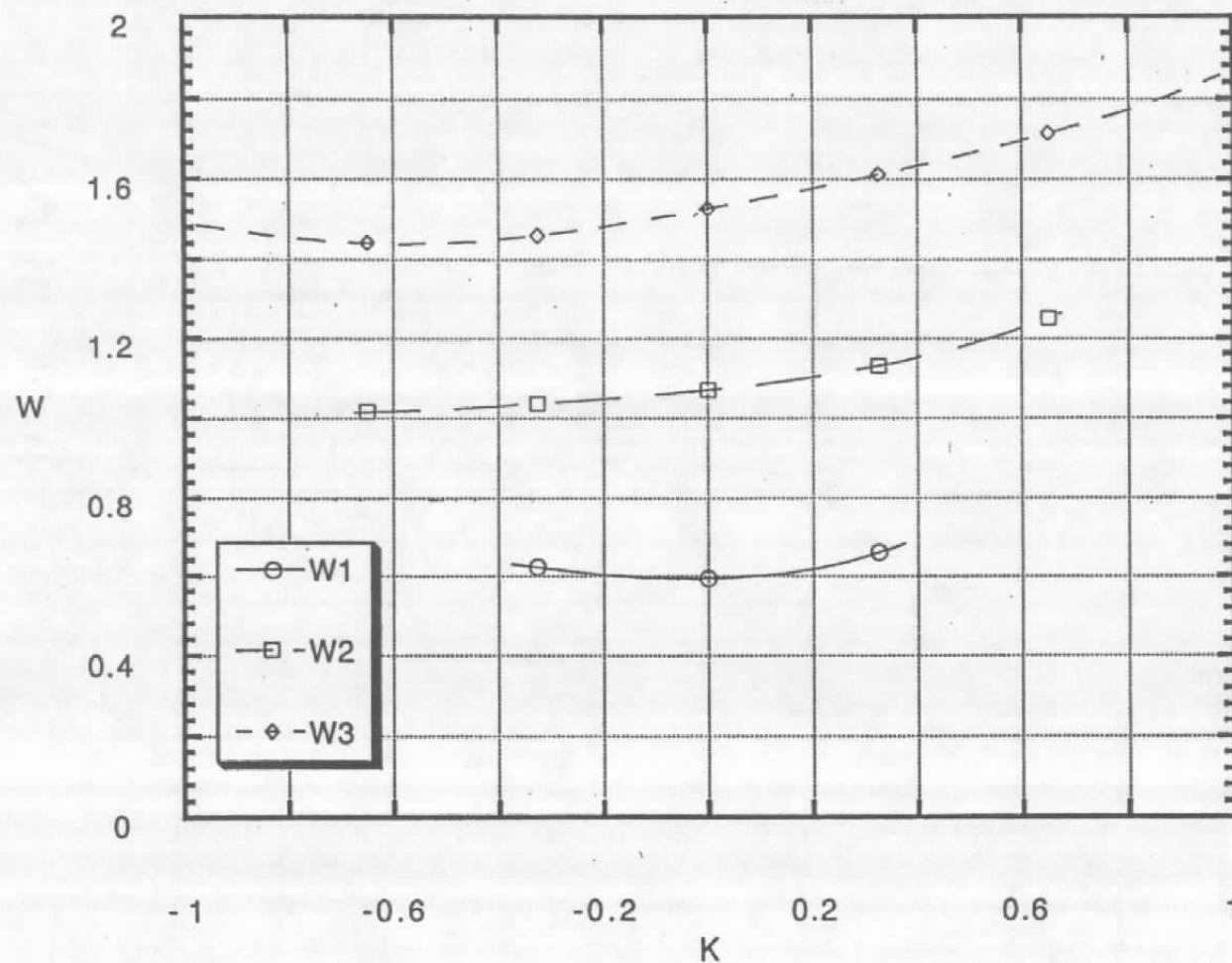


Figure 3.12 Dispersion relation of the first three radial duct modes at  $M_j=1.4$ , mode 0

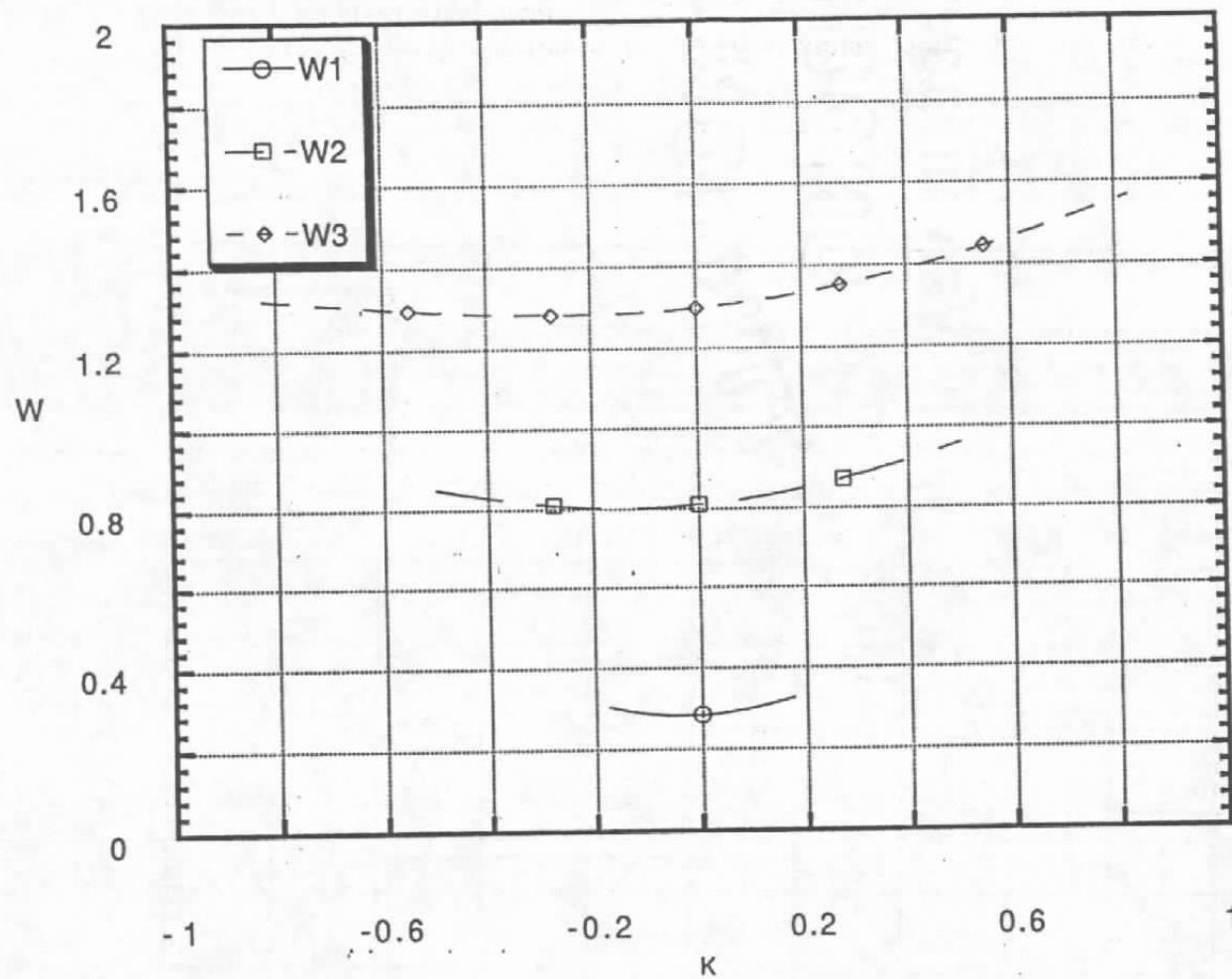


Figure 3.13 Dispersion relation of the first three radial duct modes at  $M_j=1.4$ , mode 1

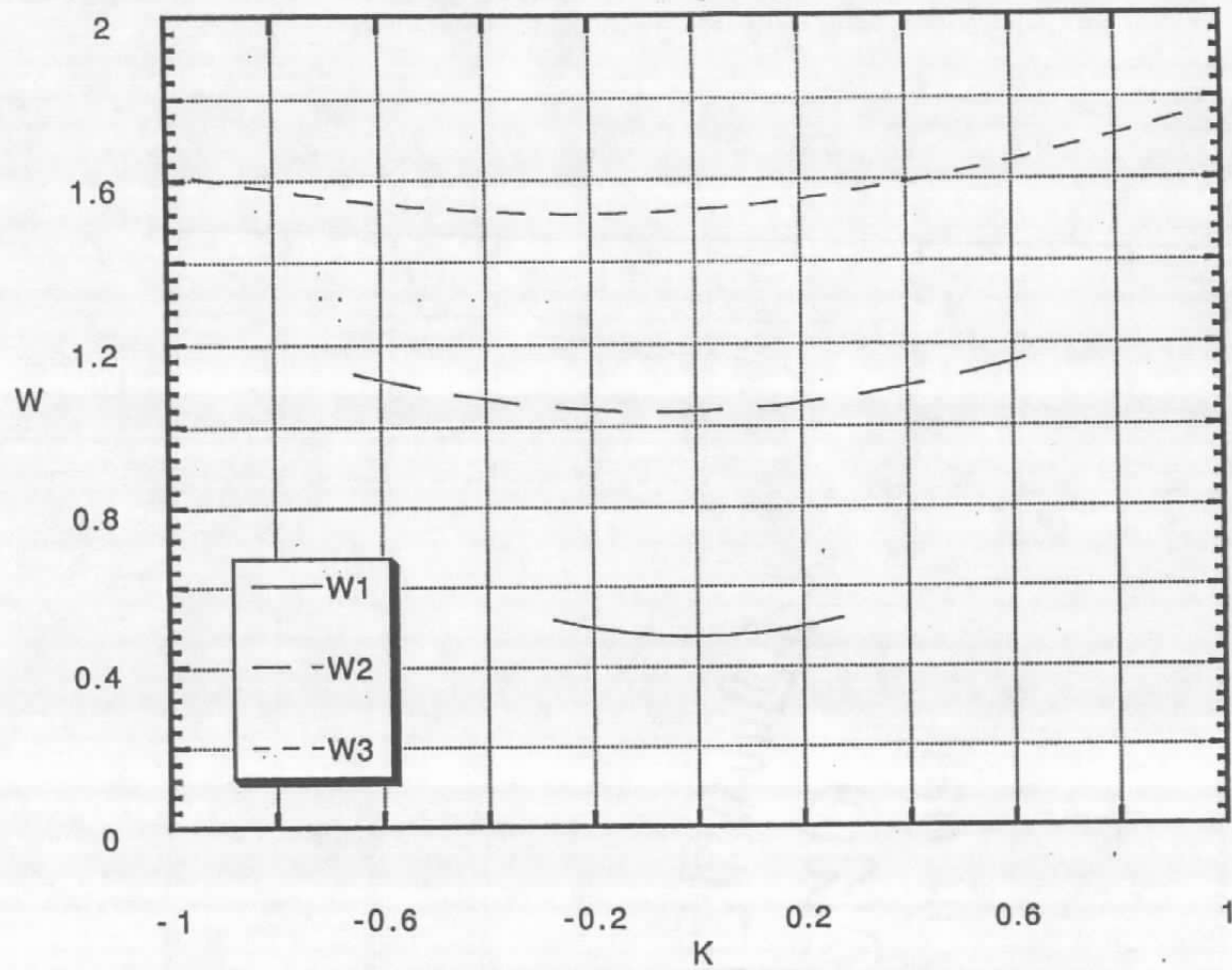


Figure 3.14 Dispersion relation of the first three radial duct modes at  $M_j=1.4$ , mode 2

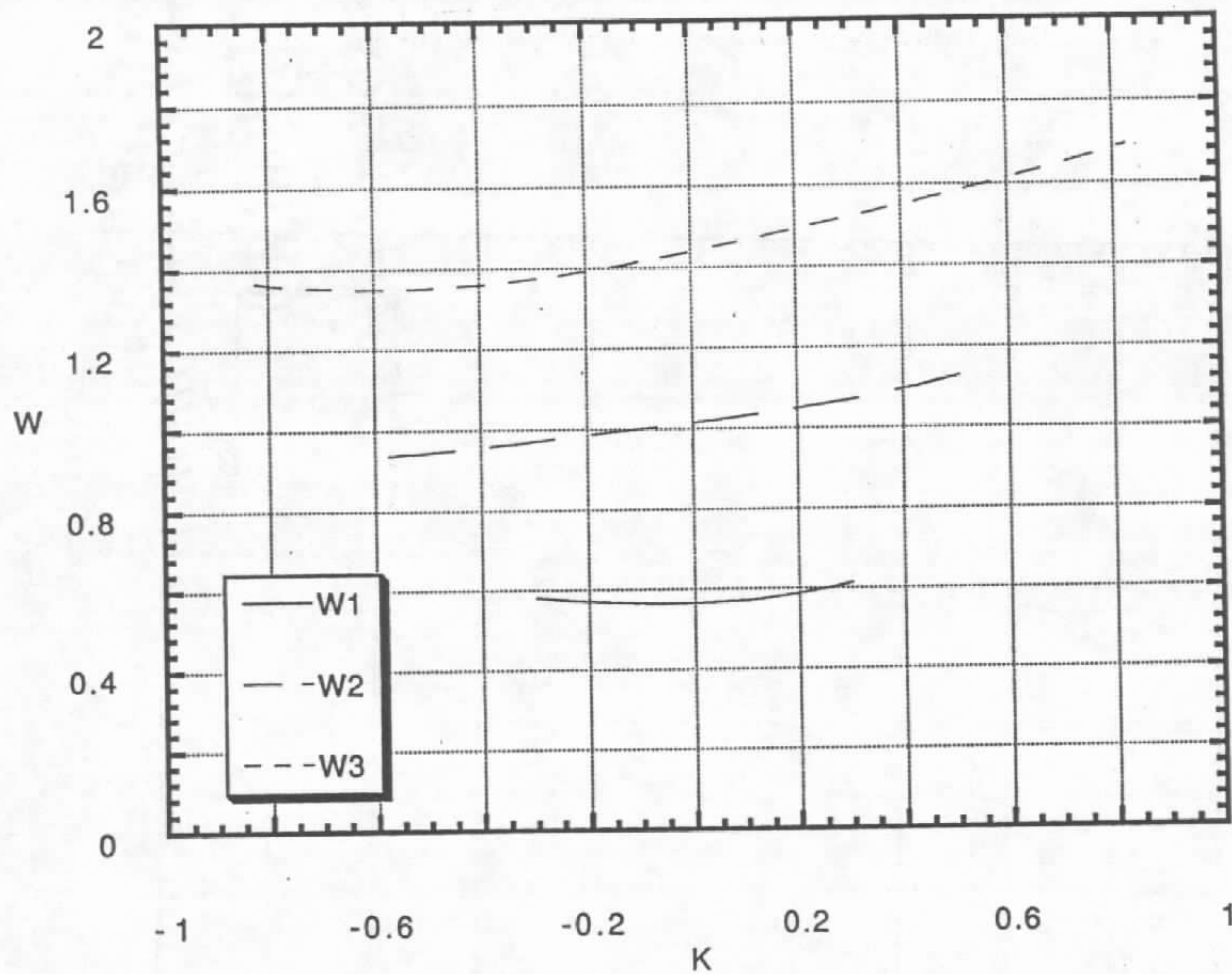


Figure 3.15 Dispersion relation of the first three radial duct modes at  $M_j=1.5$ , mode 0

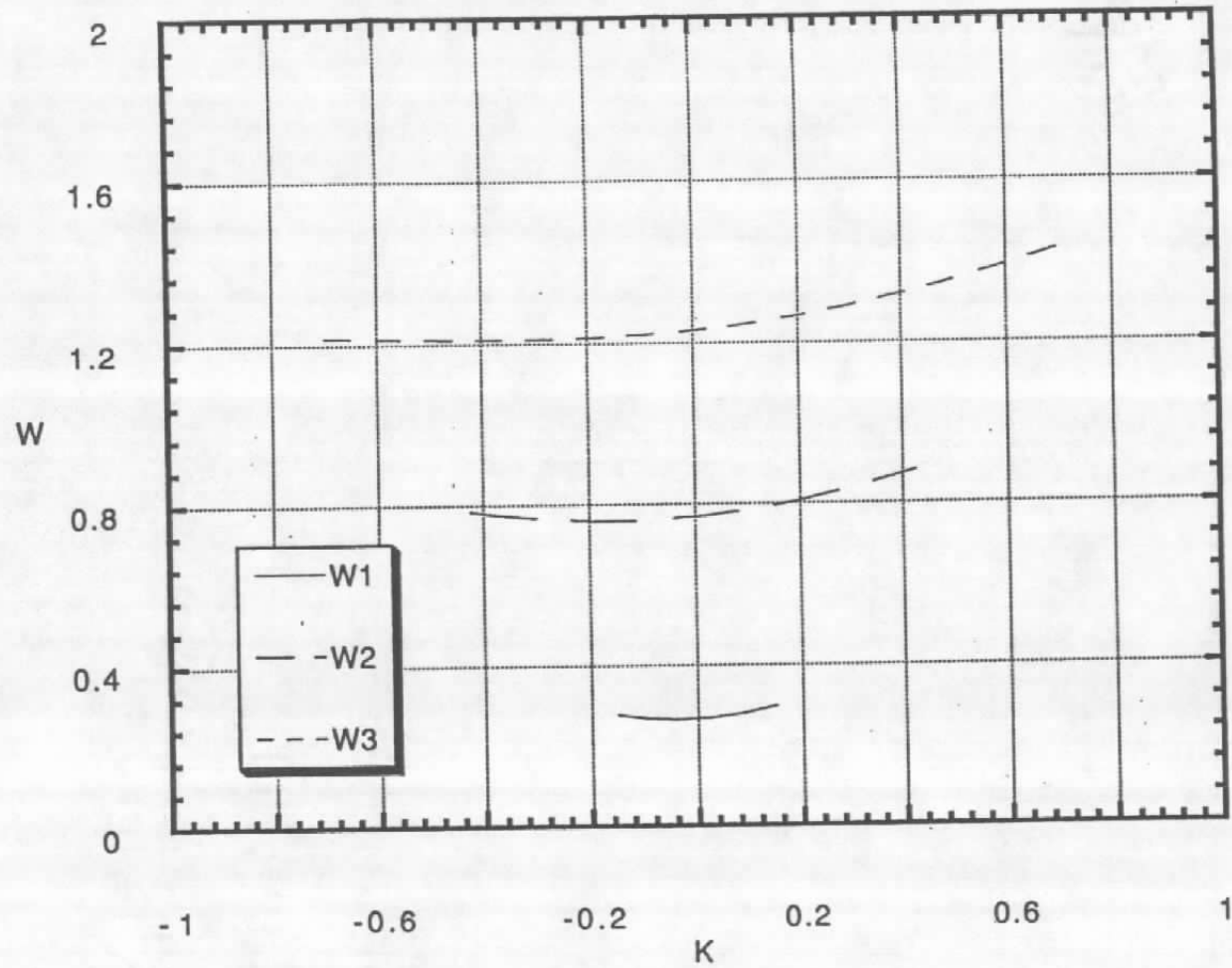


Figure 3.16 Dispersion relation of the first three radial duct modes at  $M_j=1.5$ , mode 1

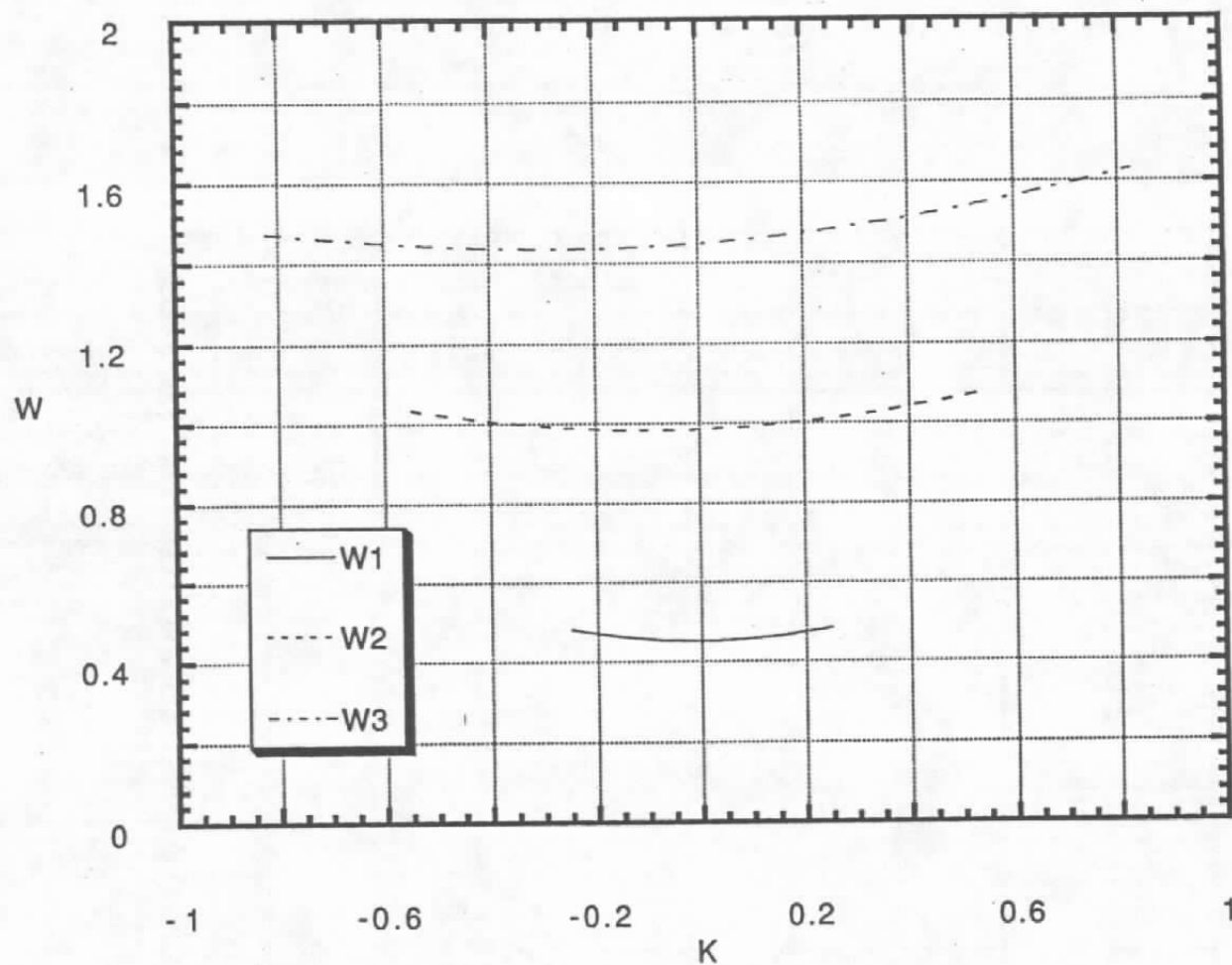


Figure 3.17 Dispersion relation of the first three radial duct modes at  $M_j=1.5$ , mode 2

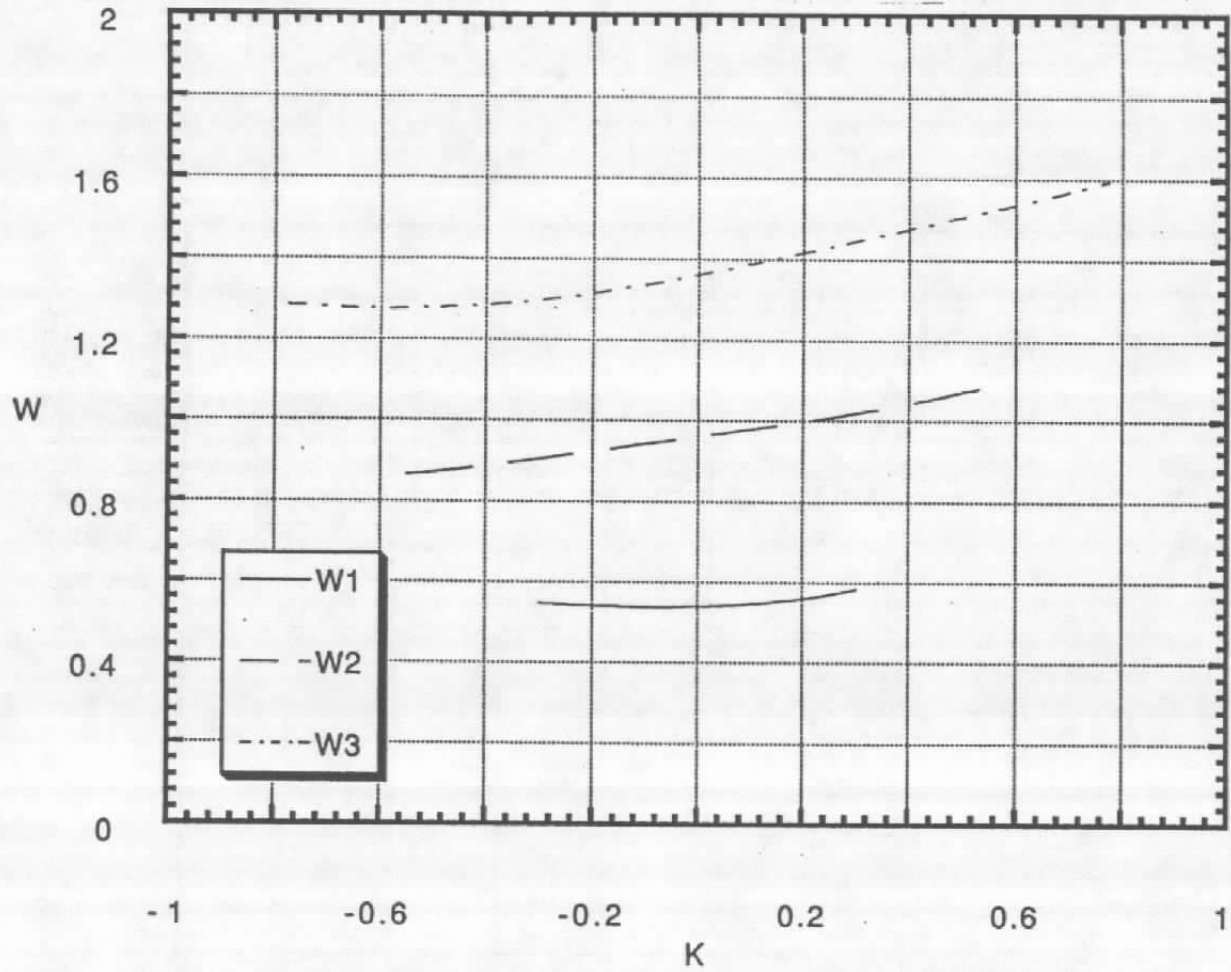


Figure 3.18 Dispersion relation of the first three radial duct modes at  $M_j=1.6$ , mode 0

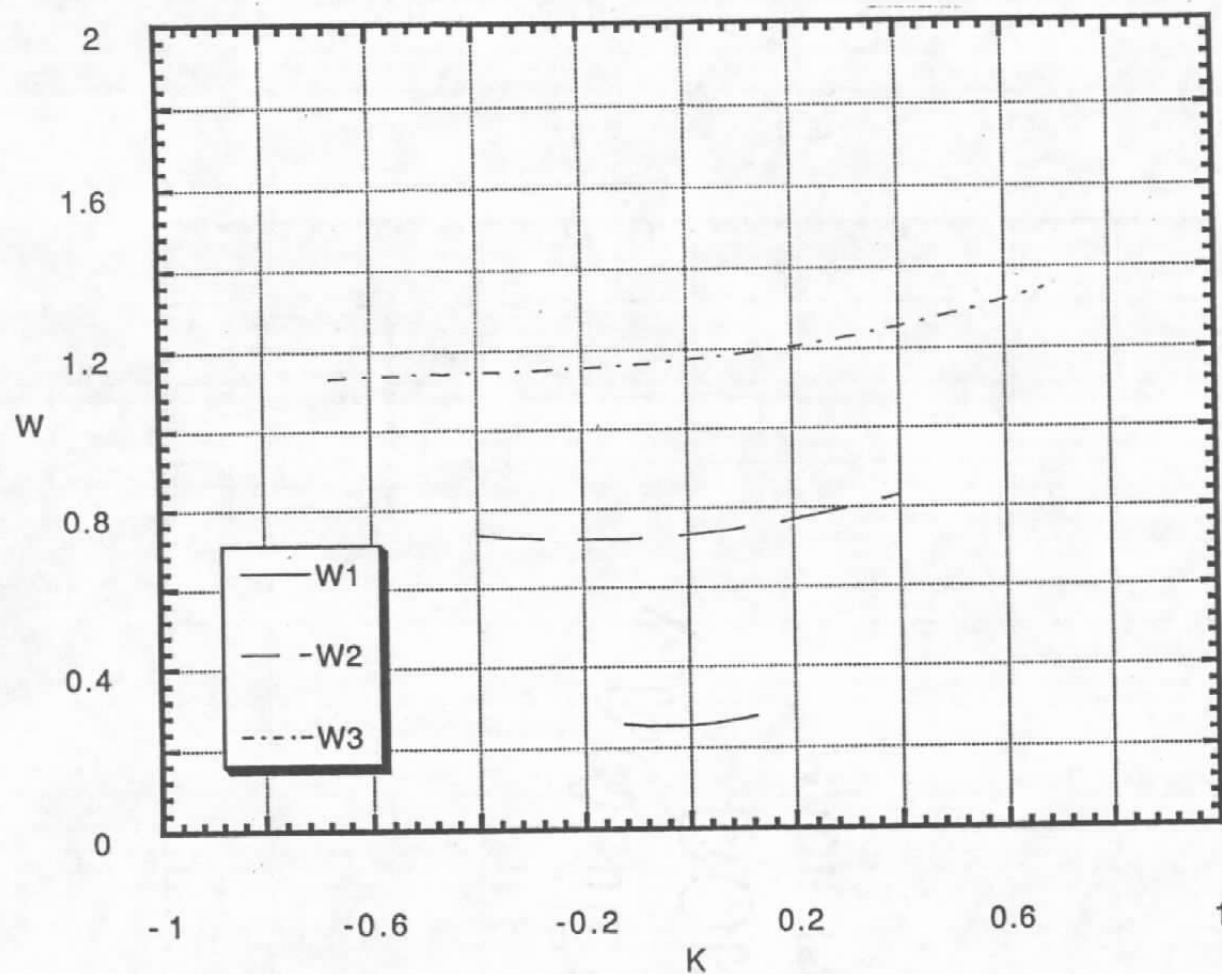


Figure 3.19 Dispersion relation of the first three radial duct modes at  $M_j=1.6$ , mode 1

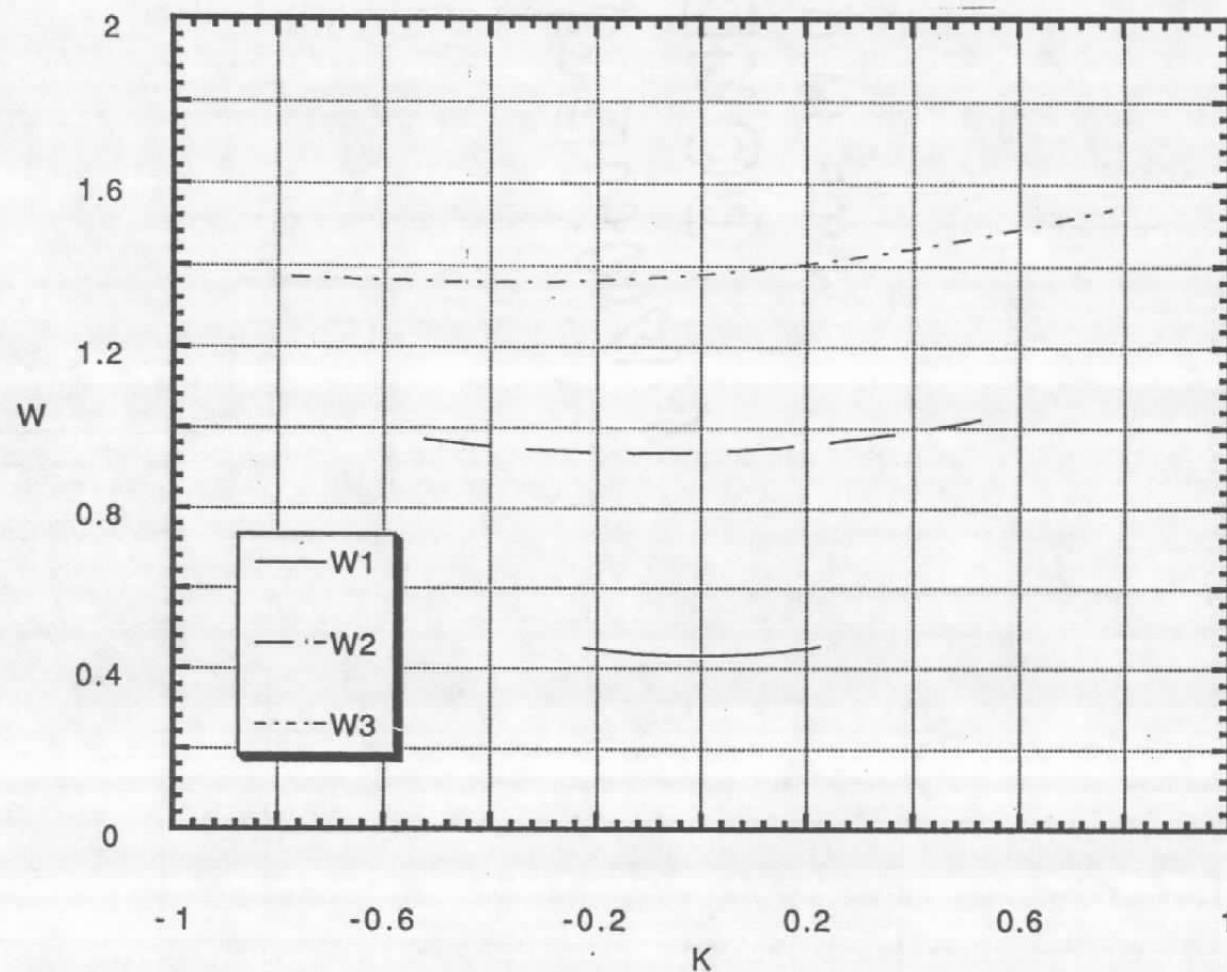


Figure 3.20 Dispersion relation of the first three radial duct modes at  $M_j=1.6$ , mode 2

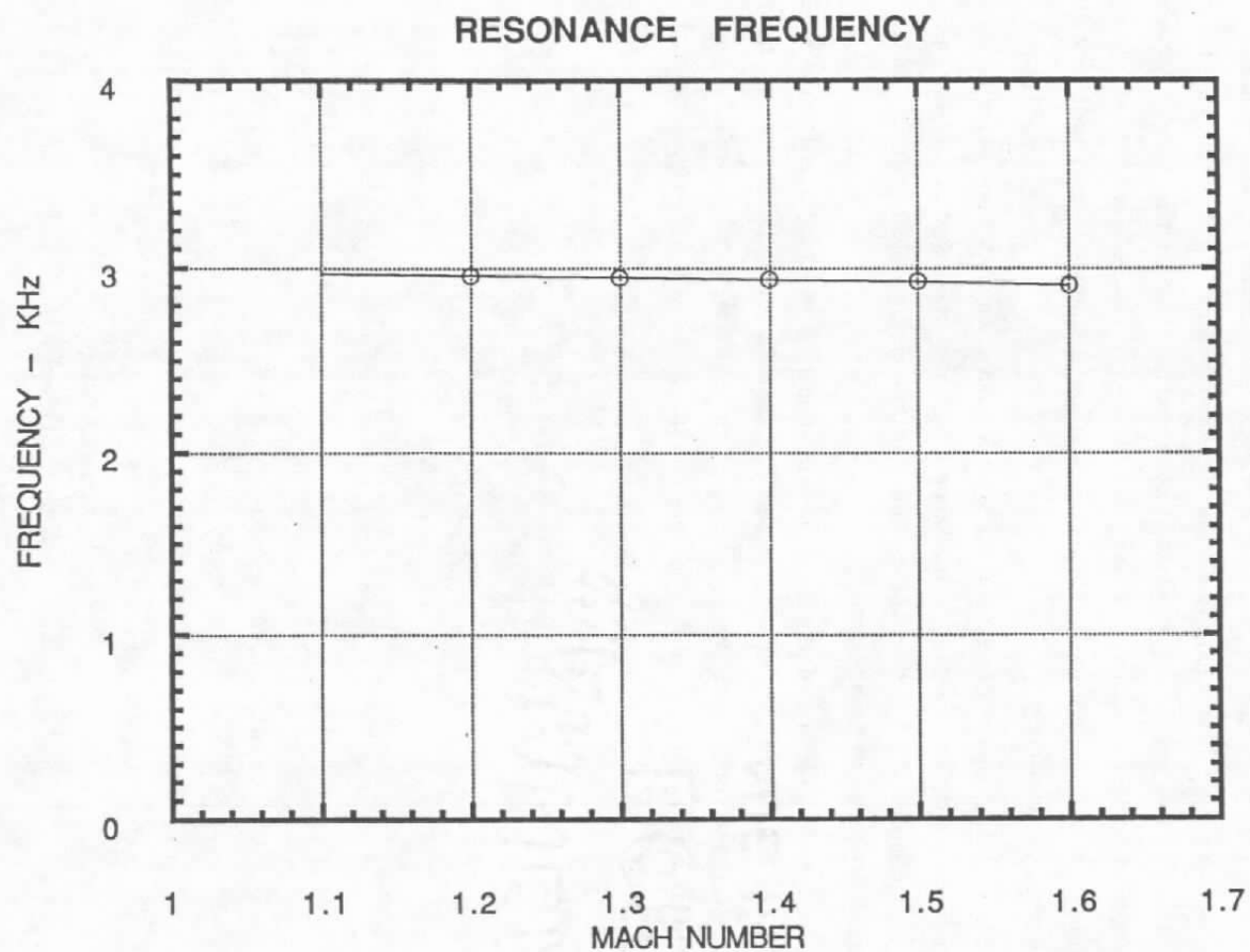


Figure 3.21 CALCULATED RESONANCE FREQUENCIES FOR THE GTRI EXPERIMENT

resonance frequency of the  $n = 1, m = 1$  duct mode as a function of jet Mach number for the companion experiments. It turns out, for all intents and purposes, the calculated resonance frequency is approximately equal to 3 KHz. The experimentally measured resonance frequency (for the long ejector) varies from 3.4 KHz at Mach number 1.1 to 4.2 KHz at the higher Mach numbers. The agreement is not perfect but is quite close. On considering the fact that a very simple mathematical model is used in the calculation the agreement must be considered as very encouraging. The relatively close agreement strongly supports the contention that the observed low frequency tone is probably due to helical duct mode resonance.

The physical model described in Figure 3.1 assumes that the ejector is infinitely long. For finite length ejector the normal acoustic modes must also satisfy the open end boundary conditions. In this case, there is no continuous dispersion relation. Instead the normal mode frequencies are discrete.

Consider an ejector of diameter  $D$  and length  $L$  as shown in Figure 3.22. It will be assumed for simplicity that the open end boundary condition  $p = 0$ , where  $p$  is the fluctuating pressure, is adequate. The solution of the Helmholtz equation (no mean flow) with solid wall and open end boundary conditions gives the following normal mode frequency formula

$$f_{lmn} = \left[ \sigma_{nm}^2 + \left( \ell \frac{\pi D}{2L} \right)^2 \right]^{1/2} \frac{a_0}{\pi D}$$

$$n, \ell = 0, 1, 2, 3, \dots$$

$$m = 1, 2, 3, \dots$$

where

$\ell$  = longitudinal mode number

$n$  = azimuthal mode number

$m$  = radial mode number

$a_0$  = ambient speed of sound

$\sigma_{nm}$  = roots of  $J'_n$  (prime denotes derivative)

i.e.,  $J'_n(\sigma_{nm}) = 0$ ,  $J_n$  is the Bessel function of order  $n$ .

For the companion experiments  $a_0/(\pi D) = 1.626$  KHz. In the order of increasing

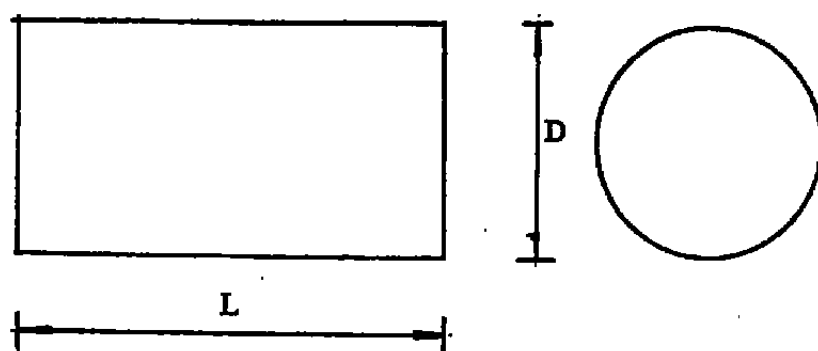


Figure 3.22 A circular ejector of length  $L$  and diameter  $D$

frequency, the first five frequencies are:

$L/D = 1$	$L/D = 3$
$f_{011} = 2.99 \text{ KHz}$	$f_{011} = 2.99 \text{ KHz}$
$f_{111} = 3.93$	$f_{111} = 3.11$
$f_{021} = 4.97$	$f_{211} = 3.44$
$f_{121} = 5.58$	$f_{021} = 4.97$
$f_{211} = 5.92$	$f_{121} = 5.04$

### 3.3 The Dominant Kelvin-Helmholtz Instability Wave

Dispersion relation (14) yields spatial instability wave (Kelvin-Helmholtz) solutions with real  $\omega$  and complex  $k(k = k_r + ik_i)$  where  $k_i < 0$ . If  $R_0 \rightarrow \infty$ , the solutions correspond to those of an unducted or free jet. It turns out for the ejector geometry of the companion experiment, there is only weak coupling between the duct and the instability waves of the jet. Thus it is sufficient to examine the instability wave characteristics of the jet as if it is totally free.

The vortex sheet model jet which gives rise to dispersion relation (14) is a good approximation of the jet flow only near the nozzle exit where the jet mixing layer is thin. Due to entrainment, the jet spreads out in the downstream direction. Experimentally, it is found that the mean velocity profile of the jet in the core region can be closely approximated by a Gaussian function.

$$\frac{u}{u_j} = \begin{cases} 1, & r < h \\ \exp[-(\ell n 2)(\frac{r-h}{h})^2], & r > h \end{cases}$$

where  $h$  is the radius of the core of the jet and  $b$  is the half-width of the mixing layer. The parameters  $h$  and  $b$  are related by the requirement of conservation of momentum flux:

$$\int_0^{\infty} \rho u^2 r dr = \frac{1}{2} \rho_j u_j^2 R_j^2$$

where  $\rho_j$ ,  $u_j$ , and  $R_j$  are the fully expanded jet density, velocity and radius respectively. The case of a vortex sheet model jet can be recovered by letting  $b/R_j \rightarrow 0$ . It is also found experimentally and justified by similarity arguments that  $b$  is a linear function of the downstream distance  $x$ , i.e.,  $db/dx = \sigma$  (constant), measured from the nozzle exit.

As an instability wave propagates downstream it sees a slowly changing mean flow. As a result its spatial growth rate,  $-k_i$ , varies in the downstream direction. Due to the

spreading of the jet, the shear gradient which drives the instability wave decreases with  $x$ , so that all instability waves regardless of frequency will eventually become neutral and then damped. For circular jets, the instability waves can be decomposed azimuthally into Fourier modes in the form of equation (5). The lowest order modes are the axisymmetric ( $n = 0$ ) and the helical or flapping modes ( $n = 1$ ). Under a given jet operating condition, generally, one of these wave modes is more dominant and most likely to be observed. The dominance depends primarily on the jet Mach number and to a lesser degree on the jet to ambient temperature ratio. The relative dominance of these waves can be quantified by determining the total spatial amplification of the waves.

The local spatial growth rate of an instability wave is given by  $-k_i$ . In general,  $-k_i$  depends on  $S$  (the Strouhal number),  $n$  (the azimuthal mode number),  $M_j$  (the Mach number of the jet) and  $b$  (the half-width of the mixing layer of the jet), i.e.,  $k_i = k_i(S, n, M_j, b)$ . Suppose at a downstream location where the mixing layer has a half-width  $b_c$ , the instability wave attains its maximum amplitude or  $k_i(S, n, M_j, b_c) = 0$ . Then the total spatial amplification of the wave would be equal to,

$$\exp \left[ -\frac{1}{\sigma} \int_{b_0}^{b_c} k_i(S, n, M_j, b) db \right]$$

where  $\sigma$  is the spreading rate and  $b_0$  is the initial half-width of the mixing layer. For a jet with a given Mach number, the most amplified instability wave is the one having a Strouhal number  $S$  and a mode number  $n$  which maximize the above integral. Numerical values of the above integral for cold jets with Mach number 1.1 to 2.0 at 0.1 Mach number increment have been computed. They are given in Figures 3.23 through 3.32 as functions of Strouhal number. In each case the lowest three modes,  $n = 0, 1, 2$ , are calculated. It is seen that, at low supersonic Mach number ( $M_j < 1.2$ ), the axisymmetric mode ( $n = 0$ ) is slightly more dominant. However, at higher Mach number, the helical mode ( $n = 1$ ) clearly is the most amplified and dominant. The switch in dominance from the axisymmetric to the helical mode as jet Mach number increases is experimentally observable. Its implication on the dynamics of the screech tone feedback loop of free or ducted supersonic jets will be discussed in the next section.

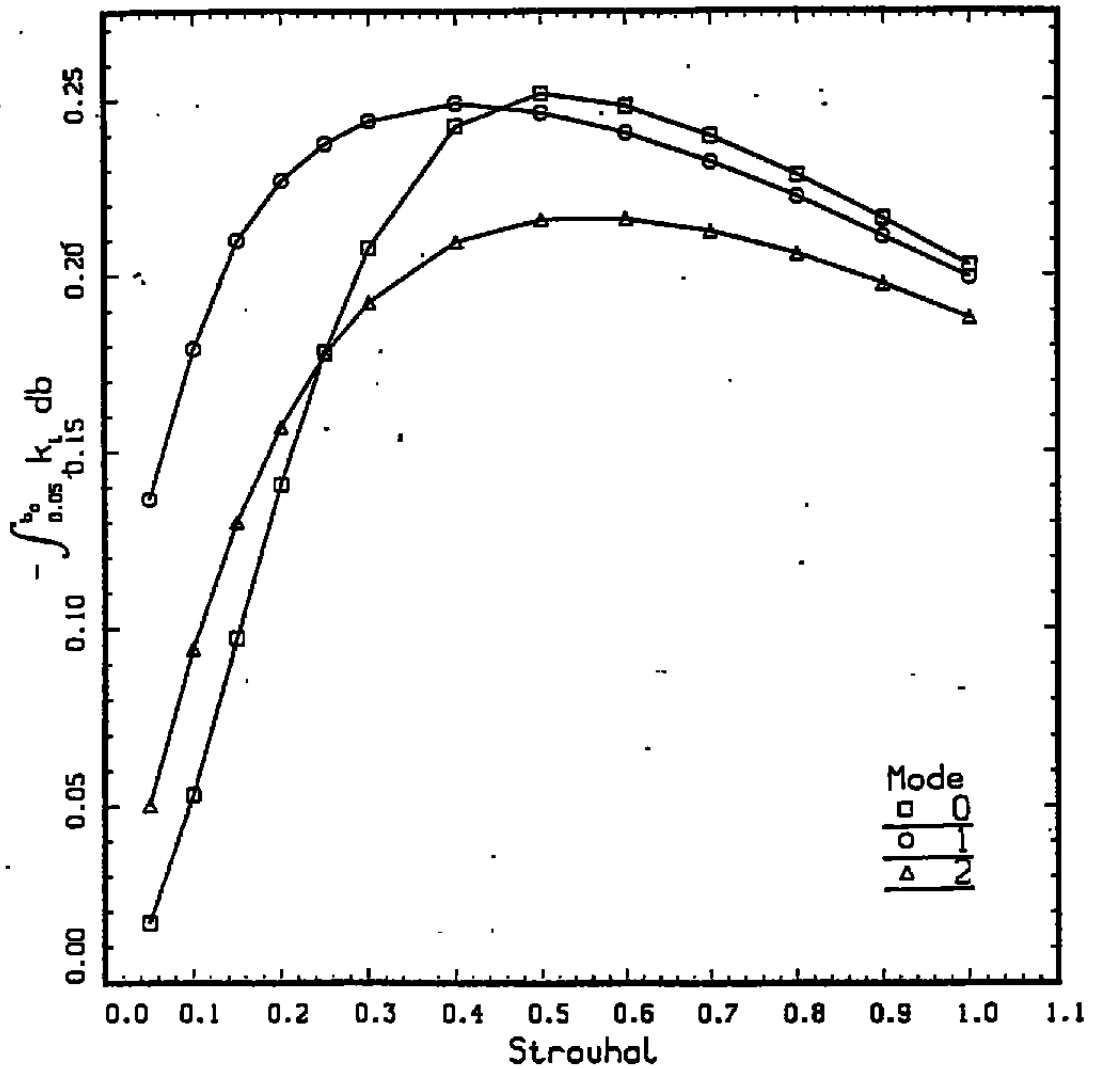


Figure 3.23 Total spatial growth rate of the instability waves of a Mach 1.1 supersonic jet as a function of Strouhal number

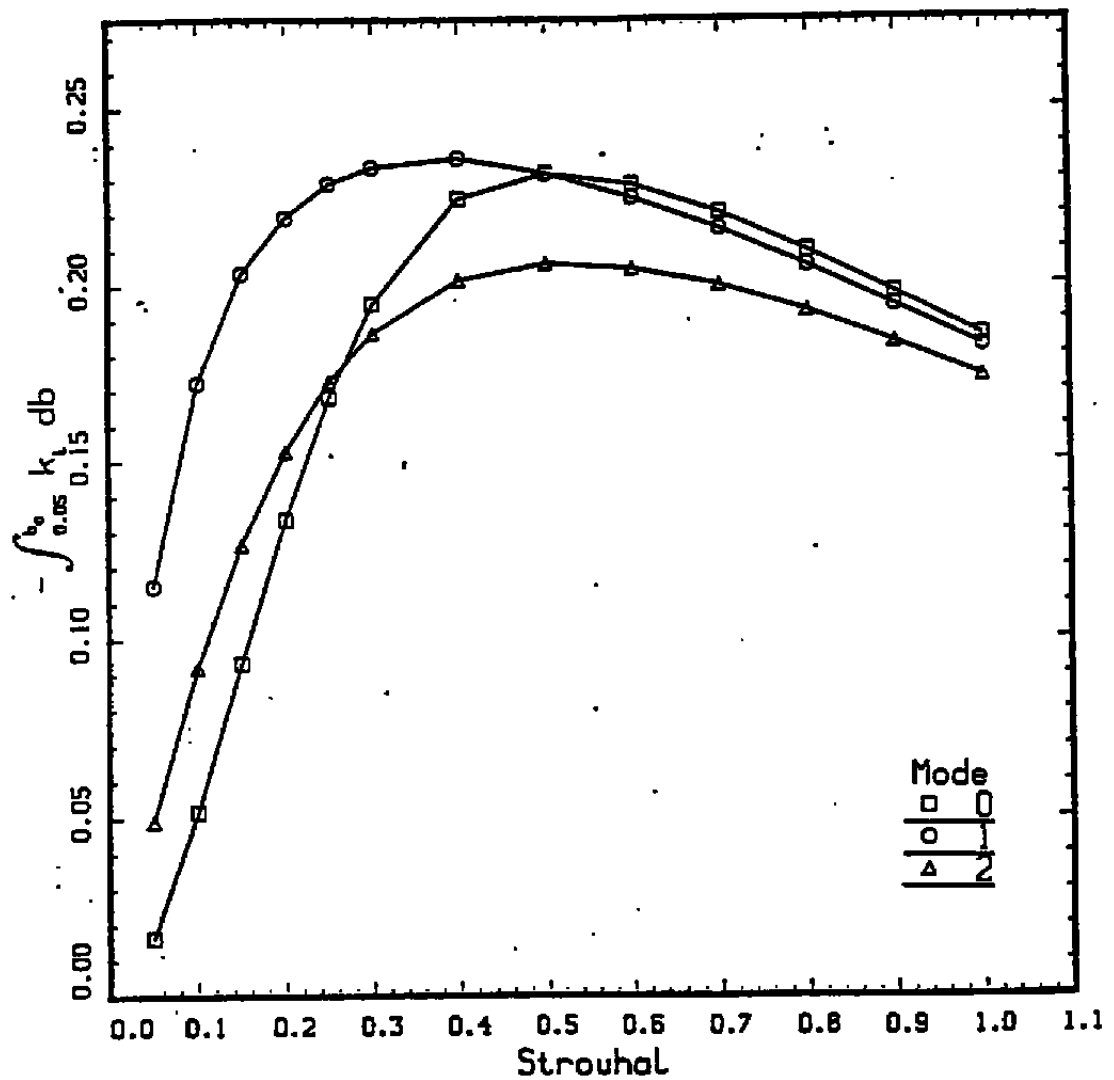


Figure 3.24 Total spatial growth rate of the instability waves of a Mach 1.2 supersonic jet as a function of Strouhal number

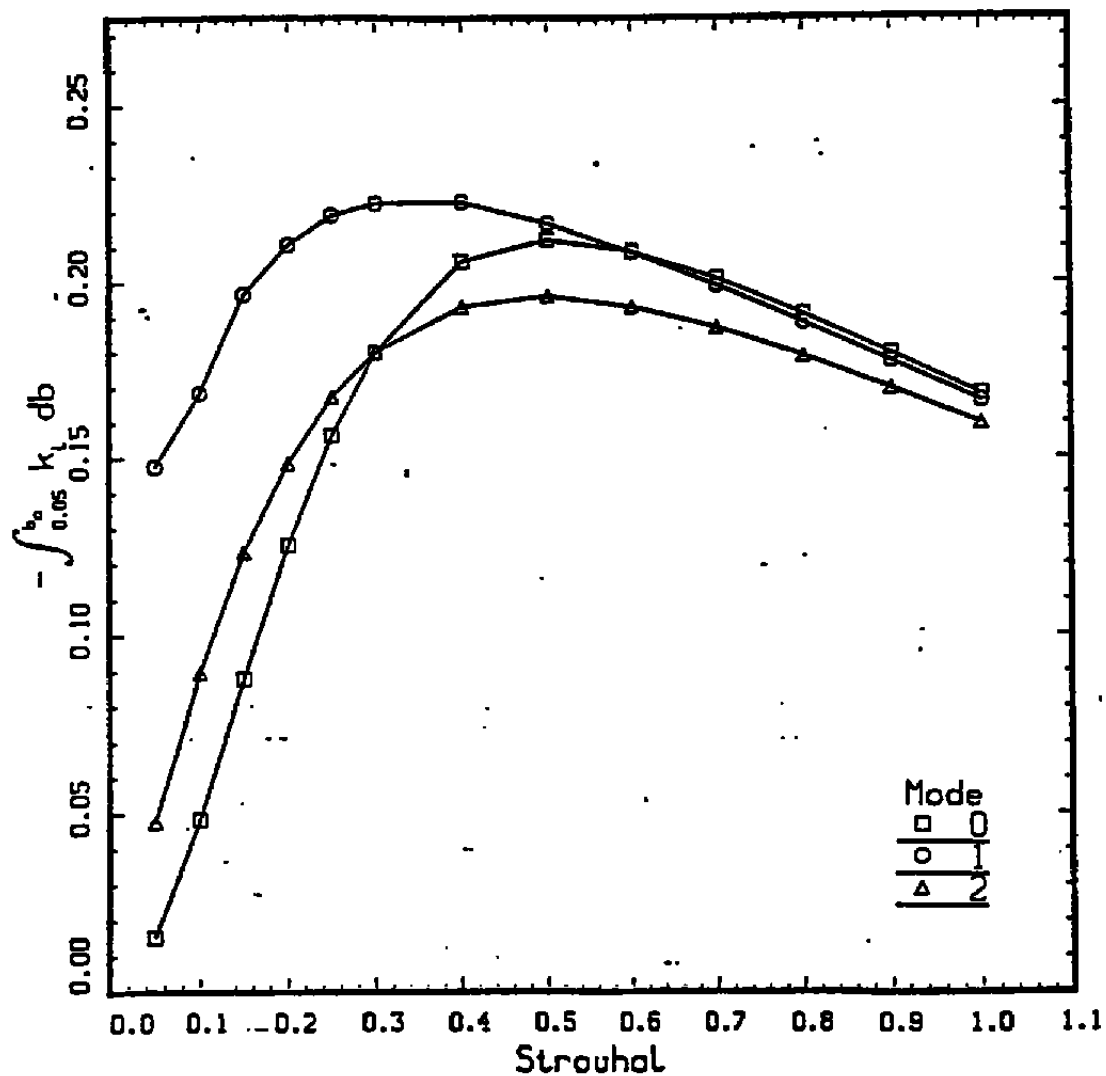


Figure 3.25 Total spatial growth rate of the instability waves of a Mach 1.3 supersonic jet as a function of Strouhal number

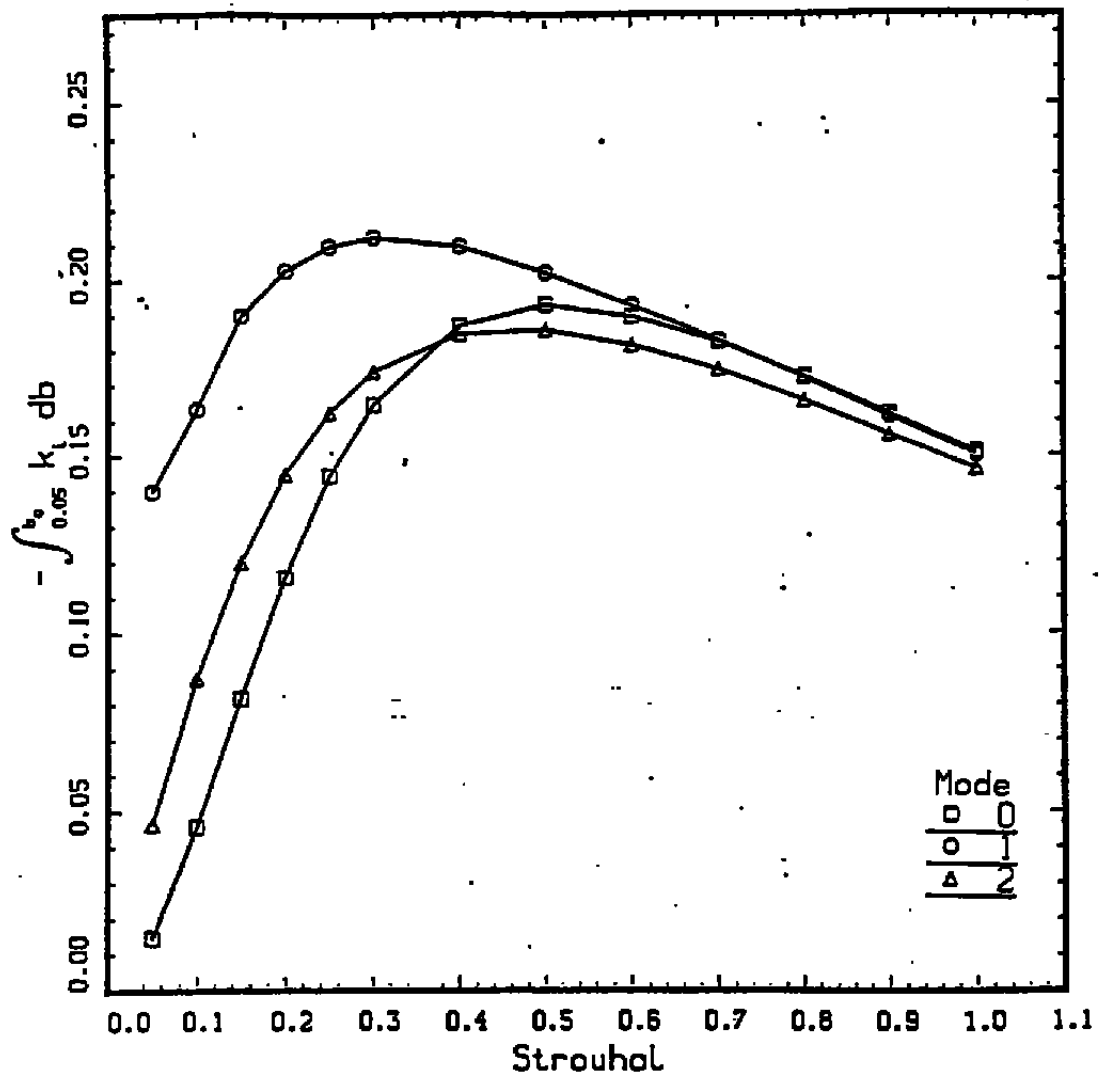


Figure 3.26 Total spatial growth rate of the instability waves of a Mach 1.4 supersonic jet as a function of Strouhal number

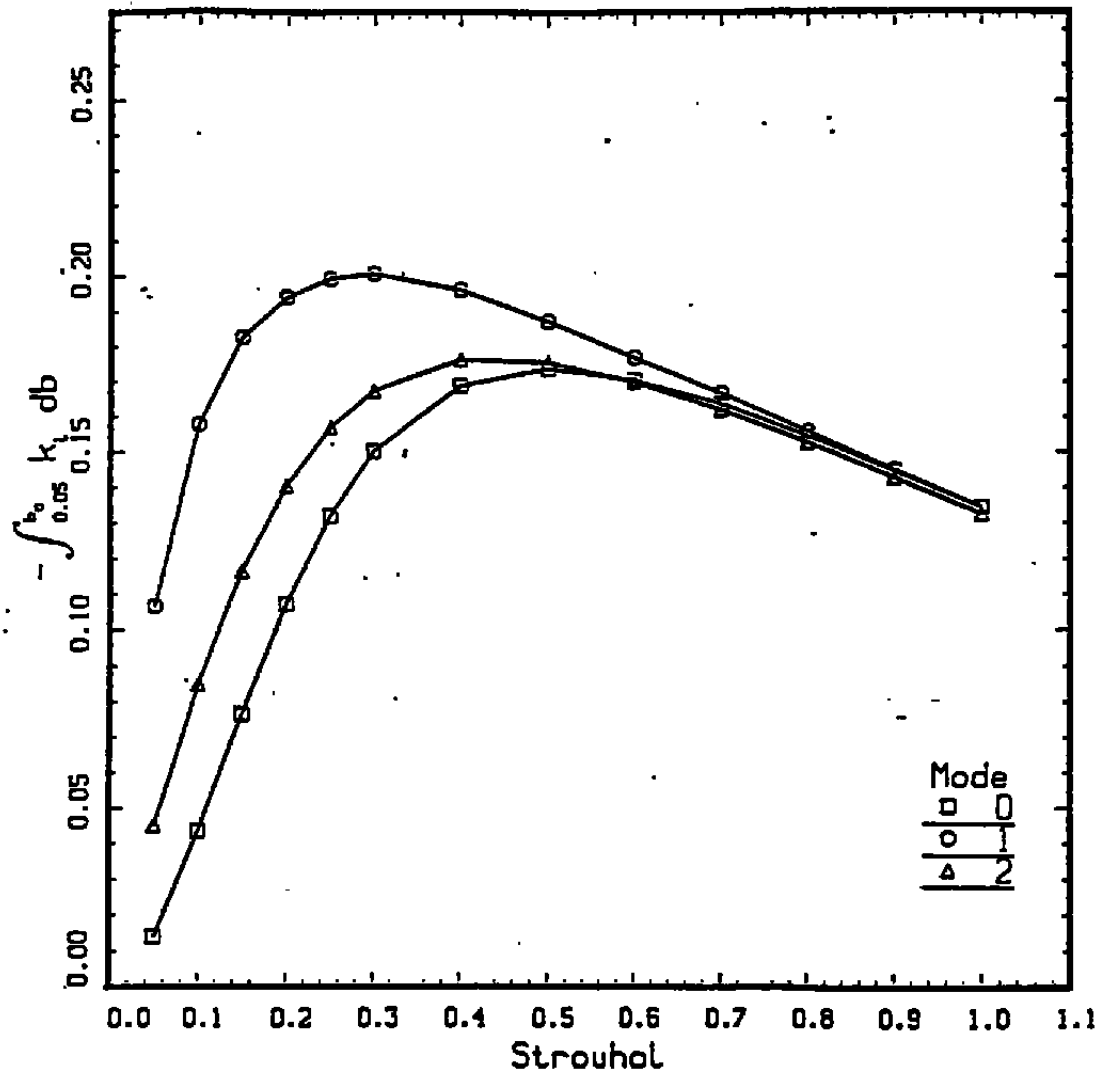


Figure 3.27 Total spatial growth rate of the instability waves of a Mach 1.5 supersonic jet as a function of Strouhal number

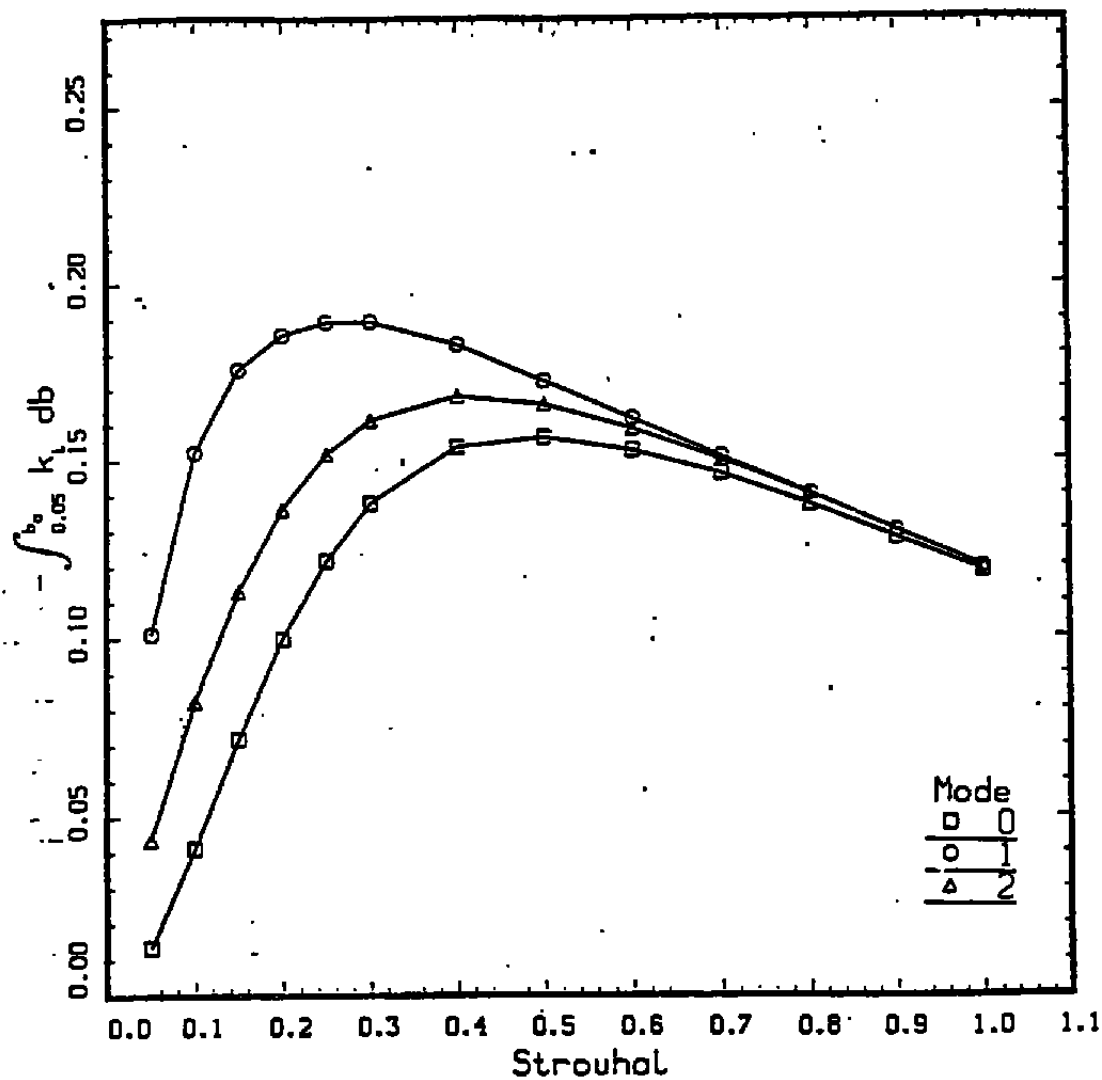


Figure 3.28 Total spatial growth rate of the instability waves of a Mach 1.6 supersonic jet as a function of Strouhal number

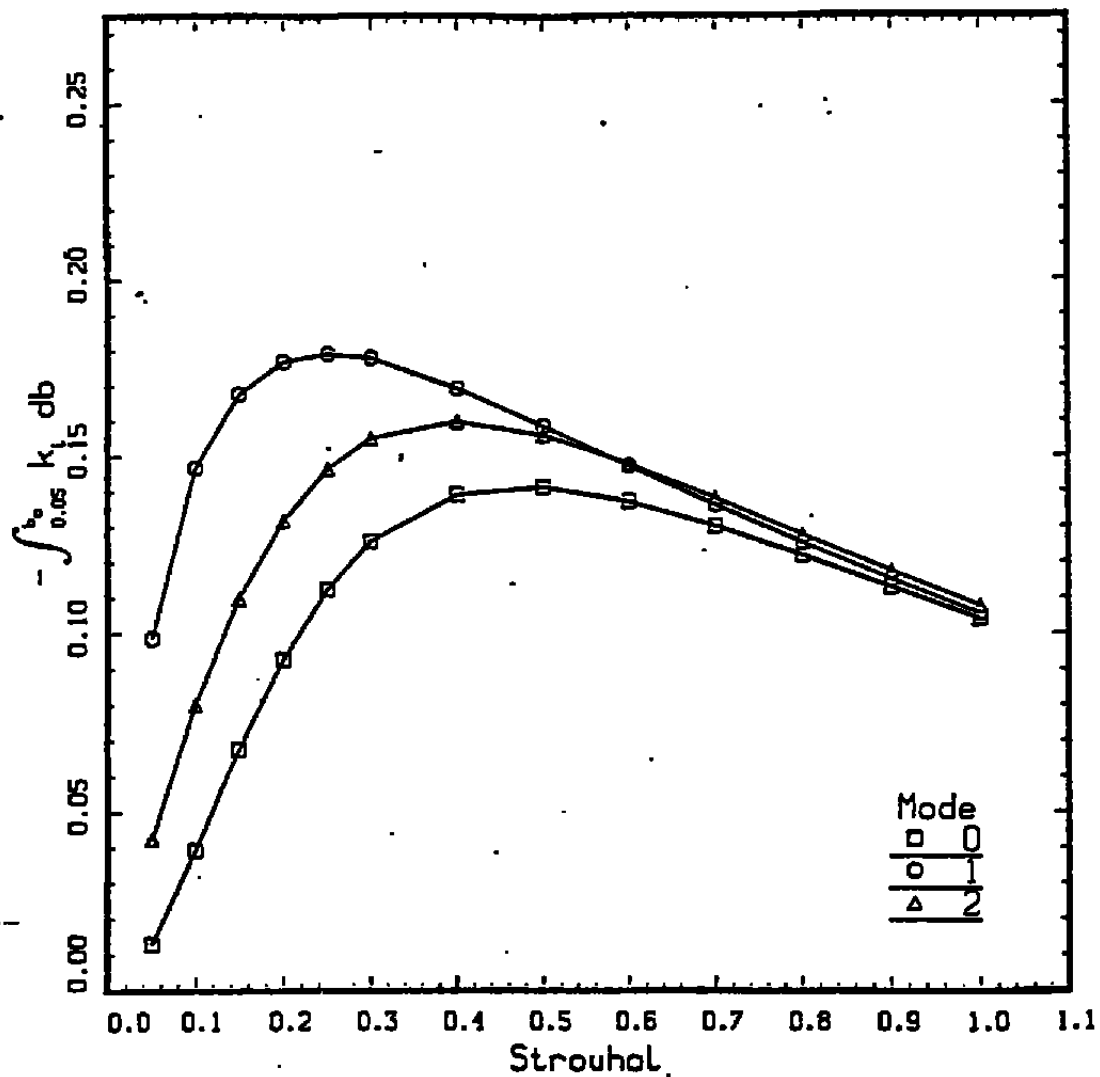


Figure 3.29 Total spatial growth rate of the instability waves of a Mach 1.7 supersonic jet as a function of Strouhal number

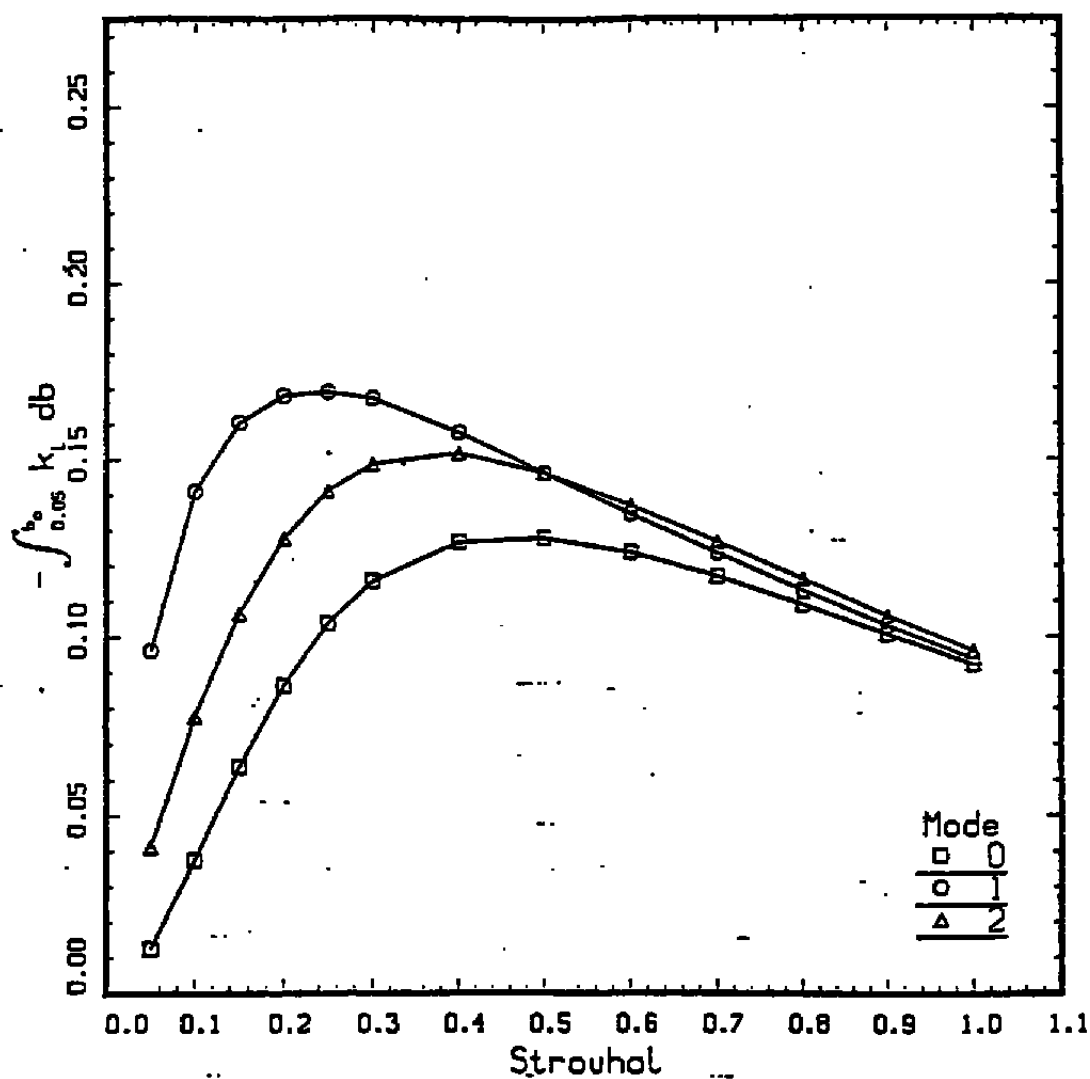


Figure 3.30 Total spatial growth rate of the instability waves of a Mach 1.8 supersonic jet as a function of Strouhal number

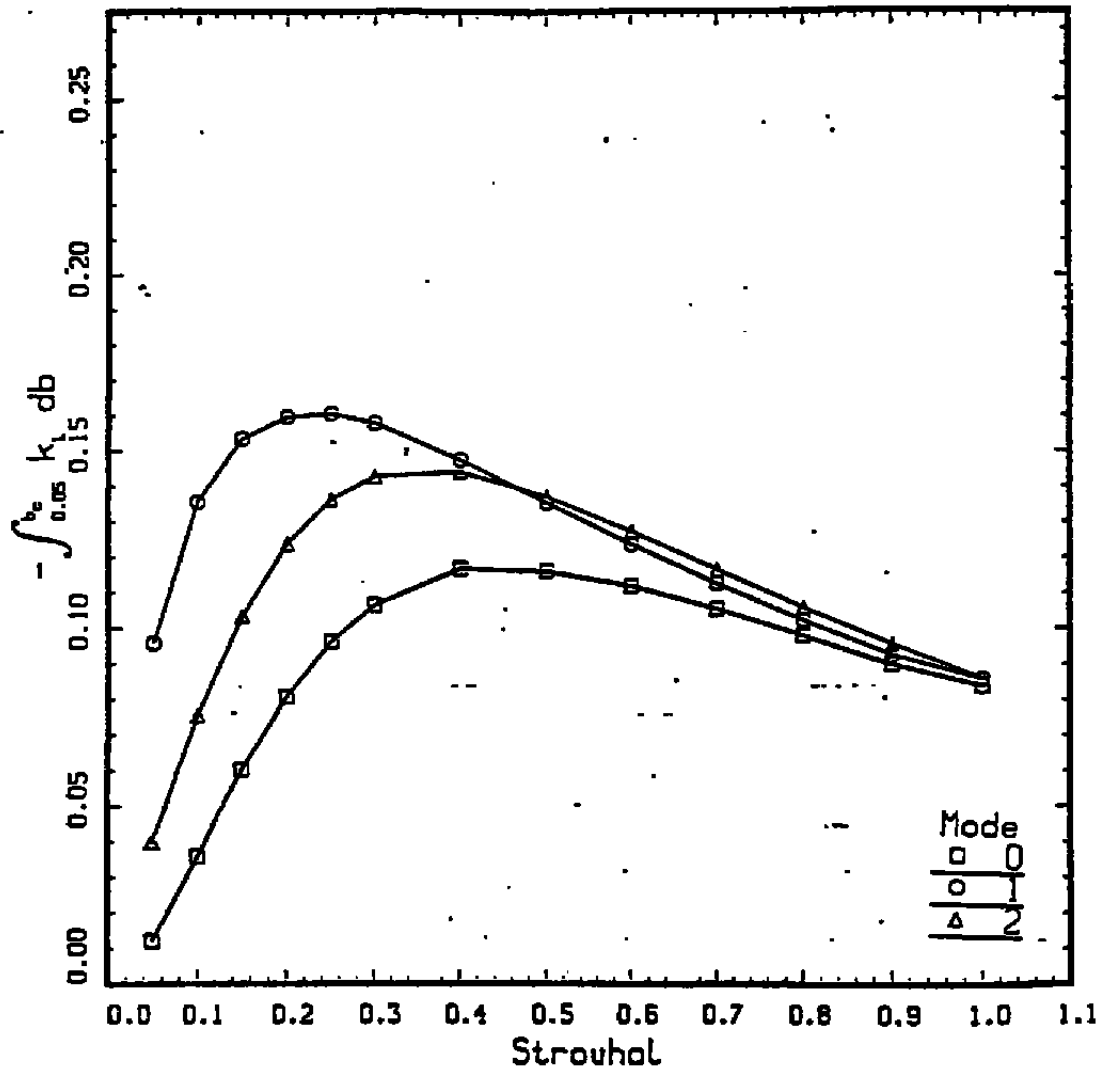


Figure 3.31 Total spatial growth rate of the instability waves of a Mach 1.9 supersonic jet as a function of Strouhal number

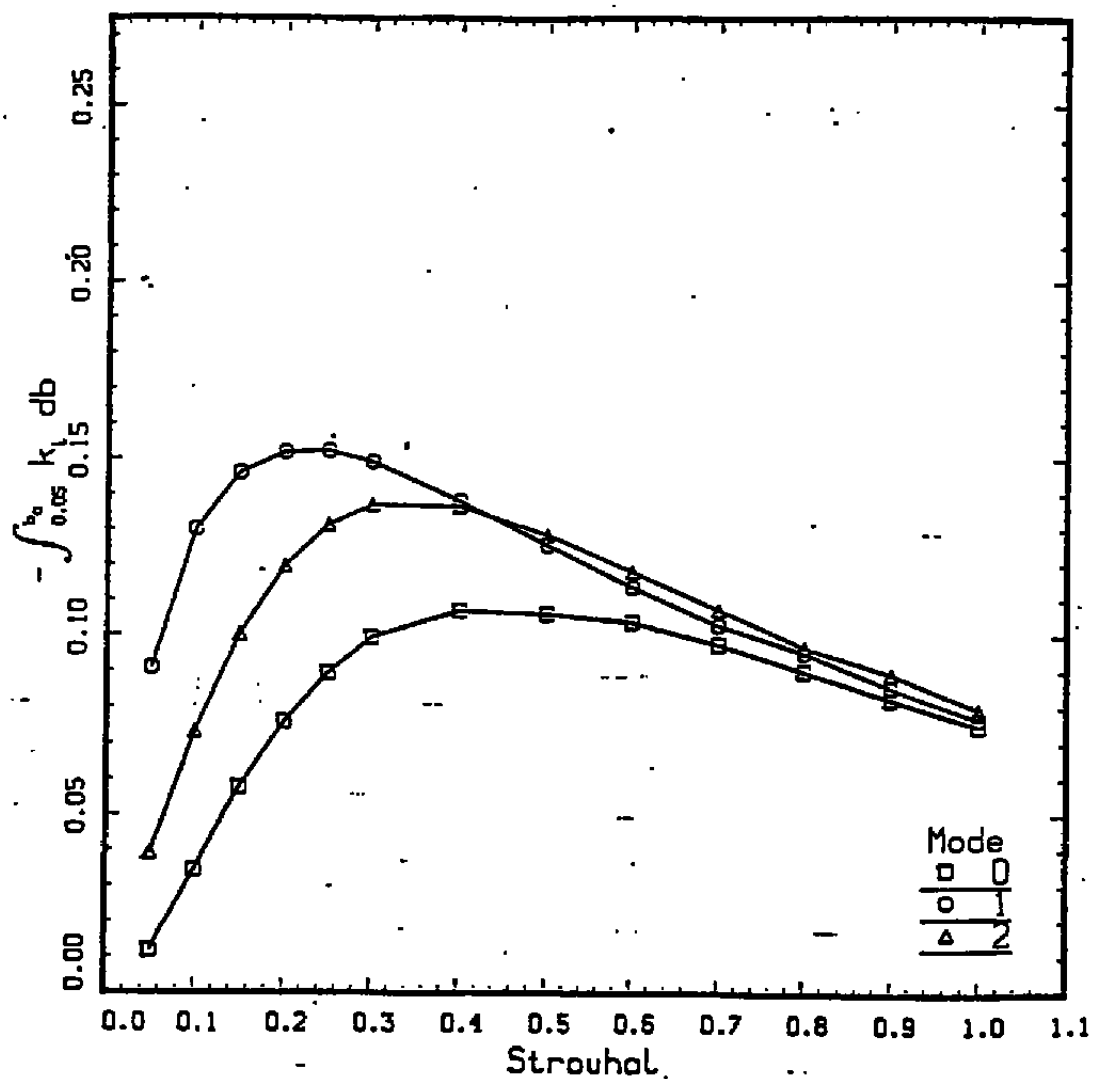


Figure 3.32

Total spatial growth rate of the instability waves of a Mach 2.0 supersonic jet as a function of Strouhal number

### 3.4 Screech Tone Characteristics and Generation

Aside from the low frequency peak, which appears to correlate with the frequency of the duct resonance mode, the noise spectrum of the jet-ejector or ducted flow is dominated by screech tones of almost discrete frequencies. In this section, an understanding of the characteristics and generation mechanism of these tones is being sought. This is done in two steps. First, an analysis of the screech tone frequency data is carried out. This provides a general classification of the tones and an identification of some of their most prominent characteristics. Second, an extension of the current theory on the generation mechanism of these tones is proposed. The extended theory incorporates the concept of dominant instability wave mode of Section 3.3 and the characteristics of the upstream propagating acoustic wave modes briefly discussed in Section 3.1 into the feedback idea of Powell ref. 3.4, Davies and Oldfield ref. 3.5, Tam, Seiner and Yu ref. 3.6 and others.

#### 3.4.1 Analysis of Screech Tone Frequency Data

Screech tone frequency data of free supersonic jets were obtained in the companion experiments. At a given jet Mach number, there are sometimes as many as three tones (not harmonics of each other). These data are plotted in Figure 3.33 as Strouhal number ( $fD_j/u_j$ ) versus fully-expanded jet Mach number,  $M_j$ , where  $D_j$  is the fully-expanded jet diameter ( $D_j = 2R_j$ ). The tones were measured at a Mach number increment of 0.1. They are not dense enough to provide a definitive pattern. In Figure 3.33, the data are supplemented by those measured by Seiner & Norum ref. 3.7. It appears that there are two basic families of tones. The tones at Mach number less than 1.2 form a family or group. Their Strouhal numbers are higher. The tones at  $M_j > 1.2$  apparently belong to another family. The frequencies of the latter family are confined to two narrow almost parallel bands. There appears to be no well-defined band structure in the first family of tones.

The tone frequencies of the supersonic jet/diffuser flow are not the same as those of a free supersonic jet at the same Mach number. In addition, the tone frequencies are not the same if the long diffuser ( $L/D = 3.0$ ) is replaced by the short diffuser ( $L/D = 1.0$ ). Figure 3.34 shows the combined tone frequency structure of the free supersonic jets and the jet/diffuser flows. By simply comparing the tone frequencies with and without the diffuser it is seen that no new tones are created in the second family of tones by enclosing a screeching jet by a diffuser. The presence of the diffuser causes only a slight shift in the tone frequency from one band to the other. With the addition of the tone frequencies of the jet/diffuser flows to the free jet data the grouping of the tone frequencies into two

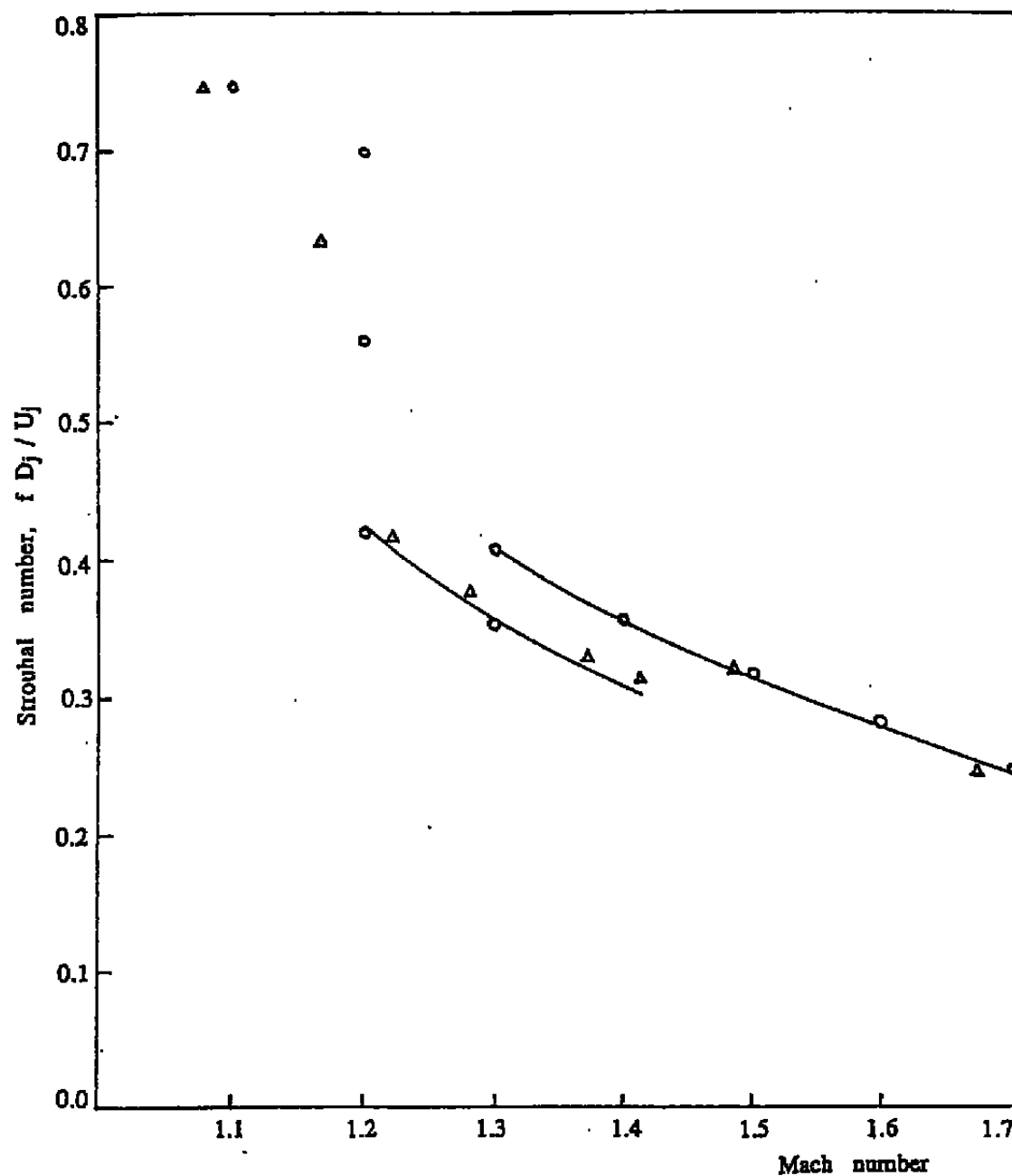


Figure 3.33 Screech tone Strouhal number versus fully expanded jet Mach number. ○ present experiment, △ Norum & Seiner

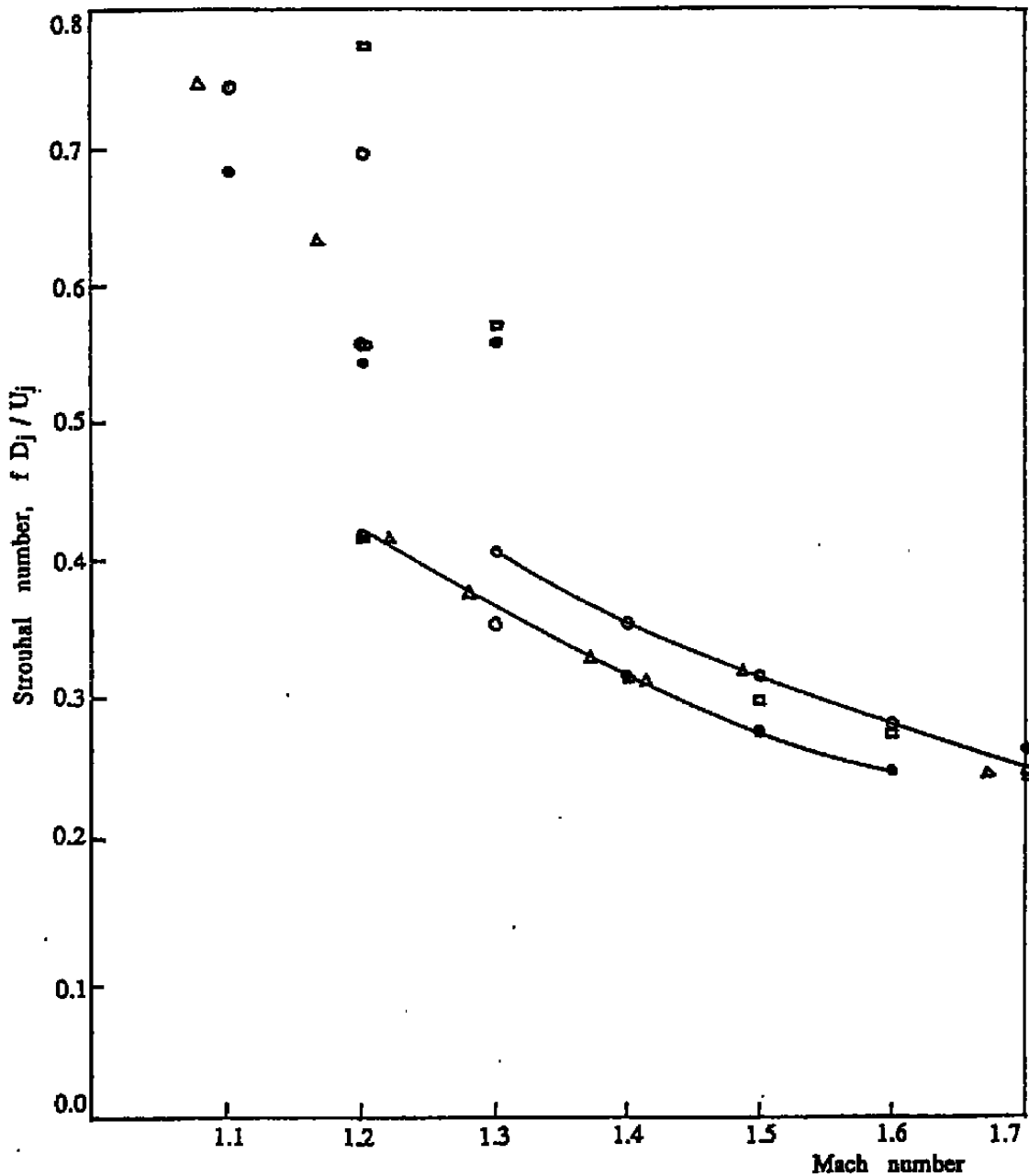


Figure 3.34 Screech tone Strouhal number versus fully expanded jet Mach number. present experiment :  $\circ$  free jet,  $\bullet$  ducted jet ( $L/D=3$ );  $\square$  ducted jet ( $L/D=1$ );  $\triangle$  Norum & Seiner (free jet)

families becomes even more prominent. The same is true with the double narrow band formation of the second family of tones.

### 3.4.2 Correlation With Dominant Instability Wave Mode of Supersonic Jets

In Section 3.3, the concept and definition of the dominant instability wave of a supersonic jet are provided and discussed. Extensive computation of the total growth rate for the  $n = 0, 1, 2$  instability wave modes of cold supersonic jets over the Mach number range of  $1.1 \leq M_j \leq 2.0$  are given in Figures 3.23 to 3.32. Here the physical meaning of these results in the Strouhal number versus jet Mach number plane is first explored. Its relationship to the screech tone frequency pattern is then examined.

Figure 3.23 shows the total growth rate as functions of Strouhal number at  $M_j = 1.1$ . At this low supersonic Mach number the axisymmetric mode ( $n = 0$ ) has a slightly larger total amplification than the helical mode ( $n = 1$ ). Both modes, however, have much larger total amplification than the higher order modes ( $n = 2, 3, \dots$ ). Instability waves with larger total amplification would attain a higher amplitude (assuming all waves have similar initial amplitude). They are the dominant waves. Thus at low supersonic jet Mach numbers, the axisymmetric instability wave mode is the most dominant. In Figure 3.23, the most dominant axisymmetric wave has a Strouhal number of 0.5. This is higher than the Strouhal number of the most dominant helical or flapping mode instability wave which has a Strouhal number of approximately 0.4. As the jet Mach number increases the axisymmetric mode waves are no longer the most dominant instabilities. Figure 3.26 shows the total growth rate at jet Mach number 1.4. Clearly now the helical ( $n = 1$ ) instability is most dominant. The dominant Strouhal number, however, has decreased to about 0.3. Beyond  $M_j = 1.4$  numerical results indicate that the dominance of the helical instability waves persists all the way to high supersonic jet Mach number.

Figure 3.35 gives a global view of the relative dominance of the axisymmetric and helical instability waves in the Strouhal number versus jet Mach number plot. At low supersonic jet Mach number, say  $M_j < 1.3$ , the dominant axisymmetric instability wave Strouhal number is around 0.5. This is indicated by a full line in Figure 3.35. Beyond Mach number 1.3, the total amplification of the axisymmetric mode is much smaller than that of the helical mode so that this mode is no longer very important. The cross-hatched areas in Figure 3.35 indicate roughly the region in which the particular instability wave mode is expected to be important and relatively dominant. The helical mode ( $n = 1$ ) is dominant at higher jet Mach number and at a lower Strouhal number. Its domain of dominance is shown in Figure 3.35. Now if the tone frequency data of Figure 3.34 is superimposed on

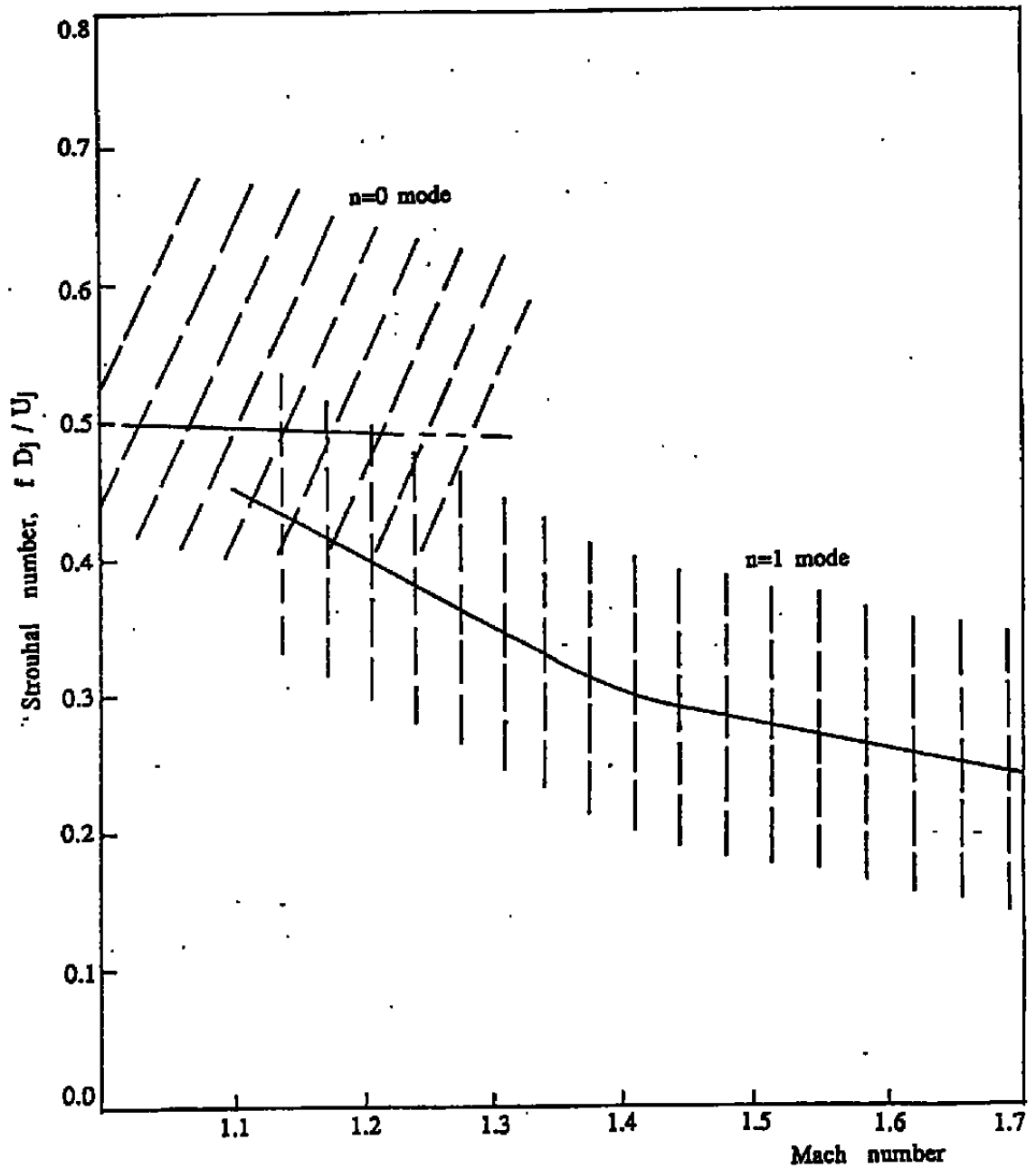


Figure 3.35 Range of the most amplified axisymmetric and helical instability wave modes of supersonic jets.

Figure 3.35 it is clear that the first family of tones is associated with the axisymmetric ( $n = 0$ ) instability waves. All the tone data points appear to fall in the region for which the  $n = 0$  instability wave mode is dominant. Similarly the second tone family is most probably associated with the helical ( $n = 1$ ) instability waves. The two frequency bands at  $M_j > 1.2$  in Figure 3.34 fit nicely into the region of dominance of the helical wave ( $n = 1$ ) in Figure 3.35. In short, the separation of the tone frequency data into two groups is a direct consequence of the change in dominance of the axisymmetric and helical instability waves of supersonic jets.

### 3.4.3 Screech Tone Generation Mechanism

The tones from the free as well as the ducted supersonic jets are believed to be screech tones. Screech tones are known to be generated by a feedback loop (see refs. 3.4, 3.5 and 3.6). Figure 3.36 shows a schematic diagram of the feedback loop. Near the nozzle exit, the shear layer of the jet is thin and is most receptive to external excitation. Acoustic disturbances reaching this region could, therefore, excite the large-scale instability waves of the jet. Once excited, the instability wave grows as it propagates downstream. After propagating downstream for a distance of four to five shock cell spacings, the instability wave, having grown in amplitude, interacts strongly with the shock cell structure generating strong acoustic radiation. Part of the acoustic disturbances propagate upstream outside the jet. On reaching the nozzle lip region, the acoustic disturbances excite the shear layer creating new instability waves. In this way, the feedback loop is closed. Suppose  $L$  is the distance between the nozzle exit and the location where the instability wave interacts strongly with the shock cell structure to produce acoustic radiation. The time needed for the instability wave to propagate from the nozzle lip to this location is equal to  $L/u_c$ , where  $u_c$  is the convective speed of the instability wave. The time taken by the acoustic wave to reach the nozzle lip region outside the jet is equal to  $L/a_0$ , where  $a_0$  is the ambient speed of sound. Since the feedback loop is closed, the total time taken around the loop once must be equal to an integral multiple of the oscillation period. If  $f$  is the frequency, the period of oscillation is  $1/f$ . Thus

$$\frac{L}{u_c} + \frac{L}{a_0} = n \frac{1}{f}; \quad n = \text{integer.}$$

Hence

$$f = \frac{nu_c}{L(1 + u_c/a_0)}. \quad (17)$$

Equation (17) gives the feedback frequency in terms of the other parameters of the feedback loop.

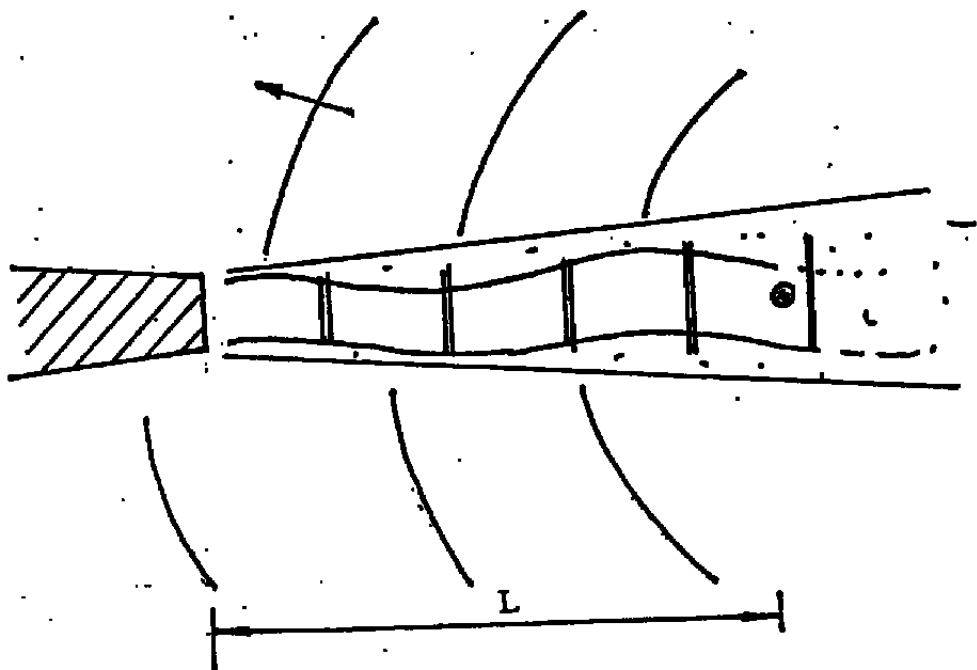


Figure 3.36 Schematic diagram of the feedback loop responsible for generating screech tones

In (17) the integer  $n$  is not specified. Because of this a phenomenon called staging often occurs. Let  $s$  be the shock cell spacing and  $m$  be such that  $L \simeq ms$ . Figure 3.37 shows two possible feedback configurations. The frequency formulas for these two configurations are:

$$f = \frac{nu_c}{ms(1 + u_c/a_0)} \quad (18)$$

$$f' = \frac{n' u_c}{m' s(1 + u_c/a_0)} \quad (19)$$

The ratio of the two feedback frequencies is, therefore, given by

$$\frac{f}{f'} = \frac{n}{m} \frac{m'}{n'} = \text{constant}. \quad (20)$$

Equation (20) implies that the feedback tone frequencies from the two feedback configurations would lie on parallel curves as observed in Figures 3.33 and 3.34. Here it is believed that the two parallel band structure of the measured tone frequency curves is simply a manifestation of the phenomenon of staging.

#### 3.4.4 Feedback Acoustic Waves

The staging phenomenon discussed above offers an explanation to the band structure of the screech tone frequencies. But there appears to be no reason for restricting the number of bands to two as in the case of Figures 3.33 and 3.34. A possible reason for limiting the number of bands to two will now be provided.

In a recent work by Tam & Hu (ref. 3.1), it was discovered that a supersonic jet could support special acoustic wave modes which propagate upstream guided by the jet. These wave modes can be calculated in the same way as the Kelvin-Helmholtz instability waves. In a more recent article by Tam & Ahuja (ref. 3.2), it was suggested that these acoustic wave modes were the feedback acoustic waves responsible for the generation of jet impingement tones. Based on this suggestion they were able to explain several aspects of seemingly puzzling phenomena associated with the impingement tones. Now it is also possible that the acoustic feedback of the present screech phenomenon is accomplished by these upstream propagating acoustic wave modes. If this is, indeed, the case then the characteristics of the screech tones must be compatible with those of the upstream propagating wave modes. One of the most prominent features of these wave modes is that the wave frequency is restricted to well defined bands. If a vortex sheet jet model is used these bands can be calculated by solving dispersion relation (14). In the case of free jets, (14) may be further simplified by letting  $R_0$  become infinitely large. As pointed out

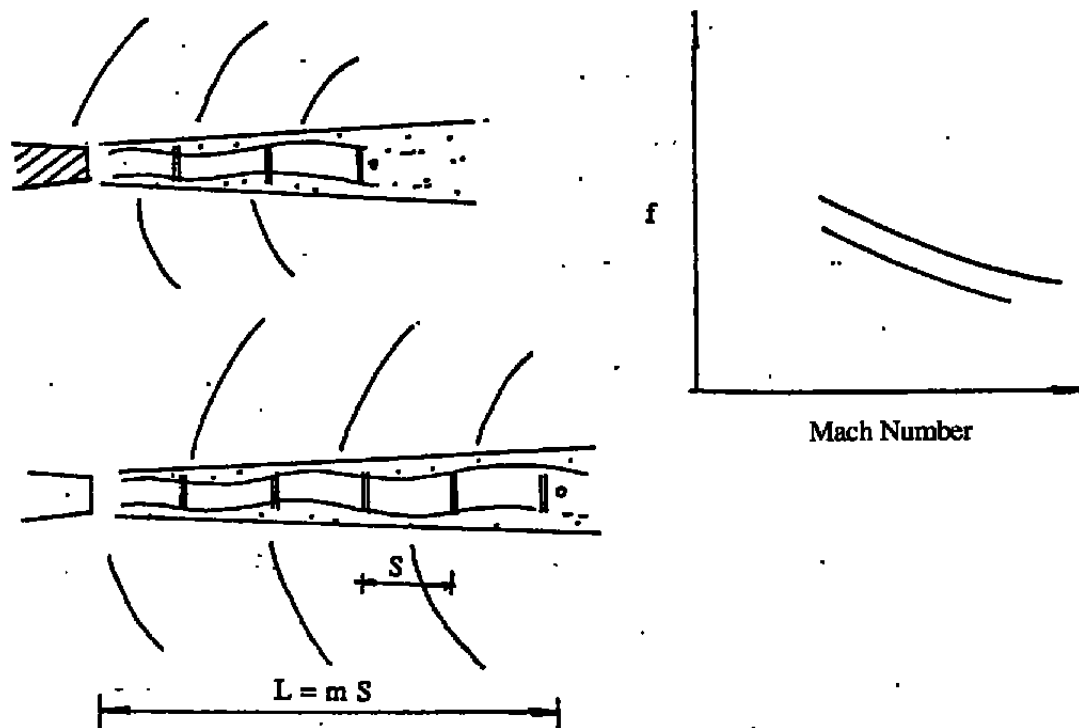


Figure 3.37 Schematic diagram showing the staging of a screeching jet

before, the presence of the diffuser does not appear to create new screech tones and that the measured tone frequencies with and without the diffuser all lie in the same two narrow bands. For simplicity, therefore, the more simple model with  $R_0 \rightarrow \infty$  is used in all the band frequency calculations in this report.

Figure 3.38 shows the calculated allowable Strouhal numbers of the axisymmetric upstream propagating acoustic wave modes as functions of jet Mach number. These waves are generally designated by two indexes  $(n, m)$ .  $n$  ( $n = 0, 1, 2, \dots$ ) is the azimuthal mode number and  $m$  ( $m = 1, 2, 3, \dots$ ) is the radial mode number. On comparing the allowable frequencies of the  $(0, 1)$  and  $(0, 2)$  upstream propagating acoustic wave modes of Figure 3.38 and the dominant frequencies of the axisymmetric instability waves of Figure 3.35 it is clear that only the  $(0, 2)$  mode and the axisymmetric Kelvin-Helmholtz instability wave of the jet can form a feedback loop. The frequencies of the  $(0, 1)$  mode are too low to match those of the instability waves. Figure 3.39 shows the allowable Strouhal numbers of the helical upstream propagating acoustic wave modes. Since a feedback loop cannot be formed unless all the different parts of the loop oscillate with the same frequency, it is evident by comparing the range of the dominant helical instability wave frequencies of Figure 3.35 with those of the feedback acoustic wave modes of Figure 3.39 that only the  $(1, 1)$  mode is relevant. Figure 3.40 shows a comparison of the measured screech tone Strouhal number (from Figure 3.34) with the allowable  $(0, 2)$  and  $(1, 1)$  upstream propagating acoustic wave mode Strouhal numbers. As can be seen the measured tone data of the first family fall within or close to the calculated band of allowable Strouhal numbers. This lends strong support to the proposition that the feedback is achieved by the upstream acoustic wave modes of the jet.

For the second family of tones, the data points all fall close to but below the very narrow allowable Strouhal number band of the  $(1, 1)$  acoustic mode. The discrepancy is believed to be due to the fact that a vortex sheet jet model is used to calculate the allowable frequencies of the  $(1, 1)$  mode. To explore this possibility the computation is repeated using a more realistic jet model with a finite thickness mixing layer. The mean velocity profile is given by equations (15) and (16).

According to the screech tone feedback model of Figure 3.36, the upstream propagating feedback acoustic waves are generated at a location approximately 4 to 5 shock cells downstream. The half-width of the mixing layer at this location is around  $b/R_j \simeq 0.8$ . As the wave propagates upstream the half-width of the mixing layer as seen by the wave decreases monotonically. This change in  $b/R_j$  leads to a change in the computed band of allowable frequencies. Here it is proposed that the effective frequency band be regarded as the aggregate of all the frequency bands with  $b/R_j \leq 0.8$ . It is to be noted that within

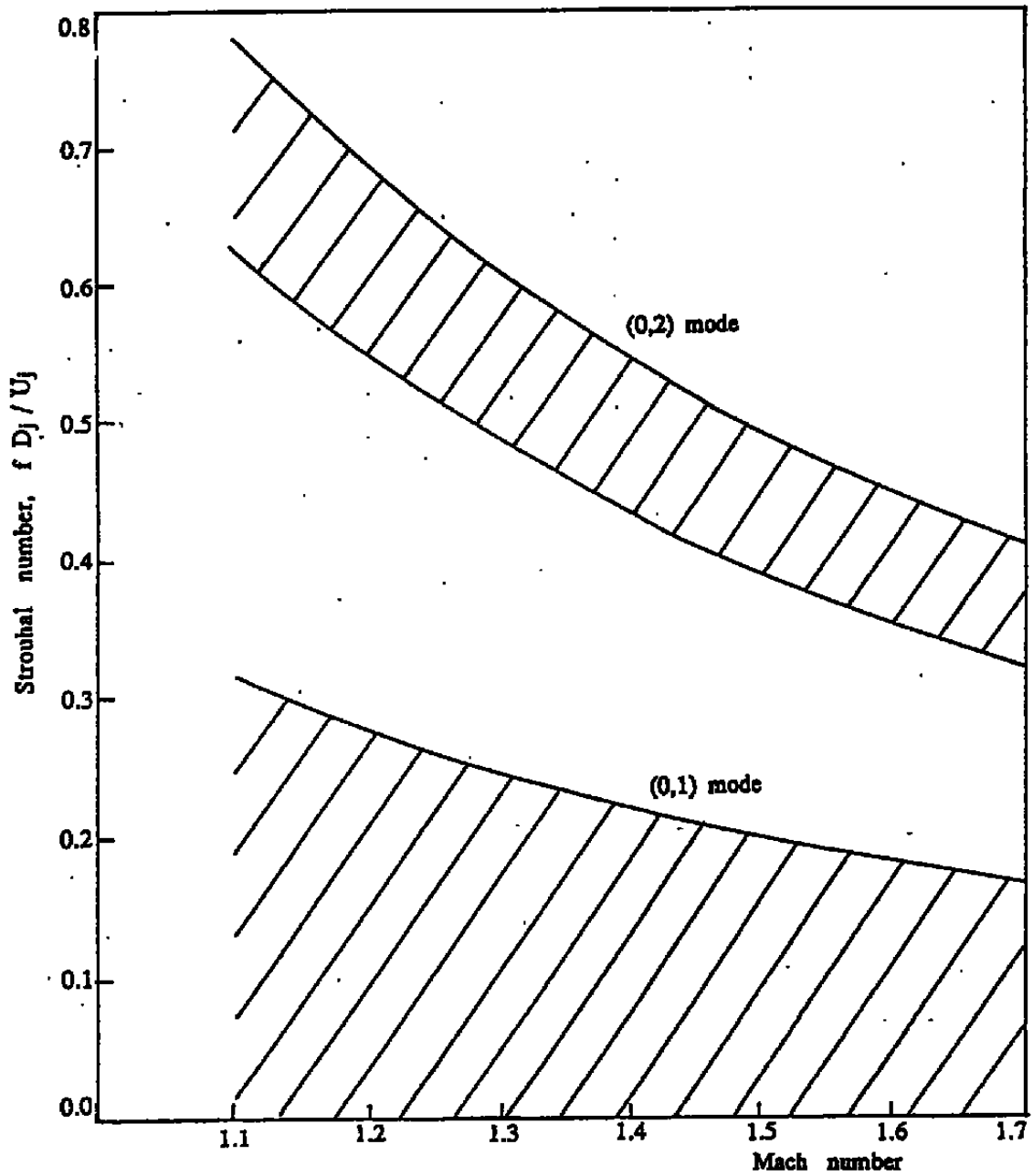


Figure 3.38 Allowable frequencies of the  $n=0$  mode upstream propagating acoustic waves (vortex sheet jet model)

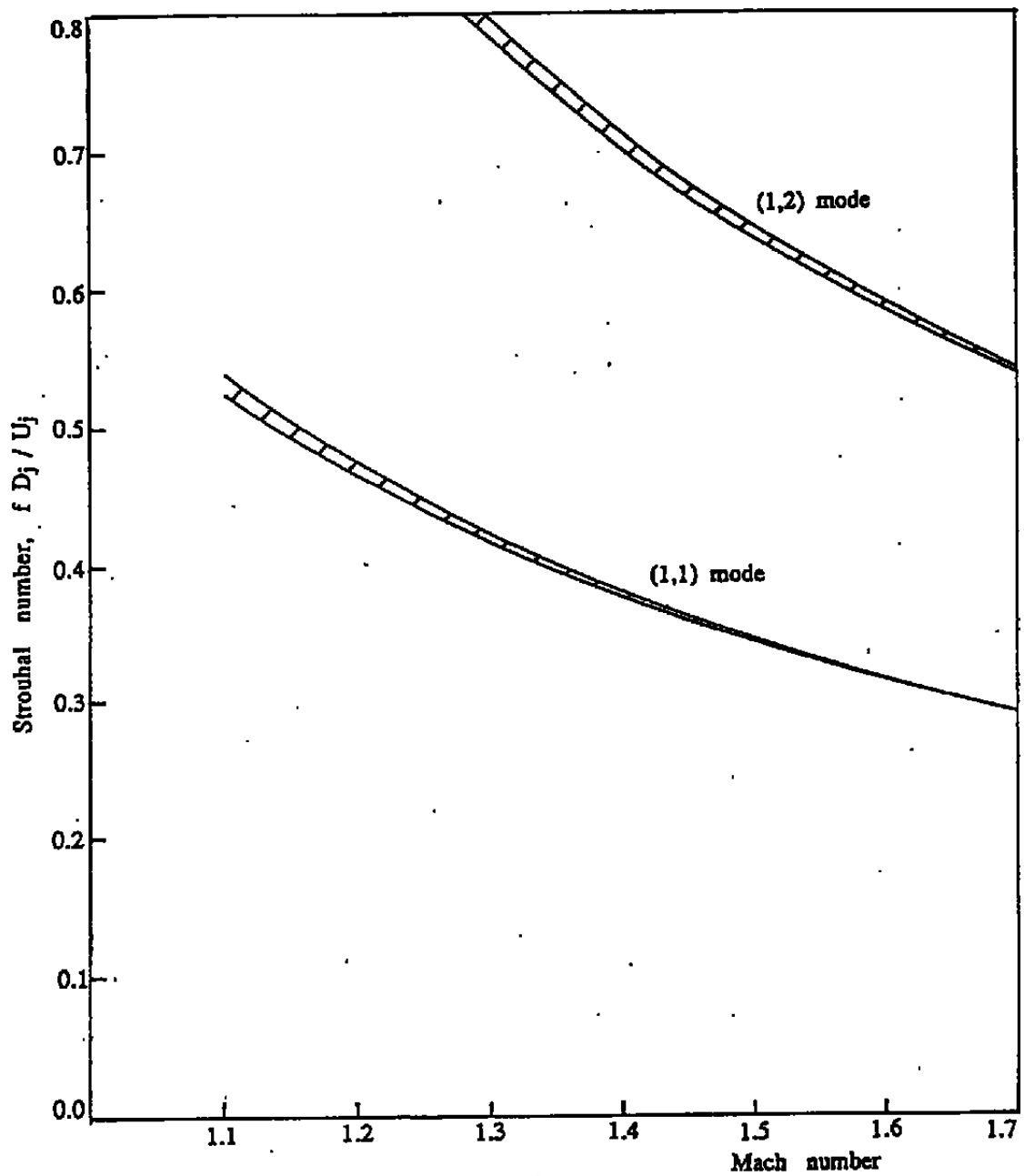


Figure 3.39 Allowable frequencies of the  $n=1$  mode upstream propagating acoustic waves (vortex sheet jet model)

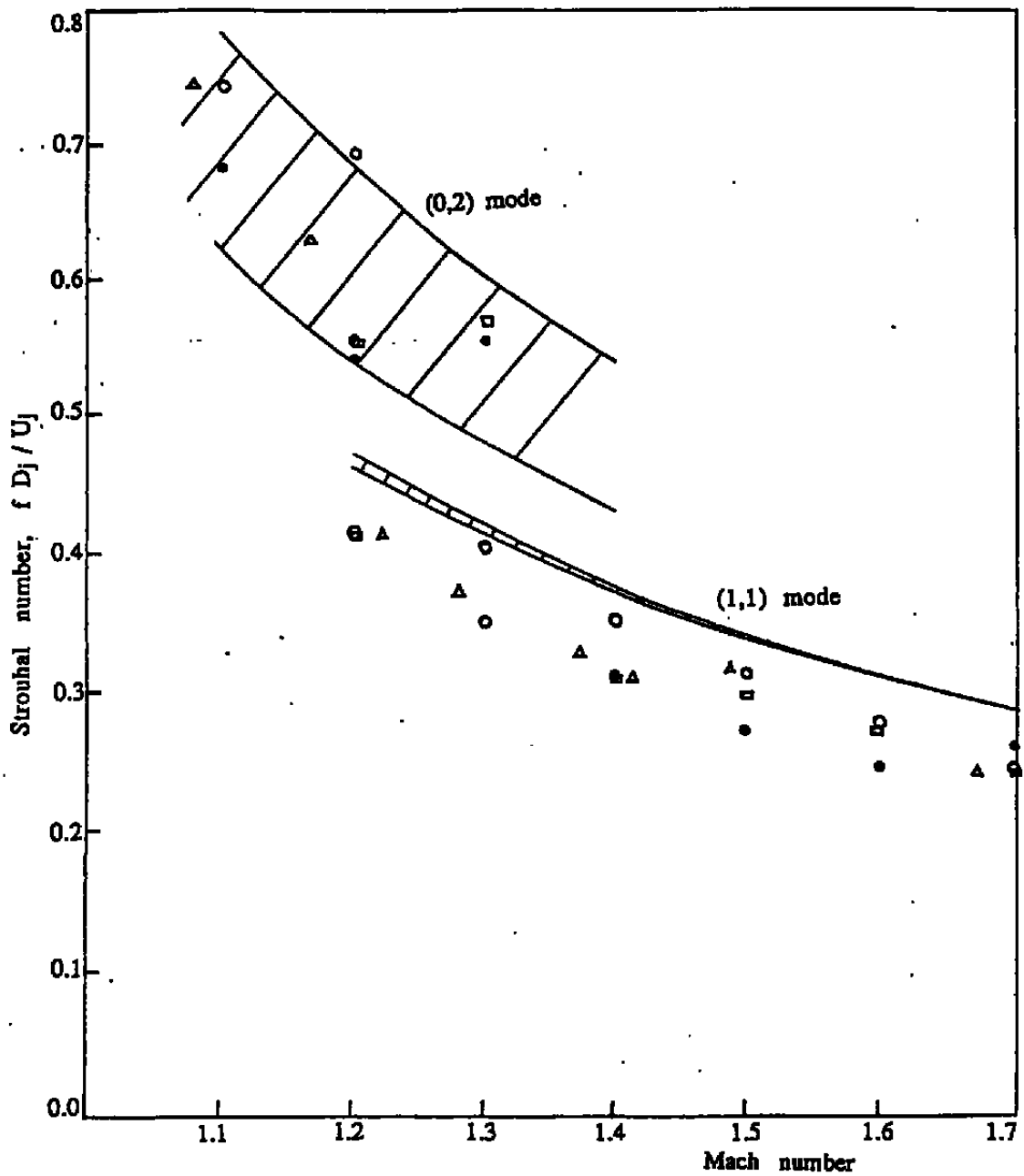


Figure 3.40 Comparison between the allowable frequencies of the upstream propagating acoustic wave modes and the measured screech tone frequencies. Vortex sheet jet model.

this definition of the effective frequency band a wave may be slightly damped in part of the region as it propagates upstream.

In the work of Tam & Hu, a procedure by which the allowable frequencies of the upstream propagating acoustic wave modes of a jet with finite thickness mixing layer is provided. Here the same computational procedure is used. Figure 3.41 shows the calculated allowable (1,1) mode Strouhal numbers at  $b/R_j = 0.0, 0.5$  and  $0.8$ . As  $b/R_j$  increases, the Strouhal number decreases. Thus the effective band of the (1,1) mode frequencies is bounded by those of  $b/R_j = 0$  and  $b/R_j = 0.8$ . Plotted in this figure also are the measured second family screech tone Strouhal numbers over the jet Mach number range of 1.2 to 1.7. It is readily seen that all the data points now lie inside or on the aggregated frequency band. The overall bandwidth is, however, still quite narrow. Accordingly, there would be no room for a third data band (see Figure 3.34) although such a band is permissible according to the staging phenomenon. Under the assumption that the screech tone feedback is accomplished by the upstream propagating acoustic wave modes of the jet, the narrow band width of these waves is the main reason for limiting the number of screech stages to two.

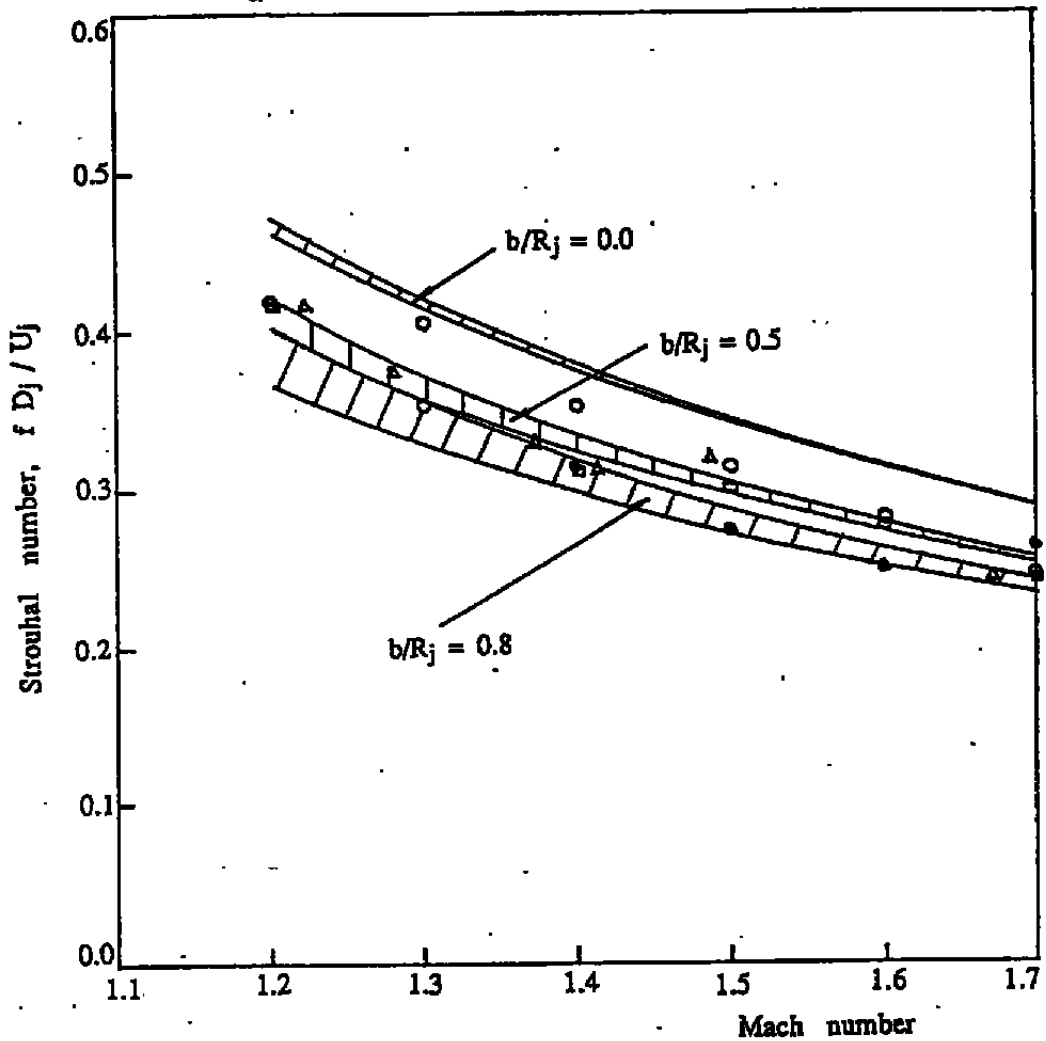


Figure 3.41 Comparison between the calculated effective frequency band of the (1,1) upstream propagating acoustic wave mode and measured screech tone frequencies.

## SECTION 4

### PLUME DEFLECTION SENSITIVITY TO SOUND

#### 4.1 Objective

Physical deflections of 2-D, C-D nozzle flows have been observed at AEDC test facilities concomitant with the presence of a strong discrete tone. It was speculated that this deflection could have been produced by this discrete tone. The purpose of the present experiments was to determine if this phenomenon could be reproduced in a model-scale facility and to assess the sensitivity of a two-dimensional convergent-divergent nozzle to external acoustic excitation at scale frequencies commensurate with those experienced in acoustic interactions at AEDC.

#### 4.2 Test Nozzle

The final design of the two-dimensional convergent-divergent nozzle was based upon the specifications and sketches provided by AEDC. The assembly drawing is shown in Figure 4.1. The details are shown in Figures 4.2 through 4.4. The nozzle exit dimensions are 1.6 inches by 0.46 inches. The area ratio of the exit to the throat is 1.222. The exit area is 0.896 square inches. The nozzle has a convergent-divergent cross-section only for the sides with the larger dimension. The sides with the smaller dimension are parallel. The nozzle is supplied by a 4-inch diameter duct of the flow visualization facility of GTRI. Design of the transition from a round to a rectangular cross-section within the constraints of nozzle wall angles imposed by AEDC was a major challenge but was accomplished by suitable contouring of the inner surfaces as shown in Figures 4.1 through 4.4. A photographic view of the nozzle is given in Figure 4.5.

#### 4.3 Acoustic Source

After appropriate scaling, the frequency for which the model scale jet was to be excited turned out to be 1kHz for the jet operated at a fully-expanded Mach number of 1.4. The noise level in the vicinity of the nozzle exit was to be about 160 dB.

A number of acoustic-driver configurations were tested to produce high intensity acoustic excitation. After testing these configurations, the multi-tube source shown in Figure 4.6 was selected as the acoustic source for this task. Since the testing was to be conducted at a single frequency of 1000 Hz, the principle of duct resonance as a function of duct length was employed to obtain very high sound pressure levels. The lengths of the tubes shown in Figure 4.6 were selected corresponding to either 1/4 wave length or 3/4 wavelength, at which high intensity

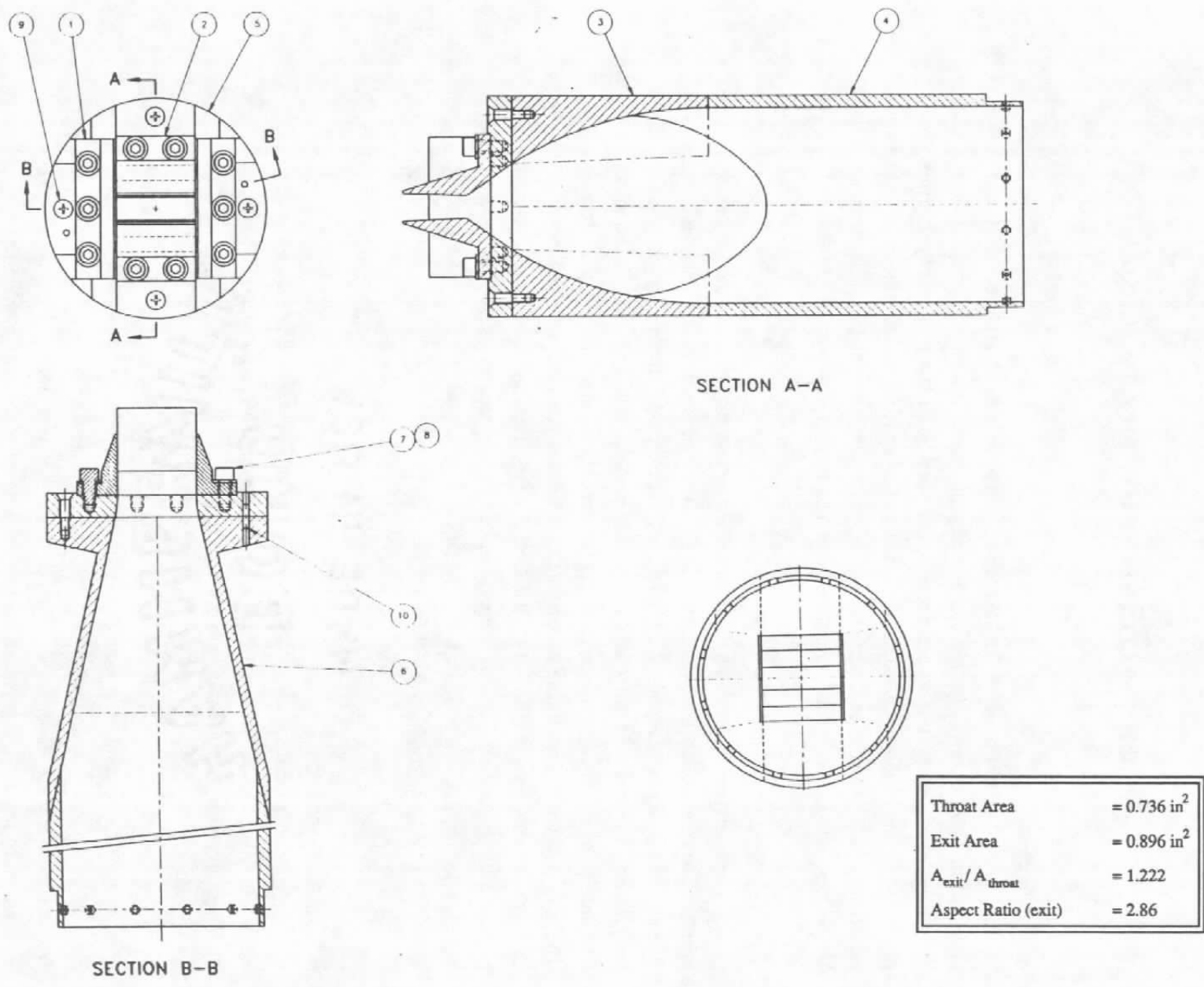
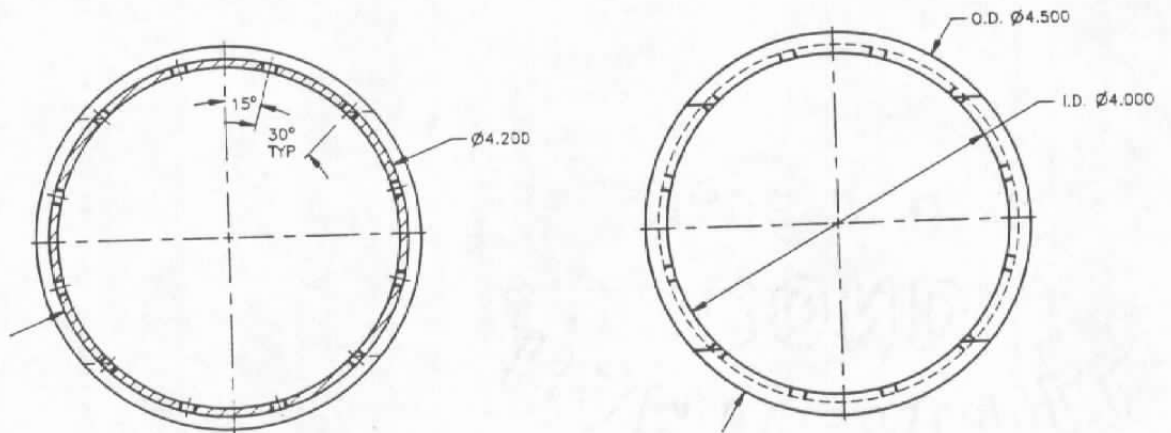


Figure 4.1 Two-dimensional convergent divergent nozzle assembly.



SECTION A-A

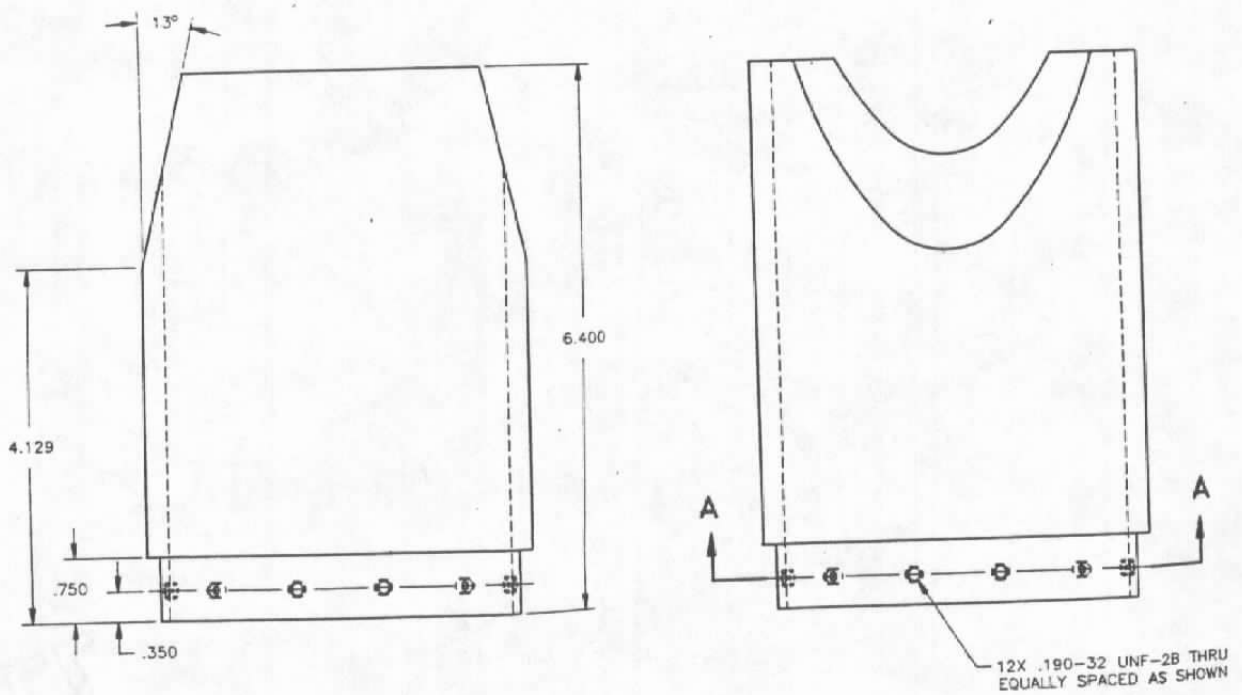


Figure 4.2 Two-dimensional convergent divergent nozzle details.

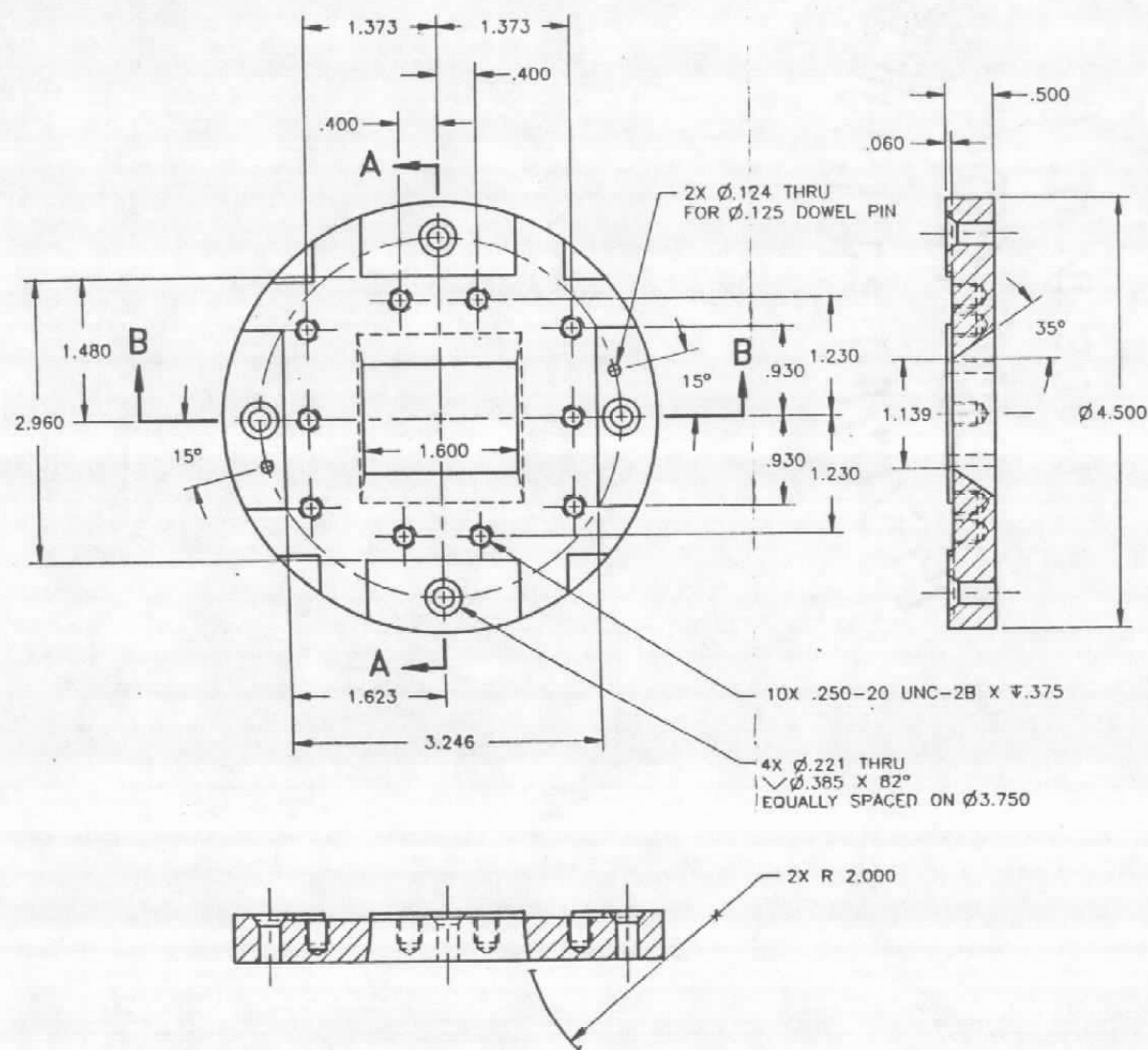


Figure 4.3 Two-dimensional convergent divergent nozzle details.

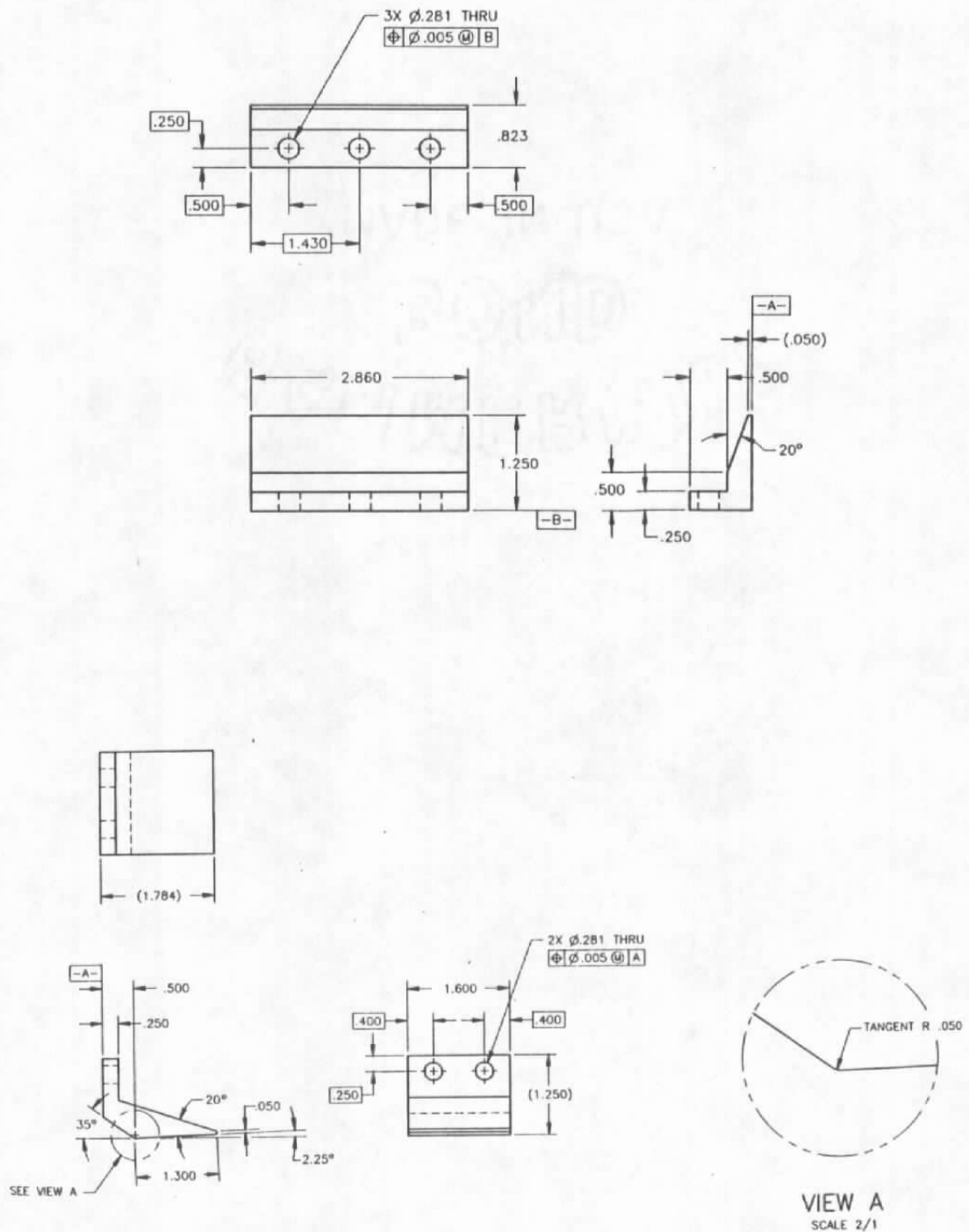
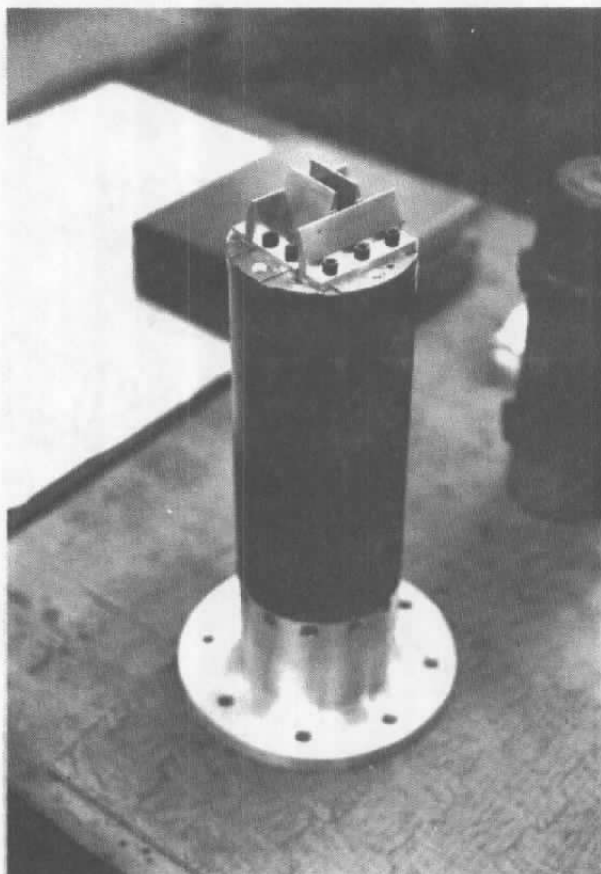


Figure 4.4 Two-dimensional convergent divergent nozzle details.



Throat Area	$= 0.736 \text{ in}^2$
Exit Area	$= 0.896 \text{ in}^2$
$A_{\text{exit}} / A_{\text{throat}}$	$= 1.222$
Aspect Ratio (exit)	$= 2.86$

Figure 4.5 The 2-D, C-D nozzle.

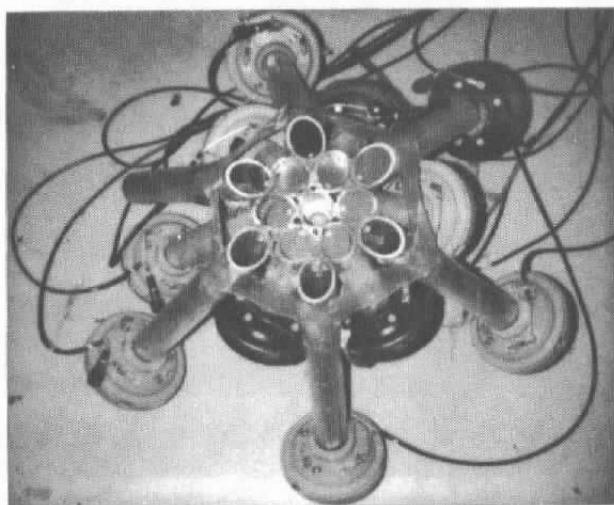


Figure 4.6 High intensity noise source.

resonance produced up to 163 decibels at 1000 Hz at about 1 inch from the exit of the center tube of the source. Three views of this configuration mounted under the 2-D, C-D nozzle in the GTRI Flow Visualization Facility are shown in Figure 4.7a-c.

#### 4.4 Plume Sensitivity Experiment

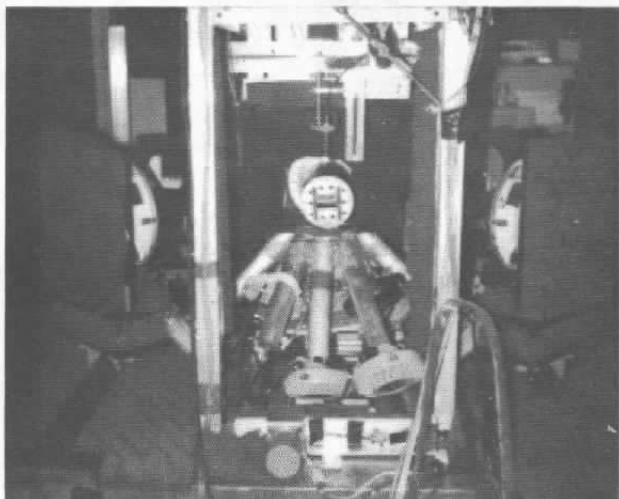
The sound source described above was mounted on the optical table of GTRI Flow Visualization Facility under the jet with the center of the noise source positioned about four inches downstream of the nozzle exit. With this configuration, although the sound pressure levels at the center of the source were about 163 dB, the sound pressure level measured at the nozzle exit was 153 dB. The data acquired consisted of schlieren and shadowgraphic flow visualizations of the jet with and without the sound excitation. The results for a pressure ratio of 3.04 (Reservoir Pressure = 30 psig) and pressure ratios just above and just below 3.04 are shown in Figures 4.8 through 4.10 in schlieren pictures and in Figures 4.11 through 4.13 in shadowgraphic pictures.

Note that the source in these flow visualization pictures appears on the upper half of each photograph. Our goal was to determine if sound could conceivably deflect the whole jet. As seen in these photographs, it did not appear to do so. Examination of video pictures produced the same conclusion. Similar conclusions were derived by placing a hard-walled plate across the jet in front of the source opening and by varying the distance of the plate from the sound source.

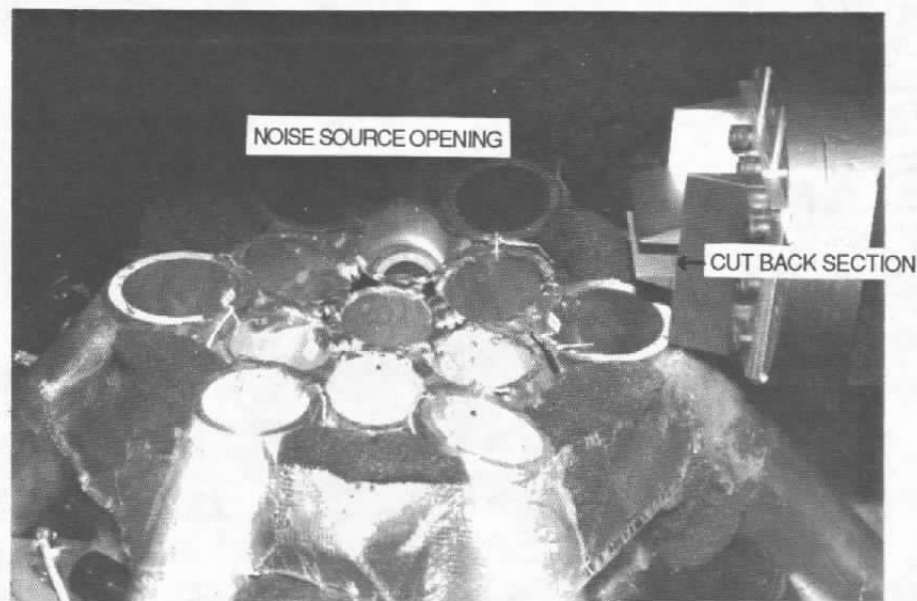
It was concluded from this simple "demonstration" type sub-scale experiment that the 2-D, C-D nozzle flow with a cut back section did not appear to respond to externally imposed sound. We were trying to replicate a qualitative observation made in the full-scale facility by AEDC personnel. No quantitative data were available. It is quite likely that the boundary layer at the plume opening was quite different in the full-scale and the sub-scale nozzles. If so, the plume sensitivity to acoustic excitation will be quite different also.

It is quite likely that in the full-scale setup, what was observed was the flapping mode of the 2-D, nozzle and depending upon the lighting conditions, this flapping mode might have been interpreted as a single-sided bodily deflection of the jet.

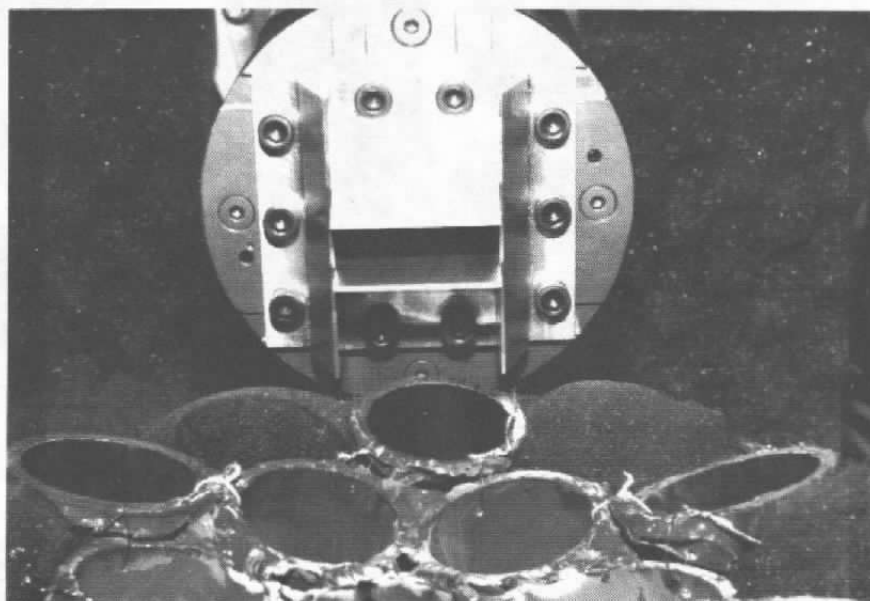
A closer examination of the schlieren pictures of the present sub-scale nozzle indicated that at higher jet Mach numbers, the flapping of the jet could be visualized. Because of the presence of the cut back section, the boundary layer of the jet at the lip of the longer sides is conceivably thickened considerably. This is likely to reduce the growth rate of instability waves in the plume. To confirm this conjecture, the cutback was closed off as shown in Figure 4.14 and schlieren photographs of the unexcited jet were acquired.



(a)



(b)



(c)

Figure 4.7 The 2-D, C-D nozzle and the high intensity noise source.

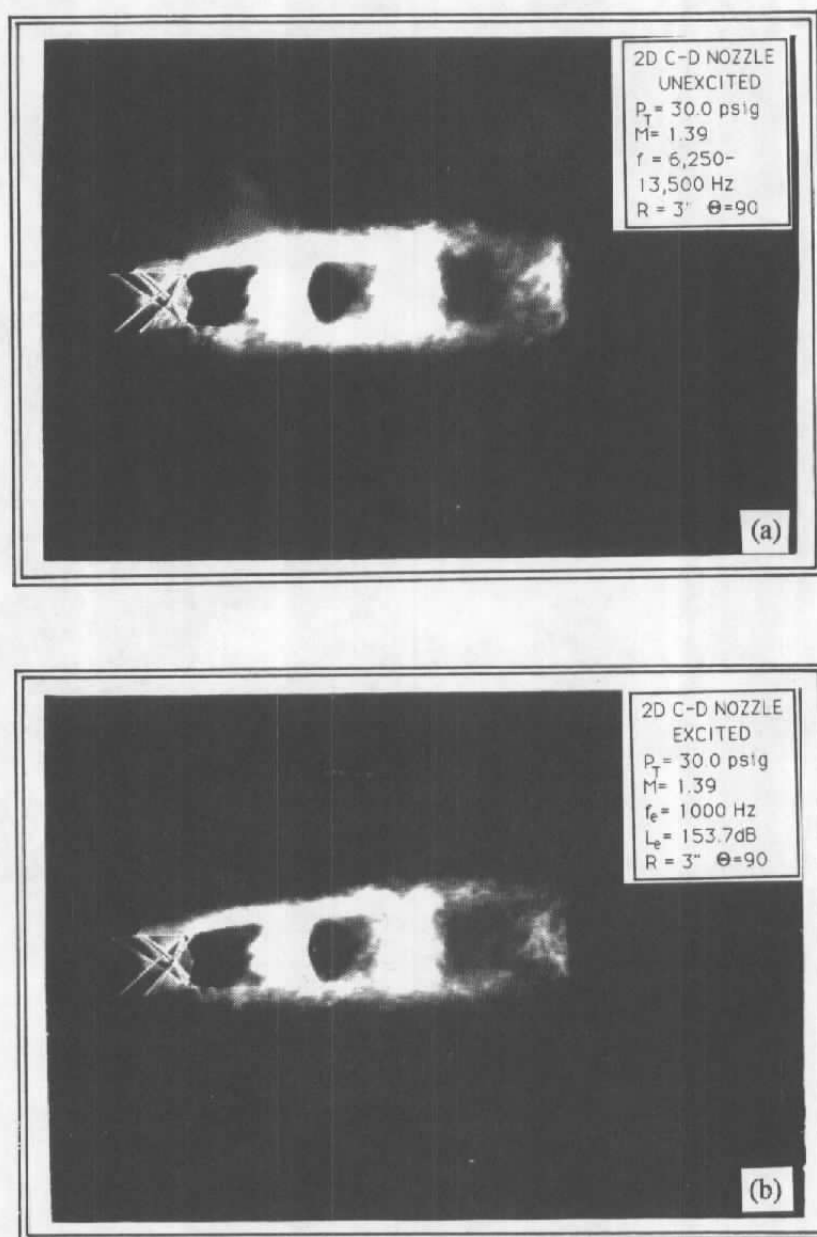


Figure 4.8 Schlieren photograph of the 2-D, C-D jet: (a) unexcited, (b) excited.

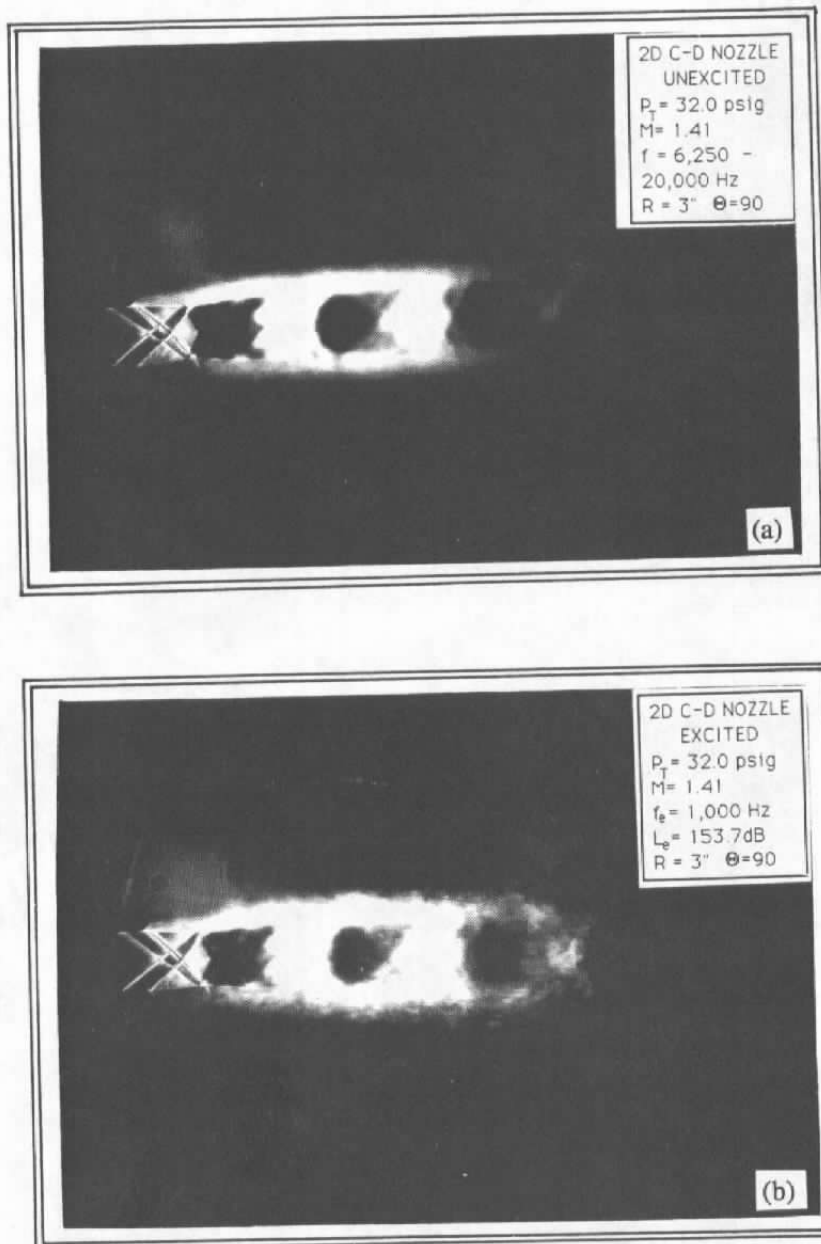


Figure 4.9 Schlieren photograph of the 2-D, C-D jet: (a) unexcited, (b) excited.

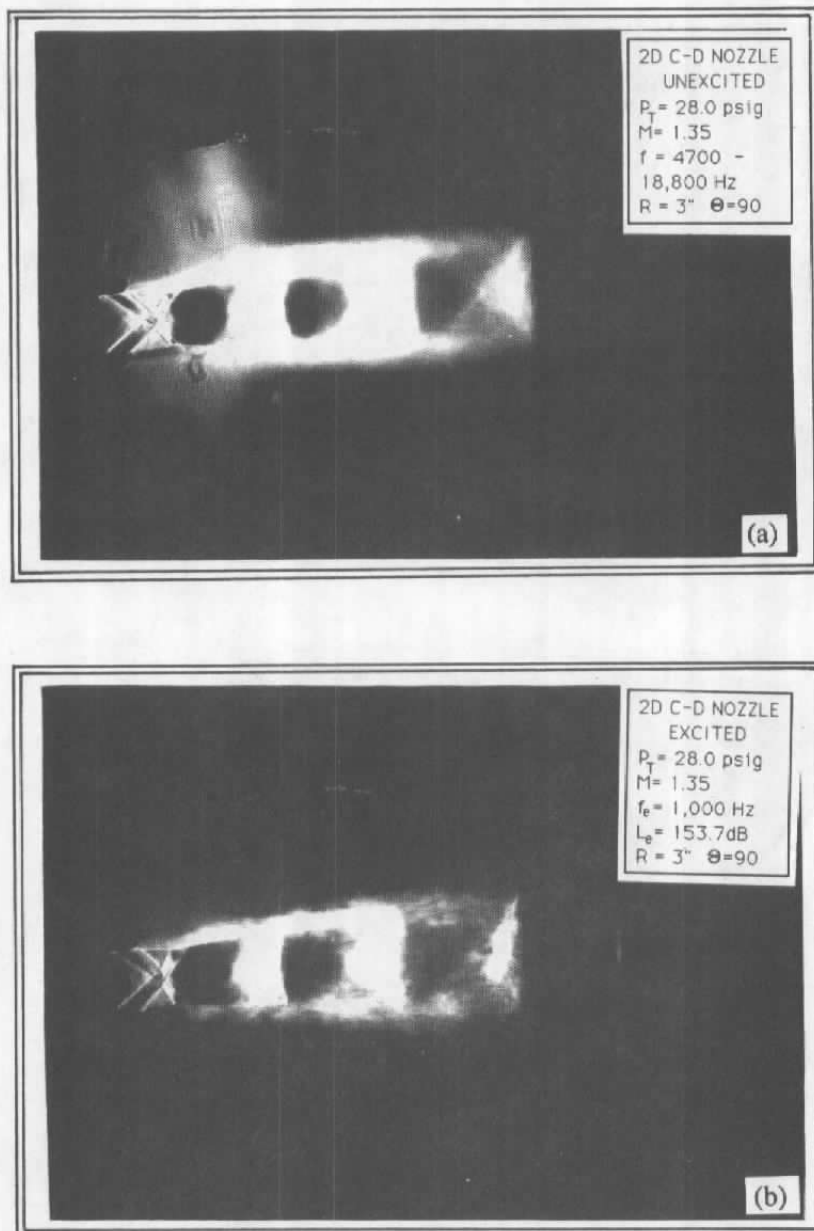


Figure 4.10 Schlieren photograph of the 2-D, C-D jet: (a) unexcited, (b) excited.

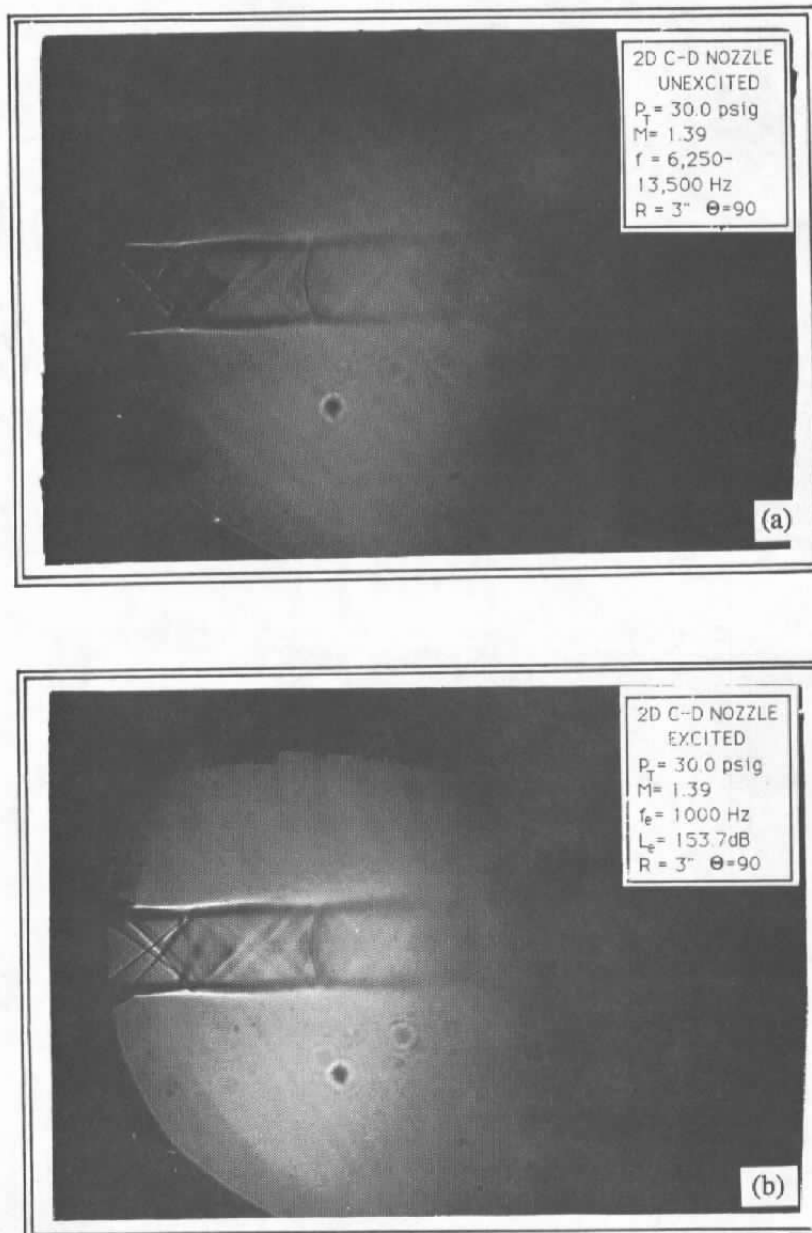


Figure 4.11 Shadowgraph of the 2-D, C-D jet: (a) unexcited, (b) excited.

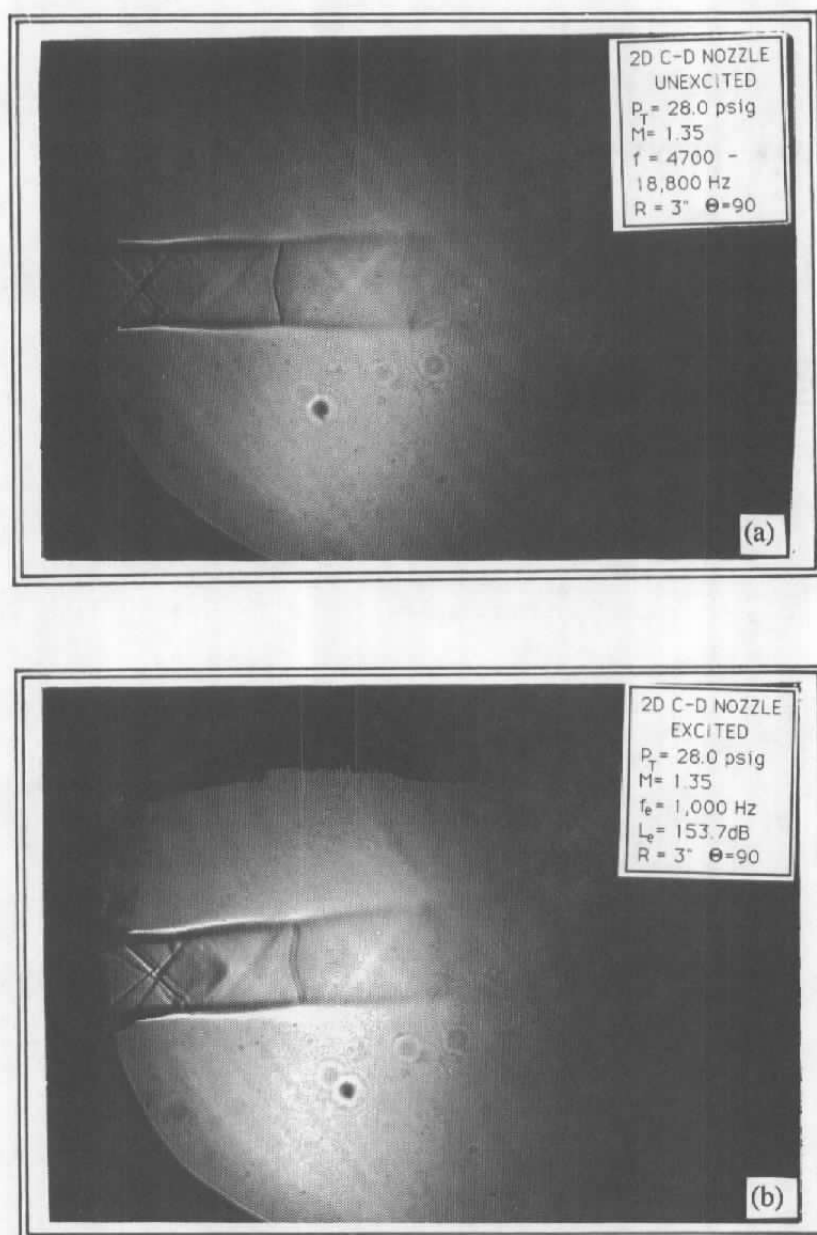


Figure 4.12 Shadowgraph of the 2-D, C-D jet: (a) unexcited, (b) excited.

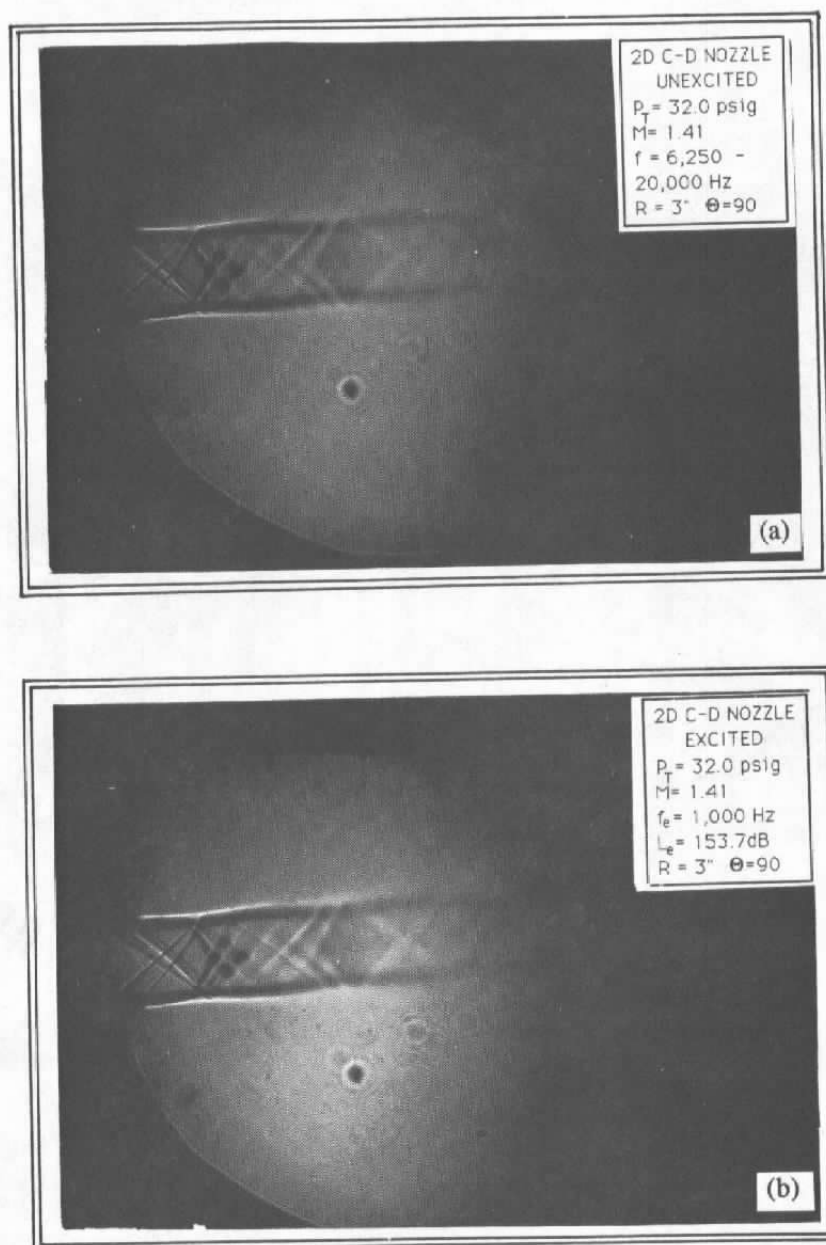


Figure 4.13 Shadowgraph of the 2-D, C-D jet: (a) unexcited, (b) excited.

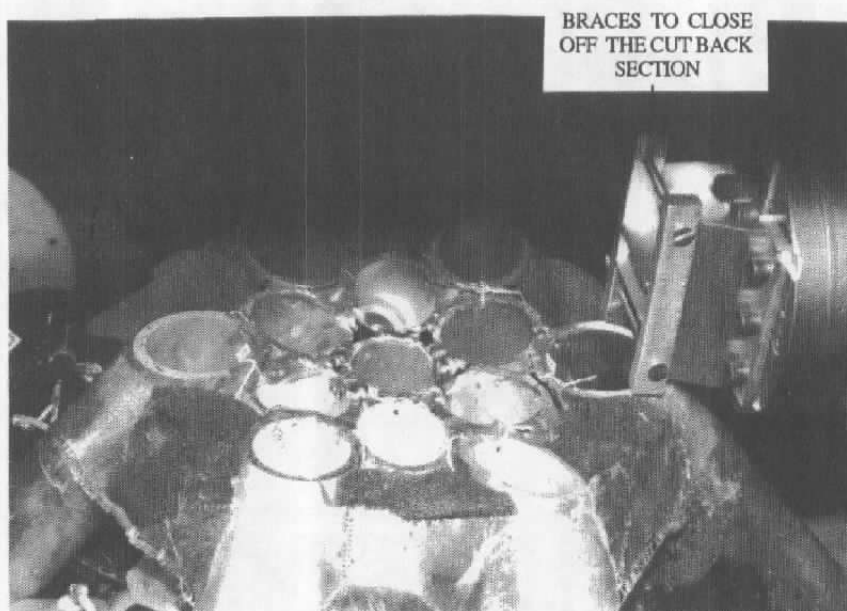


Figure 4.14 The 2-D, C-D nozzle with the cut back section closed off.

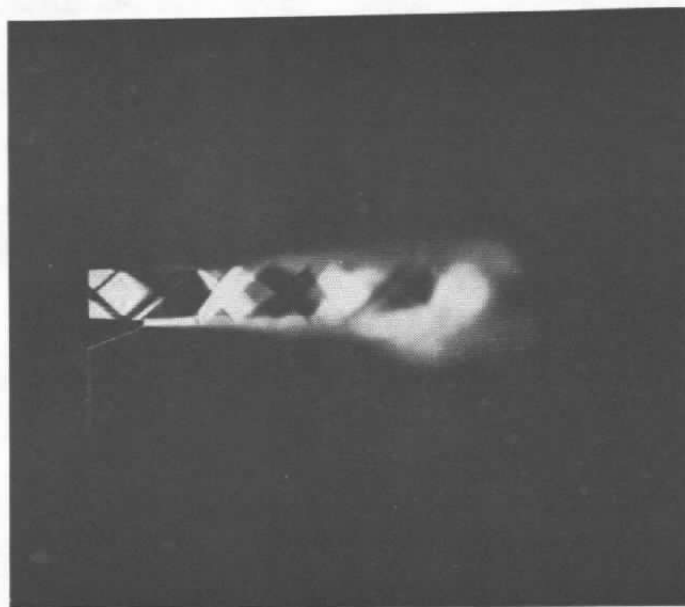
It was found that this indeed helped enhance the growth rate of the instability waves, and much stronger flapping instabilities were self excited in the jet which is typical of 2-D supersonic plumes. This is seen in comparison of jet instabilities at  $M_j = 1.49$  with the cutback open and then closed as presented in Figure 4.15.

It is recommended that if recorded data from the AEDC full-scale test are available, a closer examination be made of the data in the light of the above observations. Is it likely that the lighting conditions allowed visibility of the instability waves only on one side of the jet center line and hence giving the impression that the jet was deflected only in one direction.

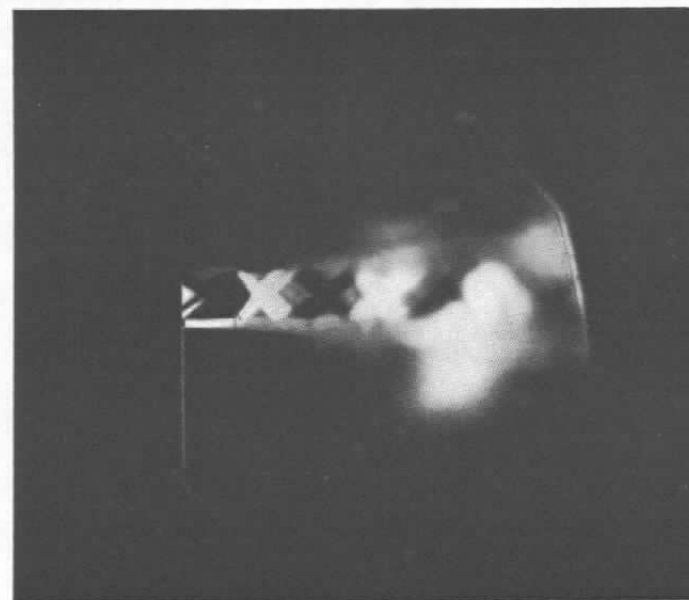
#### 4.5 Additional Interesting Data

In an effort to determine if there were other conditions for the sub-scale configurations where a bodily deflection of the jet with respect to its axis could be obtained, video pictures were taken with the jet Mach number gradually increasing. It was found that at about a pressure ratio of 1.5 such a deflection was indeed observed. This resulted from separation taking place on one of diverging walls. This separation appeared to switch randomly from one diverging wall to the other thus producing a bulk change in deflection. This is best seen in a real time video recording; a typical example is given in Figure 4.16. Figure 4.16a shows the plume development when the separation appeared to take place at the top wall (of the photograph). Figure 4.16b shows the same nozzle with the separation taking place on the lower wall. The only indication of anything being different in the two photographs is that the light shading is different just upstream of the nozzle exit and that the mixing layer on the lower side of Figure 4.16b is thicker than that in Figure 4.16a. In a full-scale configuration, any deflection produced by this wall-separation phenomenon would provide the impression of a large absolute deflection because of the larger distances involved.

It was found that when the cut-back section was closed off, the separation stabilized on one wall of the nozzle. Also it was noticed that while testing the effect of closing off the cut-back, there was a minor leak in the plate used for closing off the cut-back. On trying to stop the leak by placing the hand over it, the jet mixing appeared to reduce (the plume width decreased) in conjunction with a reduction in audible broadband noise. To explore it somewhat further, the plate to close off was attached properly to have no air leak and a 1/4 inch diameter hole was drilled on one of the plates used to close off the nozzle cut-back. The plate with the hole drilled in it is shown in Figure 4.17. A video of the schlieren flow visualization was made of the plume mixing with the hole closed or open. Typical results are shown in Figure 4.18. The jet could be modified considerably by closing off the hole itself.

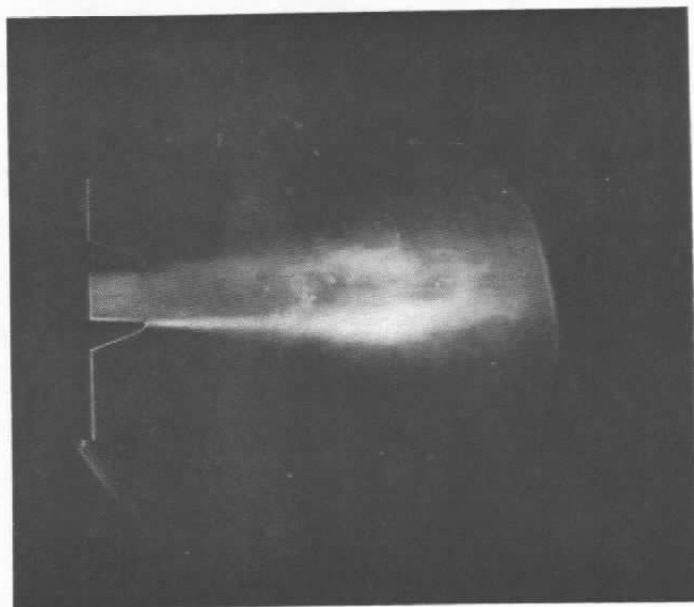


**Cut Back Open**

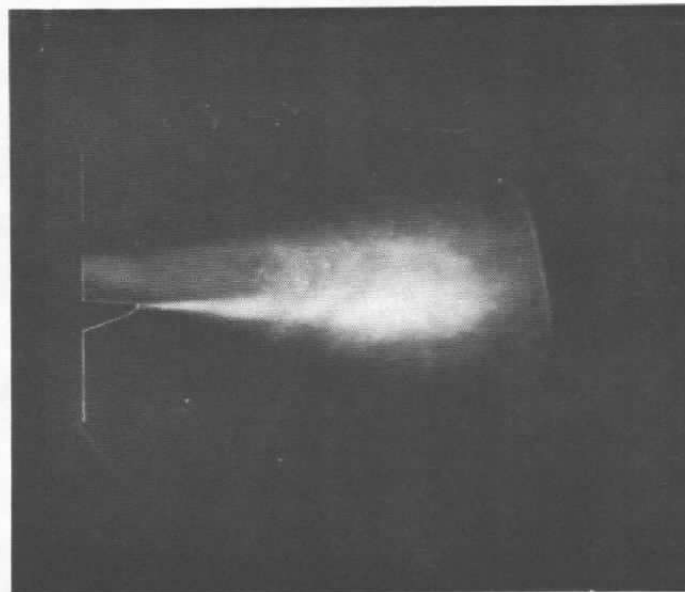


**Cut Back Closed**

Figure 4.15 Effect of closing cut back section on self-excited flapping instability.  
( $M_j = 1.49$ )



(a)



(b)

Figure 4.16 Plume visualization for two locations of nozzle wall separation.  
(Pressure ratio = 1.5)

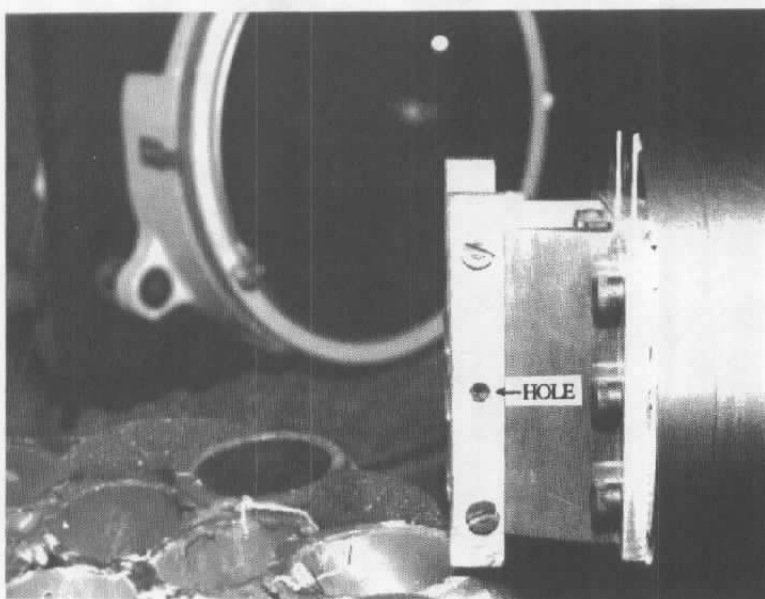


Figure 4.17 Hole drilled in the plate used to close off nozzle cut back.

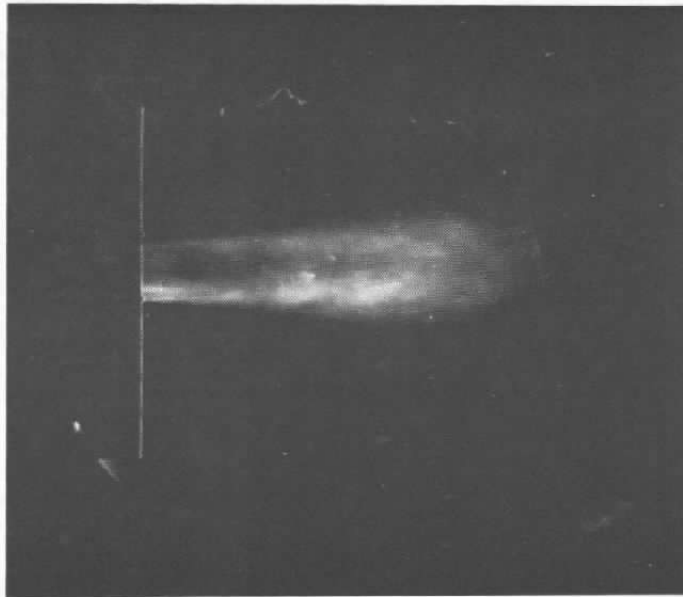
**Hole Open****Hole Closed**

Figure 4.18 Effect of opening and closing hole in cut back section.  
(Pressure ratio = 1.5)

No explanations are available for the observed phenomenon. Since detailed study of this phenomenon was beyond the scope of the present effort, no quantitative measurements were made. It is, however, recommended that further steps be taken to acquire detailed measurements to understand the physics of flow from 2-D, C-D nozzles with and without cut-backs. It is also recommended that the effects of nozzle wall boundary layer characteristics on the plume development be studied.

## SECTION 5

### OVERALL CONCLUSIONS AND RECOMMENDATIONS FOR FUTURE WORK

#### 5.1 Axisymmetric Jet Diffuser Flows

An experimental and theoretical investigation has been carried out to understand the aeroacoustics of jet/diffuser flows. Experimental measurements indicate that the spectrum of the noise of the flow is dominated by tones and resonances. Here tones refer to the spectral peaks of very narrow half-widths. On the other hand, spectral peaks with broader half-widths and not so well-defined peak frequencies are referred to as resonances. It is shown that the tones are the jet screech tones generated by feedback loops. These feedback loops are driven by the large-scale instability waves of the jet flow. The resonances are associated with the normal acoustic modes of the jet/diffuser. Because of factors outlined below plus the fact that the flow is highly turbulent, the normal mode resonances are not sharp.

To the authors' knowledge, this is the first analysis of the acoustic modes of a vortex sheet (top hot profile) supersonic jet inside a rigid circular duct.

Assuming a simple mathematical model, and assuming that the ejector is infinitely long, resonance frequencies for a helical duct mode were determined as a function of jet Mach number. The calculated frequency for the present sub-scale facility is approximately 3 kHz. The experimentally measured resonance frequency for the long ejector varies from 3.4 kHz at Mach number 1.1 to 4.2 kHz at the higher Mach numbers. The relatively close agreement strongly supports the contention that the observed low frequency tone is due in part to excitation of the helical duct mode resonance. The breadth and slight variation in this low frequency peak may be the result of the excitation of additional duct modes in this frequency range whose presence was confirmed in Section 3.2 "Duct Acoustic Modes" and the rather large resolution bandwidth of 200 Hz between each consecutive frequency in the presented spectra. In addition, the low frequency resonance measured in the sub-scale experiment appears to correlate quite well with the 85 Hz and 140 Hz tones observed in the full-scale facility when differences in scale and mean diffuser temperature are taken into account. From measurements taken from the full-scale facility, the 85 and 140 Hz tones were originally suspected to be associated with duct resonance frequencies. The present findings confirm that the full-scale phenomenon is most likely associated with some form of duct resonance and not due to a flow/acoustic interaction associated with classical jet screech. Since the amplitudes of these excited sub-scale duct modes were substantially lower than those observed in the full-scale configuration, the coupling mechanism which is presumed to have existed in the full-scale facility is still unclear. Nonetheless, the knowledge that it is the duct

resonance that is responsible for the low frequency tones is very helpful in deciding the course of action that may be necessary to eliminate the resonance tone. Or for that matter, the resonance frequency could perhaps be shifted to a more benign range by appropriately modifying the size of the diffuser.

Aside from the low frequency peak which appears to correlate with the frequency of the duct resonance mode, the noise spectrum of the jet-ejector or ducted flow is dominated by screech tones of almost discrete frequencies. An understanding of the characteristics and generation mechanism of these tones is also provided. This is done in two steps. First, an analysis of the screech tone frequencies is carried out to provide a general classification of the tones and identification of some of their most prominent characteristics. Second, the current theory on the screech tone generation has been extended by incorporating the concept of dominant instability mode developed in this report and the characteristics of the upstream propagating acoustic modes into earlier classical concepts of feedback related to screech tones.

It is shown that the tones from the free as well as the ducted supersonic jets are the screech tones. The presence of the diffuser does not appear to create new screech tones and that the measured tone frequencies with and without the diffuser all lie in the same narrow bands.

It should be noted that although this initial stage of the investigation has produced some very encouraging results, it is far from complete. Additional investigation is recommended. In particular, it is recommended that the following tasks be carried out to understand the aeroacoustics of ducted supersonic plumes as they relate to altitude test cells.

1. Using the sub-scale test facility, confirm the geometrical scaling of the resonance frequency by obtaining further acoustic data for a circular, straight ejector of a diameter different from that used in the present study. The theoretical calculation of resonance were based upon the diameter of the ejector and frequency should change linearly with ejector diameter.
2. Conduct detailed mode mapping inside the diffuser to identify diffuser modes excited by the jet. This will require mounting of pressure transducers flush with the diffuser wall in an azimuthal configuration. A mode decomposition computer code will have to be developed to accomplish this task.
3. Acquire additional screech noise data for Mach numbers that form the transition from axisymmetric mode to the helical mode. Noise spectra should be acquired at  $\Delta M$  of less than 0.1 in this region. This would provide precise Mach number demarcation line

between the modes of instabilities.

4. Conduct a study for axisymmetric heated jets similar to that for the cold jets reported here.
5. Study the conditions needed for a scale model to reproduce strong resonances observed in full-scale facilities. Simple geometrical scaling may not be enough to reproduce in scale model experiments the strong resonances observed in the full-scale facilities.
6. Develop design charts for avoiding strong resonances in the jet engine test cell environment. Development of a few simple-to-use charts by which jet-aeroacoustic sensitive frequencies (liable to cause strong acoustic resonances) can be easily estimated could be extremely beneficial to altitude test facility designers and operators.
7. Establish true scale simulation of full-scale hardware. For example, the constant diameter circular diffuser should be replaced by a conical diffuser. This would eliminate questions relative to geometric similarity on the nature of results.
8. In building any new hardware, adopt common scale for axisymmetric and 2-D nozzles. This would allow economical testing of both axisymmetric and 2-D, C-D nozzles in cell environment.
9. Continue developing theoretical models to provide insight, understanding, and analysis of the experimental measurements. Theoretical analysis will have to be extended to incorporate heated plumes and 2 dimensional nozzle geometries.

## 5.2 2-D, C-D Nozzle Flows

The purpose of this purely qualitative experimental study involving a 2-D, C-D nozzle (that had a cutback section) was to assess the sensitivity of plumes from such a nozzle to acoustic excitation at scale frequencies commensurate with those experienced in interactions in larger test facilities at AEDC.

It was concluded from this "limited-scope" study that the scaled frequency of 1000 Hz did not excite the plume from this test nozzle. In fact, because of the presence of the cutback section, the nozzle did not appear to display strong self-excited instability waves typical of 2-D nozzles without cutbacks. On closing off the cut-back section, strong flapping mode instabilities could

easily be seen in the flow. Likewise, strong screech frequencies were sensed by a far field microphone which was used to freeze the motion of the instability waves at the screech frequency.

In the experiment on plume sensitivity to externally imposed sound, we were expecting to observe some form of one sided bodily deflection of the plume as reported to have been observed in the full-scale facilities at AEDC. In view of the lack of such observation in the present experiments, it is recommended that if recorded data are available from the AEDC full-scale facilities they be examined in somewhat detail to establish if the jet indeed deflected in one direction.

It is quite likely that the flapping mode of the instability was excited in the full-scale facility, but the lighting conditions were such that the portion of the instability wave only on one side of the jet centerline could be seen. If the frequency of flapping was large enough, the observer might indeed get an impression of one-sided deflection of the plume. Note that in this case it would be difficult to precisely replicate the strength of any self-excited instability wave in the sub-scale facility from that observed in the full-scale facility. This is because the 2-D, C-D nozzle in the case of the full-scale facility was located inside the test cell, whereas that in the sub-scale facility was basically a free jet. It is well known that the amplitude of the screech which is related to the self-excited instability wave amplitude (and the sound amplitude at the nozzle lip) is a strong function of the surrounding that may help attenuate or enhance the sound energy reaching the nozzle lip. In addition, the growth rate of the instability waves is a function of the boundary layer thickness at the nozzle lip. Both of these factors could have contributed in not being able to precisely replicated the phenomenon observed in the full-scale facility.

Finally, some interesting observations were made. It was noticed that for certain jet operating conditions, separation occurred on one of the diverging walls of the nozzles. This separation randomly moved from one wall to the other. This deflected the plume flow about the nozzle axis in the manner of a fluidic jet. It was also found that when the cut back section was closed off, this separation still took place but now became stabilized on only one wall.

In another observation, it was observed that if a small hole was drilled in the section and to close off the cut back section, it modified the plume mixing and the associated jet mixing noise considerably. No quantitative data were acquired.

It is recommended that a detailed study be carried out to understand both the fluid dynamics and the aeroacoustics of 2-D, C-D nozzles. Part of this study should include 2-D, C-D nozzle wall surface pressure measurements to establish nozzle internal performance during oscillatory behavior. The walls of the nozzle wall should be made out of a transparent material to obtain

insight into the origin of the unsteadiness via schlieren photography. Finally, as already alluded to above, effect of temperature should be studied both with and without the cell.

## APPENDIX I

As pointed out earlier, all of the data presented in the report for a given nominal fully-expanded jet Mach number was acquired at a constant ratio of the plenum chamber pressure to the ambient pressure. In later measurements, it was found that because of the pumping action of the diffuser, the back pressure, downstream of the nozzle exit, was actually somewhat lower for the larger ejector than the ambient pressure. The differences in the ambient pressure and the back pressure or the test cell static pressure for the smaller ejector were insignificant. For the sake of completeness, the back pressures for both ejectors were measured as a function of the ratios of plenum pressure and ambient pressure. A relative comparison of the actual pressure ratio ( $P_{\text{plenum}}/P_{\text{test cell}}$ ) and assumed pressure ratio ( $P_{\text{plenum}}/P_{\text{ambient}}$ ) for the two ejectors is provided in Figure A1. The slope of the curve for the smaller ejector is 1.0403 while that for the larger ejector is 1.207. A comparison of assumed fully-expanded jet Mach numbers with actual Mach numbers calculated after accounting for the reduced back pressures is given in Table I.1.

Table I.1 A comparison of the assumed fully-expanded Mach numbers with the actual Mach numbers for the two ejectors.

Assumed $M_j$	Actual $M_j$ ( $L_{ej}/D_{ej} = 1$ )	Actual $M_j$ ( $L_{ej}/D_{ej} = 3$ )
0.80	0.80	0.81
1.00	1.00	1.02
1.10	1.10	1.12
1.20	1.20	1.23
1.30	1.31	1.34
1.40	1.41	1.45
1.50	1.51	1.57
1.60	1.62	1.68
1.70	1.72	1.79

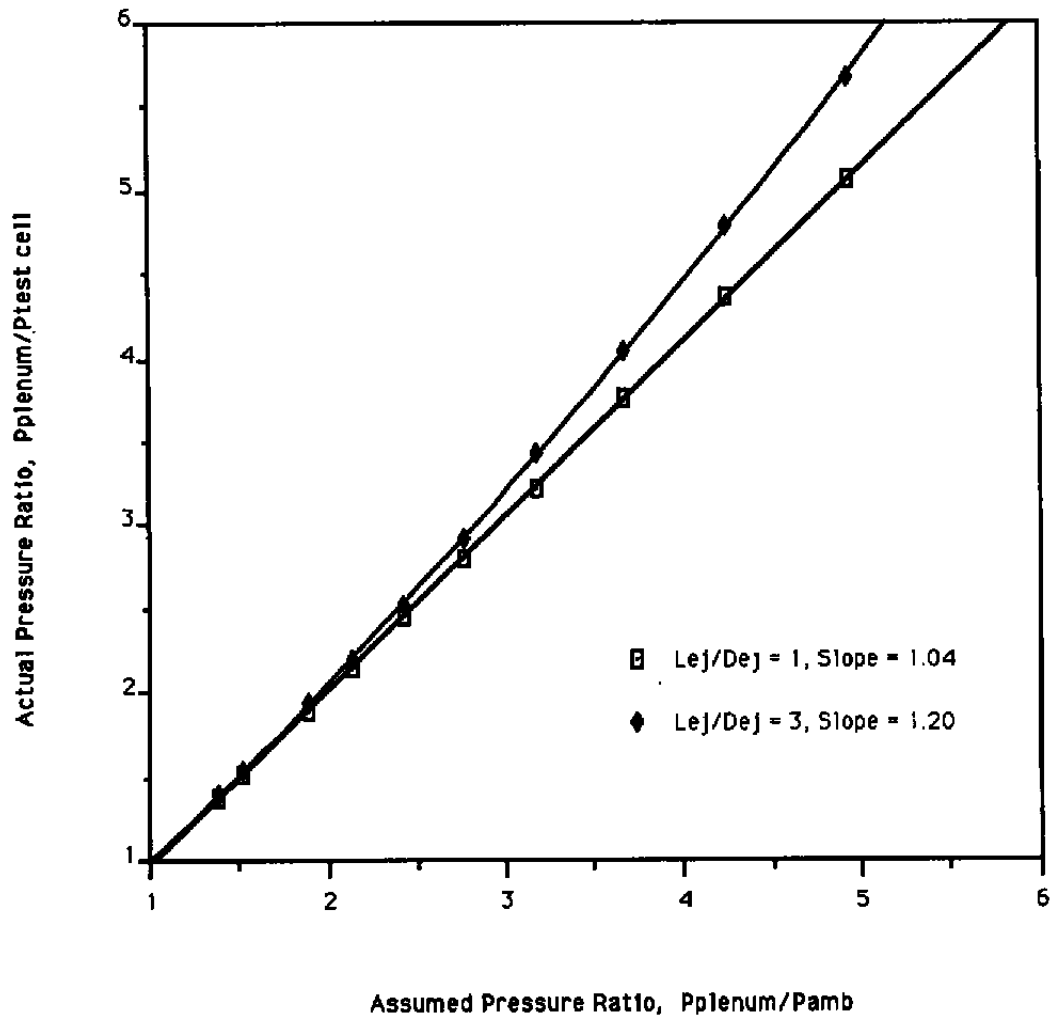


Figure I.1 Actual versus assumed pressure ratios.

## REFERENCES

- 1.1 Lazalier, G. R. 1989 Examples of acoustic interactions between a test facility and jet engine plumes. AEDC workshop on flow/acoustic interactions held at Arnold Engineering Development Center, Tennessee, Oct. 24-25 1989.
- 1.2 Tam, C. K. W. 1986 On the Screech Tones of Supersonic Rectangular Jets AIAA-86-1866.
- 2.1 Ahuja, K. K., Lepicovsky, J., Tam, C. K. W., Morris, P. J., and Burrin, R. H. 1982 Tone Excited Jet -- Theory and Experiments, NASA CR-3538.
- 2.2 Ahuja, K. K., Lepicovsky, J., and Burrin, R. H. 1982 Noise and Flow Structure of Tone-Excited Jet, AIAA Journal, Vol. 20, No. 12, pp. 1700-1706.
- 2.3 Ahuja, K. K., and Whiffen, M. C. 1985 Tone Excited Jets, Part II: Flow Visualization. Journal of Sound and Vibration, Vol. 102, No. 1, pp. 63-39.
- 3.1 Tam, C. K. W. and Hu, F. Q. 1989 On the three families of instability waves of high speed jets. Journal of Fluid Mechanics, 201, 447-483.
- 3.2 Tam, C. K. W. and Ahuja, K. K. 1990 Theoretical model of discrete tone generation by impinging jets. Journal of Fluid Mechanics, 214, 67-87.
- 3.3 Tam, C. K. W. and Norum, T. D. 1990 Impingement tones of large aspect ratio supersonic rectangular jets. AIAA paper 90-3984 (to appear in the AIAA Journal, 1991).
- 3.4 Powell, A. 1953 On the mechanism of choked jet noise. Proceedings of the Physical Society, 66, 1039-1056.
- 3.5 Davies, M. G. and Oldfield, D. E. S. 1962 Tones from a choked axisymmetric jet. Acustica, 12, 257-277.
- 3.6 Tam, C. K. W., Seiner, J. M. and Yu, J. C. 1986 Proposed relationship between broadband shock associated noise and screech tones. Journal of Sound and Vibration, 110, 309-321.

- 3.7 Seiner, J. M. and Norum, T. D. 1979 Experiments of shock associated noise on supersonic jets. AIAA paper 79-1526.